International Journal of Polymer Science

Application of Natural Biopolymers in Regenerative Medicine

Lead Guest Editor: Ramachandran Saravanan
Guest Editors: Senthilkumar Rajagopal and Panchanathan Manivasagan

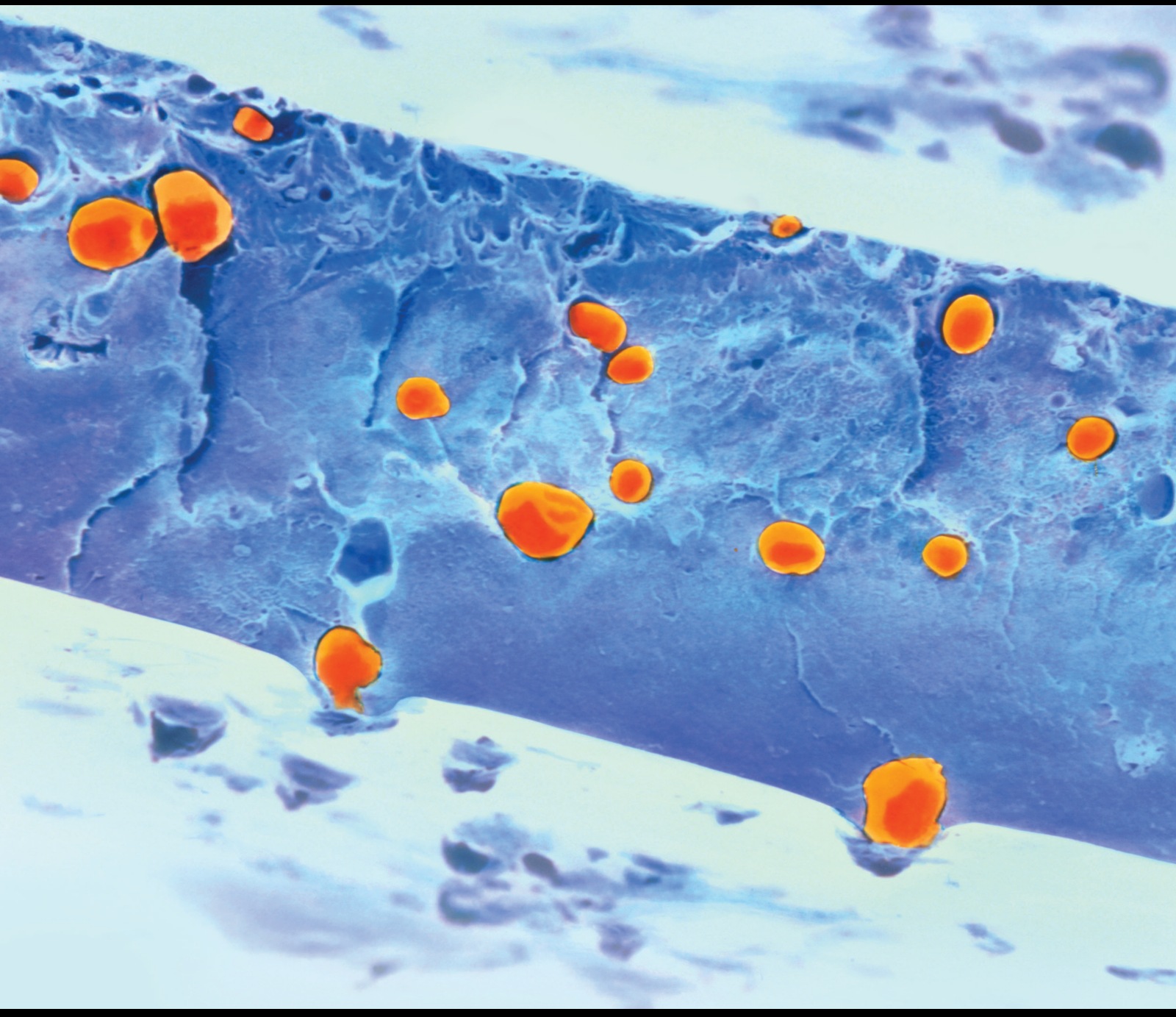

Application of Natural Biopolymers in Regenerative Medicine

International Journal of Polymer Science

Application of Natural Biopolymers in Regenerative Medicine

Lead Guest Editor: Ramachandran Saravanan
Guest Editors: Senthilkumar Rajagopal and Panchanathan Manivasagan

Contents

Hindawi
International Journal of Polymer Science
Volume 2021, Article ID 7549048, 10 pages
https://doi.org/10.1155/2021/7549048

Research Article

A Novel Study of Synthesis and Experimental Investigation on Hybrid Biocomposites for Biomedical Orthopedic Application

C. V. Subba Rao,[1] R. Sabitha,[2] P. Murugan,[3] S. Rama Rao,[4] K. Anitha,[2] and Y. Sesha Rao[1]

[1]*Department of Mechanical Engineering, QIS College of Engineering and Technology, Ongole, India*
[2]*Department of Computer Science and Engineering, Saveetha School of Engineering, SIMATS, Chennai, 602 105 Tamil Nadu, India*
[3]*Jimma Institute of Technology, Jimma University, Jimma, Ethiopia*
[4]*Tirumala Engineering College, Narasaraopet, India*

Correspondence should be addressed to P. Murugan; pmurugan14251425@gmail.com

Received 15 July 2021; Revised 20 September 2021; Accepted 8 November 2021; Published 28 November 2021

Academic Editor: Saravanan Ramachandran

In recent years the biocomposites are highly utilized in the biomedical applications, due to excellent strength as well as weight ratio. A lot of natural fibers, namely, flax, hemp, jute, kenaf, and sisal are cheaply available in colossal amount. Aim of this study, a novel approach, is executed for construction of biomedical orthopedic parts by using mixture of natural fibers. This work handled biocomposites such as flax fiber (FX), chicken feather fiber (CF), kenaf fiber (KF), and rice husk fiber (RH) effectively. From all these composites, four sets of mixed fibers with reinforcement of polylactic acid polymer used for creating orthopedic parts. The hand-lay-based methodology is undertaken for preparation of hybrid biocomposites. Parameters involved for this study are fiber types (KF + RH, RH + FX, FX + CF, and CF + KF), laminate count (2, 4, 6 and 8) infill density (30%, 60%, 90%, and 120%), and raster angle (0/60, 30/120, 50/140, and 70/160). Finding of this work is dimensional accuracy, flexural strength, and shore hardness that are analyzed by L16 orthogonal array. ANOVA statistical analysis is enhanced and enlightens the results of flexural strength and source hardness of the biocomposites. Amongst in four parameters, the fiber type parameter extremely contributes such as 40.50% in the flexural analysis. Similarly, laminate count parameter highly contributes such as 31.01% in the shore hardness analysis.

1. Introduction

In recent trends, the biomedical applications are fulfilled by the composite material especially biocomposites. The natural fibers are produced the biocomposites with reinforcement of polymer. Natural fibers possess low weight and high strength; hence, it has used in the industrial applications particularly in medical appliances. It has best suited for preparation of composites due to no environmental affects for humans. Biocomposites are prepared by blending of biofibers, namely, jute, hemp, kenaf, and sisal. Biocomposites are employed hugely in biomedical applications. Few of the biocomposites applications are tissue engineering, orthopedics, dental post, bone plate, composite pins, screws, and clips in spinal fusion. The study of chemical treatment to the natural fibers is vital role in composite preparation. Flax fiber was considered the chemical processing with 80 hours in room temperature [1]. Using of cotton cellulose and nanohydroxyapatite is excellent use in bone tissue engineering. Morphological study of the electrospun and thermal analysis is major role in the tissue engineering [2]. In bioengineering, the bone study is conducted, and the two cell lines designate the cell and proportional cell feasibility study through PVP concerned samples [3]. Blending of polylactic acid and polycaprolactone polymers into the hydroxyapatite (nHA) on the shape memory performance is conducted. The morphology study is carried out by applying of field emission scanning electron microscopy [4, 5]. A strong literature

Figure 1: Natural fibers: (a) flax fiber, (b) chicken feather fiber, (c) kenaf fiber, and rice husk fiber.

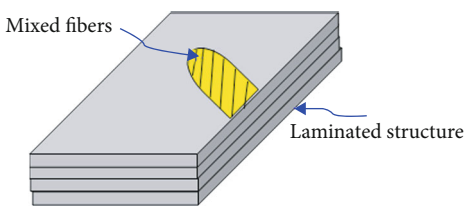

Figure 2: Natural fibers with PLA laminated structure.

Table 1: Process parameters and their values of biocomposite preparation.

Factors	Level 1	Level 2	Level 3	Level 4
Fiber types	KF + RH	RH + FX	FX + CF	CF + KF
Laminate count	2	4	6	8
Infill density (%)	30	60	90	120
Raster angle	0/60	30/120	50/140	70/160

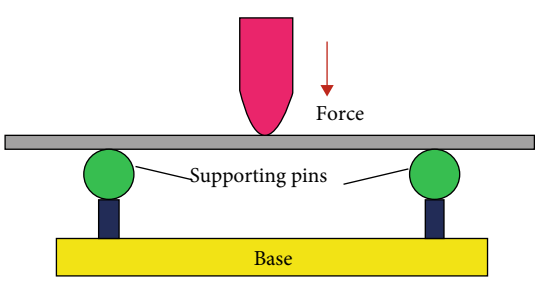

Figure 3: Flexural setup.

review is made on the natural fibers with forming of hybridization composites. The prepared composites are analyzed, parameters influences are studied, and the synthetic and natural fibers properties are briefly surveyed. Authors are

Table 2: Summary of flexural strength and influence of input parameters.

Exp. runs	Fiber types	Laminate count	Infill density (%)	Raster angle	Flexural strength (MPa)	S/N ratio
1	KF + RH	2	30	0/60	15.23	23.6540
2	KF + RH	4	60	30/120	18.34	25.2680
3	KF + RH	6	90	50/140	17.35	24.7860
4	KF + RH	8	120	70/160	20.47	26.2224
5	RH + FX	2	60	50/140	22.91	27.2005
6	RH + FX	4	30	70/160	21.05	26.4650
7	RH + FX	6	120	0/60	18.40	25.2964
8	RH + FX	8	90	30/120	17.39	24.8060
9	FX + CF	2	90	70/160	19.08	25.6116
10	FX + CF	4	120	50/140	20.05	26.0423
11	FX + CF	6	30	30/120	18.73	25.4508
12	FX + CF	8	60	0/60	17.34	24.7810
13	CF + KF	2	120	30/120	20.31	26.1542
14	CF + KF	4	90	0/60	23.07	27.2610
15	CF + KF	6	60	70/160	24.89	27.9205
16	CF + KF	8	30	50/140	19.57	25.8318

Table 3: Response table for means (flexural strength).

Level	Fiber types	Laminate count	Infill density (%)	Raster angle
1	19.94	19.38	18.65	18.51
2	18.80	20.63	20.87	18.69
3	17.85	19.84	19.92	19.97
4	21.96	18.69	19.81	21.37
Delta	4.11	1.93	2.22	2.86
Rank	1	4	3	2

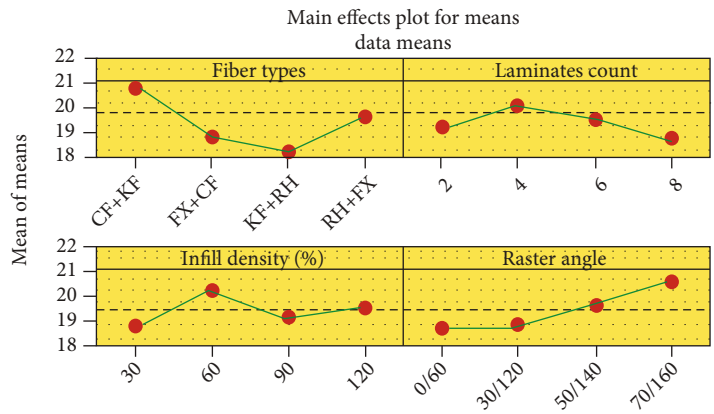

Figure 4: Main effect plot for means (flexural strength).

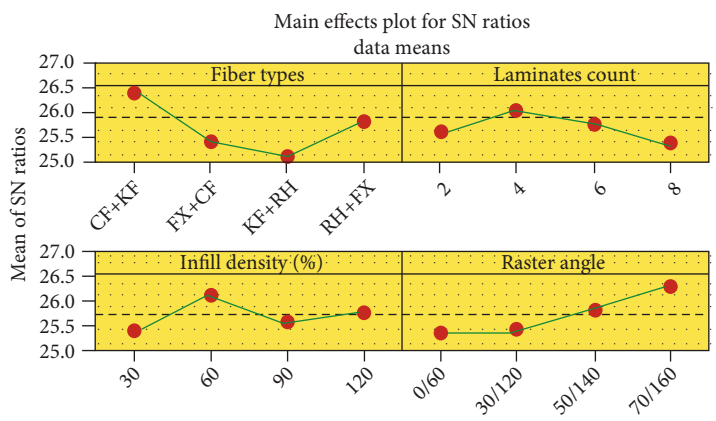

Figure 5: Main effect plot for S/N ratio (flexural strength).

putting effort to review the resulting properties of hybrid composites, namely, mechanical, thermal, water absorption, tribological behavior, and morphological [6]. In the human health bone, problems are rectified by using of biocomposites materials, and fracture of the bone is corrected by newly prepared biocomposites. Biodegradable polyesters are highly influenced in the bone engineering products, namely, implants and surgical tubing [7]. Biocomposite materials are produced by man-made effort that fibers are replace of living tissues of the human body. Human functions are restored by using of biocomposite devices named as biosensors, pacemakers, and artificial hearts [8]. The plan of this investigation is focused on the orthopedic applications by using of natural fibers such as flax fiber, chicken feather fiber, kenaf fiber, and rice husk fiber. Considered the reinforcement of polymer such as polylactic acid with the natural fibers are enhance the flexural strength and shore hardness of the biocomposites. Taguchi statistical analysis is conducted for this experimental work to improve the strength of the biocomposites [9]. Novelty of this work is combined of different natural fibers. Different combinations of fibers are offered good flexural strength and shore hardness compared to the previous research results. Novelty implemented is reflected in the results such as pair of natural fibers that enhanced the composite strength [10].

2. Materials and Methods

The objective of this study is preparing the hybrid biocomposites for orthopedic applications with using of different natural fibers. The fibers are namely flax fiber (FX), chicken feather fiber (CF), kenaf fiber (KF), and rice husk fiber (RH). All the fibers are procured from Vruksha Composites & Services, Chennai. The PLA—polylactic acid polymers—is selected for this work to reinforce into the natural fibers [11]. PLA is highly enhanced by the flexural strength and hardness of the prepared biocomposites. This composite is vastly used in the biomedical applications such as orthopedic parts [12]. Required quantity of polylactic acid polymers is procured from Natur Tec India Private Limited. The composites are prepared by hand-lay methodology with effective use of PLA polymer. Steel mould and hand roller tools are utilized to prepare the composites by the way of hand layup methodology. Using of P ratham 5.0 3D Printer (Make: Pratham, India), it can be operated by Repetier, Slicer software package. Pratham 5.0 delivers the molten material with the nozzle dimensions of 0.4 mm.

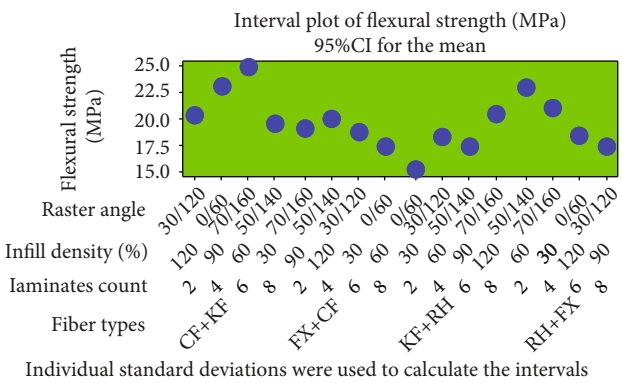

Figure 6: Interval plot of flexural strength.

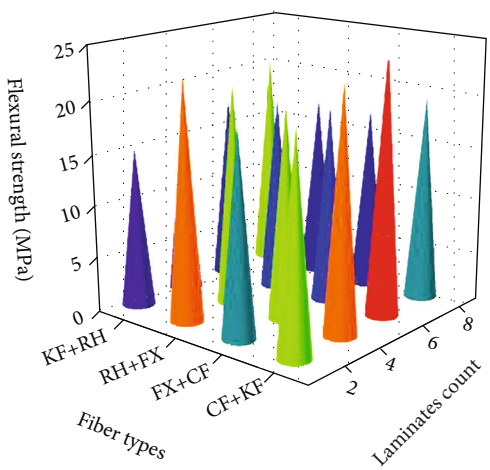

Figure 7: Flexural strength: 3D plot of fiber types and laminate count.

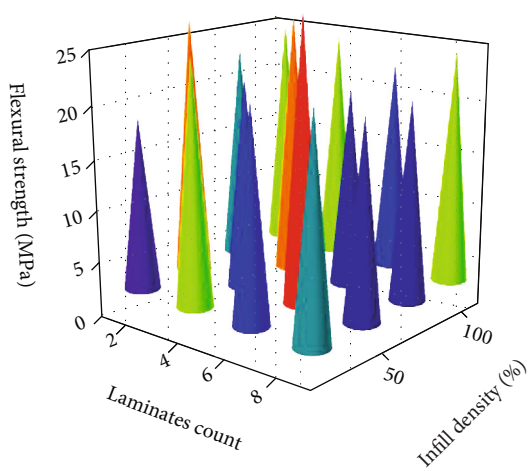

Figure 8: Flexural strength: 3D plot of laminate count and infill density.

3. Experimental Procedure

There are multiple stages that are involved to clean the fibers, and it can be discussed in detail manner. Initially, the cleansing process is carried out to clean the fibers thoroughly with the help of sodium hypochlorite (NaOCl).

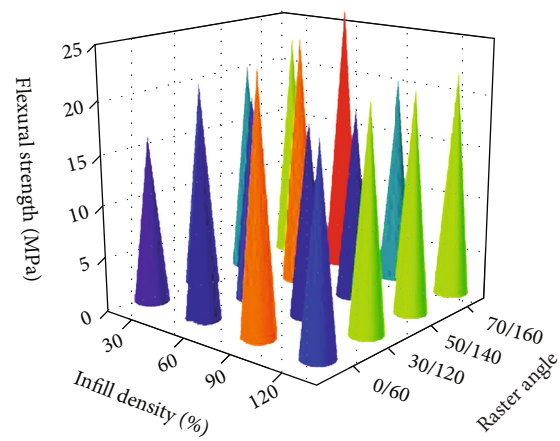

Figure 9: Flexural strength: 3D plot of infill density and raster angle.

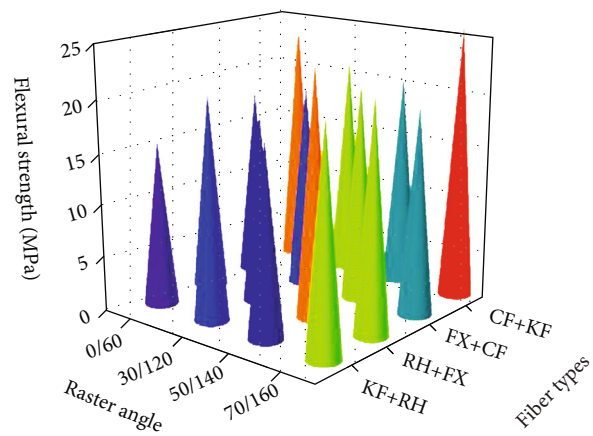

Figure 10: Flexural strength: 3D plot of raster angle and fiber types.

Table 4: Response table for signal to noise ratios (flexural strength).

Level	Fiber types	Laminate count	Infill density (%)	Raster angle
1	25.54	25.66	25.35	25.25
2	25.47	26.26	26.29	25.42
3	24.98	25.86	25.62	25.97
4	26.79	25.41	25.93	26.55
Delta	1.81	0.85	0.94	1.31
Rank	1	4	3	2

Taken of 30 liters of distilled water with mixing of 300 ml of 35% solution, namely, sodium hypochlorite, is in a vessel [13, 14]. Stirring action is maintained at a frequency level of 15 Hz with a time period of 45 min. This cleaning process carried out three times for achieve healthy fibers [15]. Further continue of washing process of the fibers is carried out by using hydrogen peroxide (H_2O_2). Using of this process, taken of 150 ml of 20% solution of H_2O_2 is mixed in 30 liters of distilled water; the homogeneous mixing is obtained by maintaining of 10 Hz and 45 min. Finally, completions of chemical processing all the fibers are dried well for 20 hrs

Table 5: Analysis of variance of flexural strength.

Source	DF	Seq SS	Contribution (%)	Adj SS	Adj MS	*F* value	*P* value
Regression	12	77.440	83.51	77.440	6.453	1.27	0.478
Fiber types	3	37.558	40.50	37.558	12.519	2.46	0.240
Laminate count	3	7.921	8.54	7.921	2.640	0.52	0.699
Infill density (%)	3	10.821	11.67	10.821	3.607	0.71	0.608
Raster angle	3	21.140	22.80	21.140	7.047	1.38	0.398
Error	3	15.293	16.49	15.293	5.098		
Total	15	92.733	100				

Table 6: Summary of shore hardness and influence of input parameters.

Exp. runs	Fiber types	Laminate count	Infill density (%)	Raster angle	Shore hardness (HD)	S/N ratio
1	KF + RH	2	30	0/60	72.13	37.1623
2	KF + RH	4	60	30/120	75.00	37.5012
3	KF + RH	6	90	50/140	74.00	37.6042
4	KF + RH	8	120	70/160	70.85	37.0068
5	RH + FX	2	60	50/140	73.00	37.2665
6	RH + FX	4	30	70/160	72.38	37.1924
7	RH + FX	6	120	0/60	75.37	37.5440
8	RH + FX	8	90	30/120	69.89	36.8883
9	FX + CF	2	90	70/160	78.25	37.8697
10	FX + CF	4	120	50/140	77.34	37.7681
11	FX + CF	6	30	30/120	72.01	37.1479
12	FX + CF	8	60	0/60	73.64	37.3423
13	CF + KF	2	120	30/120	77.29	37.7625
14	CF + KF	4	90	0/60	76.65	37.6902
15	CF + KF	6	60	70/160	74.89	37.9205
16	CF + KF	8	30	50/140	72.01	37.2318

with 600°C with the aid of hot air oven [16, 17]. In this experimental work, the automatic fiber placing mechanism is accomplished in the fiber count as well as uniform placing of the fibers [18]. The different natural fibers are chosen for this experimental work that is illustrated in Figure 1.

The composite specimen is prepared as per the ASTM D790 standard for conducting of flexural test to find the strength of the specimens. Using of solid work software package in the 3D model of the specimens is to be created as shown in Figure 2. Created 3D model is exported into the FDM machine with stereolithography layout, and this format is used for easy accessible in printing [19]. Applying of hand-lay technique, the fibers are inserted into the specimen with PLA polymer reinforcements through manually. Insertion of layer of fiber, laminate count, infill density, and raster angle is predetermined with the help of vast literature study [20–22]. The process parameters and the values of the biocomposites are presented in Table 1.

The Taguchi L16 OA is selected for estimate of the parameters that influence as well as the outcome of the work by Taguchi statistical tool.

3.1. Dimensional Accurateness. Dimensional accurateness of the composite structures is analyses by using of a digital Vernier calliper under the least count of 0.01 mm: make: aerospace. Dimensional accurateness is based on the thickness of the composite structure in this work; the insertion of fibers has the higher influence in the strength of the composites [23–25]. Dimensional accurateness is estimated by the difference between dimensions of the specimen in design stage and the production stage.

Table 7: Response table for means (shore hardness).

Level	Fiber types	Laminate count	Infill density (%)	Raster angle
1	49.60	75.17	59.02	74.45
2	75.31	75.34	61.20	73.55
3	60.49	60.07	62.20	60.48
4	72.66	58.49	75.21	61.59
Delta	25.71	26.28	16.19	25.97
Rank	3	1	4	2

3.2. Shore-D Hardness. Shore hardness is measured in the prepared biocomposites by shore hardness tester (make: Linear Instruments Chennai), avoiding the human and environmental errors while in hardness testing by taken of readings

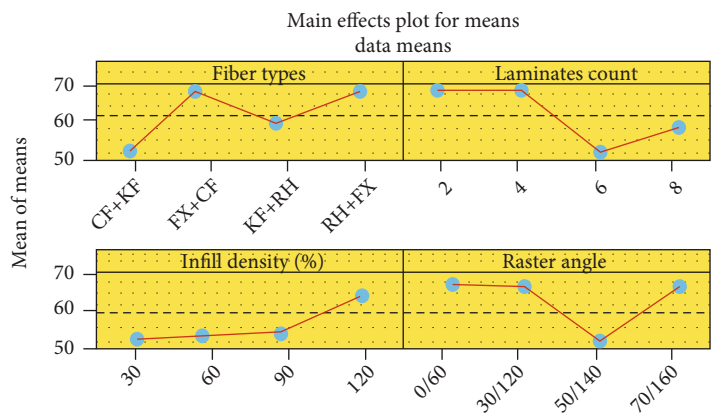

Figure 11: Main effect plot for means (shore hardness).

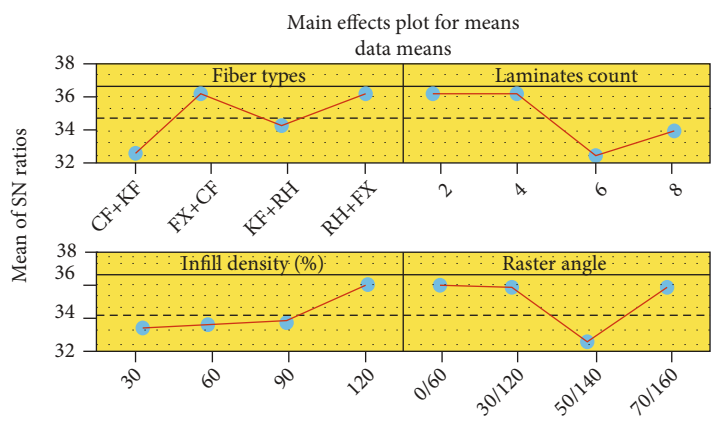

Figure 12: Main effect plot for S/N ratio (shore hardness).

in three times for each specimen finally considered the average values [26].

3.3. Flexural Testing. Using of universal testing machine the flexural test is conducted, the UTM Make: Universal grip company, Salem. This machine having a 5 kN load cell generally the testing speed for polymer composite material is set by 3 mm/min based on the ASTM standard [27]. The bottom portion of the UTM machine is utilized for conducting of flexural test, and the specimen is placed horizontally in the fixtures [28–30]. Three point flexural tests are implemented for this investigation as shown in Figure 3.

The load is acting on the center portion of the specimen with suggested span-to-depth ratio that is 18 : 1. The flexural readings are displayed digitally with the aid of computer control accessories [31–33].

4. Results and Discussion

4.1. Flexural Strength. Table 2 presents the summary of flexural strength and S/N ratio of the investigation. Maximum flexural strength was obtained as 24.89 MPa by influencing of combination of chicken feather fiber and kenaf fiber, laminate count of 6, infill density of 60%, and raster angle of 70/160.

Tables 3 and 4 present the response tables for means and S/N ratio of the flexural strength [34]. Based on the rank order, the types of fiber are highly influenced and followed by raster angle, infill density, and laminate count. The optimal parameters were obtained as mixture of chicken feather fiber and kenaf fiber, 6 counts of laminates, 60% of infill density, and 70/120 of raster angle [35].

Figures 4 and 5 present the main effect plots for both means and S/N ratio of flexural strength. Based on the types of fibers, the mixture of chicken feather fiber and kenaf fiber offered excellent flexural strength compared to other mixture of fibers. Mixture of kenaf fiber and rice husk provided minimum flexural strength [36].

Taken of laminate count the 4 number of laminates offered good flexural strength, further increasing of laminate count the strength has to be gradually decreased [37]. Infill density 60% provided the maximum flexural strength, continually increasing of infill density, and the flexural strength is decreased in little amount. Raster angle is one of the important factor for deciding the flexural strength; here, maximum flexural strength offered by influence of higher angle 70/160.

Figure 6 shows the interval plot of flexural strength and all parameter effects in a single plot. This plot shows that the maximum of flexural strength was found around

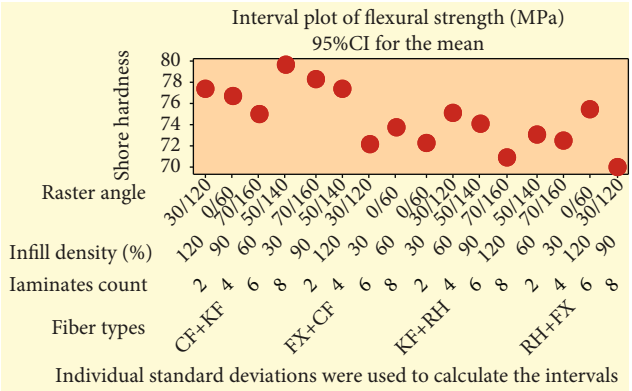

Figure 13: Interval plot of shore hardness.

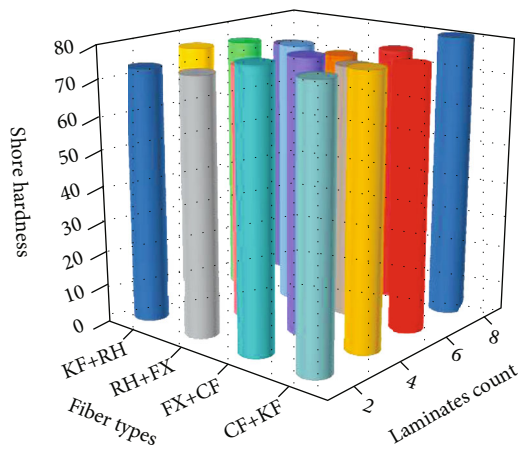

Figure 14: Shore hardness: 3D plot of fiber types and laminate count.

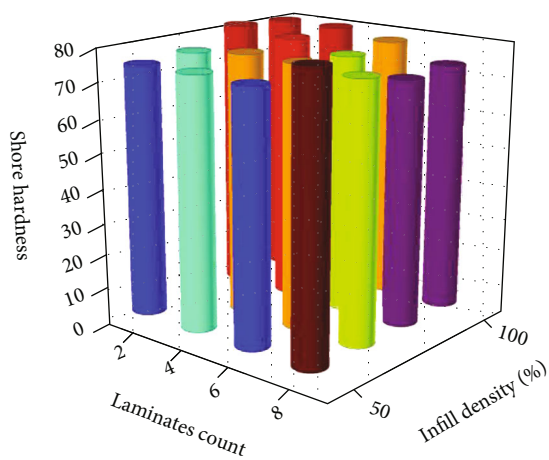

Figure 15: Shore hardness: 3D plot of laminate count and infill density.

25 MPa of flexural strength. Parameter effects were concluded as mixture of chicken feather fiber and kenaf fiber, 6 counts of laminates, 60% of infill density, and 70/120 of raster angle.

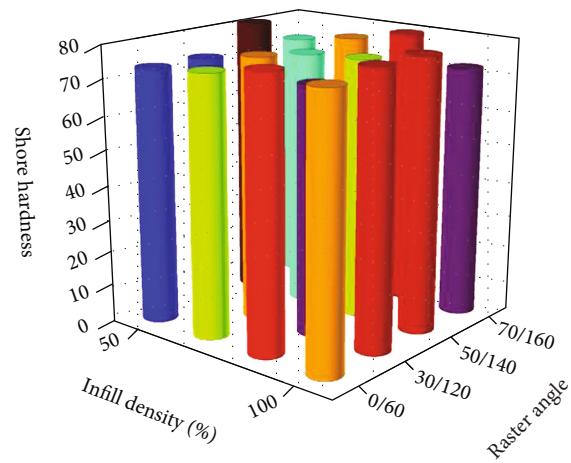

Figure 16: Shore hardness: 3D plot of infill density and raster angle.

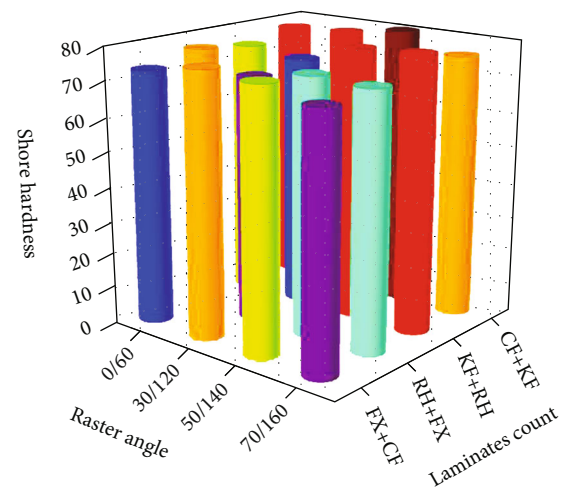

Figure 17: Shore hardness: 3D plot of raster angle and fiber types.

Table 8: Response table for signal to noise ratios (shore hardness).

Level	Fiber types	Laminate count	Infill density (%)	Raster angle
1	32.30	37.52	34.33	37.43
2	37.53	37.54	35.01	37.32
3	34.82	32.55	35.01	32.12
4	37.22	34.27	37.52	35.00
Delta	5.23	4.98	3.19	5.32
Rank	2	3	4	1

Figures 7–10 illustrate the 3D plot for the correlation between two parameters; Figure 7 presents the maximum flexural strength by chicken feather fiber and kenaf fiber relations to 6 counts of laminates [38]. Figure 8 illustrates that the 6 counts of laminates and 60% of infill density registered as excellent flexural strength. Figure 9 presents the 60% of infill density, and 70/120 of raster angle recorded more flexural strength. Figure 10 shows that the 70/120 of

Table 9: Analysis of variance of shore hardness.

Source	DF	Seq SS	Contribution (%)	Adj SS	Adj MS	*F* value	*P* value
Regression	12	6125.7	93.90	6125.7	510.5	3.85	0.147
Fiber types	3	1686.0	25.85	1686.0	562.0	4.24	0.133
Laminate count	3	2022.7	31.01	2022.7	674.2	5.09	0.107
Infill density (%)	3	633.1	9.71	633.1	211.0	1.59	0.356
Raster angle	3	1783.9	27.35	1783.9	594.0	4.49	0.125
Error	3	397.6	6.10	397.6	132.5		
Total	15	6523.3	100				

raster angle and chicken feather fiber and kenaf fiber combination registered as higher flexural strength [39].

Table 5 presented the analysis of variance of flexural strength effectively, among in all four parameters, the fiber type parameter was highly influenced such as 40.50%, followed by raster angle (22.850%), infill density (11.67%), and laminate count (8.54%).

4.2. Shore Hardness. Table 6 presents the summary of shore hardness and S/N ratio of the investigations. Highest shore hardness was found as 78.25 HD by influencing of blend of flax fiber and chicken feather fiber, minimum laminate count such as 2, 90% of infill density, and maximum raster angle (70/160).

Tables 7 and 8 present the response tables for means and S/N ratio of the shore hardness of the composite materials. Among in four parameters, the laminate count was the chief factor to effects in the shore hardness analysis. There parameter effects were analyzed through the rank order; in second rank, the raster angle was contributed'; in third, rank fiber types was influenced; finally, the infill density was involved as fourth rank of the analysis. In shore hardness analysis, the optimum parameters were found to be as mixture of rice husk fiber and flax fiber, laminate count was 4, infill density was 120%. and raster angle was 0/45.

Figures 11 and 12 illustrate the main effect plot for both means and S/N ratio of shore hardness. These plots clearly demonstrated the all four factors and the influences in the response values. From the analysis, the types of fibers, the mixture of flax fiber, and chicken feather fiber registered exceptional shore hardness contrast to remaining mixture of fibers. In the consideration of laminate count parameter, minimum count such as 2 offered better shore hardness. Increasing of laminate count decreases the shore hardness values. Parameter of infill density influences highly, and increasing of infill density raises the shore hardness values. Maximum hardness was obtained by using of 12.5 of infill density. Minimum raster angle parameter such as 0/60 recorded maximum shore hardness, and increasing of raster angle decreases the shore hardness values.

Figure 13 presents the interval plot of shore hardness with effects of all parameters in a single plot. From this plot, the highest shore hardness was noted clearly that the value of maximum shore hardness values reached 80 HD. All parameters were extremely influenced, and the effects were concluded as blending of chicken feather fiber and kenaf fiber, 8 counts of laminates, 30% of infill density, and 50/140 provided extreme value of hardness.

Figures 14–17 demonstrate the 3D plot with the relationship between two parameters, and Figure 14 illustrates that the maximum shore hardness by involvement of chicken feather fiber and kenaf fiber links to 8 counts of laminates. Figure 15 presents the correlations of 8 counts of laminates and 30% of infill density found as excellent shore hardness Figure 16 represents the 30% of infill density, and 50/140 of raster angle offered more shore hardness. Figure 17 shows that the 50/140 of raster angle and chicken feather fiber and kenaf fiber amalgamation recorded superior shore hardness.

Table 9 presents the analysis of variance of shore hardness efficiently; amongst in all four parameters, the laminate count parameter was extremely influenced such as 31.01%, pursued by raster angle (27.35%), fiber types (25.85%), and infill density (9.71%).

5. Conclusion

Biomedical applications such as orthopedic parts were produced by using of biocomposites, namely, flax fiber, chicken feather fiber, kenaf fiber, and rice husk fiber. PLA, polylactic acid polymer, was used as reinforced into the selected natural fibers to improve the flexural strength and shore hardness of the biocomposites. Taguchi optimization was involved to maximize the outcome of this investigation and estimated the optimal parameters. Results of this investigation were summarized as follows:

(i) In the flexural analysis, the maximum flexural strength was recorded as 24.89 MPa. The optimal parameters were attained as combination of chicken feather fiber and kenaf fiber, 6 counts of laminates, 60% of infill density, and 70/120 of raster angle. Mixture of chicken feather fiber and kenaf fiber offered remarkable flexural strength compared to other mixture of fibers. Among in four parameters, the fiber type parameter was extraordinarily influenced such as 40.50%, followed by raster angle (22.850%), infill density (11.67%), and laminate count (8.54%)

(ii) From shore hardness analysis, the highest shore hardness was found as 78.25 HD. The optimum parameters were registered as mixture of rice husk fiber and flax fiber, laminate counts were 4, infill

density was 120%, and raster angle was 0/45. Mixture of flax fiber and chicken feather fiber provided excellent shore hardness compare to remaining mixture of fibers. Amid in four parameters, the laminate count parameter was exceptionally influenced such as 31.01%, followed by raster angle (27.35%), fiber types (25.85%), and infill density (9.71%)

(iii) In the flexural analysis, 60% of infill density and 70/120 of raster angle recorded more flexural strength. Similarly, 70/120 of raster angle and chicken feather fiber and kenaf fiber combination registered as higher flexural strength

(iv) In shore hardness analysis, 8 counts of laminates and 30% of infill density recorded as excellent shore hardness. Similarly, 30% of infill density and 50/140 of raster angle offered more shore hardness. The 50/140 of raster angle and chicken feather fiber and kenaf fiber combination recorded better shore hardness

Data Availability

The data used to support the findings of this study are included in the article. Should further data or information be required, these are available from the corresponding author upon request.

Conflicts of Interest

The authors declare that there are no conflicts of interest regarding the publication of this paper.

Acknowledgments

The authors appreciate the technical assistance to complete this experimental work from Jimma Institute of Technology, Jimma University, Ethiopia. The authors thank Saveetha School of Engineering-Chennai for the support of technical assistance to complete this experimental work and also draft writing.

References

[1] A. Bedjaoui, A. Belaadi, S. Amroune, and B. Madi, "Impact of surface treatment of flax fibers on tensile mechanical properties accompanied by a statistical study," *International Journal of Integrated Engineering*, vol. 11, no. 6, pp. 10–17, 2019.

[2] C. Ao, Y. Niu, X. Zhang, X. He, W. Zhang, and C. Lu, "Fabrication and characterization of electrospun cellulose/nano-hydroxyapatite nanofibers for bone tissue engineering," *International Journal of Biological Macromolecules*, vol. 97, pp. 568–573, 2017.

[3] P. Basu, N. Saha, R. Alexandrova et al., "Biocompatibility and biological efficiency of inorganic calcium filled bacterial cellulose-based hydrogel scaffolds for bone bioengineering," *International Journal of Molecular Sciences*, vol. 19, no. 12, p. 3980, 2018.

[4] L. Peponi, V. Sessini, M. P. Arrieta et al., "Thermally-activated shape memory effect on biodegradable nanocomposites based on PLA/PCL blend reinforced with hydroxyapatite," *Polymer Degradation and Stability*, vol. 151, pp. 36–51, 2018.

[5] A. Belaadi, S. Amroune, and M. Bourchak, "Effect of eco-friendly chemical sodium bicarbonate treatment on the mechanical properties of flax fibres: Weibull statistics," *The International Journal of Advanced Manufacturing Technology*, vol. 106, no. 5-6, pp. 1753–1774, 2020.

[6] M. K. Gupta, M. Ramesh, and S. Thomas, "Effect of hybridization on properties of natural and synthetic fiber-reinforced polymer composites (2001–2020): a review," *Polymer Composites*, vol. 42, no. 10, pp. 4981–5010, 2021.

[7] C. Deepa and M. Ramesh, *Biocomposites for prosthesis, green biocomposites for biomedical engineering*, Elsevier, 2021.

[8] M. Ramesh and C. Deepa, *Biocomposites for Biomedical Devices, Green Biocomposites for Biomedical Engineering*, Elsevier, 2021.

[9] P. Dwivedi, P. K. Mishra, M. K. Mondal, and N. Srivastava, "Non-biodegradable polymeric waste pyrolysis for energy recovery," *Heliyon*, vol. 5, no. 8, article e02198, 2019.

[10] N. Banik, "An experimental effort on the impact of hot press forming process parameters on tensile, flexural & impact properties of bamboo fiber composites with the help of Taguchi experimental design," *Materials Today: Proceedings*, vol. 5, no. 9, pp. 20210–20216, 2018.

[11] A. Canas-Gutierrez, M. Osorio, C. Molina-Ramirez, D. Arboleda-Toro, and C. Castro-Herazo, "Bacterial cellulose: a biomaterial with high potential in dental and oral applications," *Cellulose*, vol. 27, no. 17, pp. 9737–9754, 2020.

[12] H. S. Kim and S. H. Chang, "Simulation of compression moulding process for long-fibre reinforced thermoset composites considering fibre bending," *Composite Structures*, vol. 230, article 111514, 2019.

[13] P. Anand, D. Rajesh, M. Senthil Kumar, and I. Saran Raj, "Investigations on the performances of treated jute/Kenaf hybrid natural fiber reinforced epoxy composite," *Journal of Polymer Research*, vol. 25, no. 4, pp. 1–9, 2018.

[14] A. L. Inácio, R. C. Nonato, and B. C. Bonse, "Mechanical and thermal behavior of aged composites of recycled PP/EPDM/talc reinforced with bamboo fiber," *Polymer Testing*, vol. 72, pp. 357–363, 2018.

[15] R. Kumar, M. I. Ul Haq, A. Raina, and A. Anand, "Industrial applications of natural fibre-reinforced polymer composites–challenges and opportunities," *International Journal of Sustainable Engineering*, vol. 12, no. 3, pp. 212–220, 2019.

[16] M. Yunus and M. S. Alsoufi, "Experimental investigations into the mechanical, tribological, and corrosion properties of hybrid polymer matrix composites comprising ceramic reinforcement for biomedical applications," *International Journal of Biomaterials*, vol. 2018, Article ID 9283291, 8 pages, 2018.

[17] M. Kavitha, V. M. Manickavasagam, T. Sathish et al., "Parameters optimization of dissimilar friction stir welding for AA7079 and AA8050 through RSM," *Advances in Materials Science and Engineering*, vol. 2021, Article ID 9723699, 8 pages, 2021.

[18] S. Jayaprakash, S. Siva Chandran, T. Sathish et al., "Effect of tool profile influence in dissimilar friction stir welding of aluminium alloys (AA5083 and AA7068)," *Advances in Materials Science and Engineering*, vol. 2021, Article ID 7387296, 7 pages, 2021.

[19] M. Ponnusamy, B. P. Pulla, T. Sathish et al., "Mechanical strength and fatigue fracture analysis on Al-Zn-Mg alloy with

the influence of creep aging process," *Advances in Materials Science and Engineering*, vol. 2021, Article ID 1899128, 5 pages, 2021.

[20] V. Vijayan, A. Parthiban, T. Sathish et al., "Optimization of reinforced aluminium scraps from the automobile bumpers with nickel and magnesium Oxide in stir casting," *Advances in Materials Science and Engineering*, vol. 2021, Article ID 3735438, 10 pages, 2021.

[21] N. Sezer, Z. Evis, S. M. Kayhan, A. Tahmasebifar, and M. Koç, "Review of magnesium-based biomaterials and their applications," *Journal of Magnesium and Alloys*, vol. 6, no. 1, pp. 23–43, 2018.

[22] T. Sathish, D. Chandramohan, S. Dinesh Kumar, S. Rajkumar, and V. Vijayan, "A facile synthesis of Ag/ZnO nanocomposites prepared via novel green mediated route for catalytic activity," *Applied Physics A*, vol. 127, no. 9, pp. 1–9, 2021.

[23] T. Sathish, N. Sabarirajan, and R. Saravanan, "Nano-alumina reinforcement on AA 8079 acquired from waste aluminium food containers for altering microhardness and wear resistance," *Journal of Materials Research and Technology*, vol. 14, pp. 1494–1503, 2021.

[24] B. Fiani, R. Jarrah, J. Shields, and M. Sekhon, "Enhanced biomaterials: systematic review of alternatives to supplement spine fusion including silicon nitride, bioactive glass, amino peptide bone graft, and tantalum," *Journal of Neurosurgery*, vol. 50, no. 6, 2021.

[25] T. V. Shah and D. V. Vasava, "A glimpse of biodegradable polymers and their biomedical applications," *E-Polymers*, vol. 19, no. 1, pp. 385–410, 2019.

[26] T. Sarkar, P. Nayak, and R. Chakraborty, "Storage study of mango leather in sustainable packaging condition," *Materials Today: Proceedings*, vol. 22, pp. 2001–2007, 2020.

[27] V. Dhinakaran, M. D. Vijayakumar, G. Muthu, T. Sathish, and P. M. Bupathi ram, "Experimental investigation of hybrid fibre reinforced polymer composite material and its microstructure properties," *Materials Today: Proceedings*, vol. 37, pp. 1799–1803, 2021.

[28] S. Clifton, B. H. S. Thimmappa, R. Selvam, and B. Shivamurthy, "Polymer nanocomposites for high-velocity impact applications-a review," *Composites Communications*, vol. 17, pp. 72–86, 2020.

[29] Z. Li, A. R. Shah, M. N. Prabhakar, and J. I. Song, "Effect of inorganic fillers and ammonium polyphosphate on the flammability, thermal stability, and mechanical properties of abaca-fabric/vinyl ester composites," *Fibers and Polymers*, vol. 18, no. 3, pp. 555–562, 2017.

[30] M. A. Paglicawan, M. P. Rodriguez, and J. R. Celorico, "Thermomechanical properties of woven abaca fiber reinforced nanocomposites," *Polymer Composites*, vol. 41, no. 5, pp. 1763–1773, 2020.

[31] M. Sood and G. Dwivedi, "Effect of fiber treatment on flexural properties of natural fiber reinforced composites: a review," *Egyptian Journal of Petroleum*, vol. 27, no. 4, pp. 775–783, 2018.

[32] T. Sathish, "Checking the mechanical properties of Ananas comosus leaf fiber reinforced polymer composite material," *International Journal of Pure and Applied Mathematics*, vol. 116, no. 24, pp. 243–253, 2017.

[33] A. Bourmaud, J. Beaugrand, D. U. Shah, V. Placet, and C. Baley, "Towards the design of high-performance plant fibre composites," *Progress in Materials Science*, vol. 97, pp. 347–408, 2018.

[34] R. A. J. Malenab, J. P. S. Ngo, and M. A. B. Promentilla, "Chemical treatment of waste abaca for natural fiber-reinforced geopolymer composite," *Materials*, vol. 10, no. 6, p. 579, 2017.

[35] T. Sathish, N. Sabarirajan, and S. Karthick, "Machining parameters optimization of aluminium alloy 6063 with reinforcement of sic composites," *Materials Today Proceedings*, vol. 33, pp. 2559–2563, 2020.

[36] M. Asim, M. T. Paridah, M. Chandrasekar et al., "Thermal stability of natural fibers and their polymer composites," *Iranian Polymer Journal*, vol. 29, no. 7, pp. 625–648, 2020.

[37] A. K. Sinha, S. Bhattacharya, and H. K. Narang, "Experimental determination and modelling of the mechanical properties of hybrid abaca-reinforced polymer composite using RSM," *Polymers and Polymer Composites*, vol. 27, no. 9, pp. 597–608, 2019.

[38] T. Sathish, "Experimental investigation of machined hole and optimization of machining parameters using electrochemical machining," *Journal of Materials Research and Technology*, vol. 8, no. 5, pp. 4354–4363, 2019.

[39] T. Sathish and N. Sabarirajan, "Synthesis and optimization of AA 7175–zirconium carbide (ZrC) composites machining parameters," *Journal of New Materials for Electrochemical Systems*, vol. 24, no. 1, pp. 34–37, 2021.

Hindawi
International Journal of Polymer Science
Volume 2021, Article ID 5682182, 12 pages
https://doi.org/10.1155/2021/5682182

Research Article

Improved Antibacterial Activity of Water-Soluble Nanoformulated Kaempferol and Combretastatin Polyphenolic Compounds

Y. Santhosh Kumar,[1] Langeswaran Kulanthaivel,[2] G. S. Hikku,[1] R. Saravanan,[1] Thangavelu Lakshmi,[3] C. Kirubhanand,[4] Murugesan Karthikeyan,[5] P. Vijayalakshmi,[6] and Gowtham Kumar Subbaraj[1]

[1]*Faculty of Allied Health Sciences, Chettinad Hospital and Research Institute, Chettinad Academy of Research and Education (Deemed to be University), Kelambakkam, 603 103 Tamil Nadu, India*
[2]*Molecular Oncology Lab, Department of Bioinformatics, Alagappa University, Karaikudi, 630 001 Tamil Nadu, India*
[3]*Department of Pharmacology, Saveetha Dental College and Hospital, Saveetha Institute of Medical and Technical Sciences (Deemed to be University), Chennai, India*
[4]*Department of Anatomy, All India Institute of Medical Sciences, Nagpur, Maharashtra 441108, India*
[5]*Department of Microbiology, Faculty of Medicine, Quest International University, Malaysia*
[6]*Department of Pharmacology, Asan Memorial Dental College and Hospital, Chengalpattu, Chennai, 603105 Tamil Nadu, India*

Correspondence should be addressed to Gowtham Kumar Subbaraj; gowtham_phd@yahoo.com

Received 29 June 2021; Revised 29 September 2021; Accepted 4 October 2021; Published 27 October 2021

Academic Editor: Bernabé L. Rivas

Kaempferol and combretastatin are polyphenolic compounds derived from plant sources which are known for their antibacterial activity. However, owing to their large size and water insolubility, their antibacterial activity is limited. In this context, the present study focused on the nanoformulation of kaempferol (NF-k) and combretastatin (NF-c) and their influence on water solubility and antibacterial properties. The NF-k and NF-c were prepared using the solvent evaporation method and were thoroughly characterized for evaluating the morphology, molecular vibrations, size, etc. Based on the results, it is observed that the pristine forms of kaempferol and combretastatin drugs get nanoformulated and completely soluble in water. Using particle size analyzer, the particle sizes of NF-k and NF-c were estimated as 334 nm and 260 nm, respectively, which are very fine compared to pristine kaempferol and combretastatin (5193 nm and 1217 nm, respectively). The molecular vibrations that exist in NF-k and NF-c were confirmed by the Fourier transform infrared spectra, where the nanoformulated drug showed lower intensities than the pristine form of kaempferol and combretastatin. The drug release kinetics of the nanoformulated drugs were carried out using the dialysis membrane method and were compared with their pristine forms. Owing to the size effect, the NF-k and NF-c release up to 50% of the drug in a sustained manner till 50 h showing twofold higher concentration than the control where it released 25%. The antibacterial activity was assessed by measuring the optical density at 600 nm using UV-vis spectrophotometer and displayed significant activity against gram-positive *Staphylococcus aureus* strain. The mechanisms behind the antibacterial activity of NF-k and NF-c were discussed in detail. The activation of ATP-dependent efflux pump system and the blockage of porin channels could be the cause for the bactericidal activity. Our understanding of efflux pumps and their role in antibacterial activity is still in its early stages. No studies have been performed to date using nanoformulations of kaempferol and combretastatin to investigate their roles. This complicates the determination of the exact mechanisms acting against bacterial growth when using nanoformulation drugs. Our increasing knowledge of water-soluble nanoformulation drugs and their roles in reduced bacterial activity will pave the way to developing effective treatments in the future.

1. Introduction

Bacterial diseases are an essential reason for persistent and infectious lethality. Antibiotics seem to be the preferential treatment strategy for bacterial diseases in the interest of their low-cost adequacy and incredible results. Nevertheless, a few investigations have given absolute proof that the inescapable utilization of antibiotic agents has prompted the development of multidrug-resistant bacterial strains. Previous findings have revealed that *Enterobacteriaceae* microbes express a resistance gene known as NDM-1 [1]. A significant group of antibiotics used have limited focus on translational machinery, DNA replication machinery, and cell wall synthesis. Unfortunately, microbial resistance can be created against any one of these methods of activity. The mechanism of microbial resistance comprises the expression of enzymes that change or else corrupt antibiotics, such as aminoglycosides and β-lactamase [2], alterations of cell components, like the ribosomes in tetracycline resistance, cell wall in vancomycin resistance [3], and articulation of efflux pumps, which give synchronous resistance opposing to different antibiotics [4]. To counteract multidrug resistance developed by the bacterial strains, nanoparticles are employed. However, the use of nanoparticles is inappropriate due to their method of action. The indirect contact with the bacterial cell wall facilitates antibacterial activity rather than infiltrating into the cell, which declines its commercial viability. In this context, more attention has been focused on developing novel and exhilarant nanoparticles with antibacterial activity.

Kaempferol is a flavonoid present in many vegetables, fruits, and herbs, including grapes, tomatoes, grapes, tea, and broccoli [5]. Kaempferol shows several biological activities, including antioxidant, anti-inflammatory, antimicrobial, antidiabetic, and anticarcinogenic [6–10]. Combretastatin A4 is a natural stilbenoid phenol derived from South African bushwillow (*Combretum caffrum*). Combretum species have antitumor and antimicrobial activities [11, 12]. They are extensively used to treat syphilis, abdominal pains, conjunctivitis, diarrhea, toothache, peptic ulcer, dysentery, jaundice, skin, heart, and cancer diseases [13]. However, very few studies have been reported on the antibacterial activity of nanoformulated kaempferol and combretastatin. Hence, the present research is aimed at formulating the kaempferol and combretastatin in nano regime and studying their structural, drug release kinetics, and antibacterial activity against gram-positive bacteria.

2. Materials and Methods

2.1. Materials Required. Kaempferol (≥97.0% pure), combretastatin (≥97.0% pure), and sodium dodecyl sulfate were obtained from Sigma-Aldrich. Ethanol (99% pure) was purchased from Changshu Chemicals Co., Ltd., and Luria-Bertani broth was purchased from HiMedia. N-Hexane (95% pure) and dimethyl sulphoxide (DMSO, 99% pure) were purchased from SRL laboratories Pvt. Ltd. *Staphylococcus aureus* was obtained from the research collection at Chettinad Hospital and Research Institute.

2.2. Nanoformulation of Kaempferol (NF-k). The kaempferol was nanoformulated using the solvent evaporation method (Figure 1) [14]. Briefly, kaempferol was dissolved in ethanol to achieve a final concentration of 5 mg/ml. To the above solution, a known quantity of 0.2% sodium dodecyl sulfate solution (SDS) was added and stirred. Under constant stirring, hexane (antisolvent) was added to the mixture where the ratio of solvent and antisolvent was maintained at 1 : 20. Then, the mixture was continuously stirred for 3 h at 150 rpm and held at 30°C overnight. After complete evaporation of the solvent, the powder formed was crushed. It was subjected to various physiochemical characterization studies to determine the morphology, size, and molecular vibrations in NF-k.

2.3. Nanoformulation of Combretastatin (NF-c). The combretastatin was also nanoformulated using the same solvent (Figure 2) evaporation method. Briefly, in ethanol, 5 mg/ml concentration of combretastatin was dissolved, and to this solution, 0.2% SDS was added. Under constant stirring, hexane (antisolvent) was added in a dropwise manner maintaining the ratio of solvent and antisolvent as 1 : 20. The mixture was continuously stirred for 3 h at 150 rpm and kept at 30°C overnight. After evaporating the solvent, the powder formed was crushed by mortar and pestle and subjected to various physiochemical characterization processes.

2.4. Characterization Techniques. Particle size distributions of the NF-k and NF-c were determined using the dynamic light scattering (DLS) technique (Malvern Zetasizer, USA). The particle size distributions of the nanoformulated drugs were recorded by dissolving 100 μl of prepared nanoformulation into 900 μl of solvent. To elucidate the molecular vibrations that exist in the pristine and nanoformulated drugs, fourier transform infrared (FTIR) spectroscopy was used with attenuated total reflection mode. Adequate quantity of sample was placed on the crystal surface, and the spectra of NF-k and NF-c were recorded in the range 4000 cm^{-1}–500 cm^{-1} (Model BRUKER-ALPHA, Germany) using OPUS software. FTIR spectroscopy characterizes the characteristic functional groups present in the test samples originated from the different molecular bonds unique vibration and rotational energies. The morphology and size of the nanoformulated drugs were analyzed using scanning electron microscopic (SEM) images (HITACHI SU3500, Japan).

2.5. Solubility Test. The kaempferol and combretastatin both were insoluble in water in their pristine form. After nanoformulation, both drugs become water-soluble and were validated through the solubility test using Milli-Q water. Solubility test was performed by suspending 1 mg of NF-k and NF-c in 10 ml of Milli-Q water and compared with its pristine counterpart.

2.6. Drug Release Kinetic Assay. The drug release kinetic assays were carried out for NF-k and NF-c using the dialysis membrane method. Separately, the NF-k and NF-c were suspended in water. In contrast, the kaempferol and combretastatin were suspended in DMSO (as they are insoluble in water), placed in the dialysis membrane, and immersed

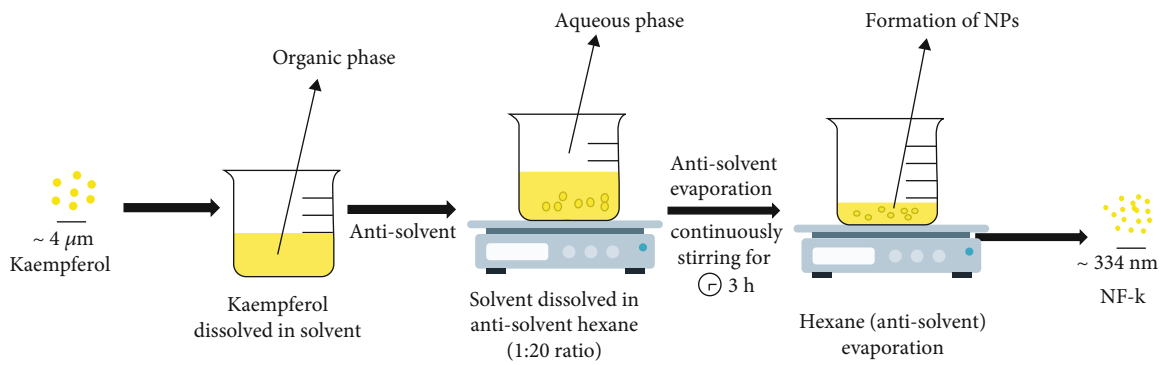

Figure 1: Schematic representation of synthesis of NF-k.

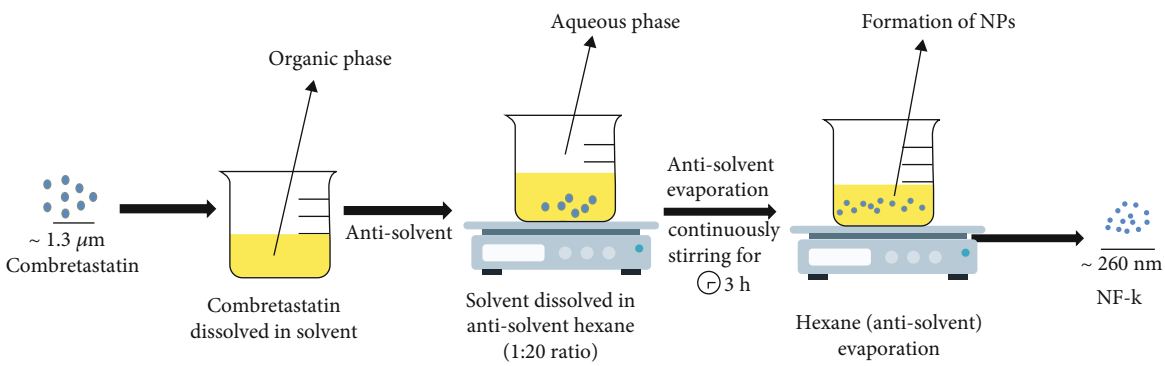

Figure 2: Schematic representation of synthesis of NF-c.

in a beaker containing 100 ml of phosphate-buffered saline (PBS). The beaker was kept on a magnetic stirrer at a speed of 250 rpm. In specified time intervals, an appropriate quantity of the samples were withdrawn from the beaker (replaced by fresh PBS medium). It was analyzed using a UV-vis spectrophotometer at 373 nm for kaempferol [15] and 289 nm for combretastatin [16]. The improvement in the absorption value was directly influenced by the quantity of drug released to the PBS solution.

2.7. Antimicrobial Activity. The antibacterial activity of NF-k and NF-c against gram-positive *Staphylococcus aureus* was assessed using UV-vis spectrophotometer. 10 ml of an overnight culture of *Staphylococcus aureus* strain was prepared. Afterward, to the 5 ml of LB broth, 0.3 ml of overnight culture was added. To the above bacterial culture, different concentrations (5 μl, 10 μl, 20 μl, 50 μl, and 100 μl) of NF-k and NF-c were added and incubated for 24 h, 48 h, and 72 h at 37°C. After the incubation period, the optical density (OD) measurements were recorded at 600 nm. The experiments were performed in triplicate, and the statistical analysis was carried out using Excel. SEM images were recorded to assess the morphology of *Staphylococcus aureus* before and after treatment with nanoformulated drugs. The NF-k and NF-c were mixed with the culture of *Staphylococcus aureus* separately and were incubated overnight at 37°C. After incubation, the samples were centrifuged, and the pellet was collected and washed thrice with PBS. After PBS wash, the samples were fixed with 2.5% glutaraldehyde solution for 2 h. Finally, samples were dropped on a sterile coverslip and air-dried at room temperature. All samples were coated with gold before recording the microscopic images.

3. Results

The kaempferol and combretastatin phytochemicals were nanoformulated through the solvent evaporation method and are subjected to various studies. The solubility of NF-k and NF-c prepared through the solvent evaporation method was evaluated by dispersing it in Milli-Q water. When nanoformulated drugs were added to the water, they were easily distributed, ensuring a hydrophilic nature (Figure 3(a)). In contrast, when pristine kaempferol and combretastatin were added to water, the drugs are found insoluble. They were floating over the surface of the water, validating the hydrophobic nature of the drug (Figure 3(b)). Therefore, it was substantiated that the nanoformulation converts the wetting behavior of the drug from hydrophobic to hydrophilic in nature.

To confirm the nano regime of prepared NF-k and NF-c compared to the micron-sized pristine drugs, DLS measurements were recorded. The nanoformulated drugs were ultrasonicated for 1 h before recording DLS measurement. The average particle size distributions of control kaempferol and NF-k were found as 5193 nm and 334.3 nm, respectively, having a polydispersity index (PDI) of 0.497 (kaempferol) and 0.207 (NF-k) (Figures 4(a) and 4(b)). Likewise, the particle size distributions of control combretastatin and NF-c were

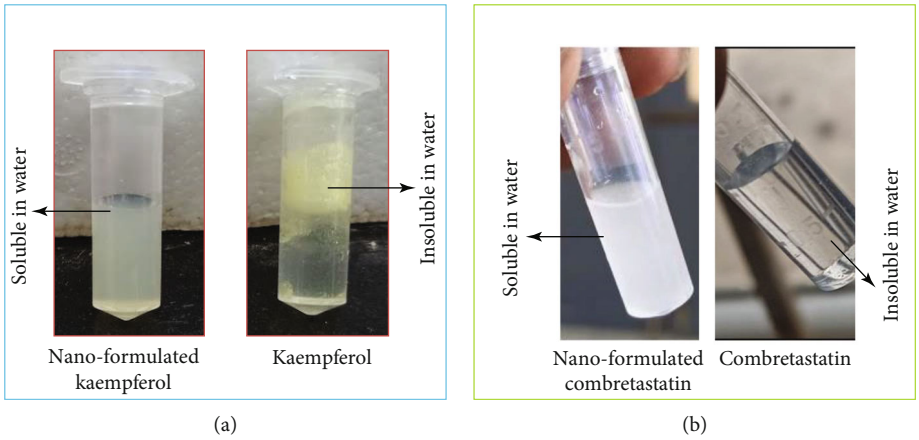

(a) (b)

Figure 3: Photographs of drugs suspended in Milli-Q water. (a) Kaempferol and NF-k. (b) Combretastatin and NF-c.

1217 nm and 260.5 nm, respectively, with PDI 0.503 and 0.125 (Figures 4(c) and 4(d)). The obtained results showed that the particle size of the drugs reduced significantly with nanoformulation and have lower PDI below 0.25.

The FTIR spectra of the pristine kaempferol and synthesized NF-k were shown in Figure 5(a). The spectrum of pristine kaempferol exhibited bands at 3314 cm^{-1} and 3420 cm^{-1}, confirming the presence of the O-H stretch. The aromatic groups and C-O, C-H, C=C, and C=O were observed at 818 cm^{-1}, 1177 cm^{-1}, 1381 cm^{-1}, 1607 cm^{-1}, and 1666 cm^{-1}, respectively. The FTIR spectrum of NF-k also shows similar peaks at 822 cm^{-1}, 1177 cm^{-1}, 1381 cm^{-1}, 1615 cm^{-1}, and 1661 cm^{-1} ascribed to the aromatic groups and C-O, C-H, C=C, and C=O functional groups, respectively. Even though similar bands were observed in the spectrum of both pure kaempferol and NF-k, the transmittance intensity originated from NF-k was lower than the pristine form. This phenomenon was due to the presence of amorphous constituents in the prepared NF-k [17]. The presence of amorphous constituents improves the solubility of the drug in water than pristine kaempferol [18]. Moreover, the peaks obtained at 2918 cm^{-1} and 2851 cm^{-1} ascribed to C-H stretching vibration originated from the long-chain C of SDS substantiate that the SDS molecules were sorbed with kaempferol while nanoformulation [19].

The FTIR spectra of the pristine combretastatin and synthesized NF-c were shown in Figure 5(b). Likewise, the FTIR spectrum of control combretastatin exhibits a band at transmission peak 3510 cm^{-1}, representing the O-H stretch. C=C, C-H, and C-O were also observed at 1584 cm^{-1}, 1329 cm^{-1}, and 1125 cm^{-1}, respectively. The NF-c also showed similar peaks at 3509 cm^{-1}, 1580 cm^{-1}, 1329 cm^{-1}, and 1125 cm^{-1}, corresponding to O-H, C=C, C-H, and C-O, respectively, with lesser intensity. Here also, the reduction in peak intensity indicates an amorphous structure, which improves the solubility and dissolution rate of NF-c than pristine combretastatin. As with NF-k, NF-c possesses peaks at 2918 cm^{-1} and 2849 cm^{-1} originated from the C-H stretching of SDS that was sorbed along with NF-c during the preparation process.

The particle size and morphology of the NF-k and NF-c were assessed through SEM micrographs (Figures 6(a) and 6(b)). From the SEM image, it was inferred that the size of the NF-k was ranged within ~270 nm with spherical-shaped structures, whereas NF-c also shows near-spherical-shaped structures with a size range within ~250 nm. The nanoformulated drugs have a certain degree of monodispersity, which is an important prerequisite for drug development.

The drug release kinetics assay for the pristine and nanoformulated drugs was performed to elucidate the superiority of the nanoformulated drugs over pristine drugs (Figures 7(a) and 7(b)). The obtained results displayed a whopping 52% release of NF-k drug in 50 h, whereas the kaempferol releases only 25%. Likewise, 47% NF-c was released in 50 h, whereas combretastatin releases only 24% of the drug. From the results, it was inferred that the nanoformulated drugs release more of their constituent molecules than their pristine forms. Further, the drug release kinetic of NF-k was better than NF-c.

The antibacterial activity of NF-k and NF-c at different concentrations was assessed by recording the OD value at 600 nm against gram-positive *Streptococcus aureus* and was compared with the control (without drug). At concentrations 5 μl, 10 μl, 20 μl, 50 μl, and 100 μl, NF-k displays OD values as 0.4, 0.39, 0.38, 0.32, and 0.25, respectively, and NF-c displays OD values as 0.49, 0.47, 0.43, 0.45, and 0.36, respectively, after 24 h of incubation, whereas the control shows OD value of 0.52. Likewise, after 72 h, NF-k and NF-c display OD values of 0.3 and 0.45 for 5 μl concentration and OD values of 0.24 and 0.35 for 100 μl concentration (Figures 8(a) and 8(b)). The obtained results substantiated that the NF-k and NF-c displayed prominent antibacterial activity showing a considerable reduction in the OD value attributed to the inhibition in bacterial growth.

The SEM micrographs of the bacterial cells were recorded before and after treating with nanoformulated drugs and were shown as Figures 9(a)–9(c). From the micrographs of the control specimen, it was clear that the *Staphylococcus aureus* with spherical morphology having a high degree of growth (Figure 9(a)). However, after treating with nanoformulated drugs, the bacterial population was found to be declined ascribed to the antibacterial activity of the nanoformulated phytochemicals (Figures 9(a) and 9(b)).

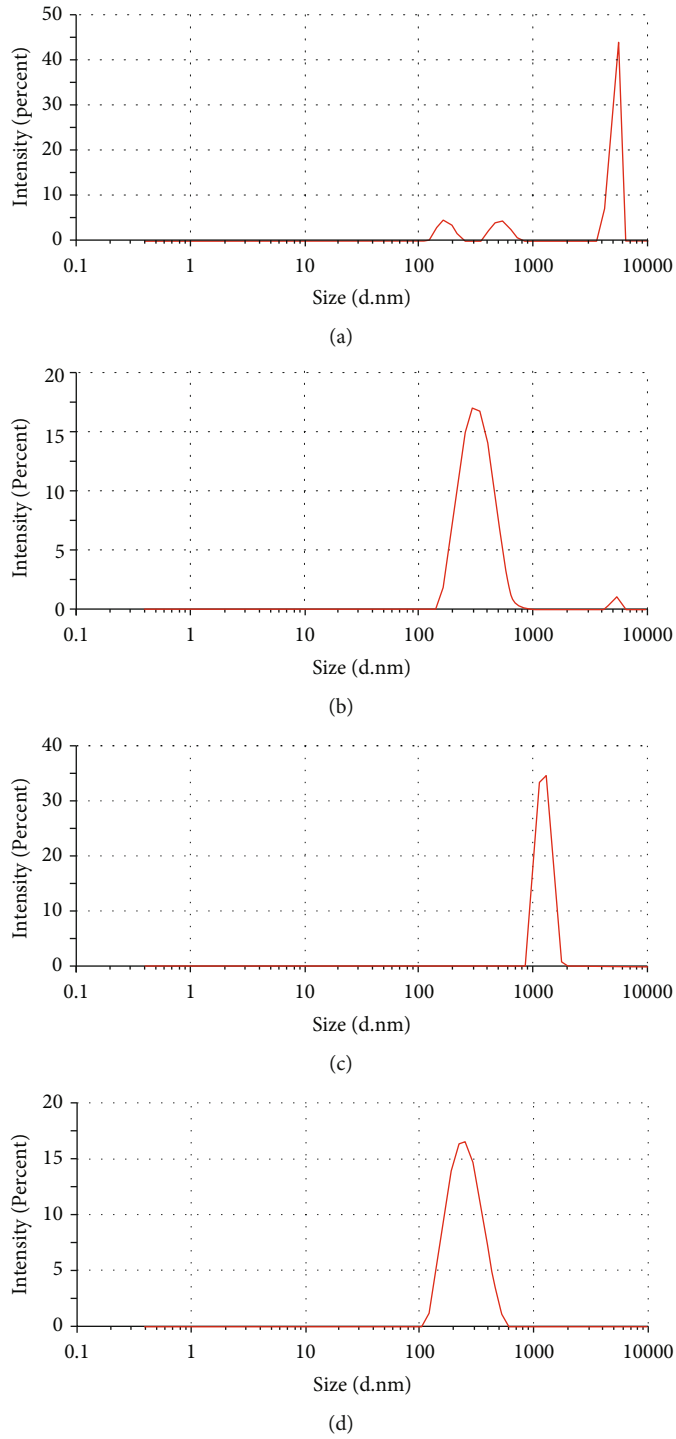

Figure 4: DLS measurements of (a) kaempferol, (b) NF-k, (c) combretastatin, and (d) NF-c.

4. Discussion

Both the kaempferol and combretastatin were insoluble in water [17] and were soluble in organic solvents like DMSO and ethanol. However, it has been reported that the poorly aqueous soluble drugs displayed better solubility through nanoformulation [18, 19]. Bhawana et al. [20] improved the solubility of the curcumin in water through nanoformulation that has more effective antibacterial activity than the curcumin suspended in DMSO. The improved activity was due to the reduction in particle size. The size was 40 nm for nanoformulated curcumin, which was much lower than the curcumin dissolved in DMSO, showing 800 nm. A 20-fold decline in the particle size resulted in improved diffusion and higher uptake by the cells, leading to better antibacterial efficacy of the nanoformulated drug.

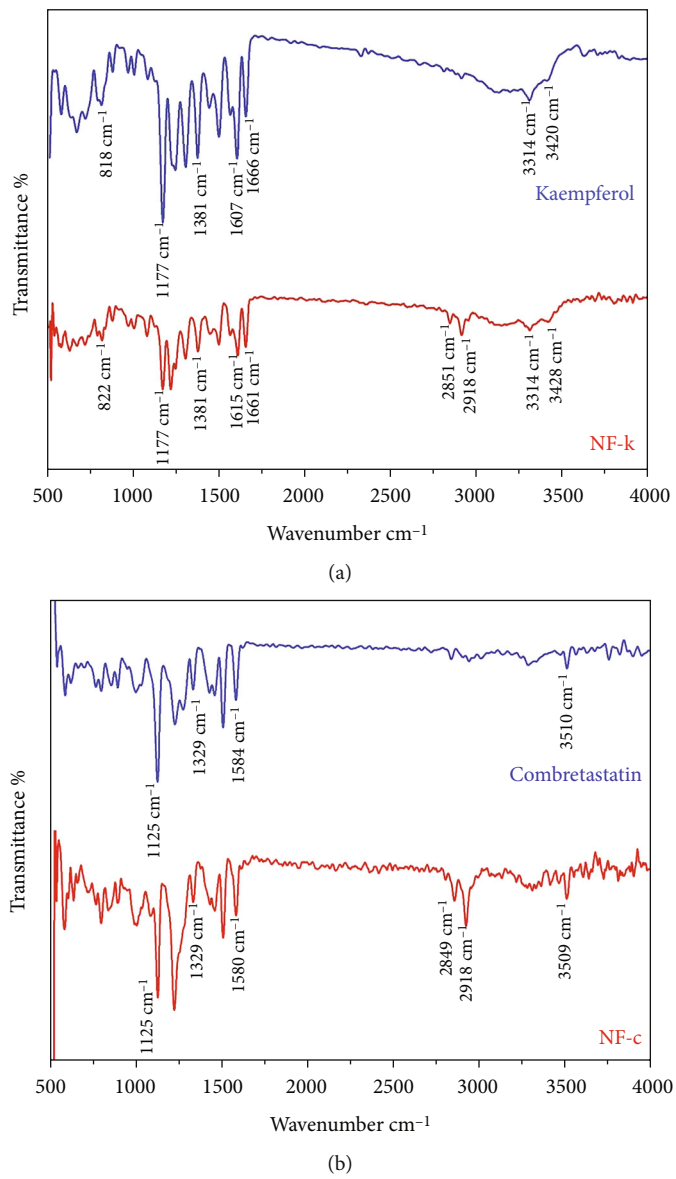

Figure 5: FTIR spectra of (a) kaempferol and NF-k and (b) combretastatin and NF-c.

Qian et al. [17] improved the bioavailability of kaempferol by 2.92 times that of pristine kaempferol through the preparation of nanosuspension. In the present study, the size of kaempferol and combretastatin wasreduced significantly through the solvent evaporation technique. From the obtained results, it was cleared that the sizes of kaempferol and combretastatin show ~15-fold and ~5-fold reduction, respectively, while nanoformulation. In the present work, the nanoformulated drugs displayed better solubility in water than their pristine forms.

As the particle size reduces, the surface energy increases, leading to the higher wetting ability of the nanoformulated drugs in the aqueous medium resulting in better solubility.

The solvent evaporation technique facilitates the formulation of drugs in a nanoregime compared to other literature techniques. Qian et al. [17] nanoformulated kaempferol through high-pressure homogenization and reduced the particle size from 1737 nm to 424 nm. Likewise, Zhao et al. [21] prepared the combretastatin nanoparticles. They reported the particle size of combretastatin nanoparticles which is 153 nm in diameter. Zhang et al. [22] formulated the combretastatin nanoparticles and noted the size of 55 nm in diameter. Shen et al. [16] prepared the PLGA-loaded combretastatin nanoparticles using the nanoprecipitation method and found that the size reduced to 208 nm. Therefore, the solubility of NF-k and NF-c in an aqueous medium can be attributed to its nanosized regime prepared through solvent precipitation technique, where SDS was used as an ionic stabilizer. Further, the PDIs of both NF-k and NF-c were less than 0.25, substantiating that the particles were uniformly distributed, which validates the solvent evaporation technique [23].

FTIR analysis was carried out to elucidate whether kaempferol and combretastatin's molecular structure has

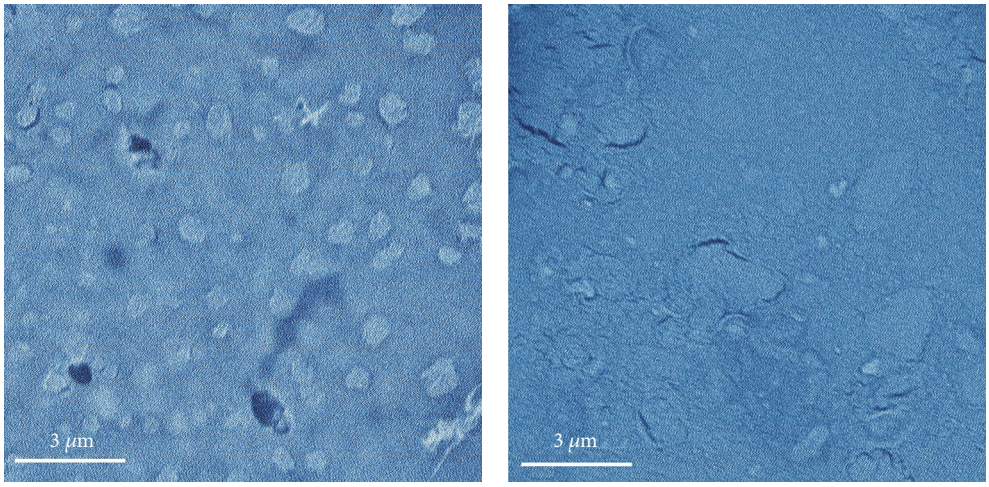

(a) (b)

Figure 6: SEM images of (a) NF-k and (b) NF-c.

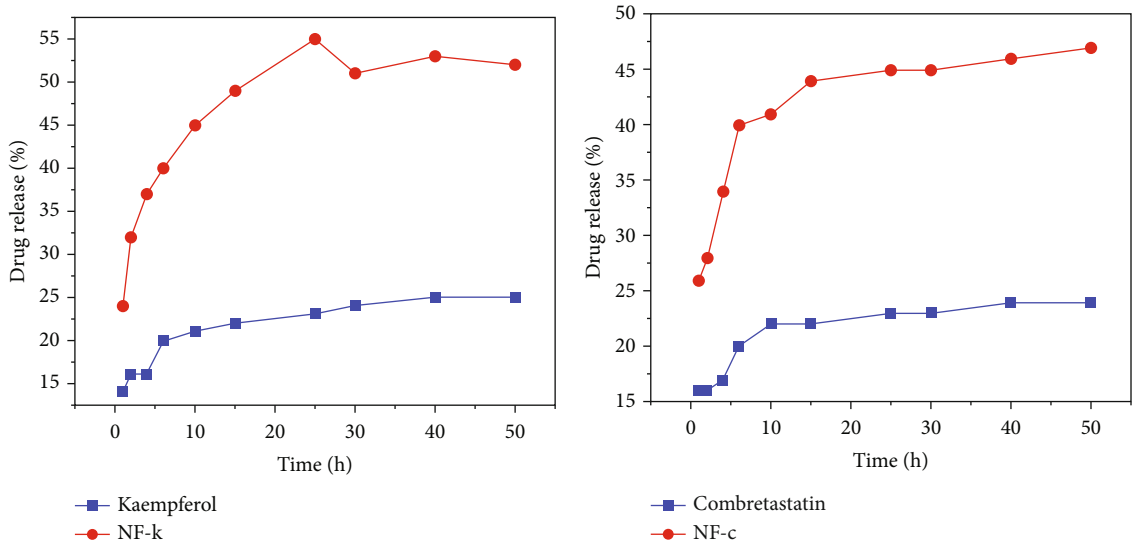

(a) (b)

Figure 7: Drug release kinetics of (a) NF-k and kaempferol and (b) NF-c and combretastatin.

changed while nanoformulation. Previously, few investigations were reported on the FTIR results of NF-k. Qian et al. [17] reported the FTIR characterization of pure kaempferol and NF-k. The results showed lower intensities and no major shifts in the FTIR peaks of NF-k compared with pure kaempferol. Telange et al. [24] reported the FTIR characterization of pure kaempferol and kaempferol-phospholipid complex. The results showed that the interaction of kaempferol with phospholipid showed novel peaks when compared to pure kaempferol. The present study results can be agreed with the earlier reports. There are no studies reported on the FTIR spectra of NF-c and combretastatin.

From Figure 3, it was clear that the FTIR of NF-k and NF-c showed peaks the same as that of their pristine forms, substantiating that the kaempferol and combretastatin molecules present in NF-k and NF-c do not lose their functional groups. Further, the intensities of the peaks werefound to be decreased with nanoformulation, which validates the formation of nanosized particles. Moreover, after nanoformulation, extra peaks emerged from the SDS molecules sorbed along with NF-k and NF-c. SDS presence also improves the solubility of the nanoformulated drug in water through its hydrophilic tail. Therefore, it is understood that the solubility of NF-k and NF-c is because of the nanosized effect and the presence of SDS molecules.

The particle size and morphology of NF-k and NF-c were determined from the SEM images. As seen in the previous literature data, the NF-k and NF-c have spherical-shaped structures [15, 25]. This may be due to the presence of SDS molecules where it may facilitate the formation of micelles while the drug may be encapsulated within the hydrophobic compartment. Similar spherical-shaped structures were

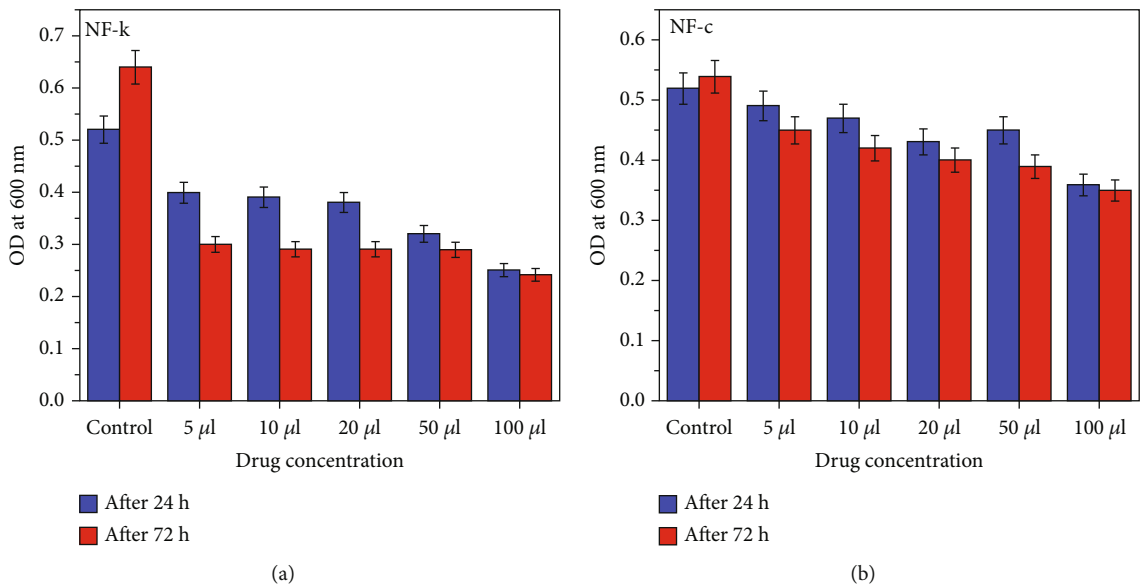

Figure 8: Antibacterial activity of (a) NF-k and (b) NF-c assessed through optical density values.

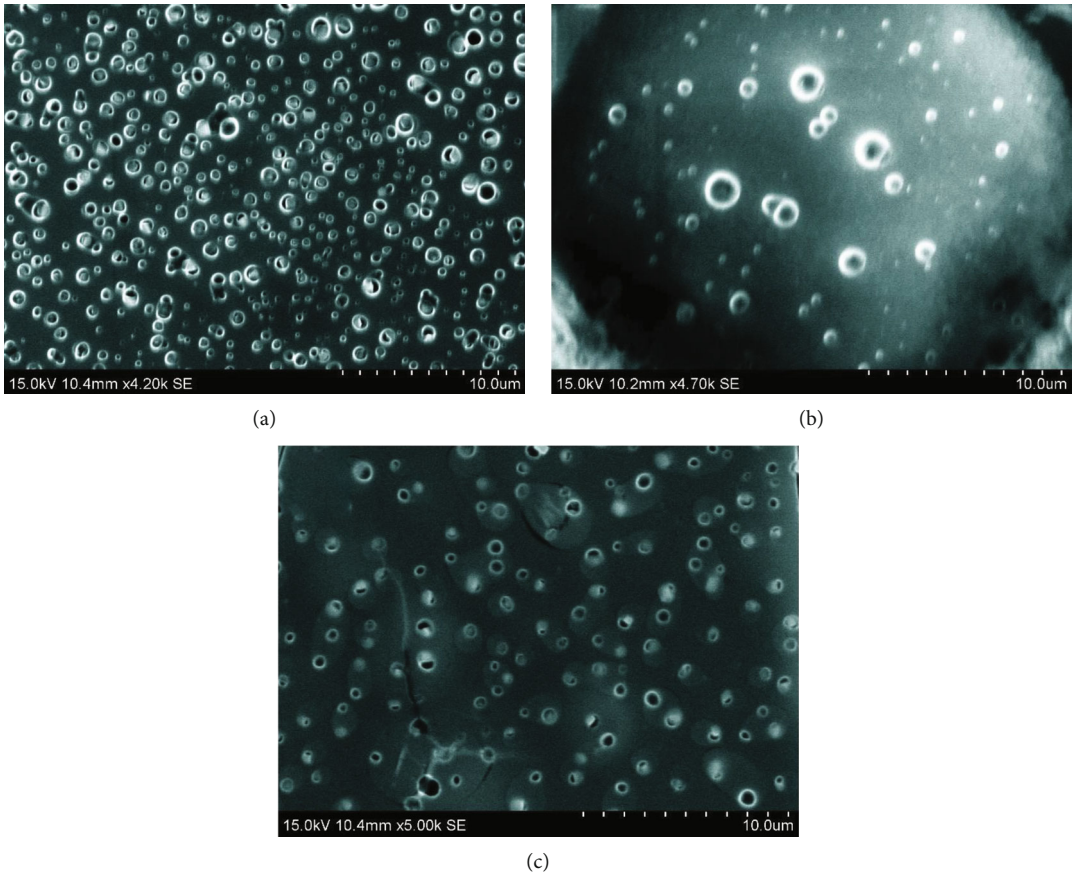

Figure 9: SEM images of bacterial cells (a) before and after treatment with (b) NF-k and (c) NF-c.

obtained for kaempferol-loaded lecithin/chitosan nanoparticles (KAE-LC NPs) when tocopheryl polyethylene glycol succinate was used as the surfactant by Sedef et al. [15]. Likewise, Paramita et al. [25] prepared near-spherical-shaped hesperetin nanoparticles using SDS as a surfactant. Further, Zaid et al. [26] used PVA as a surfactant to prepare spherical-shaped combretastatin A4-loaded poly(L-lactide-co-glycolide) (CA4-loaded PLGA NPs). Therefore, it is evident that

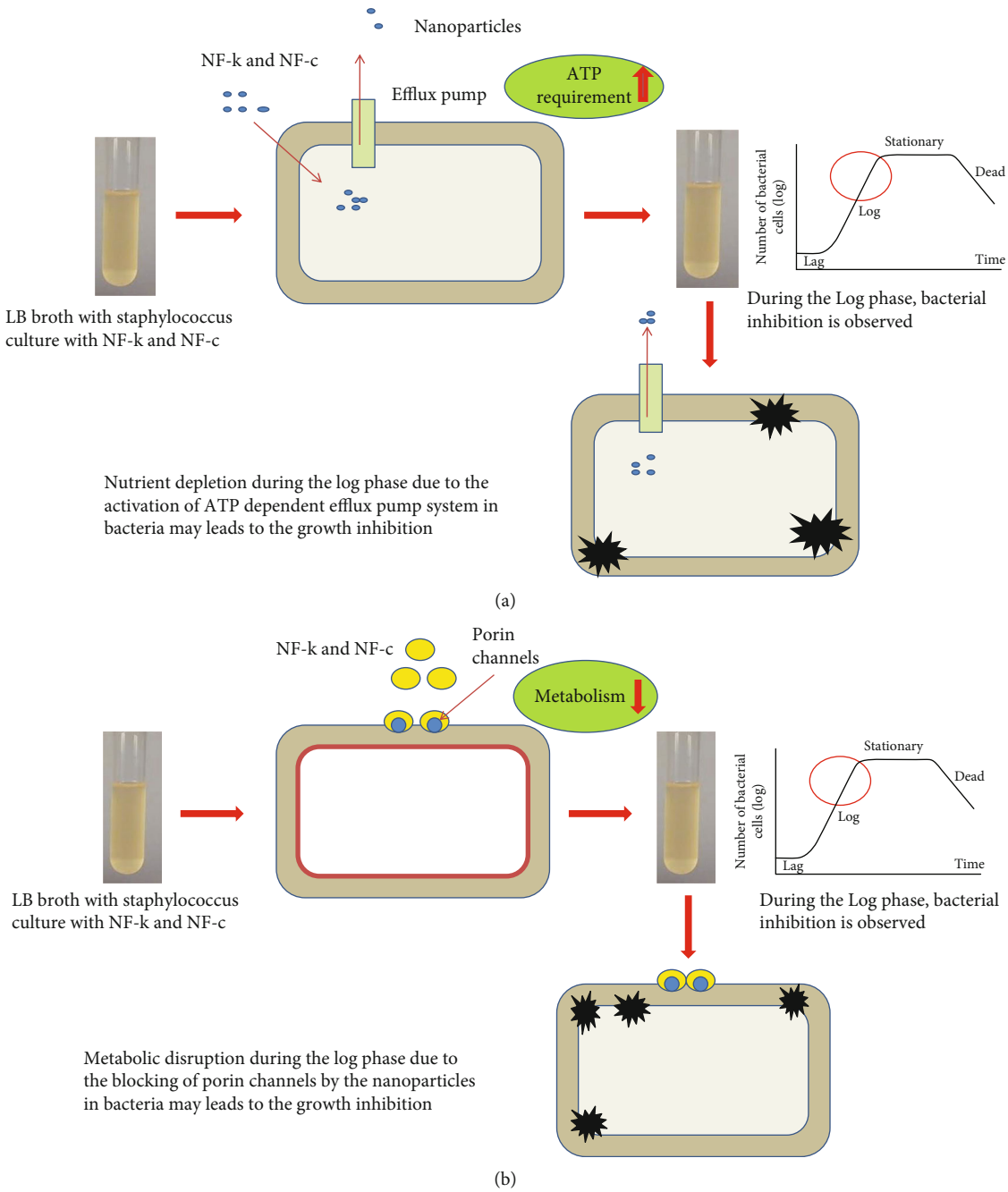

Figure 10: Possible mechanisms of antibacterial activity of nanoformulated drug through (a) blocking of porin channels and (b) activation of ATP-dependent efflux pump system.

the presence of SDS surfactant molecules promotes the formation of spherical-shaped NF-k and NF-c particles. Also, it was inferred that the sizes of NF-k and NF-c were in the nano regime, validating the superiority of the solvent precipitation technique.

The drug release kinetic assay was carried out using the dialysis membrane method. Previously, Sedef et al. [15] reported the drug release kinetics of KAE-LC NPs (200 nm to 350 nm), where the results revealed that the KAE-LC NPs released 82% of the drug in 24 h (25°C). Likewise, Zaid et al. [26] reported the drug release kinetics of CA4-loaded PLGA NPs revealed the release of 87% drug in 17 days (37°C). In the present investigation, the obtained results showed that the kaempferol and combretastatin suspended in DMSO release 20% and 21% drug, respectively, in the first 6 h after that release rate is slow down up to 50 h reaching 25% and 24%, respectively. However, in the case of NF-k and NF-c, a higher percentage of drugs, i.e., 52% and 47%, respectively, was released in a sustained manner which was found higher than the pristine drugs and lower than the reported nanoformulated drugs. The difference in the release kinetics for nanoformulated medicines with their pristine

forms and literature data was influenced by particle size and composition changes. The improved release kinetics of NF-k and NF-c than their pristine forms increase their antibacterial activity. In contrast, the declined release rate than the literature data will allow the safe circulation of nanoformulated drugs in the bloodstream without releasing a lethal amount to the healthy tissue.

The antibacterial activity of NF-k and NF-c was analyzed by evaluating the OD values after incubation with bacterial strain. For both the nanoformulated drugs, the concentration-dependent antibacterial activity trend was elucidated. Also, it was clear that the bactericidal action was higher in the first 24 h of incubation. The activity sustains for 72 h may be due to the sustained release of the nanoformulated drugs. The presence of SDS does not take part in the antibacterial activity since their percentage in the nanoformulation preparation procedure was found to be very low (0.2%) [27]. As the literatures dealing with the antibacterial activity of the NF-k and NF-c were very scarce, the mechanism behind the bacterial growth inhibition is not yet revealed. However, through previous studies on the antibacterial activity of nanoformulated phytochemicals, it is clear that the possible mechanisms behind the bactericidal activity of NF-k and NF-c are either activation of ATP-dependent efflux pump system or blocking of porin channels.

Compared with pristine drugs, the nanoformulated drugs have a small size which makes the drugs more comfortable to enter through the bacterial cell wall. The efflux pump, which is present on the surface of the cell wall, allows the bacteria to control the internal environment by removing the toxic substances, including metabolites, antibacterial agents, and quorum sensing signal molecules [28]. Previous studies revealed that the efflux pump present in *Staphylococcus*was NorA [29–31]. However, the efflux pump requires more ATP to remove the nanoformulated drugs present inside the cell wall. Due to the continuous extrusion of nanoformulated drugs, nutrient depletion occurs for the *Staphylococcus aureus* strain during the log phase leading to bacterial inhibition (Figure 10(a)).

Another possible mechanism is that the NF-k and NF-c block the porin channels on the cell wall's surface [32, 33]. Achouak et al. [34] revealed that the porins channels that regulate the nutrients into the cell for metabolism in gram-positive bacteria. Choi and Lee [35] examined the role of porins for antibiotic resistance in gram-positive bacteria. They revealed that the porins would affect the resistance to antibiotics in different classes and maintain cellular integrity. In the present work, the nanoformulated drugs may block the porin channels and cause metabolic disruption in the log phase leading to bacterial inhibition (Figure 10(b)). However, further studies are required in the future to know the exact mechanism of antibacterial activity of NF-k and NF-c.

Further, the inhibition of bacterial growth is inferred from the SEM images recorded for control and nanoformulated drugs treated bacterial culture. From the obtained results, the control shows the round-shaped, highly populated bacterial structures confirming the presence of *Staphylococcus aureus* with a smooth surface (Figure 9(a)). However, after treating with NF-k and NF-c, the bacterial population declines with distorted surfaces substantiating the antibacterial activity of the nanoformulated drugs (Figures 9(b) and 9(c)). As discussed earlier, the bacterial growth inhibition might be due to the activation of the ATP-dependent efflux pump system or/and the blockage of porin channels. Also, it is to be noted that the bacterial population is lower for NF-k than the NF-c, which is by the obtained OD values.

5. Conclusions

In the present study, NF-k and NF-c were synthesized using the solvent evaporation method and were characterized using DLS, FTIR, and SEM. The drug release kinetic assay confirmed that the NF-k and NF-c release the drugs significantly than the control up to 50 h. The present research validates the bacterial inhibition property of nanoformulated drugs. The possible mechanism behind the bacterial growth inhibition by the nanoformulated drugs may be due to the activation of ATP-dependent efflux pump system in bacteria or/and blocking of porin channels by nanosized drugs that disrupt the metabolism causing bacterial inhibition. Further, well-deliberated studies are needed in the future to elucidate the antibacterial properties of NF-k and NF-c.

Data Availability

The datasets generated and/or analyzed during the current study are available from the corresponding author on reasonable request.

Conflicts of Interest

The authors declare that there is no conflict of interest regarding the publication of this paper.

Acknowledgments

The authors would like to thank Prof. Dr. T. Balasubramanian, Honorable Vice-Chancellor, Smt. S. Jeyendra Saraswathi, Registrar, and the management of Chettinad Academy of Research and Education (Deemed to be University) for providing facilities to perform this study. This research was supported by the Department of Science and Technology-Science and Engineering Research Board (DST-SERB), Government of India, New Delhi (grant number: EMEQ/2018/000882).

References

[1] P. R. Hsueh, "New Delhi metallo-β-lactamase-1 (NDM-1): an emerging threat among Enterobacteriaceae," *Journal of the Formosan Medical Association*, vol. 109, no. 10, pp. 685–687, 2010.

[2] K. Pooled, "Mechanisms of bacterial biocide and antibiotic resistance," *Journal of Applied Microbiology*, vol. 92, pp. 55S–64S, 2002.

[3] R. Jayaraman, "Antibiotic resistance: an overview of mechanisms and a paradigm shift," *Current Science*, vol. 96, pp. 1475–1484, 2009.

[4] M. L. W. Knetsch and L. H. Koole, "New strategies in the development of antimicrobial coatings: the example of increasing usage of silver and silver nanoparticles," *Polymers*, vol. 3, no. 1, pp. 340–366, 2011.

[5] J. M. Calderon-Montano, E. Burgos-Moron, C. Perez-Guerrero, and M. Lopez-Lazaro, "A review on the dietary flavonoid kaempferol," *Mini Reviews in Medicinal Chemistry*, vol. 11, no. 4, pp. 298–344, 2011.

[6] Y.-B. Huang, M.-W. Lin, Y. Chao, C.-T. Huang, Y.-H. Tsai, and P.-C. Wu, "Anti-oxidant activity and attenuation of bladder hyperactivity by the flavonoid compound kaempferol," *International Journal of Urology*, vol. 21, no. 1, pp. 94–98, 2014.

[7] P. Rajendran, T. Rengarajan, N. Nandakumar, R. Palaniswami, Y. Nishigaki, and I. Nishigaki, "Kaempferol, a potential cytostatic and cure for inflammatory disorders," *European Journal of Medicinal Chemistry*, vol. 86, pp. 103–112, 2014.

[8] R. A. Escandón, M. del Campo, R. López-Solis, E. Obreque-Slier, and H. Toledo, "Antibacterial effect of kaempferol and (−)-epicatechin on Helicobacter pylori," *European Food Research and Technology*, vol. 242, no. 9, pp. 1495–1502, 2016.

[9] D. Piyush and V. Kiran, "Kaempferol attenuates diabetic nephropathy by inhibiting RhoA/Rho-kinase mediated inflammatory signaling," *Biomedicine & Pharmacotherap*, vol. 109, pp. 1610–1619, 2019.

[10] M. Imran, B. Salehi, J. Sharifi-Rad et al., "Kaempferol: a key emphasis to its anticancer potential," *Molecules*, vol. 24, no. 12, p. 2277, 2019.

[11] N. Martini, D. R. P. Katerere, and J. N. Eloff, "Seven flavonoids with antibacterial activity isolated from Combretum erythrophyllum," *South African Journal of Botany*, vol. 70, no. 2, pp. 310–312, 2004.

[12] N. Martini, D. R. P. Katerere, and J. N. Eloff, "Biological activity of five antibacterial flavonoids from Combretum erythrophyllum (Combretaceae)," *Journal of Ethnopharmacology*, vol. 93, no. 2-3, pp. 207–212, 2004.

[13] A. Das, K. C. Samal, A. B. Das, and G. R. Rout, "Quantification, antibacterial assay and cytotoxic effect of combretastatin, an anticancer compound from three Indian Combretum species," *International Journal of Current Microbiology and Applied Sciences*, vol. 7, no. 1, pp. 687–699, 2018.

[14] S. Kakran, N. G. Sahoo, I.-L. Tan, and L. Li, "Preparation of nanoparticles of poorly water-soluble antioxidant curcumin by antisolvent precipitation methods," *Journal of Nanoparticle Research*, vol. 14, no. 3, p. 757, 2012.

[15] S. Ilk, N. Saglam, and M. Özgen, "Kaempferol loaded lecithin/chitosan nanoparticles: preparation, characterization, and their potential applications as a sustainable antifungal agent," *Artificial Cells, Nanomedicine, and Biotechnology*, vol. 45, no. 5, pp. 907–916, 2017.

[16] N. Shen, J. Wu, C. Yang et al., "Combretastatin A4 nanoparticles combined with hypoxia-sensitive imiquimod: a new paradigm for the modulation of host immunological responses during cancer treatment," *Nano Letters*, vol. 19, no. 11, pp. 8021–8031, 2019.

[17] Y. S. Qian, S. Ramamurthy, M. Candasamy, S. Md, R. H. Kumar, and V. S. Meka, "Production, characterization and evaluation of kaempferol nanosuspension for improving oral bioavailability," *Current Pharmaceutical Biotechnology*, vol. 17, no. 6, pp. 549–555, 2016.

[18] B. C. Hancock and M. Parks, "What is the true solubility advantage for amorphous pharmaceuticals?," *Pharmaceutical Research*, vol. 17, no. 4, pp. 397–404, 2000.

[19] P. Arnnok and R. Burakham, "Retention of carbamate pesticides by different surfactant-modified sorbents: a comparative study," *Journal of the Brazilian Chemical Society*, vol. 25, no. 9, pp. 1720–1729, 2014.

[20] R. K. B. Bhawana, R. K. Basniwal, H. S. Buttar, V. K. Jain, and N. Jain, "Curcumin nanoparticles: preparation, characterization, and antimicrobial study," *Journal of Agricultural and Food Chemistry*, vol. 59, no. 5, pp. 2056–2061, 2011.

[21] B. Zhao, Z. Dong, W. Liu et al., "Co-administration of combretastatin A4 nanoparticles and anti-PD-L1 for synergistic therapy of hepatocellular carcinoma," *Journal of Nanobiotechnology*, vol. 19, no. 1, pp. 1–18, 2021.

[22] Y. Zhang, X. Liu, X. Wang et al., "Nanoparticles composed of PEGylated alternating copolymer-combretastatin A4 conjugate for cancer therapy," *Macromolecular Bioscience*, vol. 21, no. 8, article 2100077, 2021.

[23] B. Feng, M. A. Ashraf, and L. Peng, "Characterization of particle shape, zeta potential, loading efficiency and outdoor stability for chitosan-ricinoleic acid loaded with rotenone," *Open Life Sciences*, vol. 11, no. 1, pp. 380–386, 2016.

[24] D. R. Telange, A. T. Patil, A. M. Pethe, A. A. Tatode, S. Anand, and V. S. Dave, "Kaempferol-phospholipid complex: formulation, and evaluation of improved solubility, in vivo bioavailability, and antioxidant potential of kaempferol," *Journal of Excipients and Food Chemicals*, vol. 7, no. 4, p. 89, 2016.

[25] P. Paramita, S. N. Sethu, N. Subhapradha et al., "Neuro-protective effects of nano-formulated hesperetin in a traumatic brain injury model of Danio rerio," *Drug and Chemical Toxicology*, vol. 44, no. 6, pp. 1–8, 2020.

[26] A. N. Zaid, M. Hassan, N. Jaradat et al., "Formulation and characterization of combretastatin A4 loaded PLGA nanoparticles," *Materials Research Express*, vol. 6, no. 12, 2019.

[27] M. A. Díaz De Rienzo, P. Stevenson, R. Marchant, and I. M. Banat, "Anti-bacterial properties of biosurfactants against selected Gram-positive and-negative bacteria," *FEMS Microbiology Letters*, vol. 363, no. 2, p. 224, 2016.

[28] D. Gupta, A. Singh, and A. U. Khan, "Nanoparticles as efflux pump and biofilm inhibitor to rejuvenate bactericidal effect of conventional antibiotics," *Nanoscale Research Letters*, vol. 12, no. 1, 2017.

[29] S. Zimmermann, M. Klinger-Strobel, J. A. Bohnert et al., "Clinically approved drugs inhibit the Staphylococcus aureus multidrug NorA efflux pump and reduce biofilm formation," *Frontiers in Microbiology*, vol. 10, p. 2762, 2019.

[30] N. Kahzad and A. Salehzadeh, "Green synthesis of CuFe2O4@Ag nanocomposite using the Chlorella vulgaris and evaluation of its effect on the expression of norA efflux pump gene among Staphylococcus aureus strains," *Biological Trace Element Research*, vol. 198, no. 1, pp. 359–370, 2020.

[31] N. Shokoofeh, Z. Moradi-Shoeili, A. S. Naeemi, A. Jalali, M. Hedayati, and A. Salehzadeh, "Biosynthesis of Fe3O4@Ag nanocomposite and evaluation of its performance on expression of norA and norB efflux pump genes in ciprofloxacin-resistant Staphylococcus aureus," *Biological Trace Element Research*, vol. 191, no. 2, pp. 522–530, 2019.

[32] L. Liao, Y. Li, and S. Tjong, "Bactericidal and cytotoxic properties of silver nanoparticles," *International Journal of Molecular Sciences*, vol. 20, no. 2, p. 449, 2019.

[33] J. D. Prajapati, U. Kleinekathöfer, and M. Winterhalter, "How to enter a bacterium: bacterial porins and the permeation of antibiotics," *Chemical Reviews*, vol. 121, no. 9, pp. 5158–5192, 2021.

[34] W. Achouak, T. Heulin, J.-M. PagÃ¨s et al., "Multiple facets of bacterial porins," *FEMS Microbiology Letter*, vol. 199, no. 1, pp. 1–7, 2001.

[35] U. Choi and C. R. Lee, "Antimicrobial agents that inhibit the outer membrane assembly machines of Gram-negative bacteria," *Journal of Microbiology and Biotechnology*, vol. 29, no. 1, pp. 1–10, 2019.

Hindawi
International Journal of Polymer Science
Volume 2021, Article ID 9069924, 10 pages
https://doi.org/10.1155/2021/9069924

Review Article

Silk Fibroin: A Promising Tool for Wound Healing and Skin Regeneration

M. Vidya [1] and Senthilkumar Rajagopal [2]

[1]*Dept of Chemistry and Biochemistry, MS Ramaiah College of Arts, Science and Commerce, Bangalore, India*
[2]*Dept of Biotechnology, School of Applied Sciences, REVA University, Bangalore, India*

Correspondence should be addressed to Senthilkumar Rajagopal; senthilanal@yahoo.com

Received 3 July 2021; Revised 12 September 2021; Accepted 14 September 2021; Published 1 October 2021

Academic Editor: Domenico Acierno

Silk is a functional protein biomaterial produced by a variety of insects like flies, silkworms, scorpions, spiders, and mites. Silk synthesized by silkworms is extensively studied for its applications in tissue engineering and wound healing. Silk is undoubtedly a natural biocompatible material with humans and has its role in medical treatments from ancient times. The silk worm protein comprises two types of proteins namely fibroin and sericin. Silk fibroin makes up approximately 70% of cocoon weight and has wide applications in textiles and in all biomedical applications owing to its biocompatible, nontoxic, biodegradable, less immunogenic, and noncarcinogenic nature. It possesses outstanding toughness and mechanical strength, while silk sericin possesses high defensive ability against ultraviolet light and oxidation. Silk fibroin has been known to induce wound healing by increasing cell proliferation and growth and migrating various types of cells which are involved in different stages of wound healing process. With several silk varieties like silk worm fibroin, silk sericin, recombinant silk materials, and native spider silk have been investigated for its wound healing applications over the last several decades. With an objective of harnessing the silk regenerative properties, plentiful strategies have been studied and applied to develop bioartificial skin grafts and bioactive wound dressings in recent times. This review gives a detailed insight into the structure, general properties, fibroin structure-properties relationship, and biomedical applications of silk fibroin.

1. Introduction

Silks are common protein polymers produced by various insects such as silkworms, spiders, and bees. Silk fibres from various species have varying fibroin sequences, structural properties, and primary sequences. The major part of silk is produced by two types of silkworm: no mulberry (wild variety) and domesticated mulberry. Mulberry silk is produced by the domesticated silkworm family *Bombyx mori* (*B. mori*). Eri (*Philosamia ricini*/*Samia ricini*), Muga (*Anthrraea asana*/*assamensis*), and Tussar (*Antheraea mylitta*) are the primary sources of wild variety/Saturniidae/nonmulberry silk [1]. Spider silks have a higher mechanical strength than silkworm silk. However, because spider silks are in shortage, domestic *Bombyx mori* filaments are the most widely used in the commercial silk business [2]. Only silk from silkworms has been manufactured on a large scale in the past, and it has lately been employed as a biomaterial due to its long-lasting characteristics and availability [3].

1.1. Silk Fibroin's Structure and Properties. Fibroin and sericin are the two proteins found in silk from the *Bombyx mori* silkworm: The former is found in the inside of the thread and accounts for roughly 70% of the silk's weight, while the latter is located in the thin layer that surrounds the interior thread and accounts for the remaining 30% and also possesses fat/wax (0.8-1%) and colour/ash (1-1.4%) [4]. Fibroin is produced by the silkworm's posterior gland, while sericin is released by the silkworm's middle and anterior glands, the morphology of which is shown in Figure 1.

Silk is a natural protein polymer that has been recognized by the US Food and Drug Administration (FDA) for

medical usage. Silk fibroin is m4ade from mulberry silk after the outermost silk sericin is removed, which has the ability to activate an immune response when combined with fibroin [6, 7]. While spinning, the larvae releases two very thin (10 μm diameter) fibroin double strands through the spinnerets, simultaneously bonding them together with sericin from the two exocrine silk glands (aligned on both sides of the body). The protein fibre gets stronger and tougher in the presence of air [8].

The major component of silk is fibroin, which serves as the inner core and gives mechanical strength, whereas sericin serves as the exterior glue-like coating. Two silk fibroin filaments are covered with sericin in each silk fibre [9]. It is already been postulated that silk fibroin filaments are made up of 3.5 nm diameter nanofibrils, which are the building elements of silk.

These nanofibrils intertwine and have a strong interaction with one another and form into bigger fibril units, known as microfibrils that are 20-200 nm in diameter [10]. Parallel to the silk fibroin filaments, microfibrils and nanofibrils are arranged. The major structural protein of silk is silk fibroin, which includes polypeptide chains with molecular weights ranging from 200 to 350 kDa. Silk fibroin's primary structure consists of an H-L complex made up of a light- (L-) chain polypeptide and a heavy- (H-) chain polypeptide joined together by a single disulphide bond at the C-terminus of the H-chain. Furthermore, glycoprotein P25 which is noncovalently connected to the H-L-chains is present in the structure of silk fibroin and contributes to its overall integrity. The H-chain is primarily responsible for the silk fibres fibrous properties. The most common amino acids present in this chain are glycine (46 percent), serine (12 percent), and alanine (30 percent) [11]. Isoleucine, leucine, valine, and other acidic amino acids are mostly found in the nonfibrous L-chains [12].

Because of its biocompatibility, gradual disintegration, low immunogenicity, adaptability, and outstanding mechanical qualities, silk fibroin is increasingly being studied for biomedical applications [13–15]. Silk fibroin has a stronger ability to modify in response to one's biological surroundings, which could lead to better integration and possibly less material-associated thrombosis [16]. This opens up the possibility of using silk motifs as the foundation for biomaterials with specific characteristics. Historically, functional qualities have been associated with specific amino acid patterns [17] and can be genetically and/or chemically manipulated while preserving important secondary structural traits, resulting in recombinant silk polymers which control (i) chemical reactivity, (ii) polymer size, and (iii) characteristics of bulk materials [18]. Silk fibroin has been proven to stimulate adhesion of stem cells, propagation and differentiation in vitro, enhance tissue healing, and inhibit pathological adherence in vivo in various formats (fibres, films, nets, etc.) [19–21]. Silk fibroin (SF) is composed by alanine, serine, and glycine in different percentages. Because of its hydrophobic regions, silk fibroin is high in β-sheet patterns, which impact its mechanical characteristics, biodegradation rate, and ability to enhance cell adhesion and differentiation in mesenchymal stem cells.

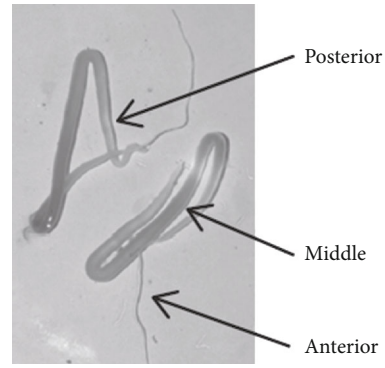

Figure 1: Silk gland morphology in *Bombyx mori* [5].

Silk fibroin is made up of both amorphous and crystalline domains. Gly-Ala repetitions are distributed throughout the crystalline domains via motifs containing tyrosine and serine amino acids. Amorphous domains are made up of bulky side chain amino acids like aspartic acid. The noncrystalline part contributes to the fibre's flexibility and elasticity, while the crystalline part adds to its strength and toughness. For *Bombyx mori* crystalline structures of silk fibroin, silks I, II, and III are the three conformations which are considered. Silk I is a water soluble version of silk fibroin that has a lot of α-helix that can be easily converted into silk II having a β-sheet structure that is antiparallel [22–24]. The unusual structural conformation of silk fibroin provides mechanical strength and flexibility [6]. Degradation studies of silk fibroin in phosphate-buffered saline for 12 weeks have shown the transition of construct from β-sheet to random coil, lowering the adhesion force and Young's modulus of the construct [25]. The β-sheet crystallization has been stimulated in silk-based scaffolds using a variety of approaches. Ethanol and methanol are two popular inorganic solvents that stimulate the development of β-sheets to a degree of 55% and 36%, respectively [26, 27]. Steam autoclaving at high temperature and pressure, on the other hand, induced the greatest β-sheet crystallinity (60 percent) [28]. Another approach that generated β-sheet (30%) production when mixed with a large proportion of silk I helical structure is water annealing at ambient temperature [29]. A single systemic procedure involving temperature-controlled water vapour annealing from 4°C to 100°C was employed to fully control the structure and properties of silk. Different kinds of silk conformations like silk I and silk II with controlled β-sheet may be made using this technology, and the degradability, mechanical strength, and biological response can be regulated [26]. Heat treatment of silk films and fibres has been examined in several lab studies. The colour, crystallinity, and mechanical strength of the silk were all changed when the temperature was raised [30, 31]. The crystallinity, mechanical strength, and colour of the silk were all modified when the temperature was raised. Several researchers have studied at the thermal treatment of silk films and fibres [30–32].

The structure of silk was highly converted to β-sheet, which is prevalent in *Bombyx mori* cocoon fibres, when the casted silk films were heated to 100°C. Furthermore,

increasing the temperature of the oriented silk fibres above the transition temperature resulted in the creation of β-sheet conformation over α-helical structure [33]. At a temperature of around 140°C, a solid-state conformational change from an α-helical structure to β-sheet silk II structure happened. The films exhibited that endothermic melting peak followed an exothermic crystallization peak, both near 140°C, according to modulated differential scanning calorimetry (DSC). Following heating above the structural transition temperature, β-sheet fibres with a structure comparable to *B. mori* cocoon fibres were generated (Figure 2) [32].

As a result, the structure and mechanical strength of silk-based substrates may be controlled by varying the temperature. Silk fibroin has also been utilised in the manufacturing of textiles and clinical sutures for generations [34]. Primary cells and cell lines can attach to, proliferate in, and differentiate in silk fibroin materials [35] and can be easily used to prepare mats [36], porous scaffolds [37], gels [38], and films [39].

1.2. Compatibility of Silk Fibroin as a Wound Healing Biomaterial. The human body's skin serves as a barrier against the infectious agents, dehydration, and environment. Wound healing is a complex process including interactions with many cells and matrices, as well as multiple overlapping phases like inflammation, new tissue creation, and tissue remodelling happening at the same time [41]. The initial phase of wound healing is inflammation, which occurs shortly after an injury and can persist up to two days. To prevent further fluid and blood losses, remove dying and dead tissues, and stop infection, the coagulation cascade, inflammatory pathways, and immune system must all be activated. Inflammatory cells like macrophages and neutrophils play a number of important roles in the repair process, including phagocytosis and the production of many cytokines and growth factors [42]. The second phase of wound healing is new tissue development that is correlated with deposition of collagen/matrix, reepithelialization, angiogenesis, and contraction of wounds [42, 43]. The remodelling or maturation phase of the wound healing process, which can last for a year or longer depending on the degree of the injury, is combined with the rebuilding of the epidermis and extracellular matrix [43, 44].

Skin regeneration is still the target of skin repair in order to minimise the long-term effects of scarring on an individual [45]. Wound healing in mammals is a reparative process that culminates in scar formation rather than a regenerative process that replaces normal tissue architecture [46]. Scar tissue is inferior to normal tissue in terms of function and appearance. It is caused by an excess of extracellular matrix (ECM) being produced following an injury [47]. Collagen I, an important protein influencing the ECM architecture during wound healing, is synthesized majorly by fibroblasts, and its synthesis is majorly regulated by cytokine transforming growth factor β_1 $(\mathrm{TGF}\beta)_1$ [48, 49]. $(\mathrm{TGF}\beta)_1$ which is secreted in inactive form is converted to active form enzymatically in order to execute its effect. $(\mathrm{TGF}\beta)_1$ changes the morphology of many cells like fibroblasts by stimulating polymerisation of the globular form of active cytoskeleton to filamentous form [48].

There really are numerous wound dressing biomaterials on the market today, to mention a few are chitosan [50], hydrocolloids [51], polyurethane [52], alginates [53], collagen [54, 55], and hyaluronic acid (Figure 3) [56]. The most widely revealed tissue engineering technique to date is still Integra, a skin substitute, which is a mix of multiple ECM proteins. The utilization of composite tissue engineering skin could be considered to speed up the second stage of repair using Integra [57].

The following characteristics should be present in an ideal wound dressing: (a) preservation of a moist wound area, (b) prevention of desiccation and excessive exudate absorption, (c) permeability of gas, (d) avoidance of bacterial infection and transmission of diseases, and (e) resistance to water [58]. The creation of optimal wound dressings, on the other hand, is still ongoing.

2. Different Forms of Silk Fibroin for Wound Healing Operations

2.1. Silk Fibroin Solution. The silk cocoon was degummed in an aqueous solution of 0.02 M Na_2CO_3 for 40 minutes boiling at 95°C, then washed with distilled water to remove the glue-like sericin proteins yields silk fibroin solution [60–62]. Degummed silk fibroin was then solubilized for 50 minutes at 98°C with calcium chloride, ethanol, and water (at a molar ratio of 1 : 2 : 8). This solution was subsequently filtered for three days over dialysis membrane to obtain silk fibroin solutions. Silk fibroin solution greatly induced healing effect both in vitro and in vivo, according to Park et al. [63]. Solubilized silk protein has also been used as an eye drop to help rabbit corneal epithelial wound repair [64].

2.2. Nanofibrous Scaffolds from Silk Fibroin. Silk fibroin scaffolds are an intriguing type of skin substitute made from silk fibroin. Electrospinning creates a pseudo-three-dimensional structure for cell adhesion and growth [60, 65–67]. Two-dimensional scaffolds produced through electrospinning technique play an important role in the manufacturing of skin substitute products which comprises all the qualities for a successful skin regeneration and wound closure [68]. Only electrospinning may confer antimicrobial activity, which is based on the movement of ionic species from the fibres, and thus produces wound dressing scaffolds or materials for long-time controlled release [69]. Fabrication of electrospun nanocomposite fibres by in situ silica gelation in poly e-caprolactone solution serves as a promising multi-bio functional material for orthopaedic applications [70]. The three-dimensional structure of nanofibrous materials supports attachment of the cell and growth of the cell and controls the cell differentiation functions [71]. The electrospun composite nanofibrous scaffolds increased the osteogenic differentiation and proliferation of mesenchymal stem cells in human and human endothelial cells angiogenic activity in vitro [72]. The biodegradable nonwoven poly (lactic-co-glycolic acid) scaffolds developed using electrospinning may improve the anisotropic and isotropic growth of cardiomyocytes [73]. Hollow electrospun nanofibrous structures manufactured by coaxial electrospinning may be a

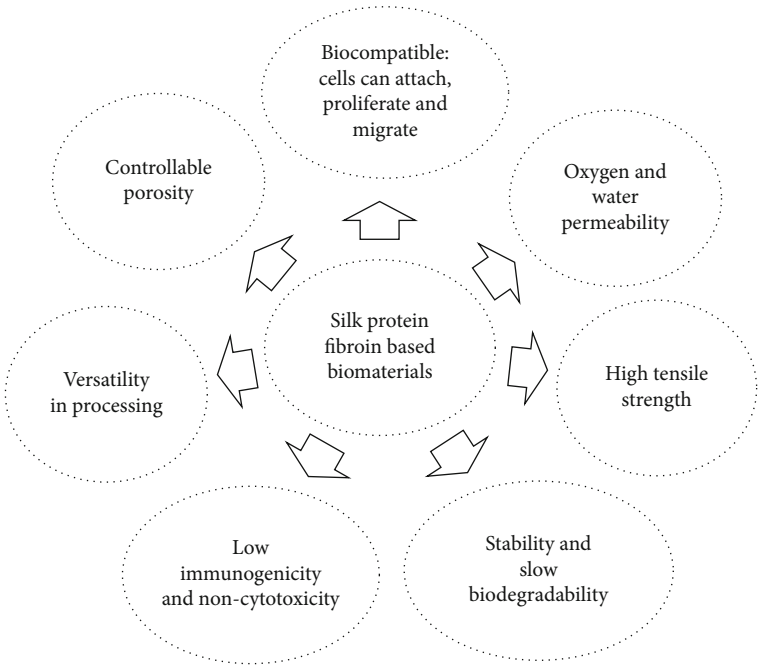

Figure 2: Diverse characteristics of biomaterials based on silk protein fibroin (adopted from Naskat et al. [40]).

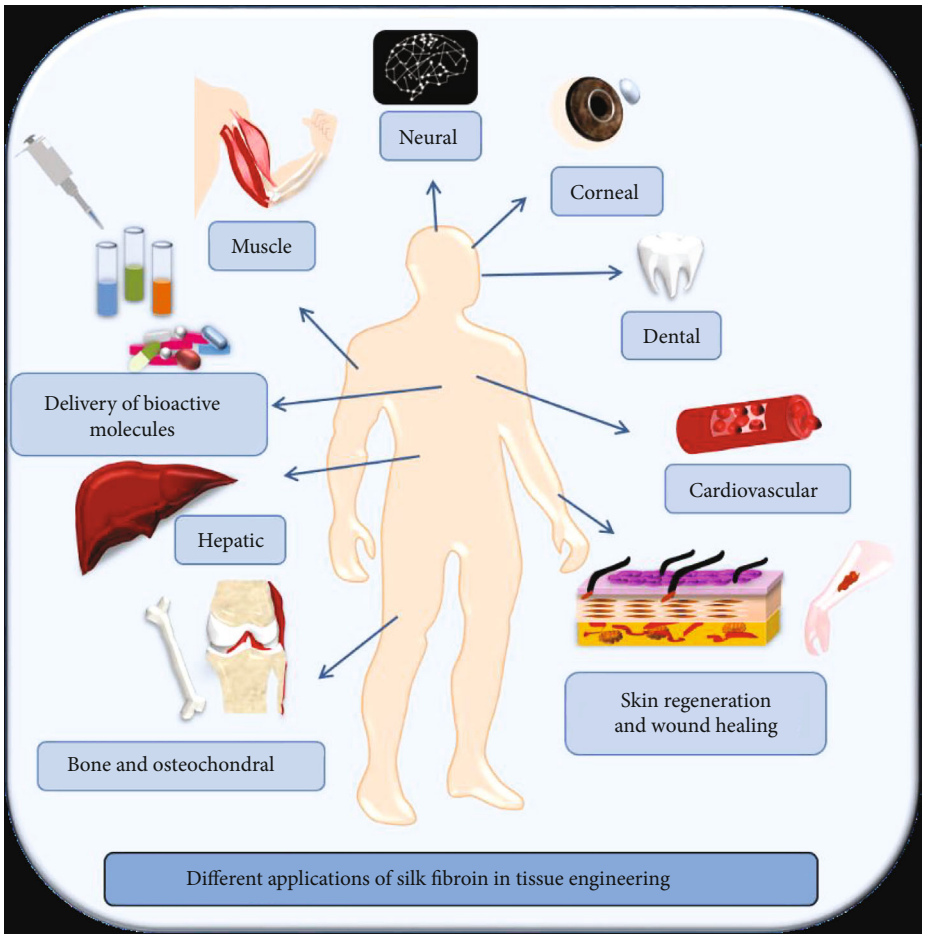

Figure 3: Silk fibroin: applications in tissue engineering and regenerative medicine (adopted from Gholipourmalekabadi et al. [59]).

Table 1: Silk fibroin morphologic forms for different wound treatments.

Forms of fibroin	Wound type	References
Fibroin in solution	Skin wound with partial thickness Burn injury Corneal epithelial wounds	[63, 101, 102]
Hydrogel	Burn injury Scrape wound	[86, 95]
Film	Skin wounds with full thickness Acute dermal wound	[100]
Fibroin sponge	Skin wounds with full thickness	[55]

promising method for drug encapsulation, which enables high drug-loading capacity and augmented solubilization of nonsoluble drugs [74].

The biological and mechanical properties of the electrospun silk fibroin (ESF) mat are directly influenced by the concentration of silk fibroin in the spinning fluid. In an in vitro and ex vivo wound model, electrospun silk fibroin with smaller size nanofibres had a stronger effect on extracellular matrix production and skin cell proliferation [75]. To develop electrospun scaffolds with biomechanical properties similar to natural skin, the fabrication process must be optimised. Research findings established increased proliferation of cells cultured on micron-sized fibres [76–78]. Cells may perceive these scaffolds as two-dimensional structures and may also allow rapid cell proliferation. Scaffolds made of this morphology of fibres may cause cells to adopt an artificial morphology, which may affect the expression of cell adhesion and migration genes and tension-sensitive expression pathways. These may be especially important in preventing pathological scarring or contracture during cutaneous wound healing [78, 79]. Cells became elongated along the fibre lengths, an aspect that may be useful to utilise for other applications where this morphology may be beneficial, including nerve tissue engineering [80, 81].

2.3. Hydrogels from Silk Fibroin. In an aqueous solution, hydrogels are three-dimensional polymeric networks with a high swelling ratio. Hydrogels are typically made from naturally occurring polymers, such as chitosan [82], alginate [83], collagen [84], hyaluronic acid [85], and silk fibroin [86, 87] due to their relatively good biocompatibility. Hydrogels have been widely used in a variety of biomedical applications, including wound healing [88]. The beneficial benefits of silk fibroin include not only inducing cell attachment, development, migration, proliferation, and creation of extracellular matrix but also improving the mechanical strength of hydrogels made from other natural polymers [89].

The wild silkworm fibre's mechanical properties such as toughness and extensibility of fibroin fibres are greater than polymers such as Kevlar and elastin [6, 90]. Collagen and silk fibroin fibrils possess a suitable interfacial adhesion, and the combined scaffolds display enhanced mechanical properties [91]. In order to couple the biological performance of collagen and mechanical resistance of fibroin,

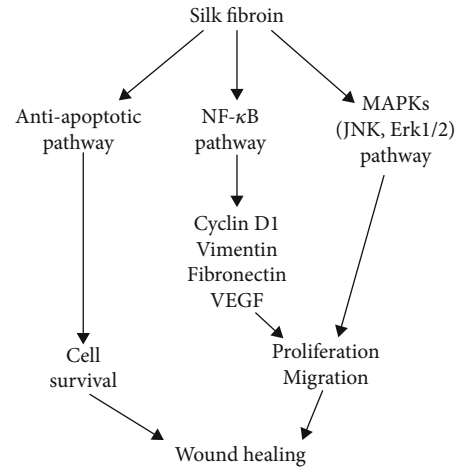

Figure 4: Biological pathways activated by silk fibroin to promote wound healing via enhancing cell viability, cell proliferation, and migration (adopted from Sultan et al. [110]).

new scaffolds were designed for vascular tissue engineering applications. The results highlighted that addition of silk fibroin fibres in collagen hydrogel improved the mechanical resistance of collagen hydrogel without any side effects [91]. Research evidences show that the inspiring mechanical properties of silk are attributed due to its hierarchical properties [92, 93]. Simulation and experimental results of β-sheet crystallites of silkworm silk show that the stiffness and strength of silk are mainly due to the presence of β-sheet crystallites. Hydrogen bonds along with intersheet hydrophobic and Van der Waals interactions significantly contribute to the stability of the structures. The exceptional strength of spider silks and silkworm, which exceeds that of steel, is due to beta-sheet nanocrystals. The remarkable strength of silkworm and spider silks, which exceeds that of steel, is due to beta-sheet nanocrystals composed of highly conserved poly-(Gly-Ala) and poly-Ala domains [94].

In vitro, a biomimetic hydrogel containing silk and L-proline showed a considerable improvement in wound healing [95]. The development of a pure silk fibroin hydrogel with a high strength and aligned microgrooved topographic structure has outstanding mechanical characteristics and is extremely strong. The hydrogel biocompatibility also allows them to sustain cell viability [96].

2.4. Silk Fibroin Sponges/Blend Films. Wound healing can be enhanced with silk fibroin blends in the form of sponges and films. Porous sponges are important tissue engineering materials, and they have also been made with regenerated silk fibroin solutions [97, 98]. Sponge scaffolds do provide a network of linked pores with a large surface area inside a predetermined three-dimensional volume, allowing for tissue ingrowth and cell adhesion. The silk/duck feet collagen hybrid sponge, according to Lee et al., could be employed as a dermal substitute for full-thickness skin abnormalities [60]. Liu et al. used a freeze-drying process to create a silk fibroin sponge for the controlled release of neurotensin-loaded gelatin microspheres in the treatment of diabetic foot ulcers [99]. The neurotensin-releasing scaffold demonstrated a good drug delivery system and wound dressing material over a 28-day posttreatment follow-up. This increased fibroblast accumulation, wound closure, and granulation of tissues at wound site, which expedited wound healing in diabetic foot ulcers with little scar formation [99]. Padol et al. showed that silk fibroin film, as a unique wound healing material, is extremely effective when combined with epidermal growth factor for acute wound healing [99] (Table 1). In rats, silk films were used to cure full-thickness skin wounds, and they showed faster healing and less inflammatory response than typical porcine-based wound dressings [100].

2.5. Wound Healing Mechanism of Silk Fibroin. The NF-κB signalling pathway is used by silk fibroin to speed up wound healing [103]. Through complicated signalling pathways, NF-κB governs different cell behaviours such as proliferation, adhesion, clearance of reactive oxygen species, and inflammation. As a result, NF-κB signalling is thought to be important in the healing of diverse wounds such as corneal epithelial wounds [104]. In the silk fibroin-induced cells, there was an increase in the expression of tumour necrosis factor receptor (TNFR) and Toll-like receptors (TLRs), two critical mediators of NF-κB. They also mediated a varied range of protein expression which regulate the healing of wounds and affected by NF-κB like epidermal growth factor (EGF), fibronectin, vascular endothelial growth factor (VEGF), vimentin, IL-10 (interleukin-10), IL-1b, transforming growth factor (TGF), and cyclin. David. Park et al. (2019) determined that silk fibroin enhanced wound healing by altering the expression of proteins involved in the remodelling and proliferation phases by stimulating NF-κB signalling (Figure 4) [103].

According to Aykac et al., silk fibroin had a protective effect in a rat model of burn injury by inactivating the apoptotic pathway [101]. Several complex cellular signalling pathways like Wnt and Notch signalling [105], transforming growth factor beta (TGFβ) signalling [105, 106], mitogen-activated protein kinase (MAPK) signalling [107], and AKT/mTOR signalling [108] take place in a tightly coordinated cascade to heal the wound during the wound healing process. MAPK signalling [109] and AKT/mTOR signalling [108] are two cellular pathways that play a role in wound healing.

2.6. Summary and Future Perspectives. Silk fibroin, due to their credible biocompatibility, significantly lowers biodegradation rates compared to other materials, is of user-friendly nature, is easily available, and has least immune response to host tissue which has attracted intense interest in recent decades for various amazing biomedical applications including wound healing. In various wound healing applications, it has been found to be a potential biomaterial in several forms, including solution, films, electrospun silk fibroin nanofibre mats, hydrogels, hydrocolloid dressings, and sponges. Because of the favourable findings obtained in vitro and in vivo, the prospects of employing fibroin alone and in blends in wound healing are highly promising. Electrospun silk fibroin techniques loaded with or without antibacterial agents are predicted to be the most effective silk fibroin-based skin substitute in future clinical trials. To construct a novel array of silk fibroin-based biomaterials for treatment of different types of wound healing, further study is required to investigate the mechanistic basis for silk fibroin on the wound. According to Belda Marin et al. [111] in a review, the behaviour of the biomaterials with ageing and liberating the inorganic phase is detrimental to find out the long-term stability of the scaffolds. Furthermore, more studies on the interaction between organic and inorganic phase is warranted. Only very few studies are available depicting the secondary structural changes of silk fibroin following after the inorganic phase interaction, which has to be studied in detail to elucidate the mechanism. The functional groups present in silk fibroin could be utilized for covalent bond formation with inorganic phase, which may give insight on scaffold designing with specific patterns.

Conflicts of Interest

The authors declare that they have no conflicts of interest.

Acknowledgments

The support provided by the Department of Biotechnology, Ministry of Science and Technology, Government of India (to Dr. Senthilkumar Rajagopal; No.: BT/RLF/Reentry/42/2012) to complete this manuscript in a successful manner is gratefully acknowledged.

References

[1] S. Gupta, H. Alrabaiah, M. Christophe, M. Rahimi-Gorji, P. D. S. Nadeem, and A. Bit, "Evaluation of silk-based bioink during pre and post3Dbioprinting: a review," *Journal of Biomedical Materials Research Part B: Applied Biomaterials.*, vol. 109, no. 2, pp. 279–293, 2021.

[2] B. K. Murugesh, "13- Silk from silkworms and spiders as high-performance fibers," in *Structure and Properties of High-Performance Fibers*, G. Bhat, Ed., pp. 327–366, Woodhead Publishing, Oxford, 2017.

[3] C. Vepari and D. Kaplan, "Silk as a biomaterial," *Progress in polymer science*, vol. 32, no. 8-9, pp. 991–1007, 2007.

[4] I. Belhaj Khalifa, N. Ladhari, and M. Touay, "Application of sericin to modify textile supports," *Journal of the Textile Institute*, vol. 103, no. 4, pp. 370–377, 2012.

[5] S. Kundu, *Silk Biomaterials for Tissue Engineering and Regenerative Medicine*, Elsevier Science, 2014.

[6] G. H. Altman, F. Diaz, C. Jakuba et al., "Silk-based biomaterials," *Biomaterials*, vol. 24, no. 3, pp. 401–416, 2003.

[7] Z. Wang, Y. Zhang, J. Zhang et al., "Exploring natural silk protein sericin for regenerative medicine: an injectable, photoluminescent, cell-adhesive 3D hydrogel," *Scientific Reports*, vol. 4, no. 1, p. 7064, 2014.

[8] S. Inoue, K. Tanaka, F. Arisaka, S. Kimura, K. Ohtomo, and S. Mizuno, "Silk fibroin of *Bombyx mori* is secreted, assembling a high molecular mass elementary unit consisting of H-chain, L-chain, and P25, with a 6:6:1 molar ratio," *Journal of Biological Chemistry*, vol. 275, no. 51, pp. 40517–40528, 2000.

[9] L.-D. Koh, Y. Cheng, C.-P. Teng et al., "Structures, mechanical properties and applications of silk fibroin materials," *Progress in Polymer Science*, vol. 46, pp. 86–110, 2015.

[10] S. Ling, W. Chen, Y. Fan et al., "Biopolymer nanofibrils: structure, modeling, preparation, and applications," *Progress in Polymer Science*, vol. 85, pp. 1–56, 2018.

[11] Q. Yu, H. Wang, K. Wei et al., "A review of structure construction of silk fibroin biomaterials from single structures to multi-level structures," *International Journal of Molecular Sciences*, vol. 18, no. 3, p. 237, 2017.

[12] K. Shimura, "Chemical composition and biosynthesis of silk proteins," *Experientia*, vol. 39, no. 5, pp. 455–461, 1983.

[13] B. Kundu, R. Rajkhowa, S. C. Kundu, and X. Wang, "Silk fibroin biomaterials for tissue regenerations," *Advanced drug delivery reviews*, vol. 65, no. 4, pp. 457–470, 2013.

[14] P. Zeplin, N. Maksimovikj, M. Jordan et al., "Spider silk coatings as a bioshield to reduce periprosthetic fibrous capsule formation," *Advanced Functional Materials*, vol. 24, no. 18, pp. 2658–2666, 2014.

[15] M. J. Rodriguez, J. Brown, J. Giordano, S. J. Lin, F. G. Omenetto, and D. L. Kaplan, "Silk based bioinks for soft tissue reconstruction using 3-dimensional (3D) printing with *in vitro* and *in vivo* assessments," *Biomaterials*, vol. 117, pp. 105–115, 2017.

[16] A. E. Thurber, F. G. Omenetto, and D. L. Kaplan, "*In vivo* bioresponses to silk proteins," *Biomaterials*, vol. 71, pp. 145–157, 2015.

[17] W. L. Stoppel, C. E. Ghezzi, S. L. McNamara, L. D. B. III, and D. L. Kaplan, "Clinical applications of naturally derived biopolymer-based scaffolds for regenerative medicine," *Annals of Biomedical Engineering*, vol. 43, no. 3, pp. 657–680, 2015.

[18] N. Shankhwar, M. Kumar, B. B. Mandal, and A. Srinivasan, "Novel polyvinyl alcohol-bioglass 45S5 based composite nanofibrous membranes as bone scaffolds," *Materials Science and Engineering: C*, vol. 69, pp. 1167–1174, 2016.

[19] M. Floren, W. Bonani, A. Dharmarajan, A. Motta, C. Migliaresi, and W. Tan, "Human mesenchymal stem cells cultured on silk hydrogels with variable stiffness and growth factor differentiate into mature smooth muscle cell phenotype," *Acta Biomaterialia*, vol. 31, pp. 156–166, 2016.

[20] W. Sun, A. Motta, Y. Shi et al., "Co-culture of outgrowth endothelial cells with human mesenchymal stem cells in silk fibroin hydrogels promotes angiogenesis," *Biomedical Materials*, vol. 11, no. 3, article 035009, 2016.

[21] J. Melke, S. Midha, S. Ghosh, K. Ito, and S. Hofmann, "Silk fibroin as biomaterial for bone tissue engineering," *Acta Biomaterialia*, vol. 31, pp. 1–16, 2016.

[22] T. Asakura, Y. Suzuki, Y. Nakazawa, G. P. Holland, and J. L. Yarger, "Elucidating silk structure using solid-state NMR," *Soft Matter*, vol. 9, no. 48, pp. 11440–11450, 2013.

[23] F. Mottaghitalab, H. Hosseinkhani, M. A. Shokrgozar, C. Mao, M. Yang, and M. Farokhi, "Silk as a potential candidate for bone tissue engineering," *Journal of Controlled Release*, vol. 215, pp. 112–128, 2015.

[24] M. Farokhi, F. Mottaghitalab, S. Samani et al., "Silk fibroin/-hydroxyapatite composites for bone tissue engineering," *Biotechnology advances*, vol. 36, no. 1, pp. 68–91, 2018.

[25] M. Farokhi, F. Mottaghitalab, J. Hadjati et al., "Structural and functional changes of silk fibroin scaffold due to hydrolytic degradation," *Journal of Applied Polymer Science*, vol. 131, no. 6, 2014.

[26] X. Hu, K. Shmelev, L. Sun et al., "Regulation of silk material structure by temperature-controlled water vapor annealing," *Biomacromolecules*, vol. 12, no. 5, pp. 1686–1696, 2011.

[27] C. Correia, S. Bhumiratana, L.-P. Yan et al., "Development of silk-based scaffolds for tissue engineering of bone from human adipose-derived stem cells," *Acta Biomaterialia*, vol. 8, no. 7, pp. 2483–2492, 2012.

[28] S.-H. Park, E. S. Gil, H. Shi, H. J. Kim, K. Lee, and D. L. Kaplan, "Relationships between degradability of silk scaffolds and osteogenesis," *Biomaterials*, vol. 31, no. 24, pp. 6162–6172, 2010.

[29] Q. Lu, X. Hu, X. Wang et al., "Water-insoluble silk films with silk I structure," *Acta Biomaterialia*, vol. 6, no. 4, pp. 1380–1387, 2010.

[30] H. Zhang, J. Magoshi, M. Becker, J. Chen, and R. Matsunaga, "Thermal properties of *Bombyx mori* silk fibers," *Journal of Applied Polymer Science*, vol. 86, no. 8, pp. 1817–1820, 2002.

[31] A. Motta, L. Fambri, and C. Migliaresi, "Regenerated silk fibroin films: thermal and dynamic mechanical analysis," *Macromolecular Chemistry and Physics-MACROMOL CHEM PHYSICS*, vol. 203, no. 10-11, pp. 1658–1665, 2002.

[32] A. Martel, M. Burghammer, R. J. Davies, and C. Riekel, "Thermal behavior of Bombyx mori silk: evolution of crystalline parameters, molecular structure, and mechanical properties," *Biomacromolecules*, vol. 8, no. 11, pp. 3548–3556, 2007.

[33] L. F. Drummy, D. M. Phillips, M. O. Stone, B. L. Farmer, and R. R. Naik, "Thermally induced α-helix to β-sheet transition in regenerated silk fibers and films," *Biomacromolecules*, vol. 6, no. 6, pp. 3328–3333, 2005.

[34] R. L. Moy, A. Lee, and A. Zalka, "Commonly used suture materials in skin surgery," *American Family Physician*, vol. 44, no. 6, pp. 2123–2128, 1991.

[35] X. Y. Luan, Y. Wang, X. Duan et al., "Attachment and growth of human bone marrow derived mesenchymal stem cells on regenerated antheraea pernyi silk fibroin films," *Biomedical materials (Bristol, England)*, vol. 1, no. 4, pp. 181–187, 2006.

[36] A. Schneider, X. Y. Wang, D. L. Kaplan, J. A. Garlick, and C. Egles, "Biofunctionalized electrospun silk mats as a topical bioactive dressing for accelerated wound healing," *Acta Biomaterialia*, vol. 5, no. 7, pp. 2570–2578, 2009.

[37] M. Li, M. Ogiso, and N. Minoura, "Enzymatic degradation behavior of porous silk fibroin sheets," *Biomaterials*, vol. 24, no. 2, pp. 357–365, 2003.

[38] S. Yan, C. Zhao, X. Wu, Q. Zhang, and M. Li, "Gelation behavior of Antheraea pernyi silk fibroin," *Science China Chemistry*, vol. 53, no. 3, pp. 535–541, 2010.

[39] M. Puerta, M. S. Peresin, and A. Restrepo-Osorio, "Effects of chemical post-treatments on structural and physicochemical properties of silk fibroin films obtained from silk fibrous

waste," *Frontiers in Bioengineering and Biotechnology*, vol. 8, article 523949, 2020.

[40] D. Naskar, R. R. Barua, A. K. Ghosh, and S. Kundu, "Introduction to silk biomaterials," in *Silk biomaterials for tissue engineering and regenerative medicine*, pp. 3–40, Woodhead Publishing, 2014.

[41] A. J. Singer and R. A. F. Clark, "Cutaneous wound healing," *New England Journal of Medicine*, vol. 341, no. 10, pp. 738–746, 1999.

[42] A. C. O. Gonzalez, T. F. Costa, Z. A. Andrade, and A. R. A. P. Medrado, "Wound healing - a literature review," *Anais Brasileiros de Dermatologia*, vol. 91, no. 5, pp. 614–620, 2016.

[43] K. S. Midwood, L. V. Williams, and J. E. Schwarzbauer, "Tissue repair and the dynamics of the extracellular matrix," *The International Journal of Biochemistry & Cell Biology*, vol. 36, no. 6, pp. 1031–1037, 2004.

[44] G. C. Gurtner, S. Werner, Y. Barrandon, and M. T. Longaker, "Wound repair and regeneration," *Nature*, vol. 453, no. 7193, pp. 314–321, 2008.

[45] F. M. Wood, "Skin regeneration: the complexities of translation into clinical practise," *The International Journal of Biochemistry & Cell Biology*, vol. 56, pp. 133–140, 2014.

[46] J. M. Reinke and H. Sorg, "Wound repair and regeneration," *European Surgical Research*, vol. 49, no. 1, pp. 39–45, 2012.

[47] M. W. Ferguson, "Wound healing–scar wars," *The Ulster medical journal*, vol. 67, Supplement 1, pp. 37–40, 1998.

[48] W. A. Border and E. Ruoslahti, "Transforming growth factor-beta in disease: the dark side of tissue repair," *The Journal of Clinical Investigation*, vol. 90, no. 1, pp. 1–7, 1992.

[49] V. Agarwal, F. M. Wood, M. Fear, and K. S. Iyer, "Polymeric Nanofibre scaffold for the delivery of a transforming growth factor $\beta 1$ inhibitor," *Australian Journal of Chemistry*, vol. 70, no. 3, pp. 280–285, 2016.

[50] S.-Y. Ong, J. Wu, S. M. Moochhala, M.-H. Tan, and J. Lu, "Development of a chitosan-based wound dressing with improved hemostatic and antimicrobial properties," *Biomaterials*, vol. 29, no. 32, pp. 4323–4332, 2008.

[51] D. Wyatt, D. N. McGowan, and M. P. Najarian, "Comparison of a hydrocolloid dressing and silver sulfadiazine cream in the outpatient management of second-degree burns," *The Journal of trauma*, vol. 30, no. 7, pp. 857–865, 1990.

[52] D. Konrad, M. Tsunoda, K. Weber, S. J. Corney, and L. Ullmann, "Effects of a topical silver sulfadiazine polyurethane dressing (Mikacure) on wound healing in experimentally infected wounds in the pig. A pilot study," *Journal of Experimental Animal Science*, vol. 42, no. 1, pp. 31–43, 2002.

[53] I. M. Vassallo and C. Formosa, "Comparing calcium alginate dressings to vacuum-assisted closure: a clinical trial," *Wounds: a compendium of clinical research and practice*, vol. 27, no. 7, pp. 180–190, 2015.

[54] H. Powell, D. Supp, and S. Boyce, "Influence of electrospun collagen on wound contraction of engineered skin substitutes," *Biomaterials*, vol. 29, no. 7, pp. 834–843, 2008.

[55] M. T. Sultan, J. Y. Jeong, Y. B. Seo et al., "Fabrication and characterization of the porous duck's feet collagen sponge for wound healing applications," *Journal of Biomaterials Science, Polymer Edition*, vol. 29, no. 7-9, pp. 960–971, 2018.

[56] R. Uppal, G. N. Ramaswamy, C. Arnold, R. Goodband, and Y. Wang, "Hyaluronic acid nanofiber wound dressing–production, characterization, and *in vivo* behavior," *Journal of biomedical materials research Part B, Applied biomaterials*, vol. 97, no. 1, pp. 20–29, 2011.

[57] F. M. Wood, "Chapter 73- Therapeutic applications: tissue engineering of skin," in *Principles of Regenerative Medicine*, A. Atala, R. Lanza, A. G. Mikos, and R. Nerem, Eds., pp. 1281–1295, Academic Press, Boston, Third Edition edition, 2019.

[58] S. Seaman, "Dressing selection in chronic wound management," *Journal of the American Podiatric Medical Association*, vol. 92, no. 1, pp. 24–33, 2002.

[59] M. Gholipourmalekabadi, S. Sapru, A. Samadikuchaksaraei, R. L. Reis, D. L. Kaplan, and S. C. Kundu, "Silk fibroin for skin injury repair: where do things stand?," *Advanced drug delivery reviews*, vol. 153, pp. 28–53, 2020.

[60] O. J. Lee, H. W. Ju, J. H. Kim et al., "Development of artificial dermis using 3D electrospun silk fibroin nanofiber matrix," *Journal of biomedical nanotechnology*, vol. 10, no. 7, pp. 1294–1303, 2014.

[61] E. J. Chung, H. W. Ju, H. J. Park, and C. Park, "Three-layered scaffolds for artificial esophagus using poly(ε-caprolactone) nanofibers and silk fibroin: an experimental study in a rat model," *Journal of Biomedical Materials Research Part A*, vol. 103, no. 6, pp. 2057–2065, 2015.

[62] C. Martínez-Mora, A. Mrowiec, E. García-Vizcaíno, A. Alcaraz, J. Cenis, and F. Nicolás, "Fibroin and sericin from *Bombyx mori* silk stimulate cell migration through upregulation and phosphorylation of c-Jun," *Plo S one*, vol. 7, no. 7, article e42271, 2012.

[63] Y. R. Park, M. T. Sultan, H. J. Park et al., "NF-κB signaling is key in the wound healing processes of silk fibroin," *Acta Biomaterialia*, vol. 67, pp. 183–195, 2018.

[64] W. Abdel-Naby, B. Cole, A. Liu et al., "Treatment with solubilized silk-derived protein (SDP) enhances rabbit corneal epithelial wound healing," *PloS one*, vol. 12, no. 11, article e0188154, 2017.

[65] M. Gholipourmalekabadi, M. Mozafari, M. Bandehpour et al., "Optimization of nanofibrous silk fibroin scaffold as a delivery system for bone marrow adherent cells: *in vitro* and *in vivo* studies," *Biotechnology and applied biochemistry*, vol. 62, no. 6, pp. 785–794, 2015.

[66] M. Gholipourmalekabadi, A. Samadikuchaksaraei, A. M. Seifalian et al., "Silk fibroin/amniotic membrane 3D bi-layered artificial skin," *Biomedical materials (Bristol, England)*, vol. 13, no. 3, article 035003, 2018.

[67] Y. R. Park, H. W. Ju, J. M. Lee et al., "Three-dimensional electrospun silk-fibroin nanofiber for skin tissue engineering," *International journal of biological macromolecules*, vol. 93, no. Part B, pp. 1567–1574, 2016.

[68] O. O. Ige, L. E. Umoru, and S. Aribo, "Natural products: a minefield of biomaterials," *ISRN Materials Science*, vol. 2012, Article ID 983062, 20 pages, 2012.

[69] H. Rodríguez-Tobías, G. Morales, and D. Grande, "Comprehensive review on electrospinning techniques as versatile approaches toward antimicrobial biopolymeric composite fibers," *Materials Science and Engineering: C*, vol. 101, pp. 306–322, 2019.

[70] S. Meka, S. Kumar Verma, V. Agarwal, and K. Chatterjee, "In situ silication of polymer nanofibers to engineer multi-biofunctional composites," *Chemistry Select*, vol. 3, no. 13, pp. 3762–3773, 2018.

[71] L. Krishna, S. Nilawar, M. Ponnalagu et al., "Fiber diameter differentially regulates function of retinal pigment and corneal epithelial cells on nanofibrous tissue scaffolds," *ACS Applied Bio Material*, vol. 3, no. 2, pp. 823–837, 2020.

[72] S. R. K. Meka, V. Agarwal, and K. Chatterjee, "In situ preparation of multicomponent polymer composite nanofibrous scaffolds with enhanced osteogenic and angiogenic activities," *Materials science & engineering C, Materials for biological applications*, vol. 94, pp. 565–579, 2019.

[73] X. Zong, H. Bien, C. Chung et al., "Electrospun fine-textured scaffolds for heart tissue constructs," *Biomaterials*, vol. 26, no. 26, pp. 5330–5338, 2005.

[74] P. X. Ma and R. Zhang, "Synthetic nano-scale fibrous extracellular matrix," *Journal of Biomedical Materials Research*, vol. 46, no. 1, pp. 60–72, 1999.

[75] T. Hodgkinson, X.-F. Yuan, and A. Bayat, "Electrospun silk fibroin fiber diameter influences in vitro dermal fibroblast behavior and promotes healing of ex vivo wound models," *Journal of Tissue Engineering*, vol. 5, 2014.

[76] A. S. Badami, M. R. Kreke, M. S. Thompson, J. S. Riffle, and A. S. Goldstein, "Effect of fiber diameter on spreading, proliferation, and differentiation of osteoblastic cells on electrospun poly(lactic acid) substrates," *Biomaterials*, vol. 27, no. 4, pp. 596–606, 2006.

[77] B. Bondar, S. Fuchs, A. Motta, C. Migliaresi, and C. J. Kirkpatrick, "Functionality of endothelial cells on silk fibroin nets: comparative study of micro- and nanometric fibre size," *Biomaterials*, vol. 29, no. 5, pp. 561–572, 2008.

[78] E. Suarez, F. Syed, T. A. Rasgado, A. Walmsley, P. Mandal, and A. Bayat, "Skin equivalent tensional force alters keloid fibroblast behavior and phenotype," *Wound repair and regeneration: official publication of the Wound Healing Society [and] the European Tissue Repair Society*, vol. 22, no. 5, pp. 557–568, 2014.

[79] E. Suarez, F. Syed, T. Alonso-Rasgado, P. Mandal, and A. Bayat, "Up-regulation of tension-related proteins in keloids: knockdown of Hsp 27, $\alpha 2\beta 1$-integrin, and PAI-2 shows convincing reduction of extracellular matrix production," *Plastic and reconstructive surgery*, vol. 131, no. 2, pp. 158e–173e, 2013.

[80] S. Ichihara, Y. Inada, and T. Nakamura, "Artificial nerve tubes and their application for repair of peripheral nerve injury: an update of current concepts," *Injury*, vol. 39, Supplement 4, pp. 29–39, 2008.

[81] I. V. Yannas, M. Zhang, and M. H. Spilker, "Standardized criterion to analyze and directly compare various materials and models for peripheral nerve regeneration," *Journal of biomaterials science Polymer edition*, vol. 18, no. 8, pp. 943–966, 2007.

[82] K. Murakami, H. Aoki, S. Nakamura et al., "Hydrogel blends of chitin/chitosan, fucoidan and alginate as healing-impaired wound dressings," *Biomaterials*, vol. 31, no. 1, pp. 83–90, 2010.

[83] K. H. Bouhadir, K. Y. Lee, E. Alsberg, K. L. Damm, K. W. Anderson, and D. J. Mooney, "Degradation of partially oxidized alginate and its potential application for tissue engineering," *Biotechnology Progress*, vol. 17, no. 5, pp. 945–950, 2001.

[84] H. Niiyama and Y. Kuroyanagi, "Development of novel wound dressing composed of hyaluronic acid and collagen sponge containing epidermal growth factor and vitamin C derivative," *Journal of Artificial Organs*, vol. 17, no. 1, pp. 81–87, 2014.

[85] J. A. Burdick and G. D. Prestwich, "Hyaluronic acid hydrogels for biomedical applications," *Advanced Materials*, vol. 23, no. 12, pp. H41–H56, 2011.

[86] H. W. Ju, O. J. Lee, B. M. Moon et al., "Silk fibroin based hydrogel for regeneration of burn induced wounds," *Tissue Engineering and Regenerative Medicine*, vol. 11, no. 3, pp. 203–210, 2014.

[87] J. M. Lee, M. T. Sultan, S. H. Kim et al., "Artificial auricular cartilage using silk fibroin and polyvinyl alcohol hydrogel," *International journal of molecular sciences*, vol. 18, no. 8, p. 1707, 2017.

[88] J. L. Drury and D. J. Mooney, "Hydrogels for tissue engineering: scaffold design variables and applications," *Biomaterials*, vol. 24, no. 24, pp. 4337–4351, 2003.

[89] S. Kapoor and S. C. Kundu, "Silk protein-based hydrogels: promising advanced materials for biomedical applications," *Acta Biomaterialia*, vol. 31, pp. 17–32, 2016.

[90] O. Hakimi, D. P. Knight, F. Vollrath, and P. Vadgama, "Spider and mulberry silkworm silks as compatible biomaterials," *Composites Part B: Engineering*, vol. 38, no. 3, pp. 324–337, 2007.

[91] M. A. de Moraes, E. Paternotte, D. Mantovani, and M. M. Beppu, "Mechanical and biological performances of new scaffolds made of collagen hydrogels and fibroin microfibers for vascular tissue engineering," *Macromolecular bioscience*, vol. 12, no. 9, pp. 1253–1264, 2012.

[92] A. Nova, S. Keten, N. M. Pugno, A. Redaelli, and M. J. Buehler, "Molecular and nanostructural mechanisms of deformation, strength and toughness of spider silk fibrils," *Nano letters*, vol. 10, no. 7, pp. 2626–2634, 2010.

[93] X. X. Xia, Z. G. Qian, C. S. Ki, Y. H. Park, D. L. Kaplan, and S. Y. Lee, "Native-sized recombinant spider silk protein produced in metabolically engineered *Escherichia coli* results in a strong fiber," *Proceedings of the National Academy of Sciences of the United States of America*, vol. 107, no. 32, pp. 14059–14063, 2010.

[94] S. Keten, Z. Xu, B. Ihle, and M. J. Buehler, "Nanoconfinement controls stiffness, strength and mechanical toughness of β-sheet crystals in silk," *Nature materials*, vol. 9, no. 4, pp. 359–367, 2010.

[95] P. Thangavel, B. Ramachandran, R. Kannan, and V. Muthuvijayan, "Biomimetic hydrogel loaded with silk and l-proline for tissue engineering and wound healing applications," *Journal of biomedical materials research Part B, Applied biomaterials*, vol. 105, no. 6, pp. 1401–1408, 2017.

[96] X. Gu, X. Chen, X. Tang et al., "Pure-silk fibroin hydrogel with stable aligned micropattern toward peripheral nerve regeneration," *Nanotechnology Reviews*, vol. 10, no. 1, pp. 10–19, 2021.

[97] H. Liu, H. Fan, Y. Wang, S. L. Toh, and J. C. H. Goh, "The interaction between a combined knitted silk scaffold and microporous silk sponge with human mesenchymal stem cells for ligament tissue engineering," *Biomaterials*, vol. 29, no. 6, pp. 662–674, 2008.

[98] W. Shen, X. Chen, J. Chen et al., "The effect of incorporation of exogenous stromal cell-derived factor-1 alpha within a knitted silk-collagen sponge scaffold on tendon regeneration," *Biomaterials*, vol. 31, no. 28, pp. 7239–7249, 2010.

[99] J. Liu, L. Yan, W. Yang et al., "Controlled-release neurotensin-loaded silk fibroin dressings improve wound

healing in diabetic rat model," *Bioactive Materials*, vol. 4, pp. 151–159, 2019.

[100] A. Sugihara, K. Sugiura, H. Morita et al., "Promotive effects of a silk film on epidermal recovery from full-thickness skin wounds," *Proceedings of the Society for Experimental Biology and Medicine Society for Experimental Biology and Medicine (New York, NY)*, vol. 225, no. 1, pp. 58–64, 2000.

[101] A. Aykac, B. Karanlik, and A. O. Sehirli, "Protective effect of silk fibroin in burn injury in rat model," *Gene*, vol. 641, pp. 287–291, 2018.

[102] D. Jao, X. Mou, and X. Hu, "Tissue regeneration: a silk road," *Journal of Functional Biomaterial*, vol. 7, no. 3, p. 22, 2016.

[103] D. W. Infanger, W. Abdel-Naby, J. J. Kalal, N. B. Paulson, Y. Bai, and B. D. Lawrence, "Silk-Derived Protein-4 (SDP-4) inhibits Nuclear Factor Kappa B (NF-κB) inflammatory signaling that underlies Dry Eye Disease (DED)," *Investigative Opthomology and Visual Science*, vol. 60, no. 9, p. 2820, 2019.

[104] L. Wang, X. Wu, T. Shi, and L. Lu, "Epidermal growth factor (EGF)-induced corneal epithelial wound healing through nuclear factor κB subtype-regulated CCCTC binding factor (CTCF) activation," *J Biol Chem.*, vol. 288, no. 34, pp. 24363–24371, 2013.

[105] Y. Shi, B. Shu, R. Yang et al., "Wnt and notch signaling pathway involved in wound healing by targeting c-Myc and Hes 1 separately," *Stem Cell Research & Therapy*, vol. 6, no. 1, p. 120, 2015.

[106] F. Cheng, Y. Shen, P. Mohanasundaram et al., "Vimentin coordinates fibroblast proliferation and keratinocyte differentiation in wound healing via TGF-β-Slug signaling," *Proceedings of the National Academy of Sciences of the United States of America*, vol. 113, no. 30, pp. E4320–E4327, 2016.

[107] J. Chen, Y. Chen, Y. Chen et al., "Epidermal CFTR suppresses MAPK/NF-κB to promote cutaneous wound healing," *Cellular physiology and biochemistry: international journal of experimental cellular physiology, biochemistry, and pharmacology*, vol. 39, no. 6, pp. 2262–2274, 2016.

[108] W. Xing, W. Guo, C. H. Zou et al., "Acemannan accelerates cell proliferation and skin wound healing through AKT/mTOR signaling pathway," *Journal of dermatological science*, vol. 79, no. 2, pp. 101–109, 2015.

[109] T. Thuraisingam, Y. Z. Xu, K. Eadie et al., "MAPKAPK-2 signaling is critical for cutaneous wound healing," *The Journal of investigative dermatology*, vol. 130, no. 1, pp. 278–286, 2010.

[110] M. T. Sultan, O. J. Lee, S. H. Kim, H. W. Ju, and C. H. Park, "Silk fibroin in wound healing process," *Advances in Experimental Medicine and Biology*, vol. 1077, pp. 115–126, 2018.

[111] C. Belda Marín, V. Fitzpatrick, D. L. Kaplan, J. Landoulsi, E. Guénin, and C. Egles, "Silk polymers and nanoparticles: a powerful combination for the design of versatile biomaterials," *Frontiers in Chemistry*, vol. 8, article 604398, 2020.

Hindawi
International Journal of Polymer Science
Volume 2021, Article ID 2462873, 8 pages
https://doi.org/10.1155/2021/2462873

Research Article

Synthesis and Characterization of Polypropylene/Ramie Fiber with Hemp Fiber and Coir Fiber Natural Biopolymer Composite for Biomedical Application

T. Sathish,[1] **Kumaran Palani**,[2] **L. Natrayan**,[1] **Anjibabu Merneedi**,[3] **Melvin Victor De Poures**,[1] **and Dinesh Kumar Singaravelu**[4]

[1]*Department of Mechanical Engineering, Saveetha School of Engineering, SIMATS, Chennai-, 600 125 Tamil Nadu, India*
[2]*Department of Mechanical Engineering, Wolaita Sodo University, Wolaita Sodo Post Box-138, Ethiopia*
[3]*Department of Mechanical Engineering, Aditya College of Engineering, Surampalem-, 533437 Andhra Pradesh, India*
[4]*Department of Mechanical Engineering, St. Peter's Institute of Higher Education and Research, Avadi, Chennai-, 600 054 Tamil Nadu, India*

Correspondence should be addressed to T. Sathish; sathish.sailer@gmail.com, Kumaran Palani; pkumaran2003et@gmail.com, and Melvin Victor De Poures; melvin.victor02@gmail.com

Received 24 June 2021; Accepted 31 August 2021; Published 17 September 2021

Academic Editor: Senthilkumar Rajagopal

In the current scenario, many natural fibers available in the world can be used in various applications in the day-to-day life of biomedical products, automobile parts, industrial products, etc. Biocomposites can replace or serve as a framework allowing the regeneration of traumatized, degenerated tissues, and organs, thus, improving the patients' quality of life. This research work is aimed at fabricating and investigating the natural biopolymer composites for biomedical applications. There are two sets of fiber composites fabricated in this research work. Ramie fiber considers a common base fiber for both composites. Hemp fibers and coir fibers were considered as filler in this research work. Biodegradable and bioresorbable polypropylene resins are used to fabricate the biocomposite using the compression moulding technique. Different proportion specimen mechanical properties were compared for bone fixtures and joint applications. The contour plots and bar charts were plotted to identify the variations in the volume percentage. The individual fiber specimens also have significant properties when compared with the composite fibers. Then, the individual superior property-based combinations such as hemp and coir fiber mixed with biodegradable and bioresorbable polypropylene/ramie fiber were recommended to produce joints and bone fixtures to alleviate pain for patients.

1. Introduction

Synthetic polymer and biodegradable polymers are commonly used in bioplastic production. Biomedical applications are currently fulfilled by using natural fibers; it can be eco-friendly and offer a safe environment. The natural fibers considered for this investigation such as (a) ramie fibers, (b) hemp fibers, and (c) coir fibers were mentioned in Figure 1. Mamtaz et al. [1] give information about the composites of natural fibers through the water absorption basis with the help of various experiments. They mentioned the impact of sodium hydroxide concentration and different theoretical considerations with the number of mathematical relation equations and definitions. Van Krevelen [2] entirely explained the various details of the polymers such as natural fiber with different verities list in a clear approach. He also gives details about the fiber matrix by way of interfacial bonding. He also produced straightforward potentials summaries regarding numerous fibers mainly the hemp fiber.

Shahzad [3] studied the important and necessary characteristics such as thermal characteristics, time versus residual weight plots, temperature versus weight plots, and heat flow for the hemp fiber. They concluded that hemp fibers are good for glass fibers based on their basic characteristics

(a) (b) (c)

Figure 1: Schematic view of natural fibers: (a) ramie, (b) hemp, and (c) coir.

except for the variability. Similarly, the matrix of biodegradable polymers, thermoset, and thermoplastic produced the greater results of the mechanical characteristics over the glass fibers. But the major disadvantage of the hemp fiber is moisture absorption which the surface treatment on the composites can reduce.

Rajak et al. [4] give the basic details of the various natural fibers like Luffa, palm, jute, banana, rice husk, kenaf, cotton, sisal, hemp, ramie, flax, and abaca also mentioned the synthetic fibers. They provide the reinforcement details and the matrix with the corresponding applications and production technique in a neat presenting method. Shahzad [5] reviewed various papers and gave details about the hemp fiber composites, and he mentioned that they could be used for automotive parts and domestic furniture. This fiber is also used as a good replacement for reinforcement of the glass fibers. The compression moulding is suitable for hemp fiber which can be used with resins like polyethylene and polypropylene. They also give recommendations for the thermoset and thermoplastic materials related to composite reinforcements.

Munde et al. [6] discussed the coir fiber, and they focused on the characteristics based on the damping and vibration. The epoxy resin, polyethylene, and polypropylene were identified as suitable for this coir fiber. The injection moulding or the extrusion methods were used to produce the components based on the structural of automobiles. Chen et al. mentioned the resins like polypropylene and polyolefin were suitable for the ramie fibers in the injection moulding method. This fiber can be used in various biomedical applications [7].

Sebe et al. [8] clearly explained the hemp fibers reinforced composites with polyester for basic mechanical properties like impact strength and flexural strength. They used the moulding method as resin transfer. The considered mechanical characteristics are improved concerning the percentage of the fiber content in the composite. Aziz and Ansell [9] investigated the polyester reinforcement of hemp fiber with Kenaf fiber composite mechanical characteristics. They used two conditions like alkali-treated and without treatment. The flexural modulus and strength reached the greatest values for the alkali-treated composites compared with the treatment condition. They also focused on the resins used for the composite preparation and concluded that polyesters had produced greater strength.

Table 1: Natural fiber composite of ramie fiber and hemp fiber set including the resin.

Sl. no	Ramie fiber (wt%)	Hemp fiber (wt%)
1	100	0
2	75	25
3	50	50
4	25	75
5	0	100

Table 2: Natural fiber composite of ramie fiber and hemp fiber set 2 including the resin.

Sl. no	Ramie fiber (wt%)	Hemp fiber (wt%)
1	100	0
2	75	25
3	50	50
4	25	75
5	0	100

Panthapulakkal et al. [10, 11] expressed that the hybridizing method is suitable for the composites of the natural fibers and synthetic fibers based on maximum mechanical characteristics. But they preferred the natural fibers because of their biodegradability. Djafar et al. [12] experimentally analysed the reinforced composites of the ramie fibers with epoxy resin and woven ramie fibers. They only focused on bending and tensile stress with SEM images and Fourier transform infrared spectroscopy analysis results. Yu et al. [13], Paiva et al. [14], and Goda et al. [15] studied and expressed ramie fiber is the suitable fiber for the reinforcement composites when compared to other fibers. It has the maximum usage in textile productions. It has the greatest tensile property from four hundred to a maximum of 1600 MPa; these values are greater than jute and flax fiber. Ramie is the preferred fiber for the research.

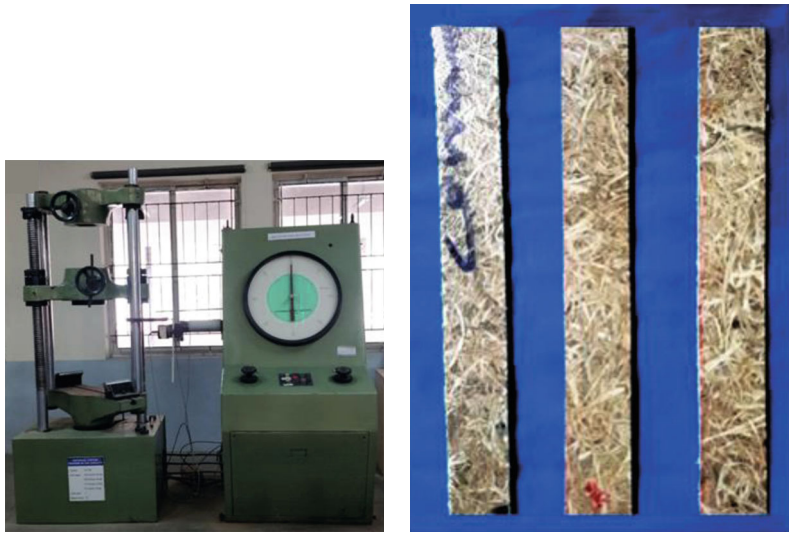

(a) (b)

Figure 2: Tensile test: (a) UTM machine and (b) composite specimens—ASTM D3822.

Table 3: Experimental results of set 1 and set 2.

Fiber with ramie fiber %	Percentage of elongation %		Tensile strength (MPa)		Density (g/cm^3)		Young's modulus (GPa)	
	Hemp	Coir	Hemp	Coir	Hemp	Coir	Hemp	Coir
0	2.6	2.6	512	512	1.57	1.57	43	43
25	2.394	6.88	608	455.6	1.552	1.514	48.25	35.8
50	2.188	11.16	704	399.2	1.534	1.458	53.5	28.6
75	1.982	15.44	800	342.8	1.516	1.402	58.75	21.4
100	1.57	24	992	230	1.48	1.29	69	7

Srinivas et al. [16] explained natural fiber composites and mentioned the basic properties of the coir, ramie, and hemp fiber. Lakshumu Naidu et al. [17] mentioned various natural fiber basic physical properties and chemical properties. Mwaikambo [18], Ticoalu et al. [19], and Sen and Reddy [20] explained the various applications of the various natural fibers among the important applications were discussed. Hemp fiber is used in products for construction, furniture, packaging materials, textiles, etc. Similarly, coir fibers are also used for roofing sheets, casing of mirrors, ropes, brushes, paper weights, etc. Likewise, ramie fiber can be used as nets for fishing, filter cloths, materials for backing the products, sewing threads, furniture, etc.

There are many reports on the mechanical and physical properties of natural fiber reinforced polymer composites, but the effect of coir fiber and hemp fiber on the mechanical behavior of ramie fiber reinforced polymer composites is scarcely reported. The objective of this research work newly attempts to prepare the biopolymer for biomedical applications using different natural fibers. The prepared composites were tested to find the tensile strength, percentage of elongation, and Young's modulus properties. Ramie fiber considers as the base fiber. The different volume percentages of hemp fiber and coir fiber were taken. There are two sets of fiber composite fabricated for the properties comparison. One set is the composites of the ramie fiber with hemp fiber and another composite created with ramie fiber with coir fiber in various combinations of volume percentage of the fiber. The basic desirable mechanical properties were measured and compared to identify the fibers' maximum output-based volume percentage contribution.

2. Experimental Setup

There are two sets of composites fabricated. They are increasing hemp fiber concentration and decreasing ramie fiber concentration in total volume. In this investigation, two sets of composite fiber combinations in each set contain the ramie fiber's participation in the percentage of volume in total volume. The fiber composite of set 1 contains the ramie fiber with hemp fiber in various proportions as per Table 1. Similarly, the composite of set 2 contains the ramie fiber with the coir fiber in different proportions as per Table 2 with reducing ramie fiber volume with the incremental volume of the coir fiber volume in the total volume of the composites.

In this investigation, the two sets of composite fiber combinations in each set contain the ramie fiber's participation in the percentage of volume in total volume. There are two sets of composites fabricated. The fiber composite of

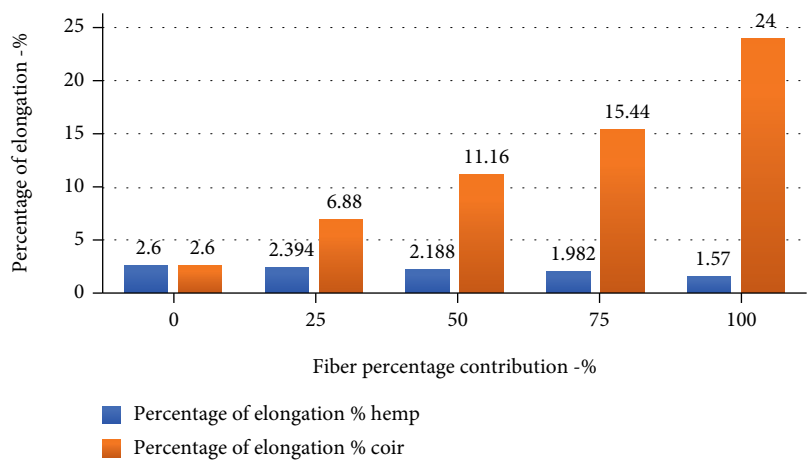

Figure 3: Comparison of the experimental results of percentage of elongation.

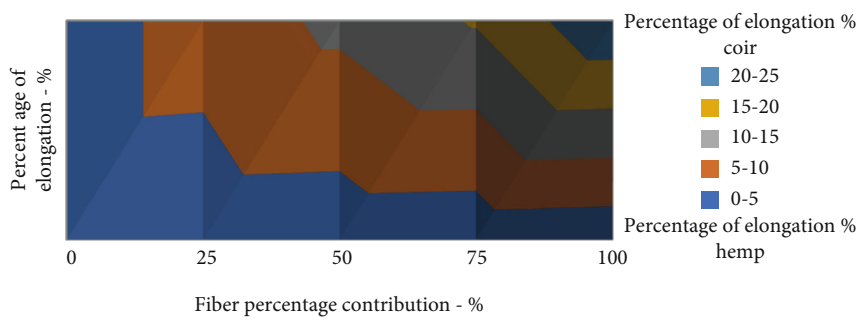

Figure 4: Comparison of the experimental results of elongation as contour plot.

set 1 contains the ramie fiber with hemp fiber in various proportions as per Table 1, like increasing hemp fiber concentration and decreasing Ramie fiber concentration in total volume. Similarly, the composite of set 2 contains the ramie fiber with the coir fiber in different proportions as per Table 2 with reducing ramie fiber volume with the incremental volume of the coir fiber volume in the total volume of the composites.

There are five composites created for each set of combinations. The biodegradable and bioresorbable polypropylene is used as a resin because it can be suitable for these three fibers. Hemp and coir have the individual mechanical properties higher and lower, respectively, when compared with the ramie fiber. So, the impacts of the combinations were considered for this investigation. The ancient method like compression moulding is selected to ASTM D3822 standard produce the specimens in 120 mm × 150 mm × 10 mm [21]. The two sets have similar dimensions. There are nine different specimens prepared because 100 percentage ramie fiber results can be used for both sets.

There are four different mechanical properties identified through testing. Tensile strength, percentage of elongation, and Young's modulus can be done with Figure 2 mentioned universal testing machines with the standard specifications of the specimens. Tensile test and percentage of elongation were done in the same specimen. Based on these two values, Young's modulus can be derived by the relation of the stress-strain equation-based calculations. The measuring weight comparison can identify the density of the specimens with the volume occupied relation such as unit mass per volume. Then, the corresponding values are identified for the analysis.

3. Results and Discussion

The experimental results were tabulated in Table 3 for set 1. They set 2 of the composite combinations, but the table mentions both coir and hemp fiber only because the ramie fiber covers the remaining percentage of the composite for both sets of composites. So the comparisons were also created with the coir and hemp fiber only, and there is also the mention for ramie fiber which is understood.

Figure 3 mentioned the percentage of elongation result comparison as a bar chart. 100% of coir have the highest percentage of elongation which is the individual composite. But the combination of 25% of ramie and 75% of coir fiber composite reached the maximum elongation (15.44%) and the minimum percentage of elongation (1.982%) obtained by the composite of the composite 25% of ramie and 75% of hemp fiber. These percentage elongation variations are also represented as the contour plot in Figure 4 with various colours. The minimum and maximum percentage variations were mentioned as the various intensity in the diagram with different colours. The minimum range starts from 0 to 5%,

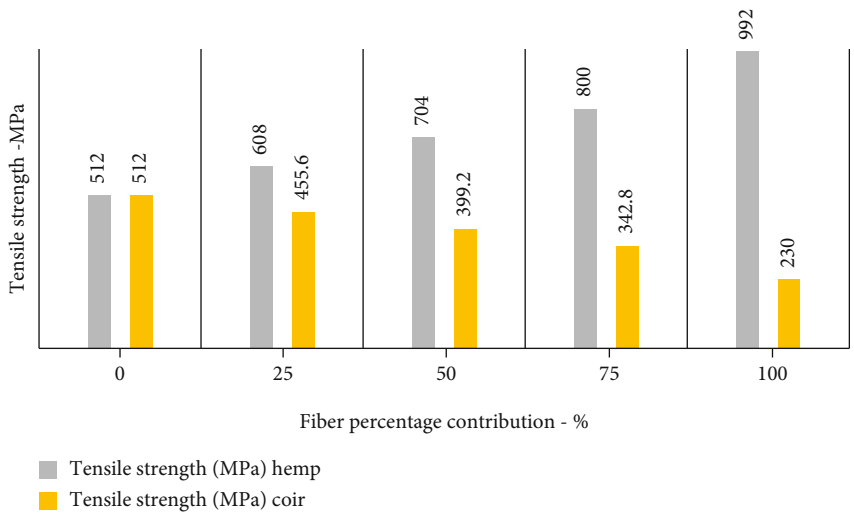

Figure 5: Comparison of the experimental results. Tensile strength as a bar chart.

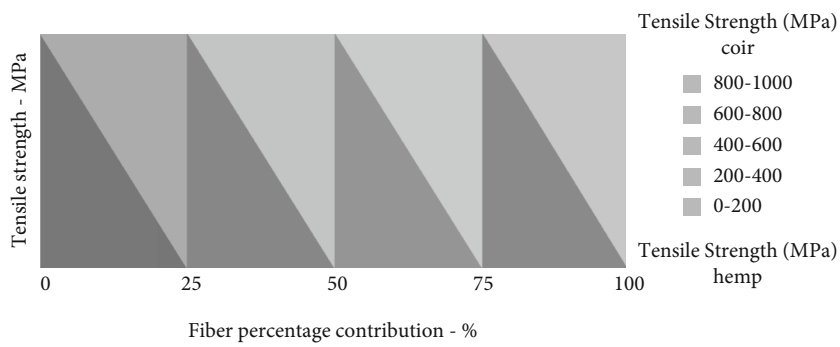

Figure 6: Comparison of the experimental results. Tensile strength as a contour plot.

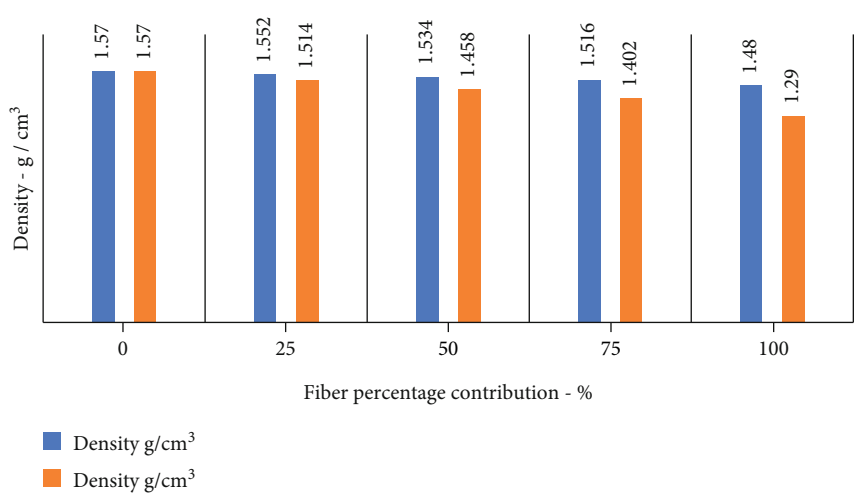

Figure 7: Experimental consequence of density as a bar chart.

and the highest intensity is reached for the 20 to 25% of elongation percentage.

The tensile strength-based result was mentioned in the bar chat in Figure 5 and the contour plot in Figure 6 for clear identification. The highest tensile strength is achieved for the 100% of the hemp fiber composite specimen. There is no ramie fiber contribution. So the maximum tensile strength such as 800 MPa is obtained for the composite with 75% of hemp fiber with 25% of the ramie fiber composite [18]. Similarly, the lowest tensile strength was obtained for the 25% ramie fiber with 75% coir fiber composite. But the coir fiber-based maximum tensile strength is obtained at

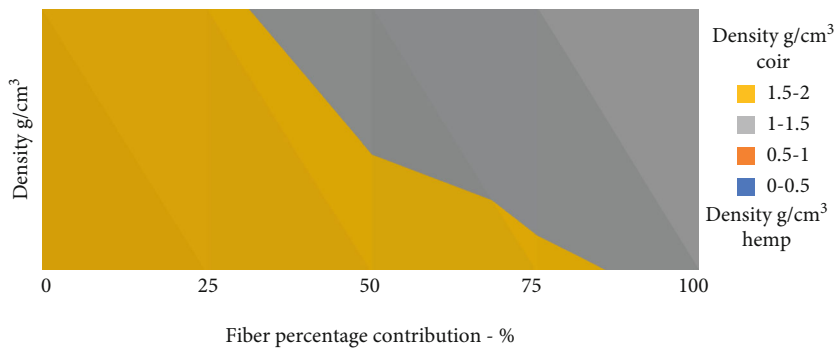

Figure 8: Experimental consequence of density as a contour plot.

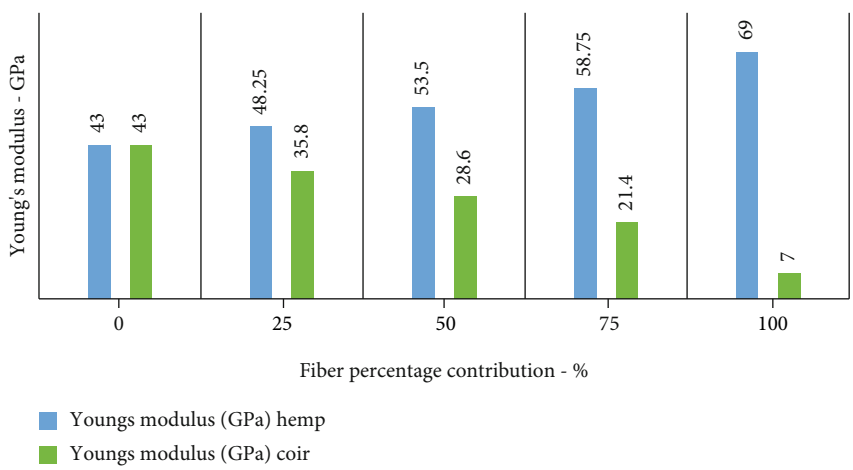

Figure 9: Experimental consequence of Young's modulus as a bar chart.

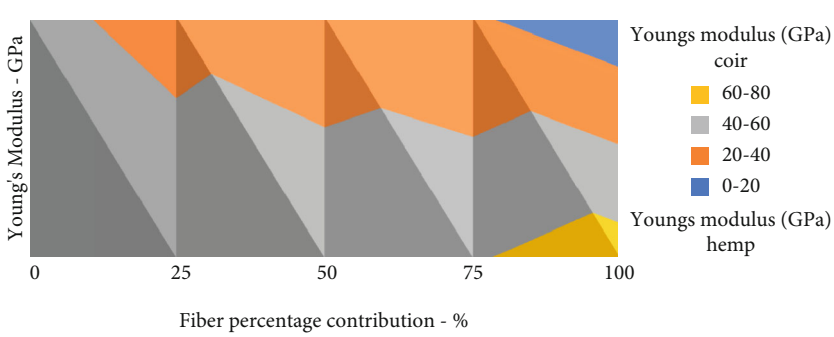

Figure 10: Experimental consequence of Young's modulus as a contour plot.

455 MPa of tensile strength for the composite with 75% of ramie fiber, and the remaining 25% is coir fiber in the total volume of the composite.

Figures 7 and 8 showed the experimentally measured and calculated density values variations of the composites as the graphical representation of bar chart and contour plot, respectively, with the standard deviation of 1.25 [19]. The maximum density is obtained for the individual fiber composite of the ramie fiber composite such as 1.57 g/cm^3. Similarly, minimum density can be reached for the individual fiber specimen of the coir fiber as 1.29 g/cm^3. But the combination-based composite of 75% ramie fiber and 25% hemp fiber reached a higher density of 1.552 g/cm^3 than the composite of the 25% coir and 75% ramie fiber-based density of 1.514 g/cm^3. Contour plots have the two variation regions only such as 1.5 to 2.0 g/cm^3 and 1.0 to 1.5 g/cm^3.

The outcomes of Young's modulus of set 1 and set 2 were mentioned in Figure 9 as a bar chart similar to Figure 10 as a contour plot. The highest Young's modulus (69 GPa) value is reached for 100% of the hemp fiber individual composite. Similarly, a very low Young's modulus value such as 7 GPa is reached for 100% of individual coir fiber composite [20]. But the combination of mixing-based composite has the following results. The 75% of hemp and 25% of ramie fiber composite reached the highest Young's modulus as 58.75 GPa.

Similarly, the 25% of coir fiber and 75% of ramie fiber composite produced 35.8 GPa of Young's modulus value [21]. The individual ramie fiber composite has Young's modulus of 43 GPa. The use of hemp fiber and coir fiber mixed with biodegradable and bioresorbable polypropylene/ramie fiber can produce joints and bone fixtures to alleviate pain for patients.

4. Conclusions

This examination of comparison of properties on ramie fiber with hemp fiber and coir fiber composites gives the following as a comparison results

(i) Both the combination of set 1 and set 2 of the fiber composite can be produced

(ii) From the tensile strength analysis, the set 1 results provided the higher tensile values (704 MPa) compared to set 2 results (399.2 MPa) for the properties such as tensile strength

(iii) In density analysis, set 1was registered as 1.54 g/cm^3, and set 2 was registered as 1.458 g/cm^3 in Young's modulus analysis. Set 1was recorded as 53.5 GPa and set 2 was recorded as 28.6 GPa

(iv) For tensile strength and Young's modulus on 75% of hemp fiber with 25% of ramie fiber composite produced the maximum values (tensile strength: 608 MPa, Young's modulus: 48.25 GPa) among the composite fibers considered for this investigation

(v) From density analysis, 25% of hemp fiber and 75% of ramie fiber reached the maximum density among the composite fibers were observed as 1.516 g/cm^3

(vi) The percentage of elongation of set 2 has greater results than the set 1 fiber composites such as 15.44%

(vii) Here, 25% of the coir fiber with 75% of the ramie fiber produced the maximum % of elongation results

(viii) Hence, the ramie fiber with hemp fiber (set 1) is suitable for the tensile strength, density, and Young's modulus-based biomedical applications. The ramie fiber with coir fiber (set 2) is suitable for elongation-based biomedical applications

(ix) The use of hemp fiber and coir fiber mixed with biodegradable and bioresorbable polypropylene/ramie fiber can produce joints and bone fixtures to alleviate pain for patients

Data Availability

The data used to support the findings of this study are included in the article. Should further data or information be required, these are available from the corresponding author upon request.

Disclosure

This study was performed as a part of the Employment of Wolaita Sodo University, Wolaita Sodo, Ethiopia.

Conflicts of Interest

The authors declare that there are no conflicts of interest regarding the publication of this paper.

Acknowledgments

The authors thank Saveetha School of Engineering, SIMATS—Chennai for the technical assistance to complete this experimental work, and the authors appreciate the supports from Wolaita Sodo University, Ethiopia.

References

[1] H. Mamtaz, M. H. Fouladi, M. Al-Atabi, and S. N. Namasivayam, "Acoustic absorption of natural fiber composites," *Journal of Engineering*, Article ID 5836107, 2016.

[2] D. W. van Krevelen, *Properties of Polymers 3th Edition*, Elsevier, New York, 1997.

[3] A. Shahzad, "A study in physical and mechanical properties of hemp fibres," *Corporation Advances in Materials Science and Engineering*, vol. 2013, article 325085, pp. 1–9, 2013.

[4] D. K. Rajak, D. D. Pagar, P. L. Menezes, and E. Linul, "Fiber-reinforced polymer composites: manufacturing, properties, and applications," *Polymers*, vol. 11, p. 1667, 2019.

[5] A. Shahzad, "Hemp fiber and its composites—a review," *J. Compos. Mater.Vol.*, vol. 46, pp. 973–986, 2011.

[6] Y. S. Munde, R. B. Ingle, and I. Siva, "Investigation to appraise the vibration and damping characteristics of coir fibre reinforced polypropylene composites," *Adv. Mater. Process. Technol.Vol.*, vol. 4, pp. 639–650, 2018.

[7] D. Chen, C. Pi, M. Chen, L. He, F. Xia, and S. Peng, "Amplitude-dependent damping properties of ramie fiber-reinforced thermoplastic composites with varying fiber content," *Polym. Compos.Vol.*, vol. 40, pp. 2681–2689, 2019.

[8] G. Sebe, N. S. Cetin, C. A. S. Hill, and M. Hughes, "RTM hemp fiber reinforced polyester composites," *Appl Compos Mater. Vol.*, vol. 7, pp. 341–349, 2000.

[9] S. H. Aziz and M. P. Ansell, "Optimising the properties of green composites," in *In: Baillie CA (ed.) Green composites*, pp. 154–180, Ch. 8. Cambridge: Woodhead Publishing Limited, 2004.

[10] S. Panthapulakkal and M. Sain, "Studies on water absorption properties of short-hemp glass fiber hybrid polypropylene composites," *Journal of Composite Materials*, vol. 41, pp. 1871–1883, 2007.

[11] S. Yogeshwaran et al., "Experimental investigation on mechanical properties of epoxy/graphene/fish scale and fermented spinach hybrid bio composite by hand lay-up technique," *Materials Today: Proceedings*, vol. 37, no. 2, pp. 1578–1583, 2021.

[12] Z. Djafar, I. Renreng, and M. Jannah, "*Tensile and bending strength analysis of ramie fiber and woven ramie reinforced epoxy composite*," *Journal of Natural Fibers*, 2020.

[13] T. Yu, J. Ren, S. Li, H. Yuan, and Y. Li, "Effect of fiber surface-treatments on the properties of poly(lactic acid)/ramie composites," *Compos Part A Appl Sci Manu.f*, vol. 41, pp. 499–505, 2010.

[14] J. C. Paiva, L. de Carvalho, V. Fonseca, S. Monteiro, and J. R. D.'. Almeida, "Analysis of the tensile strength of polyester/hybrid ramie – cotton fabric composites," *Polymer Testing*, vol. 23, pp. 131–135, 2004.

[15] K. Goda, M. S. Sreekala, A. Gomes, T. Kaji, and J. Ohgi, "Improvement of plant based natural fibers for toughening green composites – effect of load application during mercerization of ramie fibers," *Compos Part A Appl Sci Manu.f*, vol. 37, pp. 2213–2220, 2006.

[16] K. Srinivas, A. Lakshumu Naidu, and M. V. A. Raju Bahubalendruni, "A review on chemical and mechanical properties of natural fiber reinforced polymer composites," *Int. J. Performability Eng.*, vol. 13, no. 2, pp. 189–200, 2017.

[17] A. Lakshumu Naidu, V. Jagadeesh, and M. V. A. RajuBahubalendruni, "A review on chemical and physical properties of natural fiber reinforced composites," *International Journal of Advanced Research in Engineering and Technology (IJARET)*, vol. 8, no. 1, pp. 56–68, 2017.

[18] L. Mwaikambo, "Review of the history, properties and application of plant fibres," *African Journal of Science and Technology*, vol. 7, no. 2, p. 121, 2006.

[19] A. Ticoalu, T. Aravinthan, and F. Cardona, "A review of current development in natural fiber composites for structural and infrastructure applications," *In Proceedings of the Southern Region Engineering Conference(SREC '10)*, pp. 113–117, Toowoomba, Australia, 2010.

[20] T. Sen and H. N. Reddy, "Various industrial applications of hemp, kinaf, flax and ramie natural fibres," *International Journal of Innovation, Management and Technology*, vol. 2, pp. 192–198, 2011.

[21] S. Yogeshwaran et al., "Effect of waste tyre particles reinforcement on mechanical properties of jute and abaca fiber-epoxy hybrid composites with pre-treatment," *Materials Today: Proceedings*, vol. 37, no. 2, pp. 1377–1380, 2021.

Hindawi
International Journal of Polymer Science
Volume 2021, Article ID 4907027, 20 pages
https://doi.org/10.1155/2021/4907027

Review Article

Additive Manufacturing of Biopolymers for Tissue Engineering and Regenerative Medicine: An Overview, Potential Applications, Advancements, and Trends

Dhinakaran Veeman,[1] M. Swapna Sai,[1] P. Sureshkumar,[2] T. Jagadeesha,[3] L. Natrayan,[4] M. Ravichandran,[5] and Wubishet Degife Mammo[6]

[1]*Centre for Additive Manufacturing and Computational Mechanics, Chennai Institute of Technology, Chennai, 600069 Tamil Nadu, India*
[2]*Department of Mechanical Engineering, Ramco Institute of Technology, Rajapalayam, Virudhunagar, Tamil Nadu, India*
[3]*Department of Mechanical Engineering, National Institute of Technology, Calicut, India*
[4]*Department of Mechanical Engineering, Saveetha School of Engineering, SIMATS, Chennai, Tamil Nadu 602105, India*
[5]*Department of Mechanical Engineering, K. Ramakrishnan College of Engineering, Tiruchirappalli, 621 112 Tamil Nadu, India*
[6]*Mechanical Engineering Department, Wollo University, Kombolcha Institute of Technology, Kombolcha, South Wollo-208, Amhara, Ethiopia*

Correspondence should be addressed to Dhinakaran Veeman; dhinakaranv@citchennai.net, L. Natrayan; natrayanphd@gmail.com, and Wubishet Degife Mammo; wubishetdegife7@gmail.com

Received 17 July 2021; Accepted 28 August 2021; Published 9 September 2021

Academic Editor: Senthilkumar Rajagopal

As a technique of producing fabric engineering scaffolds, three-dimensional (3D) printing has tremendous possibilities. 3D printing applications are restricted to a wide range of biomaterials in the field of regenerative medicine and tissue engineering. Due to their biocompatibility, bioactiveness, and biodegradability, biopolymers such as collagen, alginate, silk fibroin, chitosan, alginate, cellulose, and starch are used in a variety of fields, including the food, biomedical, regeneration, agriculture, packaging, and pharmaceutical industries. The benefits of producing 3D-printed scaffolds are many, including the capacity to produce complicated geometries, porosity, and multicell coculture and to take growth factors into account. In particular, the additional production of biopolymers offers new options to produce 3D structures and materials with specialised patterns and properties. In the realm of tissue engineering and regenerative medicine (TERM), important progress has been accomplished; now, several state-of-the-art techniques are used to produce porous scaffolds for organ or tissue regeneration to be suited for tissue technology. Natural biopolymeric materials are often better suited for designing and manufacturing healing equipment than temporary implants and tissue regeneration materials owing to its appropriate properties and biocompatibility. The review focuses on the additive manufacturing of biopolymers with significant changes, advancements, trends, and developments in regenerative medicine and tissue engineering with potential applications.

1. Introduction

The various aspects such as type of tissue and the hormones necessary for the discrepancy and physical size are restricted to this regeneration as the body can regenerate amazingly (critical defect). Any tissue damage beyond this crucial dimension requires external assistance approaches such as tissue engineering (TE) and regenerative medicine (RM), in which the external hollows are termed yardsticks. These tissues offer a platform for cellular activity and new tissue creation [1]. In TE and RM, the scaffolds have a crucial role. These tissues are frequently supplied with growth agents in order to accelerate the differentiation between cells and selected lines to encourage the development of new tissue. For cell viability and cell prolife, the physical and chemical content plays a crucial part [2]. Biomaterial is classified

according to a wide variety of parameters, including chemical and physical composition, biodegradability, origin, and modification generations. Biomaterial is selected depending on the target tissue. Biomaterials are divided into ceramics, polymers, and composites based on their chemical composition. The biomaterial class of ceramics includes important components of inorganic metal or calcium salts [3]. The primary usage of these biomaterials has been orthodontal. Because of its resemblance with binding tissues, polymers are employed in soft tissue engineering. Mixes of ceramics and polymers comprise the composite class of biomaterials. The composites have orthopaedic and dental TE uses. Natural and manmade polymers of TE and RM are commonly employed [4]. The biodegradability and biocompatibility in natural biomaterials have plentiful availability such as collagen, chitosan, hyaluronic acid, and alginate that are commonly employed. One of the key aspects of natural polymers is the degradation of biomaterials [5].

Since these biomatters are present in the extracellular matrix (ECM), cells are very compatible and respond to growth. Collagen is one of the most frequently used natural biomaterials in several applications of scaffolds. Biopolymers have recently gathered significant interest with a view to biocomposites with a multifunctional and high efficiency that have a low environmental effect, with exclusive accessibility, renewable, environmentally friendly, and lightweight qualities [6]. Biopolymeric composites should replace for the multifaceted application of synthetic materials in optics, biochemistry, and biomedical engineering [7]. The product data is divided into two dimensions. The data are sent through the machine from the basis of the product layer by layer, and the material is dropped layer by layer, which in an additive process infuses the newest layer of material into the old layer as shown in Figure 1. The researchers have received tremendous attention in recent years from biopolymers and biodegradable synthetic polymers. Biomedical applications require the production of sustainable, stronger, and lightweight biopolymeric materials [8]. The development or choice of ways to tackle the issues of architectural design however needs a compromise between visions and aims, which generally conflicts with new biomaterials [9].

2. Need of Bioprinted Scaffolds and Its Fabrication

Tissue engineering is an alternative method for tackling the increasing need for organ transplantation. TE and RM procedures can fill the gap between the number of transplants awaiting patients and donors available [11]. Organ failure and organ transplantation from another individual is the only effective way to treat organs including the kidney, liver, pancreas, and heart in degenerative illnesses. With the production of biomaterials and scaffolds, the TE process begins. These textiles are chemically and physically changed to fulfill particular parameters in the production process including biodegradability, porosity, size, form, and bioactivity [12]. Depending on the nature of biomaterial, production, and target tissue, these requirements may be different. Cells can seed the tissue and develop the desired tissue in vitro or in the body in order to permit the host cells to enter and replace the tissue. Growth factors, hormones, and chemical indices are vital for these two methods since they define cell differentiation and tissue function [13]. Biomaterials not only permit physical cell attachment but also provide therapeutic agents such as medicines, proteins, factors for growth, and chemical indications. Most mammalian cells depend on anchor feasibility. The lack of a substratum for cellular attachment often causes the death of the cell [14]. Therefore, for surface chemical and structure of scrub materials, cell viability and function are of major importance. Three strategies—chemical alteration, change to physics, and surface coating—enhance the adhesion of cells on biomaterial and scaffold surfaces; some of the 3D porous scaffold strategies for tissue engineering purposes are represented in Table 1. The aim is to support scaffold and biomaterial cell growth and cell activity. This leads to the next stage when cells are inserted into the yards. The seeding grounds of the required cells conventionally include strategies for adding cells to scaffolds [15]. The primary cells perform the specialised function of the organ and the supporting cells, which secrete the supporting matrix, vasculature, and structural frame, during complex organ formation. Primary cells of diverse genotypes and phenotypes may be injected in order to distinguish these organisations or pluripotent cells among the required cell lines [16].

Several ways for manufacturing scaffolds exist. The manufacturing procedure is the next step to turn the biomaterials into fabrics. These manufacturing techniques are physical and chemical processes performed with the use of biomaterials for tissue engineering. Not all biomaterials are appropriate for a particular type of manufacture [17]. Biomaterials are therefore constantly updated to be used for every manufacturing procedure. Conventional production procedures include electrospinning, separating phases, drying freezes, autonomous assemblies, casting of solvents, textile technologies, injections of material, and additives. An ionic polymer solution is expelled via a fine aperture through a high voltage potential in the electrospinning process. Because of the potential difference, the solvent is sprayed in fine fibers as the solvent sprays and leaves a polymeric fragmentation [18]. Although this approach may use a wide variety of polymers, it still remains a constraint to produce scaffolds with complicated geometries and architectures. The use of a phase separation procedure can produce very porous and sophisticated three-dimensional scaffolds. A solution with distinct solvent systems is employed in this method of scaffold production [19]. One of the phases is separated with or without thermal solvents, leaving only the polymer solutions that you want. In the scaffold production method, it allows for the porosity of forged products but is restricted by the polymers and their incapacity to produce forged products with high resolution [20]. 3D printing comprises Fused Deposition Modeling (FDM), Laser Beam Melting (LBM), Selective Laser Sintering (SLS), Digital Laser Printing (DLP), PolyJet, Electron Beam Melting (EBM), and inkjet printing. Regardless of the 3D printing technique, all additives employ a common layer-by-layer design approach until the entire product is constructed. This means that a 3D structure is constructed by the continuous addition of 2D material layers. Additive production was first utilised to create

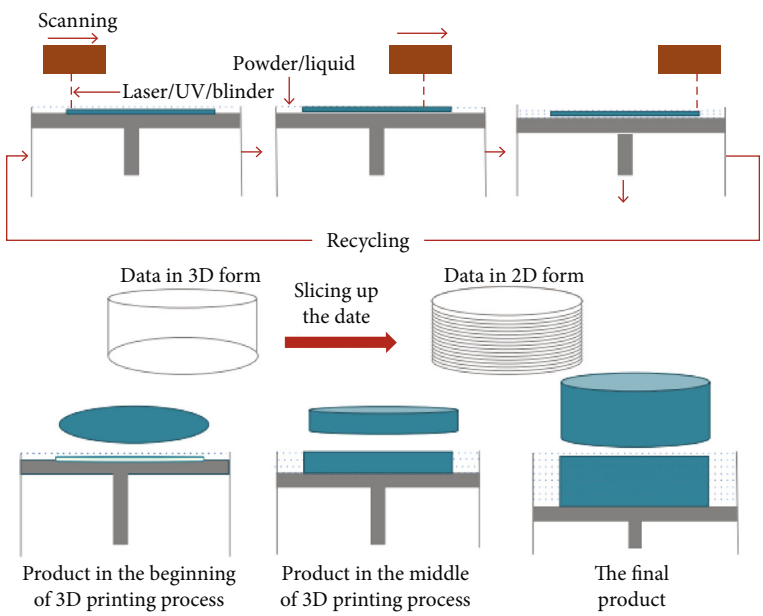

Figure 1: Schematic representation of 3D printing [10].

prototypes which were then adapted from many industries in mechanical and industrial applications [21]. This manufacturing approach has many advantages, including the capabilities to produce complex geometries, a large range of biomaterials, and various materials. Researchers have created new ideas and methods for the formation of tissues with multiple cell lines and organs using biodegradable polymers and cells [22].

3. Biopolymers and Types

Natural polymers are considered as polymers derived from living or biological resources, including plant, animal, or microorganisms and biological systems. Carbohydrate is also known as biopolymers (arabinoxylan, chitosan and starch, proteins such as gelatin and keratin, and polyhydroxyalkanoates (PHAs), poly(3-hydroxybutyrate) [P(3HB)]). In order to improve structural and functional qualities in the resulting composites, the synthesis of biopolymer composites is employed one by one or more biopolymers [30]. The composition of a biopolymer affects its functionality, while functional potential mostly depends on the behaviour of amorphous or crystalline components. Cellulose, for instance, is a structural polymer that has its crystalline shape. Chitosan is a famous component of the polysaccharide carbohydrate family. Biosustainability, biodegradability, and compatibility have been called for in the various industries [31]. It can readily be manufactured from marine sources (lobsters, crabs, and shrimps) and utilised for various biopolymer composites. Many concerns need to be considered before broad usage of biosustainable polymer are achievable, such as technical and production problems. Their functional features appear negative compared to established petroleum-based polymers and a fundamental hurdle to the wider application of biopolymer in numerous areas [32, 33]. For example, the performance of a component of biopolymers with single bonds is less than that of plastic materials as it results in a poorer mechanical characteristic. These shortcomings can be addressed in numerous methods including greasing, mixing, combining, and strengthening with other suitable ceramics and polymers [34]. Polymers come from a variety of sources including commonly manufactured polystyrene and natural biopolymers such as cellulose, protein, and microbial polyesters that are vital for a biological system structure and function [35]. The three basic forms may be categorised as biopolymers or biobased polymer composites, which depend on their source.

(1) Polymers such as starch, cellulose, arabinoxylan, and keratin are extracted or separated from biomass

(2) Polymers created from ordinary chemical processing by means of renewable biopolymer are formed through fermentation of carbohydrate by monomers such as polylactic acid (PLA) and cellulose acetate (CA)

(3) Polymers are obtained mostly from PHAs, although the creation of bacterial cellulose from digestion of microbial organisms. Biocomposite is used for the creation of materials formed from natural or biodervived polymers, like chitosan, arabinoxylane, PHAs, or PLA [36, 37]

The green composites comprising biopolymer-natural components and degradable inorganic filler are known as efficient and sustainable biocomposites. They are the topic of attention because of environmental problems and laws [39]. Biopolymers are quite strong, natural resource-derived molecules. These products are biodegradable, easily recyclable, sustainable in trade and environment and are labelled as biosustainable products [40]. In multiple possible medical applications and in other applications, chemically altered biopolymers, e.g.,

Table 1: 3D porous scaffold approaches for tissue engineering applications [23–29].

S. No.	3D technology	Materials	Growth factors	Outcomes	Application
1	Robocasting	PCL and bioactive borate glass	Human adipose-derived stem cell- (hASC-) laden	Controlled release of bioactive glass	Bone tissue engineering
2	3D bioprinting	Polycaprolactone (PCL)	Saos-2 cells seeding	The nonorthogonal structures displayed advanced E moduli than the orthogonal one, with an optimistic stimulus on the biotic performance of the cells; complex standards for the mineralization, movement of osteogenic-related genes, and deposition of the mineralized matrix	Bone tissue engineering
		Alginate/alginate-sulfate	BMP-2	Alginate/alginate sulfate bioinks allowed good 3D cell printing. Enhancement of the release of BMP-2 was achieved using alginate sulfate. Propagation and discrepancy of the reproduced osteoblasts were better	Bone tissue engineering
3	Laser sintering technique	PCL and HAp	Not defined	Subchondral bone regeneration and articular cartilage development in a rabbit model	Osteochondral tissue
4	Sol-gel method combined with 3D plotting	HAp/chitosan/silica	Mouse BMSC seeding	Compressive strength equivalent to the human trabecular bone	Bone regeneration
5	Electrospinning combined with 3D bioprinting	PCL	Laden with L929 mouse fibroblasts	Multilayered structures—3D scaffolds—with loosely packed nanofibers, with improved exterior wettability (when compared to the 2D scaffolds)	Not defined
6	Phase separation process	Cartilage ECM-derived/PLGA-βTCP-collagen type I	BMSC seeding	Improved OC regeneration. Chondro and osteogenic-induced bone marrow-derived mesenchymal stem cells (BMSC) with autonomous surroundings	Osteochondral tissue (OC)

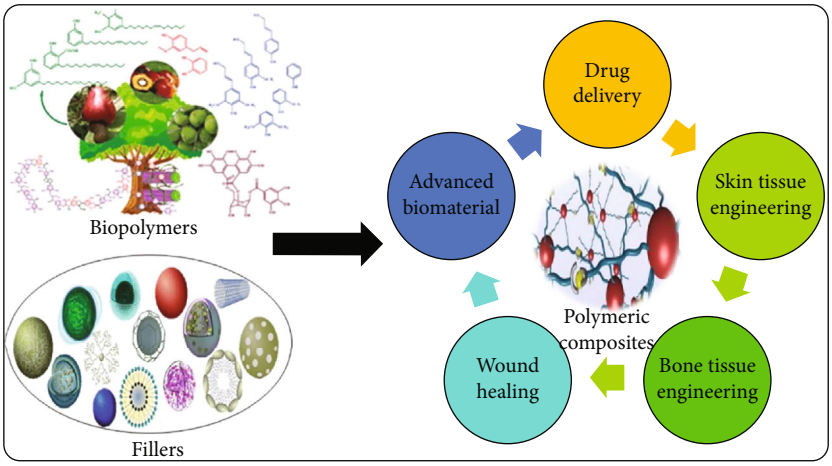

Figure 2: Potential applications of biopolymers in different aspects [38].

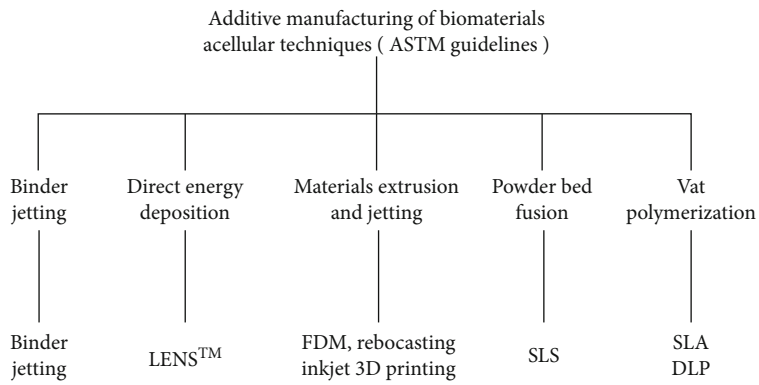

Figure 3: Acellular techniques for biomaterial additive manufacturing [46].

thiolated arabinoxylan and cellulose acetate, have been used as shown in Figure 2. Environmental factors and microbial breakdown contribute to a conducive setting for their degradation. Biodegradable biopolymer composites are known as "green organic composites." A number of in-organic fillers, including titanium, silica, and alumina, are characteristic for many green bio compounds. A number of viable and environmentally beneficial articles have already been offered with synthetic oil on the market by bioplastic advances [41].

4. Properties of Biomaterials Appropriate for 3D Printing

The principle of bioprinting consists in impressing the biomaterial using a liquid layer procedure till it is entirely produced, immediately following the biomaterial exit of the cranium in a fluid condition; the biomaterial becomes shaped. This transformation process from sol to gel or phase is the key to the bioprinting of biomaterials [42]. The most commonly used biomaterials are polymers and composites, since they may be polymerized with different ways to make them "3D-printable." Rheological characteristics and the cross-linking procedure are crucial factors which make biomaterials acceptable for 3D printing methods. Again, the criteria of bio inkjet printing are distinct from those of extrusion-based bioprinting, depending on the method of bioprinting, whose qualities differ [43]. Furthermore, appropriate printing qualities are dependent on the type of the elements of the polymer biomaterial concerned. The creation of innovative polymers or hydrogel bioprinting systems should include rheological features such as viscosity, non-Newtonian, Barus effect, and cross-linkage. Non-Newtonian systems have a low fluid dilution viscosity and are time-dependent on shear pressure [44]. Polymers are shown to have higher viscosity and tend to clog the press nozzle during 3D printing and shear-thickening fluids. Polymers are thrown by dust out of the printed head during the printing process and expanded following expulsion [45]. This phenomenon is known as the effect of Barus. Ideal bioinks should have slight or no Barus effect to reserve 3D-printed object purpose. Figure 3 displays various additive manufacturing (AM) acellular approaches for biomaterials categorised in accordance with American Society for Testing and Materials (ASTM) recommendations.

5. Polymers Fabricated by 3D Printing Technology

5.1. Natural Biomaterial. Promising options have been investigated using tissue engineering procedures while searching for

alternatives to traditional therapeutic strategies for repairing or replacing lost or dysfunctional human tissue and organ. Biomaterial-based scaffolds were beneficial for this search [47]. Gelatine, the principal hydrolyzed collagen ingredient, has spontaneously come into being in the extracellular matrix (ECM) and has the ability to suspend gel cells at low temperatures. Research studying the use of natural starch polymers with water-based binders in 3D direct printing has shown positive results, and the essential biodegradables can be mixed with the necessary mechanical qualities by synthetic polymers [48]. Polymers based on starches provide for extended time of breakdown and subsequently higher porosity with increased cellular integration which is ideal for the engineering of bone tissues [49]. For the Three-Dimensional Printing (3DP) method, a unique blend of polymer-based starch granules was produced (cornstarch, dextran, and gelatin). Scanned Electron Microscopy (SEM), Differential Scan Calorimetry (DSC), porosity evaluation, and compression testing tested the quality of the scaffolds [50, 51]. Analysis and testing have shown that new 3DP material combinations can build 3D pore scaffolding. In polymers for medication supply management, composites of starch and cellulose have demonstrated biocompatibility [52]. The density measures and mechanical tests demonstrate that, due to the small sintered level and the limit of joints, the mechanical qualities of the specimens built of bigger particles were less and that the enclosed pores were higher and more covered with small sizes of particles [53]. The results showed that biopolymer scaffolds could be produced by a process optimisation using starch and cellulose acetate to modulate laser power and scanning speed. The results are demonstrated. Specimens made of small particle size have adequate mechanical characteristics and porosities in the design and manufacture of tissue and drug delivery scaffolds with potential utility [54]. The application of 3D printing in tissue technique has permitted the production of tissue-analogous structures using innovative technologies for the printing of cells and matrix materials. The use of 3D printing to manufacture cell charging constructions has been shown to locate cells as intended and to have a high cell viability of the constructions manufactured [55, 56].

5.2. Ceramic Scaffolds. Ceramics are a sort of biomaterial, comprising calcium and phosphate, which comprises inorganic salts. Because of their osteoconductive and osteoinductivity, these biomaterials have significant potential for bone and dental TE. The inorganic composition of the bone tissue imitates calcium and phosphate salt [57]. These biomaterials stimulate the creation of new bones and are hence known as osteoconductants. Few compounds can cause a cell difference to the osteoblast linage without applying growth factors that are hence known as osteoinductive [58]. Ceramic and polymer-based biomaterials are classified as composites. Chitosan, Poly-Lactide-Glycolic Acid (PLGA), and Polyethylene-Glycol Diacrylate (PEGDA) are the common polymers added. Materials such as zirconium oxide, graphene, silica, and bioglass were added to the composition of the skin in order to build composites with mechanical properties that are bone-like [59]. Many researchers created porous materials in 3D in order to enhance vascularization in the scaffolds. Many 3D-printed ceramics will eventually be exposed to sintering and freezing techniques in order to improve mechanical characteristics and cytocompatibility [60]. The compressive strength was proven to consist of 3D-printed scaffolds employing strontium, hardystonite, gahnite, hydroxypropyl methylcellulose (HPMC), and sodium polyacrylate equal to 110 MPa bone, with 34% porous scaffolds. Because of the high mechanical qualities and the capacity to stimulate vascularization, the bone tissue engineering has a very great potential [61, 62]. 3D printing enables you to produce patient-specific grafts that fit the patient's needs with regard to histocompatibility, graft size, and bone development rates.

5.3. Synthetic Biopolymers. Bone is one of the most thoroughly studied of various tissues being actively investigated, because of its vital activities in daily living. The defective portion often must be removed by the surgery if the bone has disease or injuries. But regeneration is limited to a few millimetres away from the healthy bone [63]. The regeneration is only possible. Afterwards, the excised part of the bone is replaced by a graft, to restore its functionality. The most commonly used polymer for 3D porous scaffolds is Polycaprolactone (PCL), which is hydrophobically caused to limit cell-skin interactions, despite its strong biocompatibility and processability [64]. PCL is also semicrystalline, resulting in very lengthy degradation kinetic conditions, which is considered as soft and hard tissue compatible bioresorbable material, coupled with its hydrophobicity and its poor water absorption capacity. In the ranges 40%–85%–2,74%–55, 95 MPa and 1,17–5,03 MPa, the porosity, compressive steepness, and yield strength of the scaffolds varied. This range of rigidity closely fits the ringing bone in the maxillary region. In addition, as is apparent from the results of cytotoxicity testing, the selected manufacturing method for PCL scaffolds has proved practicable [65, 66]. In addition to PCL, some additional polymers are employed for tissue engineering in 3D printing. Poly(3-hydroxybutyrate) (PHB) is a natural, in-balanced growth-related, thermoplastic polyester that has garnered attention in biomedical fields, such as tissue engineering scaffold fabrication because of its biocompatibility and biodegradability [67]. Unlike conventional procedures, PHB may be processed by 3D printing without the need of chemicals such as plasticizers. A functional polyester with PCL-based aliphatic Phenylmagnesium Chloride (PhMgCl) has considerably greater hydrophilicity due to their backbone hydroxymethylglycolide-co-ε-caprolactone groups, which has recently been developed, leading to a significant increase in the adhesion, proliferation, and differentiation between human mesenchymal stem cells and PCL [68]. The PCL-based polyester was also developed. In order to test in vivo biodegradation and biocompatibility of 3-dimensional PhMgCl scaffoldings, 3D plasters utilising this polymer have been created via fiber filtering, increasing hydrophilicity, higher rates of degradation, and an enhanced interface between the cell material and the PCL (melt plotting). A normal external body response was seen in PhMgCl scaffolds to both types of scaffolds characterised by the presence of macrophages, lymphocytes, and fibrosis [69, 70]. The degree of interactions of tissue scaffolds and of vascularization in PhMgCl scaffolds was demonstrated to be higher

than that of PCL. Therefore, a potential biomass for bone and cartilage tissue engineering is the rapid and degradable PhMgCl that has shown good biocompatibility [71].

5.4. Synthetic Biopolymer-Based Composites. As the main scaffolding materials in the preparation of multimaterials, two photocross-linkable hydrogel biopolymers Poly-(Ethylene Glycol) (PEG-DMA, MW 1000) and poly-(PEG-DA, MW 3400) have been employed. In distinct zones of the scaffold, multimaterial scaffolds were created using a tilt of regulating concentrations, including fluorescent, fluorescent, bioactive PEG marking, or bioactive PEG [72]. Fluorescence microscopy was used for the presence of the fluorescent component in particular parts of the skull, and selective bioactivity microscopy was used to illustrate cell localization with the help of the PEG bioactive pattern in the sections. Successfully demonstrated multimaterial spatial control. Moreover, after SLS manufacture, the balance swelling behaviour of these two biopolymers was established and used to build constructions in a swollen state with the given dimensions [73]. Multimaterial SL is used, and different bioactive ligands or growth factors are relatively easy to conjugate to PEG to manufacture custom three-dimensional constructions with a specific bioactivity that can be controlled by a space [74]. Most of the present procedures use water-insoluble images incompatible with live cell manufacturing and ultraviolet (UV) radiation that harms cellular DNA. Several researches show the use of water-soluble dimethacrylate poly(ethyleneglycol) (PEG-DMA) to produce stereolithographic structured, cell-containing hydrogels. The cell viability and activity of the scaffolds with their porous internal architecture was greater than that of solid scaffolds, perhaps because of the increased exchange of oxygen and nutrients inside the scaffolds [75, 76]. A well-defined pore network, a limited pore dispersion, and significant pore interconnection characterised the porous hydrogel structures. Cell compatibility of the resin with the building structures. Human mesenchymal stem cells are attached to the surfaces of the hydrogel structures, and after seeding, they exhibited their propagating form. After five days of cultivation, cell growth was found [77]. In tissue engineering, medications, cell transplants, and other biomedical applications, these hydrogel structures can therefore be used [78].

Compared to materials such as PCL and PLA that offer a better native biocompatibility, Acrylonitrile Butadiene Styrene (ABS) is not extensively employed in medical devices. Biological applications demand protein and other biomolecular adhesion components during flow reduction [79]. The chemical modification of the ABS surface to the engineering hydrophilicity and biocompatibility is therefore very important. Surface changes have proven to be an excellent technique for increasing material biocompatibility for many years now, in particular through the grafting of PEG [80]. A method for producing watertight microfluidic equipment with chemical dissolution via acetone has proved to impair water movement between layers of a porous FDM ABS device, while keeping the structural fidelity of printed microstructures to 250 μm. The photographic grafting of PEG groups will next present a way to building a stable, biocompatible ABS surface that will improve the biocompatibility of ABS by reducing the biocompatibility of biofluidity [81, 82]. Surface and protein-adhesive studies have shown that this modified ABS is a versatile material to be used to model fusion deposition for the forming of micro-fluid-resistant biofuel channels that expand the range of potential applications in ABS-based FDM microscopic and laboratory on a chip application [83]. Compounds of polymers and inorganic bioactive materials are currently being developed to increase mechanical stabilisation of scaffolds and enhance the interaction of the tissue [84]. Combination of biodegradable polymers and ceramics such as hydroxyapatite (HA) and tricalcium phosphate (TCP) created third-party composition scaffoldings. The development of biomaterials in the nanosized osteoconductive Calcium Phosphates (Ca Ps) including HA, tricalcium phosphate, and substituted HA and TCP was recognised as being small in size, high surface-to-volume relationship, and biomechanical similarities with natural bone structure combined with bone structures such as collagen, poly(L-lactide) (PLLA), and chitosan [85, 86].

Hydroxyapatite ($Ca_{10}(PO_4)_6(OH)_2$), the chemical resemblance with calcium phosphate mineral present in biological hard tissues, has received a lot of interest. HA is used for a range of biological applications such as a controlled medication release matrix and a bone tissue transporter material [87]. Recently, the advantage of nanosized hydroxyapatite (nHA) compared with typical microsizes has been emphasised. NHA can operate as a carrier of therapeutic agents to enable the extracellular or intracellular regulated release of drugs, and, at the same time, it is highly absorbent into the body for hard tissue regeneration [88]. The bone tissue engineering application has been of major interest to PCL/HA composites. The use of PCL and HA biocomposite materials to manufacture tissue scaffolds via SLS technology. Experiments with cell culture have shown that Saos-2 cells can live on the manufactured fabric and proliferate. The results reveal that PCL/HA biocomposites have the advantage of being tissue engineering bodies produced by SLS. In addition to pure PCL, the mechanical features of the PCL-HA composites were improving. They also show that the mechanical properties of these boots can be anticipated with great precision before production [89, 90]. The ability to adjust the material properties and the anatomical form of fabric-engineered constructions for patient and site recovery strategies is an extension of mechanical features of composite materials at any loading of fillers combined with a direct production method and a complicated anatomical component production process [91, 92]. In combination with the natural manufacturing process to fabricate the sophisticated anti-anatomical protein techniques of the composite materials at all loads of fillers. It can adapt material properties and building designs for both patients and site rehabilitation plans [93].

The cell interactions of polymer engineering tissue scaffolds are known to benefit from bioactive glass. The best response will probably be obtained if the glass has no cover on the surface of the scaffold [94]. The recent creation of a 3D fiber draws technology to produce perfusable glass grills, which are similar to patterned vascular systems and are covered with a thin layer of poly-(d-lactideco-glycolide). The very porous and surface scaffolds were used to distribute bioactive glass homogenously. The presence on the surface of composite

scaffolds of calcium phosphate deposits in vitro bioactivity [95]. The metabolism of fibroblast was boosted by bioactive glass. Investigations have shown that SLS technology allows for the production of well-defined composites, where bioactive glass is equally scattered on the surface and readily available for quick cell and ion release. An undesirable polymer layer covering BG particles can be prevented by Stereolithography (SLA) on the surface of the skin [96]. The study revealed that the bioactive and biodegradable cell support of regenerative medicine photocross-linked composite and PCL scaffolds produced by SLA technology has a high potential [97].

5.5. Peptide-Based Biopolymers. A new class of biomaterials known by the outstanding chemical, physical, and biological properties of the peptide-based biopolymers is produced; protein engineering and macromolecular assembly converged to enable peptide-based biomaterial to expand [98, 99]. Prototype examples include poly-amino acids, leucine zip-based peptides, peptide amphiphiles, ionic oligopeptides in beta-sheet and peptides in beta-hairpin, and prototype peptide-based biomaterials; poly-amino acids, polypeptides, silk proteins; and coiled-coil domains. Biopolymers can also readily be functioned to strengthen cell connections and create an appropriate platform for cellular activities and functional tissues [100, 101]. This section examines two major classes of technical biopolymers based on peptides: the auto-assembly of polypeptides; the formation of gels by means of environmental stimuli and polypeptides. The application of in situ gelation chemically cross-linking elastin-like protein (ELP) hydrogels was impaired by low water soluble, toxicity problems, absence of biocompatible cross-linking reactant and product reactants, and delayed gelation kinetics [102]. While peptide biomaterials have become ever more essential materials in regenerative treatments, their use is restricted by the short lifetime and thermal instability. Many of these constraints can be overcome using new technology, and the usage of peptide-based biomaterials can therefore be further extended to applications for which it is presently impossible [103, 104].

5.6. Polymer Scaffolds. Polymers are often used in 3D printing biomaterials. The use of polymers in the manufacture of additives is extended to various tissues, including the most transplanted organs liver, kidney, and heart tissue. Biodegradable and nondegradable polymers can be used for 3D printing; however, the advantages of biodegradable polymers are greater and are therefore extensively used [105]. Biodegradable polymers are usually categorised as natural or synthetic based on their origin. In recent times, numerous synthetic polymers have been produced with programmable degradation rates. The degradation rate is vital because it needs to match the pace of the new tissue synthesis [106]. The scaffold design also incorporates natural and synthetic polymers in combination. In one or two physical stages, whether solid or fluid polymers often occur in bioprinting. Solid polymers are mainly utilised in FDM printers, while liquid polymers are used in extrusion and inkjet printers [107]. Liquid polymers are solutions of solvent systems which can be polymerized or interconnected with monomers or oligomers. Hydrogels are a polymer type that holds water and hence imitates the natural tissue environment. They are used to cell encapsulation, medication delivery systems and packs in a number of applications [108]. Vascularized tissues with tremendous promise in organ manufacturing were imprinted 3D using hydrogen and cell combinations. In efforts to build scaffolds for specific tissues, a variety of 3D printing methods were utilised. Modeling deposition fused provides an economical way of building up scaffolds that use widely available biodegradable polymer filaments with regulated porosity and architecture [109, 110]. However, thermal deterioration and spatial resolution are the limitations of FDM printers. For extrusion-based printing, the suspension, solution, or emulsion is supplied with a pneumatic, piston, or screw-driven system to produce pressure [111], given the varying viscosity of many hydrogels; pressure-oriented extrusion methods are effective.

6. Applications of Biopolymer Materials in Biomedical Fields

6.1. Drug Delivery. The revolutionary potential as carriers for the provision of genes, biomolecules, or biological agents has been displayed by polysaccharide-based composites, including arabinoxylan, xanthan gum, and chitosan [112]. These are employed as medicine carriers with excellent bioactivity, low cytotoxicity, nonantigens, processability, reversible loading, and release mechanisms for cartilage repairs and vascular grafts. They are used for treating cancer. Other assets that improve your medication delivery application are emulsification, gel formation, foaming, and moisture absorption [113]. These polymeric materials have also been acknowledged as excellent controlled drug delivery systems because of their unique mechanical and cross-link features, suitable biodegradation in various environments and at specific areas [114]. Such biomaterials can be directly synthesised or included into engineering particular and specific places of resultant nanocarriers with multifunctional features. Some biomaterial kinds have been employed efficiently as hydrogels, movies, tubes, microspheres, and microneedles and based on chitosan, guar gum, and arabinoxylan.

Controlled drug delivery tries to steadily give treatments at the desired spot, usually in the blood, and to maintain an efficient therapeutic window [115, 116]. The results are cost-effective and desirable, reducing or eliminating unpleasant side effects, complications in the dose, and increasing patient recovery and comfort. It is claimed that regulated breakdown and sustainable release following accumulating at the target site are the most wanted pharmacological properties of biomaterial systems [117]. This controlled release of implanted medicines or other therapeutic substances can be primarily controlled using triggers like temperature, pH, and ion concentration. In order to manage the release of therapeutic usage, the aimed system of drug supply must typically activate the cellular areas [118]. Therefore, to optimise the synthesis or functioning of precursors, composition conditions of manufacture, and drug encapsulation technique, a tailored drug delivery approach must fit into the required release kinetics [119]. The medicine or other nutrient should be delivered at a controlled rate and dosage by ensuring that all factors such as size, shape, surface

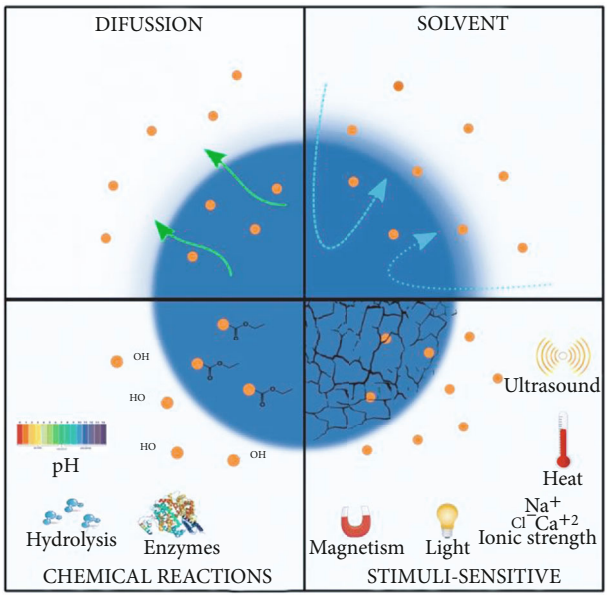

Figure 4: Mechanisms for controlled drug release using diverse types of carriers [121].

morphology, bioavailability, and biodegradability are suitable and particular to the intended spot. The biomimetic polymer nanoparticles were made in various sizes, and the therapeutic ingredients were loaded effectively. Such accurate nanodrug carriers assisted to imagine inflammatory regions in molecular form and resolved possible inflammations and immune responses [120]. Figure 4 shows various types of carriers to control drug release mechanisms.

6.2. Tissue Engineering (TE). Tissue engineering involves the treatment or regeneration of faulty tissue through biomaterial scaffolds. It requires polymer composites with the requisite composition, desired technical qualities, and adequate physicochemical behaviour in order to promote the formation of biological tissue. It has expanded in depth and importance as an advanced discipline of its own, having been classified as a biomaterial subsection [122]. As tissue technology deals with different applications, the result is usually related to applications which substitute, repair, or rebuild part or complete tissues (bone, cartilage, blood vessels, bladder, skin, and muscle). The tissues implicated are typically responsible for the appropriate functioning of particular architecture, morphology, and mechanics [123]. Tissue engineering phrase also is employed in the artificially produced protection and support system to combine complex biochemical pathways via cells (skin, hip replacement). Capable technology for 3D bone scaffolding is bone tissue engineering (BTE) that contains living cells and bioactive chemicals. BTE focuses on the perception of the skeletal structure as the bone dynamics increase the clinical ability to address unsettling skeletal and segmental anomalies [124, 125]. In other circumstances, contemporary technology and advancement of bone biochemistry are important to efficiently grow or rebuild bone tissue. Bone can be used for a wide range of multifunction, leading to physiological and endocrine stimulation [126].

The bone endures a continual resorption and repair process which takes place due to internal intermediates and external mechanical standards, exchanges of chemicals, and structural remodeling [127]. Bone had been named the greatest intelligent material historically and most precisely due to its limited regenerative flexibility. The freshly cured bone with adjacent host bone and, most importantly, the native bone functions include bone fusion [128, 129]. Functional bone tissue engineering adds to functional and architectural diversity; the bone is an exceedingly complex tissue. Particularly, the Extracellular Bone Matrix is made from a nonmineralized organic matrix as well as an inorganic mineralized component [130]. For nanocomposite construction, the compressive strength and resistance of the thigh-bone fractures and the load-bearing applications are important [131]. Suitable compounds for extracellular matrixes or sticky ligands which enable stem cells and regenerate bone tissue might be applied so quickly in different procedures of engineering [132, 133]. Bone tissue engineering should focus on producing scaffolds of angiogenesis, combining growth stimuli and the porosity structure necessary for vascular growth [134, 135]. The processing of these scaffolds with micro- and nanometre-surface geomorphology is indispensable to cell bond, propagation, and discrepancy as shown in Figure 5.

However, bone tissue engineering is regarded as an alternative in situations when donor availability is restricted, or where there is a risk of disease transmission, donor site difficulties, or even limitations of external materials to reshape and respond to physiological conditions. This is true whether the scaffold is acellular or seeded with stem cells, which can directly develop into bone cells, to replace a broken portion of bone. The scaffold's composition and structure are critical. Bone tissue engineering's primary goal is to create scaffolds that not only act as a scaffolding for the implantation of cells but also send regenerative signals to cells to accelerate bone healing and repair. Structural bone scaffolds are 3D architectures and environments that are designed to (1) promote cell adhesion and survival, (2) accelerate bone remodeling and remodeling, (3) provide osteoconductive structural guidance, and (4) in some cases, act as carriers for growth factors, antibiotics, or gene therapy. The epidermis which works as an anti-illness shield is the most waterproof layer and plays a significant role in bodily temperature and humidity regulation. More than 90 percent of epidermal cells are keratinocytes [137]. Langerhans, melanocytes, and Merkel cells dominate the bulk of epidermal cell populations. The dermis and skin base are around 90 percent of the skin's weight. It is an extracellular matrix of soft tissues consisting of a variety of cells, lenses, and hair follicles. The dermis has a strong vascularization, and the nerve ends with a blood vessel [138]. Fibroblast is the largest dermal cell containing collagen and elastin and giving mechanical strength to the skin. A more deeply elastic, mucous tissue-cell skin that store fat, blood vessels, and nerve is present in the pulmonary hypoderm. Traumas such as physical penetration, venom, fire, illness, and operation are the major reason and contribute to the chance that important organs are infected, injured, or dehydrated by this disease [139]. Skin replacement technology offers a potential foundation for better care for combating chronic

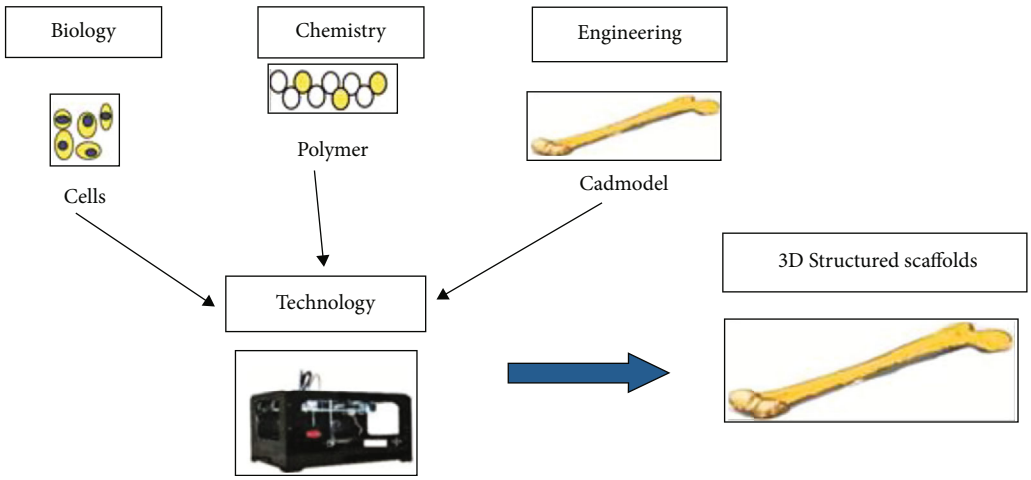

Figure 5: Representation of multidisciplinary fields used in the 3D printing technique for TE applications [136].

Table 2: Biopolymeric materials in tissue engineering and wound healing [146–155].

Biomedical field	S. No.	Polymeric material	Prominent characteristics
Tissue engineering	1	Chitosan	Recyclable, biocompatible, uncontaminated
	2	Gelatin	Bioactive, biocompatible, hemocompatible, cell adherence
	3	Arabinoxylan	Biocompatible, uncontaminated, cell observance, bioactive, cell explosion
	4	Collagen	Biodegradable, fibrous, biodegradable, cell proliferation
	5	Xyloglucan	Cell explosion, environmental, cell discrepancy, biocompatible
	6	Fibrinogen	Biocompatible, hemocompatibility, cell propagation, decomposable
	7	Arabinoxylan/guar gum/gelatin/ collagen	Antiseptic, biocompatible, decomposable, bioactive, continuous drug release, cell propagation
Wound healing	8	Chitosan	Biocompatible, antibacterial, cell proliferation, bioactive
	9	Alginate/fibrinogen/hyaluronic acid/ xyloglucan	Fiber protein, biocompatible, recyclable, rubbery, sterile, cell obedience
	10	Bacterial cellulose/pectin	Antibacterial, cell adherence, cell differentiation, biocompatible, bioactive, cytocompatible

and acute skin damage. However, given the mechanical and physiological aspects of active skin, cellular basis technology and simulated extracellular matrix are required for skin tissue engineering to connect with the surrounding tissue [140, 141]. No substantial skin prototype is currently available to accurately replicate the natural skin structure, composition, organic consistency, or visual environment. Alternatives of the skin might have crucial, easy-to-use, and wound-specific characteristics [142].

These biomaterials are sufficiently water-sensitive and have specific affinity to host places. Their biochemical and mechanical qualities are sufficient, their privation is controlled, their disinfection is nontoxic and nonantigenic, and their inflammation is minor [143]. They can also join the congregation at low operational cost with minimum injury and suffering of angiogenesis. The ultimate objective of tissue technology is to achieve the maximum of these needs to prepare intelligent skin substitutes [144]. In addition, the new skin electronic properties or aesthetic structure do not restore polymeric composite materials. In order to extend skin growth to provide the typical usefulness and beauty of healthy skin, the changes in stem cell biology and skin morphogenesis are necessary [145]. Some of the biopolymeric materials and their features are represented in Table 2.

6.3. Wound Healing. Wounds are a form of uneven skin punching, breakdown, or skin deformation owing to a chronic or thermal trauma. Injuries can be classed as chronic or acute injuries depending on the healing procedure. Chronic injury is predominantly tissue lesions, usually within 8 to 12 weeks, which appear to have totally resolved [156]. Acute injuries continue to occur and are still more than 12 weeks of recuperation. Various neurological factors can lead to wound-healing impairments or the failure to correctly heal. Chronic injury examples are bedsores and leg ulcers. As the basis for the wound gradation, skin layers and polluted areas are used and only the epidermal skin surface is involved with surface wounds [157, 158]. The word partial thickness injury is

defined as injury involving the epidermis, deep epidermis, muscles, soft tissue, and follicular tissues. The wounds are combined with subcutaneous fat or deep tissues besides the epidermis and the skin surface [159]. The physiological wound repair is part of coordinated teamwork among various biological systems. The wound is entirely treated in a cascade with controlled operations. Hysteresis and coagulation of your blood start with lesions, mainly in order to avoid first sight exsanguinations, taking place in every area of the body [160]. The lesion is also a long-term secondary target and a matrix for cell adherence. A carefully managed balance of endothelial cells and thrombocytes relies on the homeostasis and fibrin produced at a site of the injury [161]. The neurological system of response in damaged veins causes vascularization, which blocks blood flow over several minutes. The waterfall of coagulation is caused by homeostatic behaviours and proliferation and differentiation [162]. Platelets bond when blood spills, causing a release of the coagulation factor: fibronectin, fibrin, vitronectin, and thrombospondin. Coagulation retains homosexuality and a cell migration matrix in homosexual and inflammatory treatments [163, 164]. Many biopolymers are routinely used in wound care and treatment, including fibrous proteins and different polysaccharides. These biocompatible, biodegradable polymer matrices preserve an atmosphere similar to the extracellular environment. The process of sluggish wound treatment is accelerated [165]. For cell adhesion, proliferation, migration, and differentiation, the biopolymeric matrix provides an ideal microenvironment Using biopolymer-based wound care materials, three-dimensional cross-linked polymeric networks can keep the wound wet and oxygenated. As a result of the use of wound healing dressings, the wound is regenerated, prevented, and protected from disease-causing bacteria. Dermal and epidermal tissue healing and regeneration rely on it. This wound healing material is identified as hydrogels that can be packed for localised therapeutic delivery with spatially and temporally controlled cells, medications, and peptides. Hydrogels have been utilised for biomedical and therapeutic applications, such as tissue engineering, regenerative medicine, cancer treatment and infectious diseases, controlled drug delivery, and peptide delivery [166]. Hydrogels adhere to the application site shape to provide for considerably more therapeutically practical formulation of loaded hydrogels in biomedical applications. While hydrogels are believed to be exceptionally biocompatible with poly(ethyleneglycol) (PEG), hydrogels based on PEG, hydrogels used on are considered extremely biocompatible. High systemic biocompatibility of PEG and utilisation of biomaterials generated from ECM increase the distribution of cell growth [167]. As a result, the multifunctional wound-care material PEG-based cross-linking hydrogels with good loading components, such as cells, medicines, and peptides, are being developed [168].

6.4. Bioprinting. Bioprinting includes production of AMs in complex and functioning living tissues, utilising biocompatible cells, supported components and materials. In regenerative medicine, biopharmaceutical products are generally used to support tissue and organ transplant, especially the development of hydrogel [169]. Many forms of bioprinting are available, including inkjet printing and AM-based extrusion. One study generated 3D cell architectures through neural cell sheets employing an alternative human pluripotent embryonal carcinoma (NT-2) cells and fibrin gel inkjet printing approach [170]. The Vascular Endothelial Growth Factor (VEGF) presence in 3D-bioprinted scaffolds that incorporates alginate into one of their matrix mixes promotes vascularization in gelatine microparticles.

The hydrogels developed containing hyaluronic acid and semi-interpenetrating systems with a dextran basis [171]. The use of neural stem cells to produce artificial neural tissue was organically printed with collagen and VEGF-releasing fibrin gel. Hyaluronic acid-based scaffolds were created through layer-by-layer deposition through bioprinting [7]. In order to print bespoke steaks with cell inclusion, many such techniques have integrated other conjoined natural polymers such as dextrin and gelatin. This has led to the development of sophisticated materials with biological activity by adding growth factors such as Bone Morphogenetic Proteins (BMP-2) by use of microfabrication technologies [172]. Many of the bioprinting approaches mentioned could be adjusted and optimised with or without cell utilisation for bone tissue engineering. The survivability of cells in situ following the printing method is part of many issues related to cell printing [173]. New methods used for obtaining 3D cell-charged structures with proper mechanical and biological properties have been applied with collagen-based bioinks [174]. The 3D printing techniques for polymers are shown in Figure 6.

6.5. Advanced Functional Biomaterials. In order to design and synthesise multifunctional polymer material, a better understanding of the sequence, structural, and functional features of natural polymers plays an essential role. These innovative artificial biomaterials are self-assembled and stimulated to encourage cell contact and growth under particular conditions [176, 177]. The complexity of posttranscriptional changes has limited sophisticated and multifunctional biomaterial protein synthesis that utilises bacterial resources and the conundrum of target genes [178]. Other changes have been intended to properly control spatial and temporal releases. The development of the structure and de novo design for protein-based biomaterials has been made easier by progression in gene therapy and manipulation approaches [179]. Due to the existence of multifunctional domains on the protein structure, the structure of produced biomaterials is linked to significant versatility, such as cell binding places and enzymatic domains. The design and production of new biomaterials based on artificial proteins have been promised recently in genetic engineering. Compared with its native counterparts, these biomaterials have a unique performance, such as improving self-assembly in fiber architectures [180, 181]. The significant necessities for choosing a bioink for 3D printing in biomaterial characteristics is shown in Figure 7.

6.6. Materials and Manufacturing Advances and Trends. The selection of optimum biomaterials will be a vital part of effective bioprinting of therapeutically relevant tissue. Based on the availability and knowledge of these materials, numerous polymers were examined during the bioprinting stage for traditional 3D printing and fabric production [183].

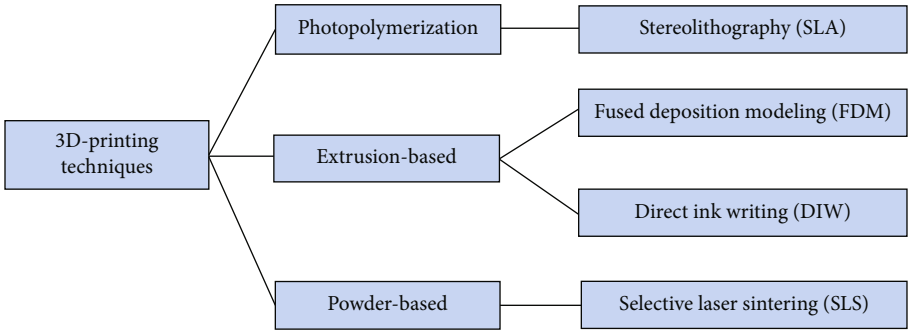

Figure 6: 3D printing techniques for polymers [175].

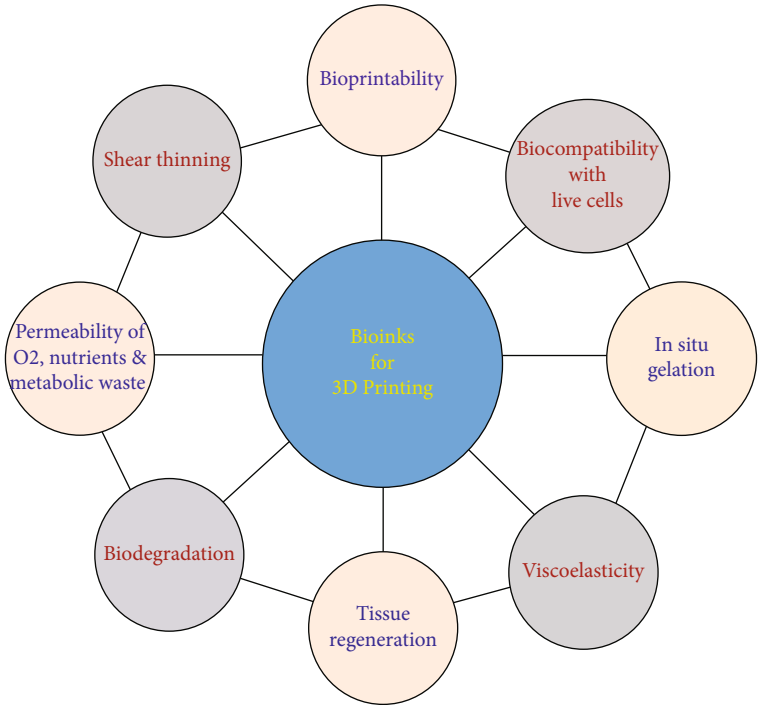

Figure 7: Bioink for 3D printing in biomaterial features [182].

However, in bioprint applications, materials are not the most physiologically suitable. Many of these are exceedingly physiologically active, leading to improper cell contact and premature or undesired differentiation of the stem cells [184]. The focus is currently on new biopolymers and hydrogels, which imitate better the nanostructural characteristics and reactivity of ECM and other constituents in the true tissue microenvironment. But those new hydrogels and biopolymers more biocompatible are not necessarily appropriate to conventional methods of bioprinting [185]. Many lack the structural stability to optimise bioprinting and can collapse if they are too soft. An interesting field of research is to optimise the microarchitecture for these biopolymers. Substances are combined with the proliferative and cytocompatible impact of a softer material to optimise the usefulness of all of them, the mechanical properties of one single substance [186, 187]. For example, an "integrated tissue organ printer" is utilised to put companies into the soft hydrogel cell scaffold. Tricalcium phosphates with gelatine and hyaluronic acid bioprinting can be successfully combined [188]. In general, the effectiveness of the bioprinting process has to be enhanced. The existing bioprinting method is time consuming and currently cannot reliably supply the number of cells needed for varied tissue types.

As mentioned before, a change in cell shape, changed signalling pathways, and even cell death is often caused by imposed force through the printing process [189]. In order to make more efficient cell death and loss, the huge effort is involved in each bioprinting project. Improved methods for monitoring and assessing cell death are part of the solution. Vascular networks may be the main task in converting bioprinting into the lab for the production of functional tissues [190]. Tissues of even minimal complexity will not survive without proper channels for nutrition delivery and waste removal. In vivo, the diffusion of oxygen is limited by a vascular network for tissues that are beyond 100-200 mm. Infected tissues will have nutritional restrictions without a vascular network which result in inadequate development of tissue or necrosis [191]. In order to properly

perfect bioprinted tissue, an early enough developmental network must be established for the prevention of death of tissue and for the endothelium to be attached and grown. As a result of the development process, all tasks in normal development must be played by the vascular structures, including the maintenance of selective waste and nutrient barriers, and inflammatory reactions, coagulation, and other homeostatic processes [192, 193]. Today, problems with bioprints are mostly related to restrictions on printing resolution and speed. Capillaries, for instance, can have a diameter of about 3 mm while a droplet of 20 mm is currently used by the highest-resolution laser-based bioprinters.

Conventional methods or additive manufacturing can be used to create bone scaffolds. Pore size, shape, distribution, and interconnectedness of pores are all difficult to manage using conventional approaches. To add living cells in conventional procedures would be very impossible because of manufacturing circumstances. If pores are distributed in an unintended manner, it could have a negative impact on cell distribution and, ultimately, the development of new tissue. Other organic solvents left behind in the scaffold microstructure can negatively affect cell survival or function. Due to low-cost items and simple instrumentation, these techniques are still employed today [194]. As a result of the absence of hazardous solvents in AM procedures, the biocompatibility of scaffolds is much improved as well. If necessary, scaffolds can be constructed with two or more materials. Despite the high resolution of SLA and SLS, their applicability in the manufacture of bone scaffolds is extremely limited. Photosensitive polymers required for SLA use in bone tissue have a low biocompatibility. As a result of the high-intensity laser beam, SLS is not generally used in bone tissue applications. In spite of its low resolution and limited material options, FDM solvent-free and ultraclean procedure is likely to be the greatest technology for incorporating live cells, which could explain why FDM-created PCL bone scaffolds have won FDA approval.

Even if printing resolution is increased to such an extent that a complex capillary network can be produced, time with the currently available technology is prohibitive [195]. The cell viability may be impacted if the printing cannot be finalised fast. In consideration of these issues, several solutions have been proposed. One of the most promising is attempts to vascularize in vivo with the addition of angiogenic substances to biomedical tissue implants, inducing the host vasculature growth. This method has to be refined, despite encouraging outcomes [196, 197]. Alternatively, vascular networks of synthetic origin have been attempted. While the bioprinting of vessels with bigger diameters has been successful, synthetically created small microvascular grafts with fewer than 5 mm show poor patentability and are now unrealistic [198]. Inappropriately, the basic problem of tissue death prevention and timely growth of mature, functional vasculature has still to be overcome [199].

6.7. Challenges and Future Directions. Two types of tissue engineering difficulties exist: novel bioink research and development for specific tissues or universal bioink for all tissues and the regulatory category. Ideally, a universal bioink must be a biomaterial mix that promotes survival in the angiogenesis and in nerve intercalation of natural tissues, chemical indicators, and growth factors. These challenges can be overcome by providing new technologies, such as additive fabrication, which allow the production of complicated fabrics. Vascularization is one of the most essential difficulties for developing sustainable angiogenesis solutions involving the addition of angiogenic growth factors, platelet additions, bone marrow clots, and bioreactors. Since numerous heads loaded with cell type can be used by bioprinters, a vasculature is placed into a 3D imprint. The use of sacrificial biomaterials within the skin is another technique to address vascularization. Sacrificial materials provide mechanical support throughout the construction of the 3D printing process. During the postprocessing, processing of the buildings from the channels or empty regions in the building can be quickly dissolved or removed as circulatory channels.

Graphene and their composites and metal nanoparticles have also taken on a crucial importance as fillers into biopolymers reinforced their mechanical characteristics, such as tensile, effect, bending, and other structural qualities in medical applications, to create the necessary biomaterials. The main issues of the usage of biopolymers for synthesising biocomposites are mechanical behaviours and inadequate dispersion. The fillers produce agglomerates with a matrix of biopolymers that leads to feeble interfacial connection with defective structural harmonics and imperfect mechanical characteristics. The outcome is a large number of additional unusual properties, such as susceptibility to high temperatures, humidity, low impact strength, shelf life, and more. Future guidelines lead to new biomaterial in order to meet the above concerns and to be economically viable, recycled, and eco-friendly.

7. Conclusion

The biopolymers are the greatest option for synthetic petroleum polymers with considerably renewable, biodegradable, and environmentally sound characteristics. Biopolymers are not supported by mechanical properties such as high strength of tensile, impact strength, bending force, and thermal stability. However, they are able to perform load-bearing applications using their ceramic composites using a mechanical strength. There is yet more attention to be paid, inventions and improvements by using reinforced elements to adapt biocomposite microstructural features, the standard mixing techniques.

(i) These composites lead to many other unusual qualities such as sensitivity to high temperatures, susceptibility to moisture, low impact, and shelf life

(ii) In order to address the specified factors and to fit economic viability, recyclability, and eco-friendly ways, future direction leads to new biomaterials. This combination of synthetic and natural macromolecular chemistry leads essentially to biomedical applications since polymer structure management can lead to functionality being manipulated

(iii) Bioprinters can automate the assembly process and permit the preprogram and intricate manipulation

of biopolymers, from macromolecular to the live cell. This is done to achieve architectural and biochemical complexity which is never previously achievable especially in biomedical fields of tissue engineering and regenerative medicine

(iv) Tissue engineering has generated both natural and synthetic polymers through the technique of 3D printing, and various other materials have been developed. In combination with polymers, fiber and particles are developed to produce materials with enhanced bioactivity, biocompatibility, and physical and chemical qualities

Data Availability

The data used to support the findings of this study are included within the article. Should further data or information be required, these are available from the corresponding author upon request.

Conflicts of Interest

The authors declare that there are no conflicts of interest regarding the publication of this paper.

Acknowledgments

The authors thank Chennai Institute of Technology, Chennai, and Saveetha School of Engineering, SIMATS, Chennai, for the technical assistance. The authors appreciate the supports from Wollo University, Kombolcha Institute of Technology, Ethiopia. This research was performed as a part of the employment of Wollo University, Kombolcha Institute of Technology, Ethiopia.

References

[1] S. Bose, C. Koski, and A. V. Ashley, "Additive manufacturing of natural biopolymers and composites for bone tissue engineering," *Materials Horizons*, vol. 7, no. 8, pp. 2011–2027, 2020.

[2] T. Kuhnt and S. Camarero-Espinosa, "Additive manufacturing of nanocellulose based scaffolds for tissue engineering: beyond a reinforcement filler," *Carbohydrate Polymers*, vol. 252, article 117159, 2021.

[3] J. Kundu, J.-H. Shim, J. Jang, S.-W. Kim, and D.-W. Cho, "An additive manufacturing–based PCL–alginate–chondrocyte bioprinted scaffold for cartilage tissue engineering," *Journal of Tissue Engineering and Regenerative Medicine*, vol. 9, no. 11, pp. 1286–1297, 2015.

[4] S. Pina, J. M. Oliveira, and R. L. Reis, "Natural–based nanocomposites for bone tissue engineering and regenerative medicine: a review," *Advanced Materials*, vol. 27, no. 7, pp. 1143–1169, 2015.

[5] B. Dhariwala, E. Hunt, and T. Boland, "Rapid prototyping of tissue-engineering constructs, using photopolymerizable hydrogels and stereolithography," *Tissue Engineering*, vol. 10, no. 9-10, pp. 1316–1322, 2004.

[6] S. Pina, V. P. Ribeiro, C. F. Marques et al., "Scaffolding strategies for tissue engineering and regenerative medicine applications," *Materials*, vol. 12, no. 11, p. 1824, 2019.

[7] N. Di Marzio, D. Eglin, T. Serra, and L. Moroni, "Bio-fabrication: convergence of 3D bioprinting and nano-biomaterials in tissue engineering and regenerative medicine," *Frontiers in Bioengineering and Biotechnology*, vol. 8, p. 326, 2020.

[8] B. Nagesha, V. Dhinakaran, M. V. Shree, K. M. Kumar, D. Chalawadi, and T. Sathish, "Review on characterization and impacts of the lattice structure in additive manufacturing," *Materials Today: Proceedings*, vol. 21, pp. 916–919, 2020.

[9] C. Vyas, R. Pereira, B. Huang, F. Liu, W. Wang, and P. Bartolo, "Engineering the vasculature with additive manufacturing," *Current Opinion in Biomedical Engineering*, vol. 2, pp. 1–13, 2017.

[10] X. Li, R. Cui, L. Sun et al., "3D-printed biopolymers for tissue engineering application," *International Journal of Polymer Science*, vol. 2014, Article ID 829145, 13 pages, 2014.

[11] S. Mantha, S. Pillai, P. Khayambashi et al., "Smart hydrogels in tissue engineering and regenerative medicine," *Materials*, vol. 12, no. 20, p. 3323, 2019.

[12] J. Lee, S.-H. Lee, B. S. Kim, Y.-S. Cho, and Y. Park, "Development and evaluation of hyaluronic acid-based hybrid bio-ink for tissue regeneration," *Tissue Engineering and Regenerative Medicine*, vol. 15, no. 6, pp. 761–769, 2018.

[13] M. Sahranavard, A. Zamanian, F. Ghorbani, and M. H. Shahrezaee, "A critical review on three dimensional-printed chitosan hydrogels for development of tissue engineering," *Bioprinting*, vol. 17, article e00063, 2020.

[14] J. E. Kim, S. H. Kim, and Y. Jung, "Current status of three-dimensional printing inks for soft tissue regeneration," *Tissue Engineering and Regenerative Medicine*, vol. 13, no. 6, pp. 636–646, 2016.

[15] C. R. Lynch, P. P. D. Kondiah, and Y. E. Choonara, "Advanced strategies for tissue engineering in regenerative medicine: a biofabrication and biopolymer perspective," *Molecules*, vol. 26, no. 9, article 2518, 2021.

[16] S. Safinsha and M. Mubarak Ali, "Composite scaffolds in tissue engineering," *Materials Today: Proceedings*, vol. 24, pp. 2318–2329, 2020.

[17] S. Kashte and S. Kadam, "Advances and innovations and impediments in tissue engineering and regenerative medicine," in Crimson Publishers, 2019.

[18] S. Gupta and A. Bit, "3D bioprinting in tissue engineering and regenerative medicine," *Cell and Tissue Banking*, pp. 1–14, 2021.

[19] K. Dzobo, N. E. Thomford, D. A. Senthebane et al., "Advances in regenerative medicine and tissue engineering: innovation and transformation of medicine," *Stem Cells International*, vol. 2018, Article ID 2495848, 24 pages, 2018.

[20] S. Stratton, O. S. Manoukian, R. Patel, A. Wentworth, S. Rudraiah, and S. G. Kumbar, "Polymeric 3D printed structures for soft–tissue engineering," *Journal of Applied Polymer Science*, vol. 135, no. 24, p. 45569, 2018.

[21] B. J. Tricomi, A. D. Dias, and D. T. Corr, "Stem cell bioprinting for applications in regenerative medicine," *Annals of the New York Academy of Sciences*, vol. 1383, no. 1, pp. 115–124, 2016.

[22] A. Alblawi, A. S. Ranjani, H. Yasmin, S. Gupta, A. Bit, and M. Rahimi-Gorji, "Scaffold-free: a developing technique in

field of tissue engineering," *Computer Methods and Programs in Biomedicine*, vol. 185, p. 105148, 2020.

[23] C. Murphy, K. Kolan, W. Li, J. Semon, D. Day, and M. Leu, "3D bioprinting of stem cells and polymer/bioactive glass composite scaffolds for bone tissue engineering," *International Journal of Bioprinting*, vol. 3, p. 11, 2017.

[24] D. R. Fonseca, R. Sobreiro-Almeida, P. C. Sol, and N. M. Neves, "Development of non-orthogonal 3D-printed scaffolds to enhance their osteogenic performance," *Biomaterials Science*, vol. 6, no. 6, pp. 1569–1579, 2018.

[25] A. L. Oliveira, S. C. Sampaio, R. A. Sousa, and R. L. Reis, "Controlled mineralization of nature-inspired silk fibroin/hydroxyapatite hybrid bioactive scafolds for bone tissue engineering applications," in *Proceedings of the 20th European Conference on Biomaterials*, Nantes, France, 2006.

[26] Y. Du, H. Liu, Q. Yang et al., "Selective laser sintering scaffold with hierarchical architecture and gradient composition for osteochondral repair in rabbits," *Biomaterials*, vol. 137, pp. 37–48, 2017.

[27] Y. F. Dong, J. N. Liang, Y. H. Cui, S. Xu, and N. R. Zhao, "Fabrication of novel bioactive hydroxyapatite-chitosan-silica hybrid scaffolds: combined the sol-gel method with 3D plotting technique," *Carbohydrate Polymers*, vol. 197, pp. 183–193, 2018.

[28] Q. Gao, H. Gu, P. Zhao et al., "Fabrication of electrospun nanofibrous scaffolds with 3D controllable geometric shapes," *Materials and Design*, vol. 157, pp. 159–169, 2018.

[29] H. Da, S. J. Jia, G. L. Meng et al., "The impact of compact layer in biphasic scaffold on osteochondral tissue engineering," *PLoS One*, vol. 8, no. 1, article e54838, 2013.

[30] M. Mehrpouya, H. Vahabi, M. Barletta, P. Laheurte, and V. Langlois, "Additive manufacturing of polyhydroxyalkanoates (PHAs) biopolymers: materials, printing techniques, and applications," *Materials Science and Engineering: C*, vol. 127, article 112216, 2021.

[31] L. Chaunier, S. Guessasma, S. Belhabib, G. Della Valle, D. Lourdin, and E. Leroy, "Material extrusion of plant biopolymers: opportunities & challenges for 3D printing," *Additive Manufacturing*, vol. 21, pp. 220–233, 2018.

[32] R. Velu, D. K. Jayashankar, and K. Subburaj, "Additive processing of biopolymers for medical applications," in *Additive Manufacturing*, pp. 635–659, Elsevier, 2021.

[33] F. Cruz, "Fabrication of HA/PLLA composite scaffolds for bone tissue engineering using additive manufacturing technologies," *Biopolymers*, vol. 11, pp. 227–242, 2010.

[34] V. Dhinakaran, M. Lavanya, K. Vigneswari, M. Ravichandran, and M. Vijayakumar, "Review on exploration of graphene in diverse applications and its future horizon," *Materials Today: Proceedings*, vol. 27, pp. 824–828, 2020.

[35] C.-S. Wu, "Characterization, functionality and application of siliceous sponge spicules additive-based manufacturing biopolymer composites," *Additive Manufacturing*, vol. 22, pp. 13–20, 2018.

[36] J. V. Ecker, M. Kracalik, S. Hild, and A. Haider, "3D-material extrusion-printing with biopolymers: a review," *Chemical and Materials Engineering*, vol. 5, no. 4, pp. 83–96, 2017.

[37] L. Chaunier, G. D. Valle, D. Lourdin, A.-L. Réguerre, K. Cochet, and E. Leroy, "Viscous sintering kinetics of biopolymer filaments extruded for 3D printing," *Polymer Testing*, vol. 77, article 105873, 2019.

[38] M. U. Aslam Khan, S. I. Abd Razak, W. S. al Arjan et al., "Recent advances in biopolymeric composite materials for tissue engineering and regenerative medicines: a review," *Molecules*, vol. 26, no. 3, p. 619, 2021.

[39] R. A. Ilyas and S. M. Sapuan, "Biopolymers and biocomposites: chemistry and technology," *Current Analytical Chemistry*, vol. 16, no. 5, pp. 500–503, 2020.

[40] M. D. Sarker, S. Naghieh, N. K. Sharma, L. Ning, and X. Chen, "Bioprinting of vascularized tissue scaffolds: influence of biopolymer, cells, growth factors, and gene delivery," *Journal of Healthcare Engineering*, vol. 2019, Article ID 9156921, 20 pages, 2019.

[41] V. Dhinakaran, J. Ajith, A. F. Y. Fahmidha, T. Jagadeesha, T. Sathish, and B. Stalin, "Wire arc additive manufacturing (WAAM) process of nickel based superalloys – a review," *Materials Today: Proceedings*, vol. 21, pp. 920–925, 2020.

[42] P. Zarrintaj, H. Vahabi, T. J. Gutiérrez, M. Mehrpouya, M. R. Ganjali, and M. R. Saeb, "Nanocomposite biomaterials made by 3D printing: achievements and challenges," in *Handbook of Polymer Nanocomposites for Industrial Applications*, pp. 675–685, Elsevier, 2021.

[43] C. Yu, J. Schimelman, P. Wang et al., "Photopolymerizable biomaterials and light-based 3D printing strategies for biomedical applications," *Chemical Reviews*, vol. 120, no. 19, pp. 10695–10743, 2020.

[44] B. I. Oladapo, S. A. Zahedi, and A. O. M. Adeoye, "3D printing of bone scaffolds with hybrid biomaterials," *Composites Part B: Engineering*, vol. 158, pp. 428–436, 2019.

[45] A. E. Jakus, N. R. Geisendorfer, P. L. Lewis, and R. N. Shah, "3D-printing porosity: a new approach to creating elevated porosity materials and structures," *Acta Biomaterialia*, vol. 72, pp. 94–109, 2018.

[46] M. J. Zafar, D. Zhu, and Z. Zhang, "3D printing of bioceramics for bone tissue engineering," *Materials*, vol. 12, no. 20, p. 3361, 2019.

[47] K. Tappa and U. Jammalamadaka, "Novel biomaterials used in medical 3D printing techniques," *Journal of Functional Biomaterials*, vol. 9, no. 1, p. 17, 2018.

[48] D. J. Richards, Y. Tan, J. Jia, H. Yao, and Y. Mei, "3D printing for tissue engineering," *Israel Journal of Chemistry*, vol. 53, no. 9–10, pp. 805–814, 2013.

[49] M. Guvendiren, J. Molde, R. M. D. Soares, and J. Kohn, "Designing biomaterials for 3D printing," *ACS Biomaterials Science & Engineering*, vol. 2, no. 10, pp. 1679–1693, 2016.

[50] H. N. Chia and M. W. Benjamin, "Recent advances in 3D printing of biomaterials," *Journal of Biological Engineering*, vol. 9, no. 1, pp. 1–14, 2015.

[51] D. J. Whyte, R. Rajkhowa, B. Allardyce, and A. Z. Kouzani, "A review on the challenges of 3D printing of organic powders," *Bioprinting*, vol. 16, article e00057, 2019.

[52] Q. Yan, H. Dong, S. Jin et al., "A review of 3D printing technology for medical applications," *Engineering*, vol. 4, no. 5, pp. 729–742, 2018.

[53] R. J. Mondschein, A. Kanitkar, C. B. Williams, S. S. Verbridge, and T. E. Long, "Polymer structure-property requirements for stereolithographic 3D printing of soft tissue engineering scaffolds," *Biomaterials*, vol. 140, pp. 170–188, 2017.

[54] N. Poomathi, S. Singh, C. Prakash et al., "3D printing in tissue engineering: a state of the art review of technologies and biomaterials," *Rapid Prototyping Journal*, vol. 26, no. 7, pp. 1313–1334, 2020.

[55] D. M. Kirchmajer and R. G. Iii, "An overview of the suitability of hydrogel-forming polymers for extrusion-based 3D-printing," *Journal of Materials Chemistry B*, vol. 3, no. 20, pp. 4105–4117, 2015.

[56] A. Skardal and A. Atala, "Biomaterials for integration with 3-D bioprinting," *Annals of Biomedical Engineering*, vol. 43, no. 3, pp. 730–746, 2015.

[57] H. Seitz, W. Rieder, S. Irsen, B. Leukers, and C. Tille, "Three–dimensional printing of porous ceramic scaffolds for bone tissue engineering," *Journal of Biomedical Materials Research Part B: Applied Biomaterials: An Official Journal of The Society for Biomaterials, The Japanese Society for Biomaterials, and The Australian Society for Biomaterials and the Korean Society for Biomaterials*, vol. 74, no. 2, pp. 782–788, 2005.

[58] B. Leukers, H. Gülkan, S. H. Irsen et al., "Biocompatibility of ceramic scaffolds for bone replacement made by 3D printing," *Materialwissenschaft und Werkstofftechnik: Entwicklung, Fertigung, Prüfung, Eigenschaften und Anwendungen technischer Werkstoffe*, vol. 36, no. 12, pp. 781–787, 2005.

[59] V. Dhinakaran, B. Stalin, M. S. Sai, J. Vairamuthu, and S. Marichamy, "Recent developments of graphene composites for energy storage devices," *Materials Today: Proceedings*, vol. 45, pp. 1779–1782, 2021.

[60] Y. Wen, S. Xun, M. Haoye et al., "3D printed porous ceramic scaffolds for bone tissue engineering: a review," *Biomaterials Science*, vol. 5, no. 9, pp. 1690–1698, 2017.

[61] J.-B. Lee, W.-Y. Maeng, Y.-H. Koh, and H.-E. Kim, "Porous calcium phosphate ceramic scaffolds with tailored pore orientations and mechanical properties using lithography-based ceramic 3D printing technique," *Materials*, vol. 11, no. 9, p. 1711, 2018.

[62] X. Du, F. Shengyang, and Y. Zhu, "3D printing of ceramic-based scaffolds for bone tissue engineering: an overview," *Journal of Materials Chemistry B*, vol. 6, no. 27, pp. 4397–4412, 2018.

[63] U. G. Sampath, Y. C. Ching, C. H. Chuah, J. J. Sabariah, and P.-C. Lin, "Fabrication of porous materials from natural/synthetic biopolymers and their composites," *Materials*, vol. 9, no. 12, p. 991, 2016.

[64] M. Hassan, K. Dave, R. Chandrawati, F. Dehghani, and V. G. Gomes, "3D printing of biopolymer nanocomposites for tissue engineering: nanomaterials, processing and structure-function relation," *European Polymer Journal*, vol. 121, p. 109340, 2019.

[65] K. Li, D. Wang, K. Zhao, K. Song, and J. Liang, "Electrohydrodynamic jet 3D printing of PCL/PVP composite scaffold for cell culture," *Talanta*, vol. 211, p. 120750, 2020.

[66] S. Balasubramanian, M.-E. Aubin-Tam, and A. S. Meyer, "3D printing for the fabrication of biofilm-based functional living materials," *ACS Synthetic Biology*, vol. 8, no. 7, pp. 1564–1567, 2019.

[67] F. Pati, J.-H. Shim, J.-S. Lee, and D.-W. Cho, "3D printing of cell-laden constructs for heterogeneous tissue regeneration," *Manufacturing Letters*, vol. 1, no. 1, pp. 49–53, 2013.

[68] S. Nagarajan, S. Radhakrishnan, S. N. Kalkura, S. Balme, P. Miele, and M. Bechelany, "Overview of protein–based biopolymers for biomedical application," *Macromolecular Chemistry and Physics*, vol. 220, no. 14, article 1900126, 2019.

[69] W. Xu, X. Wang, N. Sandler, S. Willför, and X. Chunlin, "Three-dimensional printing of wood-derived biopolymers: a review focused on biomedical applications," *ACS Sustainable Chemistry & Engineering*, vol. 6, no. 5, pp. 5663–5680, 2018.

[70] J. Saroia, Y. Wang, Q. Wei, K. Zhang, T. Lu, and B. Zhang, "A review on biocompatibility nature of hydrogels with 3D printing techniques, tissue engineering application and its future prospective," *Bio-Design and Manufacturing*, vol. 1, no. 4, pp. 265–279, 2018.

[71] G. Vozzi, A. Previti, D. De Rossi, and A. R. T. I. Ahluwalia, "Microsyringe-based deposition of two-dimensional and three-dimensional polymer scaffolds with a well-defined geometry for application to tissue engineering," *Tissue Engineering*, vol. 8, no. 6, pp. 1089–1098, 2002.

[72] S. Yang, K.-F. Leong, Z. Du, and C.-K. Chua, "The design of scaffolds for use in tissue engineering. Part II. Rapid prototyping techniques," *Tissue Engineering*, vol. 8, no. 1, pp. 1–11, 2002.

[73] T. Rasheed, M. Bilal, Y. Zhao, A. Raza, S. Z. H. Shah, and H. M. N. Iqbal, "Physiochemical characteristics and bone/-cartilage tissue engineering potentialities of protein-based macromolecules – a review," *International Journal of Biological Macromolecules*, vol. 121, pp. 13–22, 2019.

[74] Y. Wan, X. Li, and S. Wang, "Recent advances in biohybrid materials for tissue engineering and regenerative medicine," *Journal of Molecular and Engineering Materials*, vol. 4, no. 1, p. 1640001, 2016.

[75] A. George, M. R. Sanjay, R. Srisuk, J. Parameswaranpillai, and S. Siengchin, "A comprehensive review on chemical properties and applications of biopolymers and their composites," *International Journal of Biological Macromolecules*, vol. 154, pp. 329–338, 2020.

[76] E. C. Novosel, C. Kleinhans, and P. J. Kluger, "Vascularization is the key challenge in tissue engineering," *Advanced Drug Delivery Reviews*, vol. 63, no. 4-5, pp. 300–311, 2011.

[77] D. Chouhan, S. Kaushik, and D. Arora, "Trends in bio-derived biomaterials in tissue engineering," in *Biomaterials in Tissue Engineering and Regenerative Medicine: From Basic Concepts to State of the Art Approaches*, pp. 163–213, Springer, 2021.

[78] G. P. Udayakumar, S. Muthusamy, B. Selvaganesh et al., "Biopolymers and composites: properties, characterization and their applications in food, medical and pharmaceutical industries," *Journal of Environmental Chemical Engineering*, vol. 9, no. 4, article 105322, 2021.

[79] V. C.-F. Li, C. K. Dunn, Z. Zhang, Y. Deng, and H. J. Qi, "Direct ink write (DIW) 3D printed cellulose nanocrystal aerogel structures," *Scientific Reports*, vol. 7, no. 1, pp. 1–8, 2017.

[80] E. Arkan, A. H. Azandaryani, P. Moradipour, and L. Behbood, "Biomacromolecular based fibers in nanomedicine: a combination of drug delivery and tissue engineering," *Current Pharmaceutical Biotechnology*, vol. 18, no. 11, pp. 909–924, 2017.

[81] R. Pérez-Pedroza, A. Ávila-Ramírez, Z. Khan, M. Moretti, and C. A. E. Hauser, "Supramolecular biopolymers for tissue engineering," *Advances in Polymer Technology*, vol. 2021, Article ID 8815006, 23 pages, 2021.

[82] M. Azizi-Lalabadi and S. M. Jafari, "Bio-nanocomposites of graphene with biopolymers; fabrication, properties, and applications," *Advances in Colloid and Interface Science*, vol. 292, article 102416, 2021.

[83] F. S. Rezaei, A. Khorshidian, F. M. Beram, A. Derakhshani, J. Esmaeili, and A. Barati, "3D printed

chitosan/polycaprolactone scaffold for lung tissue engineering: hope to be useful for COVID-19 studies," *RSC Advances*, vol. 11, no. 32, pp. 19508–19520, 2021.

[84] K. R. Shoueir, N. El-Desouky, M. M. Rashad, M. K. Ahmed, I. Janowska, and M. El-Kemary, "Chitosan based-nanoparticles and nanocapsules: overview, physicochemical features, applications of a nanofibrous scaffold, and bioprinting," *International Journal of Biological Macromolecules*, vol. 167, pp. 1176–1197, 2020.

[85] A. Vinod, M. R. Sanjay, S. Suchart, and P. Jyotishkumar, "Renewable and sustainable biobased materials: an assessment on biofibers, biofilms, biopolymers and biocomposites," *Journal of Cleaner Production*, vol. 258, article 120978, 2020.

[86] A. M. Al-Ghraibah, M. Al-Qudah, and F. M. AL-Oqla, "Medical implementations of biopolymers," in *Advanced Processing, Properties, and Applications of Starch and Other Bio-Based Polymers*, pp. 157–171, Elsevier, 2020.

[87] B. Leukers, H. Gülkan, S. H. Irsen et al., "Hydroxyapatite scaffolds for bone tissue engineering made by 3D printing," *Journal of Materials Science: Materials in Medicine*, vol. 16, no. 12, pp. 1121–1124, 2005.

[88] A. M. Cakmak, S. Unal, A. Sahin et al., "3D printed polycaprolactone/gelatin/bacterial cellulose/hydroxyapatite composite scaffold for bone tissue engineering," *Polymers*, vol. 12, no. 9, p. 1962, 2020.

[89] C. Liu, "Collagen–hydroxyapatite composite scaffolds for tissue engineering," in *Hydroxyapatite (HAp) for Biomedical Applications*, pp. 211–234, Woodhead Publishing, 2015.

[90] S. Mondal and U. Pal, "3D hydroxyapatite scaffold for bone regeneration and local drug delivery applications," *Journal of Drug Delivery Science and Technology*, vol. 53, p. 101131, 2019.

[91] Y. E. Arslan, T. S. Arslan, B. Derkus, E. Emregul, and K. C. Emregul, "Fabrication of human hair keratin/jellyfish collagen/eggshell-derived hydroxyapatite osteoinductive biocomposite scaffolds for bone tissue engineering: from waste to regenerative medicine products," *Colloids and Surfaces B: Biointerfaces*, vol. 154, pp. 160–170, 2017.

[92] C. E. Corcione, F. Gervaso, F. Scalera et al., "3D printing of hydroxyapatite polymer-based composites for bone tissue engineering," *Journal of Polymer Engineering*, vol. 37, no. 8, pp. 741–746, 2017.

[93] K. K. Moncal, D. N. Heo, K. P. Godzik et al., "3D printing of poly(ε-caprolactone)/poly(D,L-lactide-co-glycolide)/hydroxyapatite composite constructs for bone tissue engineering," *Journal of Materials Research*, vol. 33, no. 14, pp. 1972–1986, 2018.

[94] S.-J. Kim, E. M. Kim, M. Yamamoto, H. Park, and H. Shin, "Engineering multi–cellular spheroids for tissue engineering and regenerative medicine," *Advanced Healthcare Materials*, vol. 9, no. 23, article 2000608, 2020.

[95] S. Datta, R. Barua, and J. Das, "Importance of alginate bioink for 3D bioprinting in tissue engineering and regenerative medicine," IntechOpen, London, UK, 2020.

[96] N. Asadi, A. R. Del Bakhshayesh, S. Davaran, and A. Akbarzadeh, "Common biocompatible polymeric materials for tissue engineering and regenerative medicine," *Materials Chemistry and Physics*, vol. 242, p. 122528, 2020.

[97] I. O. Smith, X. H. Liu, L. A. Smith, and P. X. Ma, "Nanostructured polymer scaffolds for tissue engineering and regenerative medicine," *Wiley Interdisciplinary Reviews: Nanomedicine and Nanobiotechnology*, vol. 1, no. 2, pp. 226–236, 2009.

[98] J. L. Ifkovits and J. A. Burdick, "Review: photopolymerizable and degradable biomaterials for tissue engineering applications," *Tissue Engineering*, vol. 13, no. 10, pp. 2369–2385, 2007.

[99] P. Ramiah, L. C. du Toit, Y. E. Choonara, P. P. D. Kondiah, and V. Pillay, "Hydrogel-based bioinks for 3D bioprinting in tissue regeneration," *Frontiers in Materials*, vol. 7, p. 76, 2020.

[100] M. K. McHale, L. A. Setton, and A. Chilkoti, "Synthesis and in vitro evaluation of enzymatically cross-linked elastin-like polypeptide gels for cartilaginous tissue repair," *Tissue Engineering*, vol. 11, no. 11-12, pp. 1768–1779, 2005.

[101] W. He, T. Yong, W. E. Teo, Z. Ma, and S. Ramakrishna, "Fabrication and endothelialization of collagen-blended biodegradable polymer nanofibers: potential vascular graft for blood vessel tissue engineering," *Tissue Engineering*, vol. 11, no. 9-10, pp. 1574–1588, 2005.

[102] G. D. Nicodemus and S. J. Bryant, "Cell encapsulation in biodegradable hydrogels for tissue engineering applications," *Tissue Engineering Part B: Reviews*, vol. 14, no. 2, pp. 149–165, 2008.

[103] K. J. Shields, M. J. Beckman, G. L. Bowlin, and J. S. Wayne, "Mechanical properties and cellular proliferation of electrospun collagen type II," *Tissue Engineering*, vol. 10, no. 9-10, pp. 1510–1517, 2004.

[104] C. M. Magin, D. L. Alge, and K. S. Anseth, "Bio-inspired 3D microenvironments: a new dimension in tissue engineering," *Biomedical Materials*, vol. 11, no. 2, article 022001, 2016.

[105] T. B. F. Woodfield, C. A. Van Blitterswijk, J. De Wijn, T. J. Sims, A. P. Hollander, and J. Riesle, "Polymer scaffolds fabricated with pore-size gradients as a model for studying the zonal organization within tissue-engineered cartilage constructs," *Tissue Engineering*, vol. 11, no. 9-10, pp. 1297–1311, 2005.

[106] J. D. Kretlow and A. G. Mikos, "Review: mineralization of synthetic polymer scaffolds for bone tissue engineering," *Tissue Engineering*, vol. 13, no. 5, pp. 927–938, 2007.

[107] P. Danilevicius, S. Rekštyte, R. Gadonas et al., "Micro-structured polymer scaffolds fabricated by direct laser writing for tissue engineering," *Journal of Biomedical Optics*, vol. 17, no. 8, article 081405, p. 081401, 2012.

[108] A. Prasopthum, Z. Deng, I. M. Khan, Z. Yin, B. Guo, and J. Yang, "Three dimensional printed degradable and conductive polymer scaffolds promote chondrogenic differentiation of chondroprogenitor cells," *Biomaterials Science*, vol. 8, no. 15, pp. 4287–4298, 2020.

[109] J. L. Walker and M. Santoro, "Processing and production of bioresorbable polymer scaffolds for tissue engineering," in *Bioresorbable Polymers for Biomedical Applications*, pp. 181–203, Woodhead Publishing, 2017.

[110] P. X. Ma and J.-W. Choi, "Biodegradable polymer scaffolds with well-defined interconnected spherical pore network," *Tissue Engineering*, vol. 7, no. 1, pp. 23–33, 2001.

[111] K. Seunarine, N. Gadegaard, M. Tormen, D. O. Meredith, M. O. Riehle, and C. D. W. Wilkinson, "3D polymer scaffolds for tissue engineering," *Nanomedicine*, vol. 1, no. 3, pp. 281–296, 2006.

[112] J. Jacob, J. T. Haponiuk, S. Thomas, and S. Gopi, "Biopolymer based nanomaterials in drug delivery systems: a review," *Materials Today Chemistry*, vol. 9, pp. 43–55, 2018.

[113] A. T. Neffe, C. Wischke, M. Racheva, and A. Lendlein, "Progress in biopolymer-based biomaterials and their application

in controlled drug delivery," *Expert Review of Medical Devices*, vol. 10, no. 6, pp. 813–833, 2013.

[114] S. Gopi, A. Amalraj, and S. Thomas, "Effective drug delivery system of biopolymers based on nanomaterials and hydrogels-a review," *Drug Designing: Open Access*, vol. 5, no. 129, p. 2169, 2016.

[115] J. Chen, F. Xie, X. Li, and L. Chen, "Ionic liquids for the preparation of biopolymer materials for drug/gene delivery: a review," *Green Chemistry*, vol. 20, no. 18, pp. 4169–4200, 2018.

[116] G. V. Patil, "Biopolymer albumin for diagnosis and in drug delivery," *Drug Development Research*, vol. 58, no. 3, pp. 219–247, 2003.

[117] D. Das and S. Pal, "Modified biopolymer-dextrin based cross-linked hydrogels: application in controlled drug delivery," *RSC Advances*, vol. 5, no. 32, pp. 25014–25050, 2015.

[118] M. C. García, "Drug delivery systems based on nonimmunogenic biopolymers," in *Engineering of Biomaterials for Drug Delivery Systems*, pp. 317–344, Woodhead Publishing, 2018.

[119] L. Grøndahl, G. Lawrie, A. Anitha, and A. Shejwalkar, "Applications of alginate biopolymer in drug delivery," in *Biointegration of Medical Implant Materials*, pp. 375–403, Woodhead Publishing, 2020.

[120] M. Rai, A. P. Ingle, I. Gupta, and A. Brandelli, "Bioactivity of noble metal nanoparticles decorated with biopolymers and their application in drug delivery," *International Journal of Pharmaceutics*, vol. 496, no. 2, pp. 159–172, 2015.

[121] J. K. Patra, G. Das, L. F. Fraceto et al., "Nano based drug delivery systems: recent developments and future prospects," *Journal of Nanobiotechnology*, vol. 16, no. 1, pp. 1–33, 2018.

[122] M. Okamoto and B. John, "Synthetic biopolymer nanocomposites for tissue engineering scaffolds," *Progress in Polymer Science*, vol. 38, no. 10-11, pp. 1487–1503, 2013.

[123] V. Vlierberghe, P. D. Sandra, and E. Schacht, "Biopolymer-based hydrogels as scaffolds for tissue engineering applications: a review," *Biomacromolecules*, vol. 12, no. 5, pp. 1387–1408, 2011.

[124] D. Martino, M. S. Alberto, and M. V. Risbud, "Chitosan: a versatile biopolymer for orthopaedic tissue-engineering," *Biomaterials*, vol. 26, no. 30, pp. 5983–5990, 2005.

[125] T. G. Sahana and P. D. Rekha, "Biopolymers: applications in wound healing and skin tissue engineering," *Molecular Biology Reports*, vol. 45, no. 6, pp. 2857–2867, 2018.

[126] C. J. Pérez-Guzmán and R. Castro-Muñoz, "A review of zein as a potential biopolymer for tissue engineering and nanotechnological applications," *Processes*, vol. 8, no. 11, p. 1376, 2020.

[127] H. P. S. A. Khalil, F. Jummaat, E. B. Yahya et al., "A review on micro- to nanocellulose biopolymer scaffold forming for tissue engineering applications," *Polymers*, vol. 12, no. 9, article 2043, 2020.

[128] S. K. Nitta and K. Numata, "Biopolymer-based nanoparticles for drug/gene delivery and tissue engineering," *International Journal of Molecular Sciences*, vol. 14, no. 1, pp. 1629–1654, 2013.

[129] T. Biswal, "Biopolymers for tissue engineering applications: a review," *Materials Today: Proceedings*, vol. 41, pp. 397–402, 2021.

[130] R. S. Ambekar and B. Kandasubramanian, "Progress in the advancement of porous biopolymer scaffold: tissue engineering application," *Industrial & Engineering Chemistry Research*, vol. 58, no. 16, pp. 6163–6194, 2019.

[131] N. Goonoo, A. Bhaw-Luximon, G. L. Bowlin, and D. Jhurry, "An assessment of biopolymer- and synthetic polymer-based scaffolds for bone and vascular tissue engineering," *Polymer International*, vol. 62, no. 4, pp. 523–533, 2013.

[132] M. Swetha, K. Sahithi, A. Moorthi, N. Srinivasan, K. Ramasamy, and N. Selvamurugan, "Biocomposites containing natural polymers and hydroxyapatite for bone tissue engineering," *International Journal of Biological Macromolecules*, vol. 47, no. 1, pp. 1–4, 2010.

[133] D. Li, T. Liu, X. Yu, D. Wu, and S. Zhiqiang, "Fabrication of graphene–biomacromolecule hybrid materials for tissue engineering application," *Polymer Chemistry*, vol. 8, no. 30, pp. 4309–4321, 2017.

[134] J. Velema and D. Kaplan, "Biopolymer-based biomaterials as scaffolds for tissue engineering," in *Tissue Engineering I*, pp. 187–238, Springer, 2006.

[135] A. Mokhtarzadeh, A. Alibakhshi, M. Hejazi, Y. Omidi, and J. E. N. Dolatabadi, "Bacterial-derived biopolymers: advanced natural nanomaterials for drug delivery and tissue engineering," *TrAC Trends in Analytical Chemistry*, vol. 82, pp. 367–384, 2016.

[136] M. Devi, M. Amutheesan, R. Govindhan, and B. Karthikeyan, "A review of three-dimensional printing for biomedical and tissue engineering applications," *The Open Biotechnology Journal*, vol. 12, no. 1, pp. 241–255, 2018.

[137] K. Kolan, Y. Liu, J. Baldridge et al., "Solvent based 3D printing of biopolymer/bioactive glass composite and hydrogel for tissue engineering applications," *Procedia CIRP*, vol. 65, pp. 38–43, 2017.

[138] T. A. E. Ahmed, E. V. Dare, and M. Hincke, "Fibrin: a versatile scaffold for tissue engineering applications," *Tissue Engineering Part B: Reviews*, vol. 14, no. 2, pp. 199–215, 2008.

[139] S. A. Sell, M. J. McClure, K. Garg, P. S. Wolfe, and G. L. Bowlin, "Electrospinning of collagen/biopolymers for regenerative medicine and cardiovascular tissue engineering," *Advanced Drug Delivery Reviews*, vol. 61, no. 12, pp. 1007–1019, 2009.

[140] S. Gomes, I. B. Leonor, J. F. Mano, R. L. Reis, and D. L. Kaplan, "Natural and genetically engineered proteins for tissue engineering," *Progress in Polymer Science*, vol. 37, no. 1, pp. 1–17, 2012.

[141] A. Kumar, S. Mandal, S. Barui et al., "Low temperature additive manufacturing of three dimensional scaffolds for bone-tissue engineering applications: processing related challenges and property assessment," *Materials Science and Engineering: R: Reports*, vol. 103, pp. 1–39, 2016.

[142] R. LogithKumar, A. KeshavNarayan, S. Dhivya, A. Chawla, S. Saravanan, and N. Selvamurugan, "A review of chitosan and its derivatives in bone tissue engineering," *Carbohydrate Polymers*, vol. 151, pp. 172–188, 2016.

[143] H. Nosrati, S. Pourmotabed, and E. Sharifi, "A review on some natural biopolymers and their applications in angiogenesis and tissue engineering," *Journal of Applied Biotechnology Reports*, vol. 5, no. 3, pp. 81–91, 2018.

[144] A. Salerno and C. D. Pascual, "Bio-based polymers, supercritical fluids and tissue engineering," *Process Biochemistry*, vol. 50, no. 5, pp. 826–838, 2015.

[145] M. Khan, A. Aslam, H. Mehboob et al., "Development of polymeric nanocomposite (xyloglucan-co-methacrylic

acid/hydroxyapatite/SiO_2) scaffold for bone tissue engineering applications—in-vitro antibacterial, cytotoxicity and cell culture evaluation," *Polymers*, vol. 12, 2020.

[146] J. X. Law, L. L. Liau, A. Saim, Y. Yang, and R. Idrus, "Electrospun collagen nanofibers and their applications in skin tissue engineering," *Tissue Engineering and Regenerative Medicine*, vol. 14, no. 6, pp. 699–718, 2017.

[147] A. Olad and H. B. K. Hagh, "Graphene oxide and amin-modified graphene oxide incorporated chitosan-gelatin scaffolds as promising materials for tissue engineering," *Composites. Part B, Engineering*, vol. 162, pp. 692–702, 2019.

[148] J. Wang, J. Bai, M. Fan et al., "Cereal-derived arabinoxylans: structural features and structure-activity correlations," *Trends in Food Science and Technology*, vol. 96, pp. 157–165, 2020.

[149] Y. Song, H. Wu, Y. Gao et al., "Zinc silicate/nano-hydroxyapatite/collagen scaffolds promote angiogenesis and bone regeneration via the p38 MAPK pathway in activated monocytes," *ACS Applied Materials & Interfaces*, vol. 12, no. 14, pp. 16058–16075, 2020.

[150] V. Bourquin, N. Nishikubo, H. Abe et al., "Xyloglucan endotransglycosylases have a function during the formation of secondary cell walls of vascular tissues," *The Plant Cell*, vol. 14, no. 12, pp. 3073–3088, 2002.

[151] S. Underwood, A. Afoke, R. Brown, A. MacLeod, P. A. Shamlou, and P. Dunnill, "Wet extrusion of fibronectin-fibrinogen cables for application in tissue engineering," *Biotechnology and Bioengineering*, vol. 73, no. 4, pp. 295–305, 2001.

[152] B. Balakrishnan, M. Mohanty, P. Umashankar, and A. Jayakrishnan, "Evaluation of an in situ forming hydrogel wound dressing based on oxidized alginate and gelatin," *Biomaterials*, vol. 26, no. 32, pp. 6335–6342, 2005.

[153] V. Patrulea, V. Ostafe, G. Borchard, and O. Jordan, "Chitosan as a starting material for wound healing applications," *European Journal of Pharmaceutics and Biopharmaceutics*, vol. 97, Part B, pp. 417–426, 2015.

[154] K. Stapelfeldt, S. Stamboroski, I. Walter et al., "Controlling the multiscale structure of nanofibrous fibrinogen scaffolds for wound healing," *Nano Letters*, vol. 19, no. 9, pp. 6554–6563, 2019.

[155] B. Kocaaga, O. Kurkcuoglu, M. Tatlier, S. Batirel, and F. S. Guner, "Low-methoxyl pectin–zeolite hydrogels controlling drug release promotein vitrowound healing," *Journal of Applied Polymer Science*, vol. 136, no. 24, p. 47640, 2019.

[156] A. Khalid, B. Dongbi, A. Abraham et al., "Electrospun nanodiamond-silk fibroin membranes: a multifunctional platform for biosensing and wound-healing applications," *ACS Applied Materials & Interfaces*, vol. 12, no. 43, pp. 48408–48419, 2020.

[157] W. He, J. Wu, J. Xu, D. A. Mosselhy, Y. Zheng, and S. Yang, "Bacterial cellulose: functional modification and wound healing applications," *Advances in Wound Care*, vol. 10, pp. 623–640, 2021.

[158] S. Sapkota and S. Chou, "Electrospun chitosan-based fibers for wound healing applications," *Journal of Biomaterials*, vol. 4, no. 2, pp. 51–57, 2020.

[159] R. G. Auddy, M. F. Abdullah, S. Das, P. Roy, S. Datta, and A. Mukherjee, "New guar biopolymer silver nanocomposites for wound healing applications," *BioMed Research International*, vol. 2013, Article ID 912458, 8 pages, 2013.

[160] K. Varaprasad, T. Jayaramudu, V. Kanikireddy, C. Toro, and E. Sadiku, "Alginate-based composite materials for wound dressing application:a mini review," *Carbohydrate Polymers*, vol. 236, article 116025, 2020.

[161] S. Gilotra, D. Chouhan, N. Bhardwaj, S. Nandi, and B. Mandal, "Potential of silk sericin based nanofibrous mats for wound dressing applications," *Materials Science & Engineering. C, Materials for Biological Applications*, vol. 90, pp. 420–432, 2018.

[162] H. Bakhsheshi-Rad, A. Ismail, M. Aziz et al., "Development of the PVA/CS nanofibers containing silk protein sericin as a wound dressing: *in vitro* and *in vivo* assessment," *International Journal of Biological Macromolecules*, vol. 149, pp. 513–521, 2020.

[163] A. Iacob, M. Drăgan, O. Ionescu et al., "An overview of biopolymeric electrospun nanofibers based on polysaccharides for wound healing management," *Pharmaceutics*, vol. 12, no. 10, p. 983, 2020.

[164] M. Ahmed, M. Zayed, S. El-Dek, M. A. Hady, D. H. El Sherbiny, and V. Uskoković, "Nanofibrous ε-polycaprolactone scaffolds containing Ag-doped magnetite nanoparticles: physicochemical characterization and biological testing for wound dressing applications *in vitro* and *in vivo*," *Bioactive Materials*, vol. 6, no. 7, pp. 2070–2088, 2021.

[165] H. El-Hamshary, M. El-Naggar, A. El-Faham, M. Abu-Saied, M. K. Ahmed, and M. Al-Sahly, "Preparation and characterization of nanofibrous scaffolds of Ag/vanadate hydroxyapatite encapsulated into polycaprolactone: morphology, mechanical, and in vitro cells adhesion," *Polymers*, vol. 13, no. 8, p. 1327, 2021.

[166] T. A. Jeckson, Y. Neo, S. P. Sisinthy, and B. Gorain, "Delivery of therapeutics from layer-by-layer electrospun nanofiber matrix for wound healing: an update," *Journal of Pharmaceutical Sciences*, vol. 110, pp. 635–653, 2020.

[167] E. G. Lemraski, J. Hossein, M. Dashti et al., "Antimicrobial double-layer wound dressing based on chitosan/polyvinyl alcohol/copper: in vitro and in vivo assessment," *International Journal of Nanomedicine*, vol. 16, pp. 223–235, 2021.

[168] E. Matei, C. Gaidău, M. Râpă et al., "Sustainable rabbit skin glue to produce bioactive nanofibers for nonactive wound dressings," *Materials*, vol. 13, no. 23, p. 5388, 2020.

[169] V.-T. Duong, J. P. Kim, K. Kim, H. Ko, C. H. Hwang, and K.-I. Koo, "Three-dimensional bio-printing technique: trend and potential for high volume implantable tissue generation," *Journal of Biomedical Engineering Research*, vol. 39, no. 5, pp. 188–207, 2018.

[170] C. Starmer, A. Stead, J. Wyngaarden et al., *A Biased History of the Physics of Neuro- and Cardiac Electrophysiology*Medical University of South Carolina.

[171] Z. Xie, M. Gao, A. Lobo, and T. Webster, "3D bioprinting in tissue engineering for medical applications: the classic and the hybrid," *Polymers*, vol. 12, no. 8, p. 1717, 2020.

[172] A. Babbar, V. Jain, D. Gupta, C. Prakash, S. Singh, and A. Sharma, "3D bioprinting in pharmaceuticals, medicine, and tissue engineering applications," in *Advanced Manufacturing and Processing Technology*, pp. 147–161, CRC Press, 2020.

[173] Z. Wang, W. Kapadia, C. Li et al., "Tissue-specific engineering: 3D bioprinting in regenerative medicine," *Journal of Controlled Release*, vol. 329, pp. 237–256, 2020.

[174] E. S. Bishop, S. Mostafa, M. Pakvasa et al., "3-D bioprinting technologies in tissue engineering and regenerative medicine: current and future trends," *Genes & Diseases*, vol. 4, no. 4, pp. 185–195, 2017.

[175] M. Silva, I. S. Pinho, J. A. Covas, N. M. Alves, and M. C. Paiva, "3D printing of graphene-based polymeric nanocomposites for biomedical applications," *Functional Composite Materials*, vol. 2, no. 1, pp. 1–21, 2021.

[176] X. Wang, N. Rivera-Bolaños, B. Jiang, and G. Ameer, "Advanced functional biomaterials for stem cell delivery in regenerative engineering and medicine," *Advanced Functional Materials*, vol. 29, no. 23, article 1809009, 2019.

[177] R. T. Chung, "Development of advanced functional biomaterials," Naval Academy Annapolis MD Annapolis, 2019.

[178] K. Sharma, M. Mujawar, and A. Kaushik, "State-of-art functional biomaterials for tissue engineering," *Frontiers in Materials*, vol. 6, 2019.

[179] Y. Wang, G. Chen, H. Zhang, C. Zhao, L. Sun, and Y. Zhao, "Emerging functional biomaterials as medical patches," *ACS Nano*, vol. 15, no. 4, pp. 5977–6007, 2021.

[180] A. Lendlein, B. F. Pierce, L. Ambrosio, and D. Grijpma, "Advanced functional polymers for medicine: multifunctional biomaterials," *Acta Biomaterialia*, vol. 8, no. 12, article 4199, 2012.

[181] M. Raucci, U. D'Amora, A. Ronca, and L. Ambrosio, "Injectable functional biomaterials for minimally invasive surgery," *Advanced Healthcare Materials*, vol. 9, no. 13, article e2000349, 2020.

[182] J. Gopinathan and I. Noh, "Recent trends in bioinks for 3D printing," *Biomaterials Research*, vol. 22, no. 1, pp. 1–15, 2018.

[183] N. M. Seale, Y. Zeng, and S. Varghese, "Biomimetic tissue engineering for musculoskeletal tissues," in *Developmental Biology and Musculoskeletal Tissue Engineering*, pp. 207–223, Academic Press, 2018.

[184] P. Katyal, F. Mahmoudinobar, and J. Montclare, "Recent trends in peptide and protein-based hydrogels," *Current Opinion in Structural Biology*, vol. 63, pp. 97–105, 2020.

[185] E. Doğan, A. Bhusal, B. Cecen, and A. Miri, "3D printing metamaterials towards tissue engineering," *Applied Materials Today*, vol. 20, article 100752, 2020.

[186] A. Sivashanmugam, R. A. Kumar, M. V. Priya, S. Nair, and R. Jayakumar, "An overview of injectable polymeric hydrogels for tissue engineering," *European Polymer Journal*, vol. 72, pp. 543–565, 2015.

[187] S. Kumar, M. Nehra, D. Kedia, N. Dilbaghi, K. Tankeshwar, and K.-H. Kim, "Nanotechnology-based biomaterials for orthopaedic applications: recent advances and future prospects," *Materials Science & Engineering. C, Materials for Biological Applications*, vol. 106, article 110154, 2020.

[188] J. Patel, T. Sheth, D. Thakore, and D. Dhamat, "Biomimetics in endodontics: a review of the changing trends in endodontics," *Journal of Advanced Oral Research*, vol. 9, no. 1-2, pp. 11–14, 2018.

[189] N. Mukherjee, A. Adak, and S. Ghosh, "Recent trends in the development of peptide and protein-based hydrogel therapeutics for the healing of CNS injury," *Soft Matter*, vol. 16, no. 44, pp. 10046–10064, 2020.

[190] L. Muthukrishnan, "Imminent antimicrobial bioink deploying cellulose, alginate, EPS and synthetic polymers for 3D bioprinting of tissue constructs," *Carbohydrate Polymers*, vol. 260, p. 117774, 2021.

[191] J.-O. Lim, J. Huh, S. I. H. Abdi, S. Ng, and J. J. Yoo, "Functionalized biomaterials-oxygen releasing scaffolds," *Journal of Biotechnology & Biomaterials*, vol. 5, pp. 1–11, 2015.

[192] R. Birla, "Bioengineered bioartificial ventricles," in *Tissue Engineering for the Heart*, pp. 199–226, Springer, Cham, 2016.

[193] S. GV, V. N. Borovkov, A. V. Eremin, A. A. Orlov, and I. N. Saburina, "The stimulation of reparative regeneration in the treatment of fractures of the extremities with the use of new biotechnologies," *Patologicheskaia Fiziologiia i Èksperimental'naia Terapiia*, vol. 81, 2013.

[194] J. Ma, I. Noh, I. Lee, and S. Zhang, "Frontiers in regenerative medical materials: comments from the participants of the 2014 China-Korea Symposium on Biomimetic and Regenerative Medical materials," *Regenerative Biomaterials*, vol. 2, no. 1, pp. 71–76, 2015.

[195] S. Anju, N. Prajitha, V. Sukanya, and P. Mohanan, "Complicity of degradable polymers in health-care applications," *Materials Today Chemistry*, vol. 16, p. 100236, 2020.

[196] S. Mahfouzi, S. A. S. Tali, and G. Amoabediny, "3D bioprinting for lung and tracheal tissue engineering: criteria, advances, challenges, and future directions," *Bioprinting*, vol. 21, article e00124, 2021.

[197] A. Tatara, D. Kontoyiannis, and A. Mikos, "Drug delivery and tissue engineering to promote wound healing in the immunocompromised host: current challenges and future directions," *Advanced Drug Delivery Reviews*, vol. 129, pp. 319–329, 2018.

[198] A. Moshiri, A. Oryan, and M. Shahrezaee, "An overview on bone tissue engineering and regenerative medicine: current challenges, future directions and strategies," *Journal of Sports Medicine & Doping Studies*, vol. 5, 2015.

[199] J. Zhang, Y. Liu, Y. Chen et al., "Adipose-derived stem cells: current applications and future directions in the regeneration of multiple tissues," *Stem Cells International*, vol. 2020, Article ID 8810813, 26 pages, 2020.

Hindawi
International Journal of Polymer Science
Volume 2021, Article ID 4865733, 14 pages
https://doi.org/10.1155/2021/4865733

Research Article

Synthesis of Biomaterial-Based Hydrogels Reinforced with Cellulose Nanocrystals for Biomedical Applications

Pavan Kumar Dara,[1] Mahadevan Raghavankutty,[1] Karthik Deekonda,[2] Anil Kumar Vemu,[3] Visnuvinayagam Sivam,[4] Suseela Mathew,[1] Anandan Rangasamy,[1] Ravishankar Chandragiri Nagarajarao,[1] and Senthilkumar Subramanian[5]

[1]*Biochemistry and Nutrition Division, ICAR-Central Institute of Fisheries Technology, Cochin, 682029 Kerala, India*
[2]*-Chimertech Innovations LLP, Veterinary Incubation Foundation @ TANUVAS, CUL Building, Madhavaram Milk Colony, Chennai, 600 051 Tamil Nadu, India*
[3]*Department of Microbiology, Government Medical College, Ongole, 523001 Andhra Pradesh, India*
[4]*Microbiology and Biotechnology, ICAR-Central Institute of Fisheries Technology, Cochin, 682029 Kerala, India*
[5]*College of Medicine and Health Science, Jigjiga University, Ethiopia*

Correspondence should be addressed to Senthilkumar Subramanian; senthilkumarsubramanian@jju.edu.et

Received 21 June 2021; Accepted 17 August 2021; Published 8 September 2021

Academic Editor: Senthilkumar Rajagopal

Cellulose nanocrystals (CNC) were prepared by formic acid hydrolysis and TEMPO- (2,2,6,6-tetramethyl-piperidine-1-oxyl-) mediated oxidation. The prepared CNCs were reinforced into biopolymers chitosan (CHI), alginate (ALG), and gelatin (GEL) to obtain "CNC-ALG-GEL" and "CNC-CHI-GEL" hydrogels. The synthesized hydrogels were characterized for physicochemical, thermal, and structural characterization using Fourier transform infrared spectroscopy (FT-IR), scanning electron microscopy (SEM), thermal gravity analysis (TGA), and X-ray diffraction (XRD) analyses. Notably, the reinforcement of CNC has not altered the molecular structure of a biopolymer as revealed by FT-IR analysis. The hydrogels reinforced with CNC have shown better thermal stability and miscibility as revealed by thermal gravity analysis. The physicochemical, thermal, and structural characterization revealed the chemical interaction and electrostatic attraction between the CNC and biopolymers. The biocompatibility was investigated by evaluating the viability of the *L929* fibroblast cell, which represents good biocompatibility and nontoxic nature. These hydrogels could be implemented in therapeutic biomedical research and regenerative medicinal applications.

1. Introduction

Cellulose is one of the naturally occurring renewable biopolymers. It plays a key position as an abundant raw organic material which is capable of meeting the demands for green and biobased products [1]. Nanocellulose materials such as cellulose nanocrystals (CNC) and cellulose nanofibrils (CNF) prepared from cellulose have gained tremendous attention in tissue engineering, biomedical applications, and regenerative medicine due to their superior biocompatibility and favourable rheological and biological active properties [2].

CNCs are rod-shaped-like nanoparticles that can be obtained from different types of diversified rich cellulose bioresources such as rice husk, wheat straw, cotton, and wood pulp [3]. It possesses a diameter of 2-20 nm with a length of 100-500 nm. Generally, CNC can be extracted from cellulose biomaterial through acid hydrolysis using acids such as sulfuric acid, formic acid, hydrochloric acid, nitric acid, and phosphoric acid. Nevertheless, among all the acids,

formic acid is mostly preferable due to its certain desirable abilities like being less corrosive, reusable, and easily recoverable and having a low boiling point [4]. Due to minimal cytotoxicity and immunogenicity properties, CNCs have the ability to be utilised as an extracellular matrix in tissue culture medium which enhances cell growth and cell proliferation [5].The immense capacity of CNC for surface charge modification allows researchers to improve their hydrophilicity and stability and thereby enhance the bioavailability of CNC [6]. The nanocrystals with high carboxyl content have been found to be suitable for drug delivery applications [7].

Over the past years, many researchers have attempted to develop extraction methods for the preparation of CNC. Many researchers have developed biopolymer-based materials such as hydrogels and scaffolds for wound dressing, biomedical applications, and therapeutic research. Several research studies have been extensively made for the incorporation/fabrication/injection of CNC into biopolymers such as alginate, chitosan, gelatin, polyvinyl alcohol, and hydroxyapatite [2, 5, 8–11]. Jeddi and Mahkam synthesized nanocarboxymethyl cellulose from CNC to incorporate in bilayer alginate-chitosan hydrogel beads and successfully use as a carrier for the controlled delivery of dexamethasone [12]. In another study, Ntoutoume et al. demonstrated that the curcumin and cyclodextrin complexes with CNC have an antiproliferative effect on colorectal and prostatic cancer cell lines [13]. Further, according to Bertsch et al., the presence of CNC in the polymer complex enhanced the physiological and rheological characteristics of the wound dressing material [14]. Due to the outstanding mechanical properties of CNC, innovative research could evolve for the development of artificial organs such as blood vessels, nuclear pulposus, and soft tissues by the application of CNC [15]. With this rationale, the aim of the present research investigation was to synthesize the CNC from cellulose by formic acid hydrolysis and reinforcement of synthesized CNC into the biopolymers chitosan, alginate, and gelatin for the preparation of hydrogels. The physicochemical, structural rheological, and cytotoxicity properties were assessed that play an important role in biomedical and tissue engineering applications.

2. Materials and Methods

Low molecular weight chitosan (degree of deacetylation with 75–85%, 50–190 kDa), sodium alginate, ferric (III) chloride ($FeCl_3$), formic acid, TEMPO (2,2,6,6-tetramethylpiperidine-1-oxyl), EDC (1-ethyl-3-(3-dimethylaminopropyl)carbodiimide), and sodium bromide (NaBr) were purchased from Sigma, St. Louis, USA. All other chemicals and reagents used in the present study were of either analytical grade (AR) or guaranteed grade (GR).

2.1. Preparation of Cellulose Nanocrystals. CNC was prepared by formic acid hydrolysis according to the following method as described by Du et al. [4]. Briefly, 3 gm of cellulose was added in 100 ml of 0.015 M $FeCl_3$ containing 90 ml formic acid in a spherical flask. The flask was kept at 95°C for 4 h under stirring using a magnetic stirrer (Heidolph Instruments, GmbH and Co., Germany). The flask was cooled down to room temperature followed by centrifugation at 8000 rpm for 10 min using centrifuge (Sorvall Legend XTR, Thermo Fisher Scientific, New Hampshire, USA). The obtained white residue was washed repeatedly with distilled water until pH 6 was achieved. After separation of the supernatant, the white residue nanocrystals were freeze dried at −40°C for 72 h using a freeze dryer (Lark, Tamil Nadu, India) and stored at 4°C until further analysis.

The obtained white residue nanocrystals were subjected to cationic modification using TEMPO and sodium hypochlorite (NaOCl) according to the following method as described by Akhlaghi et al. [6]. 1.5 gm of nanocrystals was added to 100 ml of deionised water and sonicated for 15 min. 20 mg of TEMPO and 400 mg of NaBr were added to the CNC suspension. The pH of the CNC suspension was adjusted to 10 using 1 M NaOH. The oxidation reaction was initiated by adding 10 ml of 13% NaOCl to the CNC suspension under gentle stirring continuously for 3 h, simultaneously maintaining constant pH 10. An aliquot of 10 ml of methanol was added to quench the reaction, and pH was adjusted to 7 using 1 M HCl. Finally, the oxidised nanocrystals were dialysed against deionised water using 14 kDa dialysis membranes (Sigma, St. Louis, USA). The resultant freeze-dried cellulose nanocrystals were designated as "CNC."

2.2. Preparation of Hydrogels Reinforced with CNC. The biomaterial-based hydrogels reinforced with CNC were prepared according to the following method described by Wang et al. [16], with slight modifications. A 1% CNC (20 ml) was dispersed in 40 ml of 2% alginate and 2% chitosan homogenous solutions separately *via* sonication for 15 min and designated as "CNC-ALG" and "CNC-CHI," respectively. Further, a 2% gelatin was dissolved in 40 ml of deionised water with 20 mg of EDC (1-ethyl-3-(3-dimethylaminopropyl)carbodiimide) and stirred continuously for 24 h at room temperature. Fish gelatin was used in the present study, which was prepared according to the following method as described by Dara et al. [17]. This gelatin solution with EDC was added to CNC-ALG and CNC-CHI solutions followed by the addition of 0.5 ml of 50 mM $ZnSO_4$. The suspension was stirred continuously for 6 h at room temperature for ionic cross-linking. Finally, the obtained hydrogels were rinsed with 1x phosphate buffer saline (PBS) and designated as "CNC-ALG-GEL" and "CNC-CHI-GEL," respectively. The hydrogels were stored at 4°C until further analysis. The procedure for the preparation of hydrogels is shown in Figure 1.

2.3. Particle Size Distribution and Zeta Potential Analysis. The particle size distribution (PSD) and zeta potential of CNC and hydrogel samples were determined by dynamic light scattering analyses (DLS) using a Zetasizer Nano Series (Malvern, Worcestershire, UK). For PSD analysis, the CNC and hydrogel samples were loaded into a quartz cuvette with 1 cm path-length and were subjected to DLS measurement with a detection angle of 90° at 25 ± 0.1°C. The *Z*-average

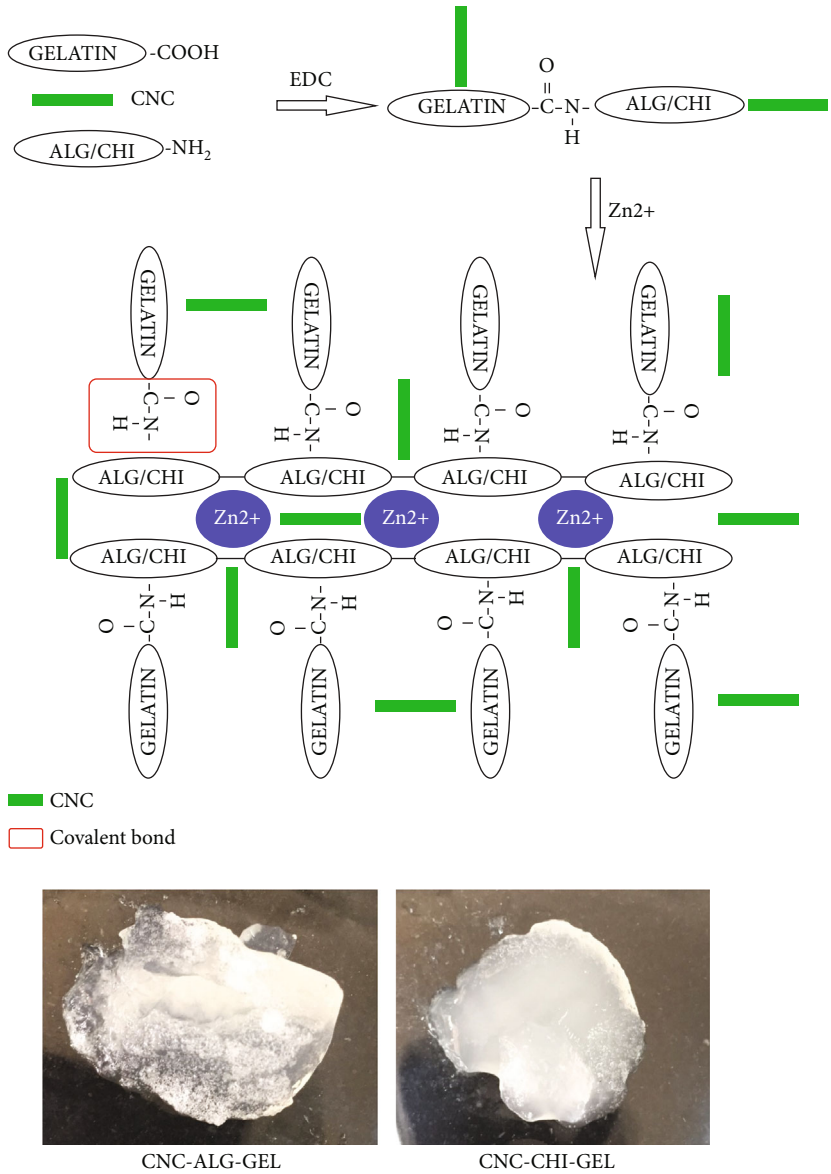

Figure 1: Procedure for the preparation of hydrogels reinforced with CNC.

hydrodynamic diameters and polydispersity index (PDI) of hydrogels were determined and recorded based on the scattering intensity. For analysing the zeta potential, the CNC and hydrogel samples were filtered using a 0.45 μm syringe filter membrane to remove large particles and measured with an angle of 15° at 25°C.

2.4. FT-IR Spectra and SEM Morphology. The FT-IR spectra of CNC and hydrogels were analysed using a FT-IR spectrometer (Bruker Optik GmBH, Germany), in the region of 4000 cm^{-1}–500 cm^{-1} wave numbers at 4 cm^{-1} resolution. The surface morphology was examined using scanning electron microscopy (SEM JSM, Japan), and samples were observed at an accelerated 15 kV voltage.

2.5. X-Ray Diffraction (XRD) Pattern. X-ray powder diffraction patterns of CNC and hydrogels were recorded using an Analytical X'Pert Pro X-ray diffractometer. The X-ray source was Cu-Kα radiation (40 kV, 80 mA). The XRD patterns of samples were taken in the 2θ range of 10°–80° in a fixed time mode at room temperature at a scanning rate of 4° min^{-1}.

2.6. Thermal Characteristics. Prior to the analyses, the CNC and hydrogel samples were conditioned at 25°C and 53% relative humidity. DTG (derivative thermogravimetry) and DTA (differential thermal analysis) of hydrogels were analysed using a thermogravimetric analyser (Seiko Exstar 6300, Italy). Samples were heated from 600°C, at 20°C/min heating rate, using nitrogen flow (250 ml/min). The T_o (onset temperature), T_m (melting temperature), and ΔH (enthalpy) of hydrogel samples were obtained from DTG/DTA curves.

2.7. Rheological Study. The rheological flow properties (shear stress and viscosity vs. shear rate) of CNC and hydrogels

were measured using a Brookfield DV-III Ultra™ Programmable Rheometer (Brookfield Engineering Laboratories Inc., Middleboro, USA). The cone and plate spindle (CP-41 model) with measuring geometry of 5 cm was used with a gap of 0.05 mm and a shear rate ranging from 10 to 100 s^{-1}. A flow curve was obtained by plotting shear stress and viscosity vs. shear rate values using a steady state flow program. The Herschel–Bulkley model was selected as the best-fit model based on standard error of shear stress-shear rate and shear stress-viscosity data.

The Herschel–Bulkley model equation is as follows:

$$\tau = \tau_o + kD^{\eta}, \quad (1)$$

where τ is the shear stress (Pa), τ_o is the yield stress (Pa), D is the shear rate (s^{-1}), k is the consistency coefficient, and η is the flow behaviour index (dimensionless). The consistency coefficient (k) and flow behaviour index (η) of CNC and hydrogels were determined by the steady state flow program software.

2.8. In Vitro Degradation. In vitro degradation of CNC and hydrogels was studied using the enzymatic digestion method. A known weight of the hydrogel sample was taken and placed in an aliquot (10 ml) of PBS with 10 U/ml of trypsin at 37°C for the duration of 7 days. The weight of hydrogel samples was taken periodically.

2.9. Cytotoxicity. Cytotoxicity/biocompatibility of CNC and hydrogels was investigated by MTT (3-(4,5-dimethylthiazol-2-yl)-2,5-diphenyltetrazolium bromide) assay according to the method followed Dara et al. [18]. The viability of cells was calculated and was expressed in percentage (%).

$$\text{Cell viablity (\%)} = \frac{\text{OD of sample}}{\text{OD of control}} \times 100. \quad (2)$$

2.10. Statistical Analysis. One-way ANOVA was used to analyse the data. Experiments were carried out in triplicates independently. Significant differences between the means of triplicates were determined by Duncan's multiple comparison test using statistical software IBM SPSS 20 (SPSS Inc., Illinois, USA).

3. Results and Discussion

3.1. Particle Size Distribution and Zeta Potential Analysis. Particle size distribution is one of the most important characteristic properties that determine its functionality, whereas the zeta potential defines the potential difference between the dispersion medium and the layer of fluid attached to the dispersed nanocrystals in a colloidal system of charged particles [10]. The Z-average hydrodynamic diameter, polydispersity index (PDI), and zeta potential data of hydrogels are displayed in Table 1. The Z-average hydrodynamic diameter and zeta potential of synthesized CNC were found to be 192 nm and -48.40 mV, respectively. The particle size of the CNC depends on several factors such as type of acid used for the hydrolysis, reaction temperature, and reaction time [1]. In the present study, formic acid was used for the hydrolysis, and the reaction time and temperature were 4 h and 95°C, respectively. The smaller particle size and higher zeta potential of synthesized CNC were most likely due to the improved dispersibility and conversion of hydroxyl groups to carboxyl groups on the biopolymer cellulose surface during the TEMPO-mediated oxidation process [19]. The Z-average hydrodynamic diameter and zeta potential of hydrogels CNC-ALG-GEL and CNC-CHI-GEL were found to be 415 nm and 572 nm and -61.6 mV and +16.9 mV, respectively. It can be noted that the changes in the particle size and zeta potential of CNC-ALG-GEL and CNC-CHI-GEL represent the colloidal electrostatic interactions between the incorporated CNC, chitosan, and alginate biopolymers. The negative zeta potential value of CNC-ALG-GEL (-61.6 mV) indicates the presence of carboxyl groups, and the positive value of CNC-CHI-GEL confers the cationic characteristics of chitosan chains [18, 20]. Further, the lowest zeta potential (+16.9 mV) of CNC-CHI-GEL might be due to the neutralization of amino groups on biopolymer chitosan that results from the separation from CNC and aggregation at the surface of nanocrystals [21]. Nevertheless, the nature of the biopolymers used for the surface modification defines the surface charge. In the present study, the positive zeta potential of CNC-CHI-GEL and CHI-GEL represents the cationic characteristic of chitosan, whereas the negative zeta potential of CNC-ALG-GEL and ALG-GEL could be originated from the carboxylic groups of alginate. The smaller particle size of CNC-ALG-GEL might be due to more affinity and adsorption of the cellulose nanocrystal to the surface of the biopolymer. Moreover, the swelling of cellulose nanocrystals tends to create repulsion between polymeric chains which results in increasing the particle size [15]. It can be noticed that the synthesized CNC and hydrogels were monodispersed which was evident by the low PDI (<0.5). Furthermore, the detailed morphological studies of CNC and hydrogels were confirmed by SEM. From this data, it can be deduced that the biopolymer hydrogels were highly stable due to reinforcement of CNC.

Table 1: Particle size distribution and zeta potential of hydrogels.

Samples	Particle size (d·nm)	PDI	Zeta potential (mV)
CNC	192 ± 6.82	0.275 ± 0.0013	−48.4 ± 0.62
ALG-GEL	251 ± 7.80	0.376 ± 0.0110	−24.4 ± 2.06
CHI-GEL	308 ± 9.87	0.405 ± 0.0236	61.5 ± 5.87
CNC-ALG-GEL	415 ± 14.30	0.464 ± 0.0215	−61.6 ± 7.89
CNC-CHI-GEL	572 ± 13.74	0.488 ± 0.0255	16.9 ± 1.96

3.2. FT-IR Spectra. FT-IR spectral analysis was performed to study the alterations in the functional groups of the hydrogels that would have occurred due to cross-linking of CNC. The FT-IR spectra of CNC were found to have

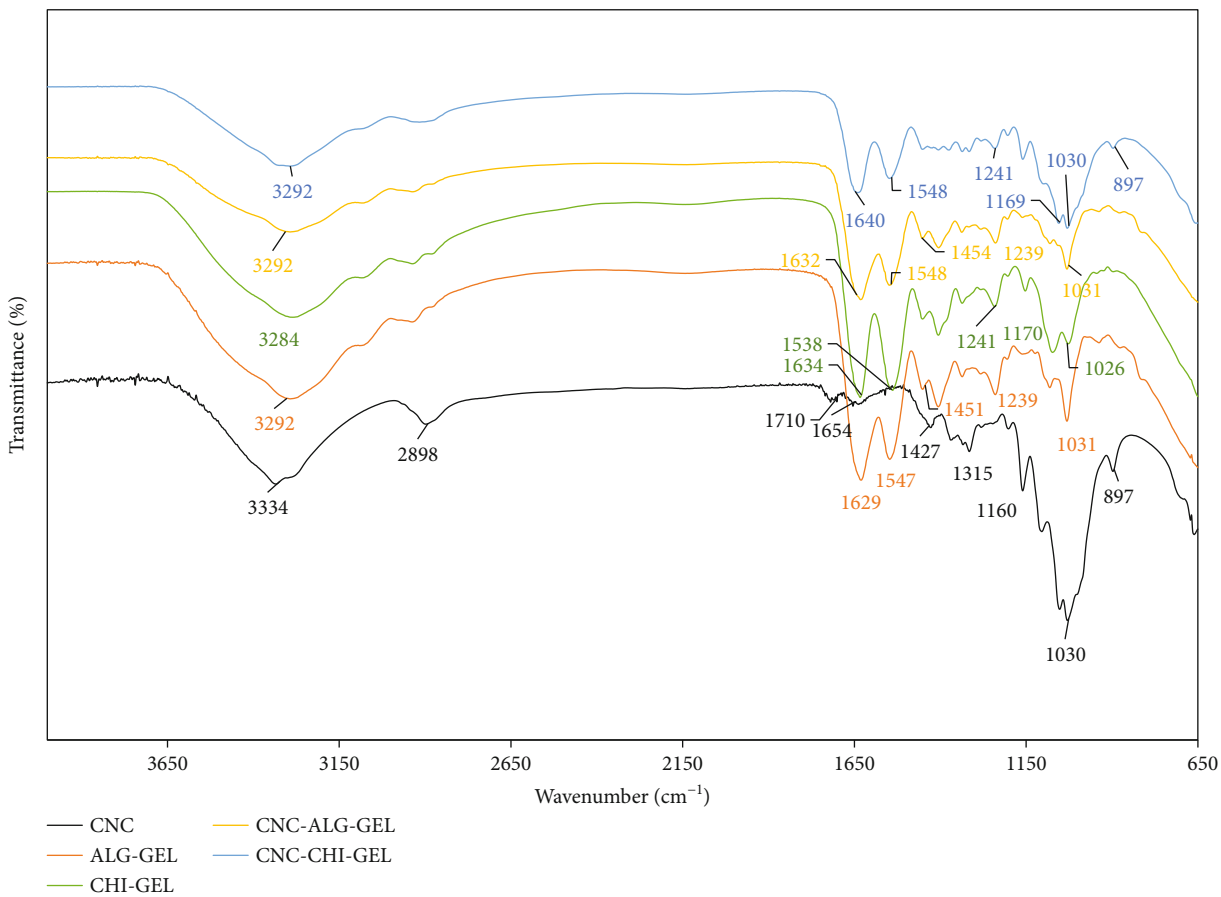

Figure 2: FT-IR spectra of CNC and hydrogels.

absorption bands at wave numbers at 3334 cm^{-1}, 2898 cm^{-1}, 1654 cm^{-1}, 1427 cm^{-1}, 1315 cm^{-1}, 1150 cm^{-1},1030 cm^{-1}, and 897 cm^{-1}, which can be attributed to O-H, C-H, COO^{-}, O-H bending, C-O stretching, CO-O-CO stretching, and C-H bending, respectively (Figure 2). The spectral data of CNC were in accordance with the spectral data of CNC extracted from rice husk [3]. The absorption band of CNC at a wave number at 1710 cm^{-1} can be attributed to stretching of carbonyl groups (C=O) resulting from the TEMPO reaction [22]. The characteristic absorption peaks of CNC-CHI-GEL and CHI-GEL at wave number ≈ 1170 cm^{-1} can be assigned to the free amine group (-NH_2) of the chitosan molecule, whereas on the other hand, the absorption peak of CNC-ALG-GEL and ALG-GEL wave number ≈ 1450 c m^{-1} could be related to the carboxylic group (-COOH) of alginate [5]. In line with these reports, our findings correlated well with the results of zeta potential analyses as reported earlier. The pattern of absorption bands of all the hydrogels was in accordance with the FT-IR spectra of fish gelatin [17]. It can be noted that the appearance of a broad absorption band at wave number ≈ 1625 cm^{-1} of all hydrogel samples is an indicator of the successful formation of a complex between carboxylic groups of CNC and amino groups of biopolymers. Furthermore, it is stated that the intensity of the peak at region ~1625 cm^{-1} of all hydrogel samples represents the successful cross-linking of the gelatin chain with

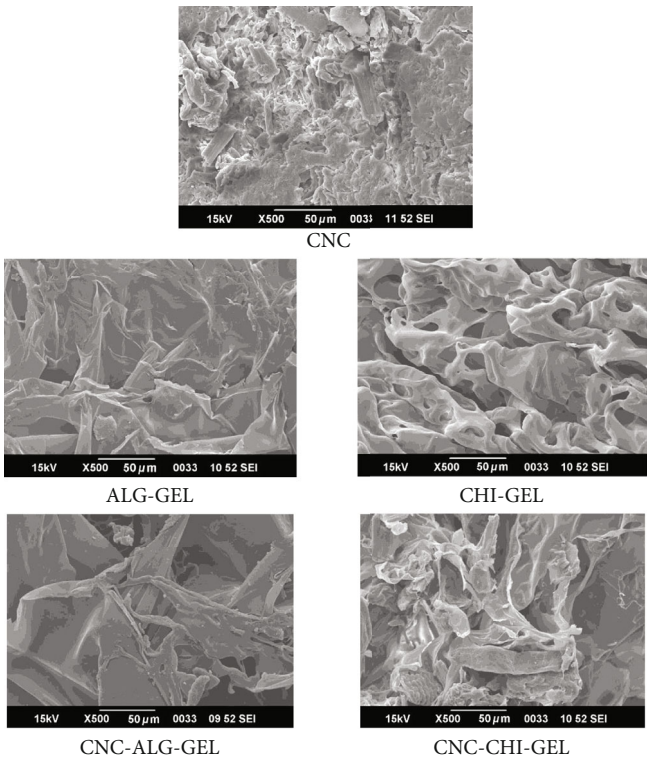

Figure 3: SEM of CNC and hydrogels.

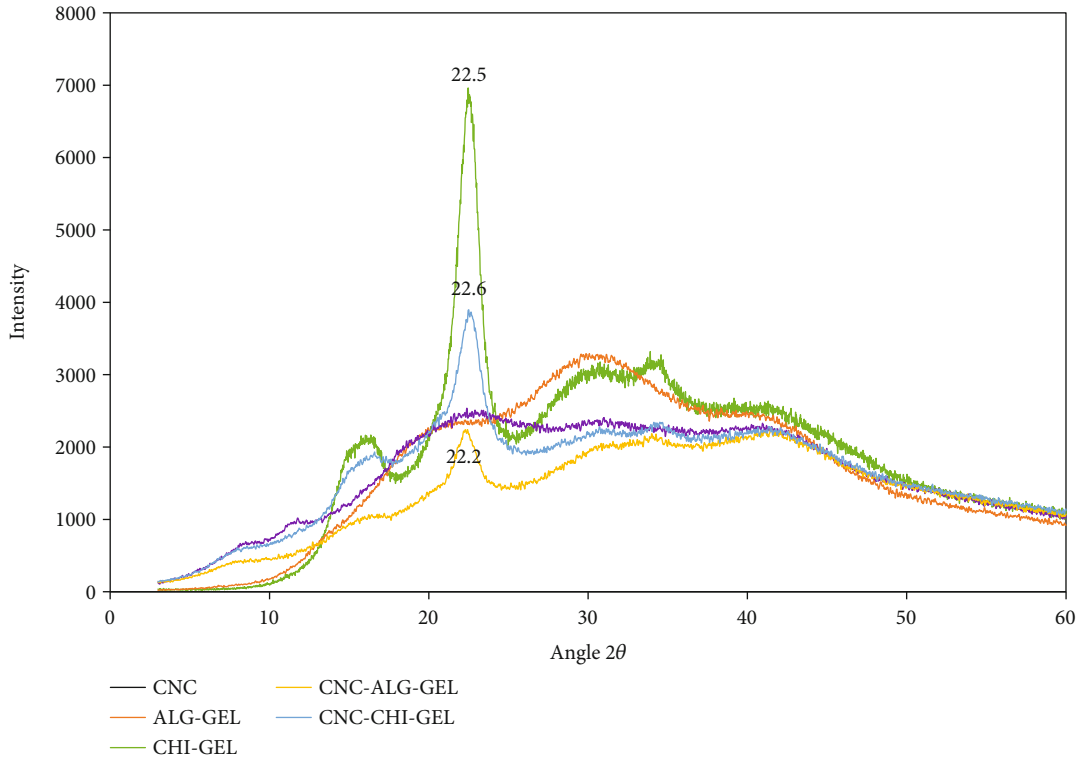

Figure 4: XRD of CNC and hydrogels.

the biopolymer hydrogels by overlapping the amide group of the gelatin molecule [3]. In another study by Wang et al., it was mentioned that the broad absorption peaks in the region (3200 cm^{-1}–2900 cm^{-1}) of the spectrum of hydrogels illustrate the strong O-H bond interaction between the biopolymer-gelatin backbone and CNC molecules [16]. The absorption bands of CNC at regions ~1425 cm^{-1} and ~1225 cm^{-1} were shifted to different frequencies in hydrogel samples after reinforcement, and this emphasizes the formation complex inter- and intrahydrogen bonding between CNC and polymer matrix [23]. The FT-IR results of the present study clearly indicated that the reinforcement of CNC has not altered the network structure of biopolymer molecules.

3.3. SEM Morphology. The morphology and microstructures of CNC and hydrogels were depicted in Figure 3. The morphology of CNC was found to have roughness with fractured surface. It is well known that the morphology of nanocrystals depends upon the severity of hydrolysis used for the reaction [4]. In the present study, the formic acid hydrolysis method was used for the preparation of CNC. The SEM micrographs of ALG-GEL, CNC-ALG-GEL, CHI-GEL, and CNC-CHI-GEL appeared to be smooth and also showed porous structures compared to the micrograph of CNC, which indicated the blend miscibility, high homogeneity, and *in situ* dissolution of biopolymers to form blend mixtures [22]. The impact of smoothness and porosity was high in CNC-ALG-GEL and CNC-CHI-GEL hydrogels as compared to ALG-GEL and CHI-GEL. It is noticed that certain factors such as hydrogen bonding and complexity of CNC with biopolymers define the network structure formation of hydrogel membranes [24]. The uniform distribution of pores in the CNC-ALG-GEL and CNC-CHI-GEL hydrogels reflected the embedded nature of CNC which resulted from strong interfacial adhesion between the CNC and the biopolymer matrix. Technically, the roughness and smoothness of hydrogel membranes depend upon the concentration of CNC added to hydrogels [9]. In the present study, the interpenetrated networks in the hydrogel membranes due to the reinforcement of CNC were a good indication of superior mechanical properties and good stability against degradation, which correlated well with an earlier report [16]. Moreover, the hydrogels with these characteristics also support other features such as easy injectability and cost-effectiveness which are more suitable for tissue engineering and regenerative medicine applications [1].

3.4. X-Ray Diffraction (XRD) Pattern. As shown in Figure 4, the CNC showed three cellulose characteristic peaks at $2\theta = 14.2^\circ$, 16.4°, and 22.5°, where the prominent characteristic sharp peak at $2\theta = 22.5^\circ$ attributing to (200) plane reflection of crystal lattice of alpha-cellulose and hemicelluloses [25]. The peak at $2\theta = 20^\circ$ of CHI-GEL indicates the semiamorphous nature of chitosan, whereas the peak at $2\theta = 19.9^\circ$ of ALG-GEL indicates the amorphous and crystalline nature of alginate [5, 18]. The characteristic peak of CNC at $2\theta = 22^\circ$ appeared in the CNC-ALG-GEL and CNC-CHI-GEL which indicated the presence of CNC in the hydrogel membrane matrix. However, this characteristic peak was slightly shifted, and the disparity in crystallinity can be due to intermolecular interactions. It was noticed that the intensity of

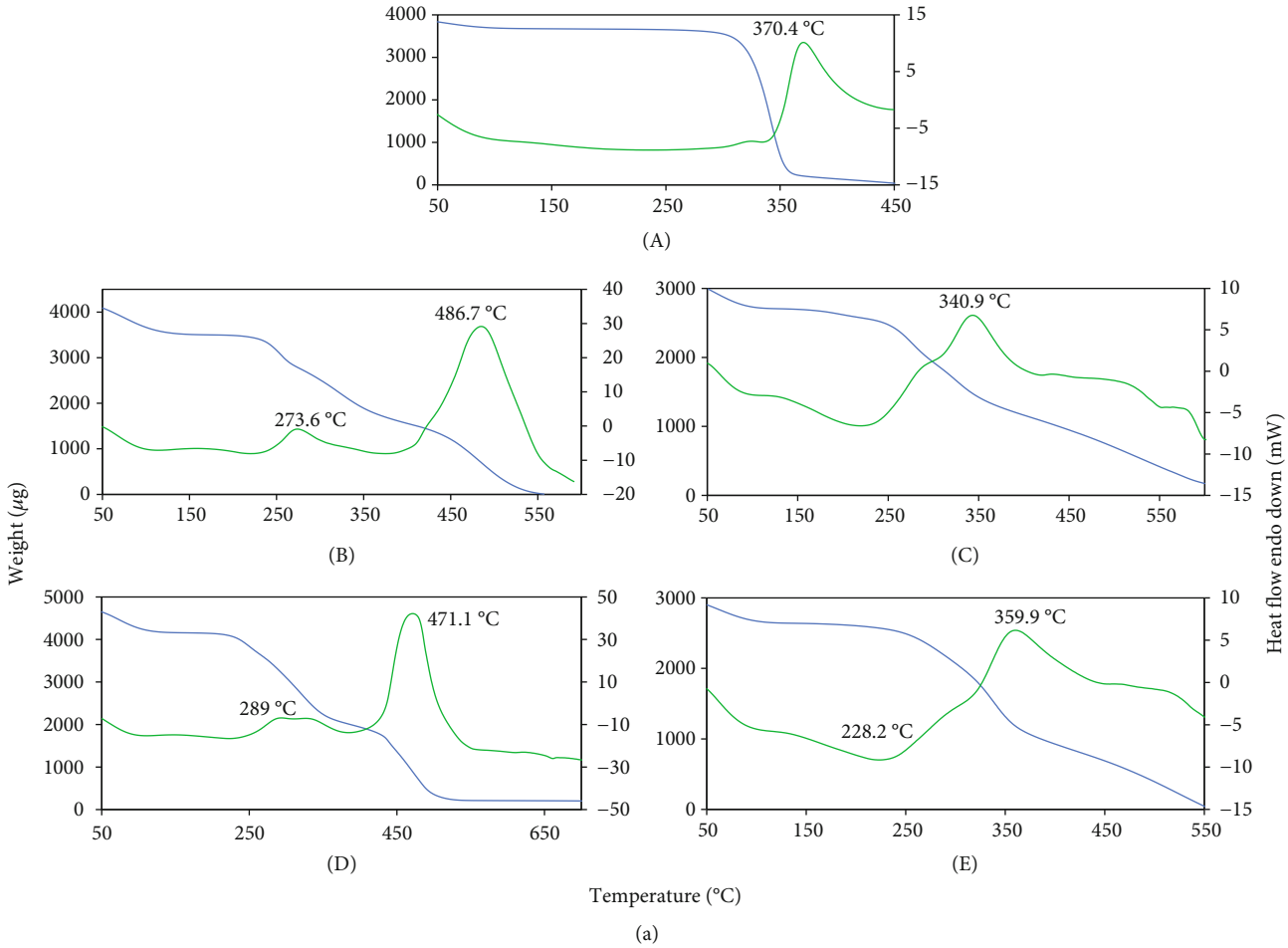

(a)

Figure 5: Continued.

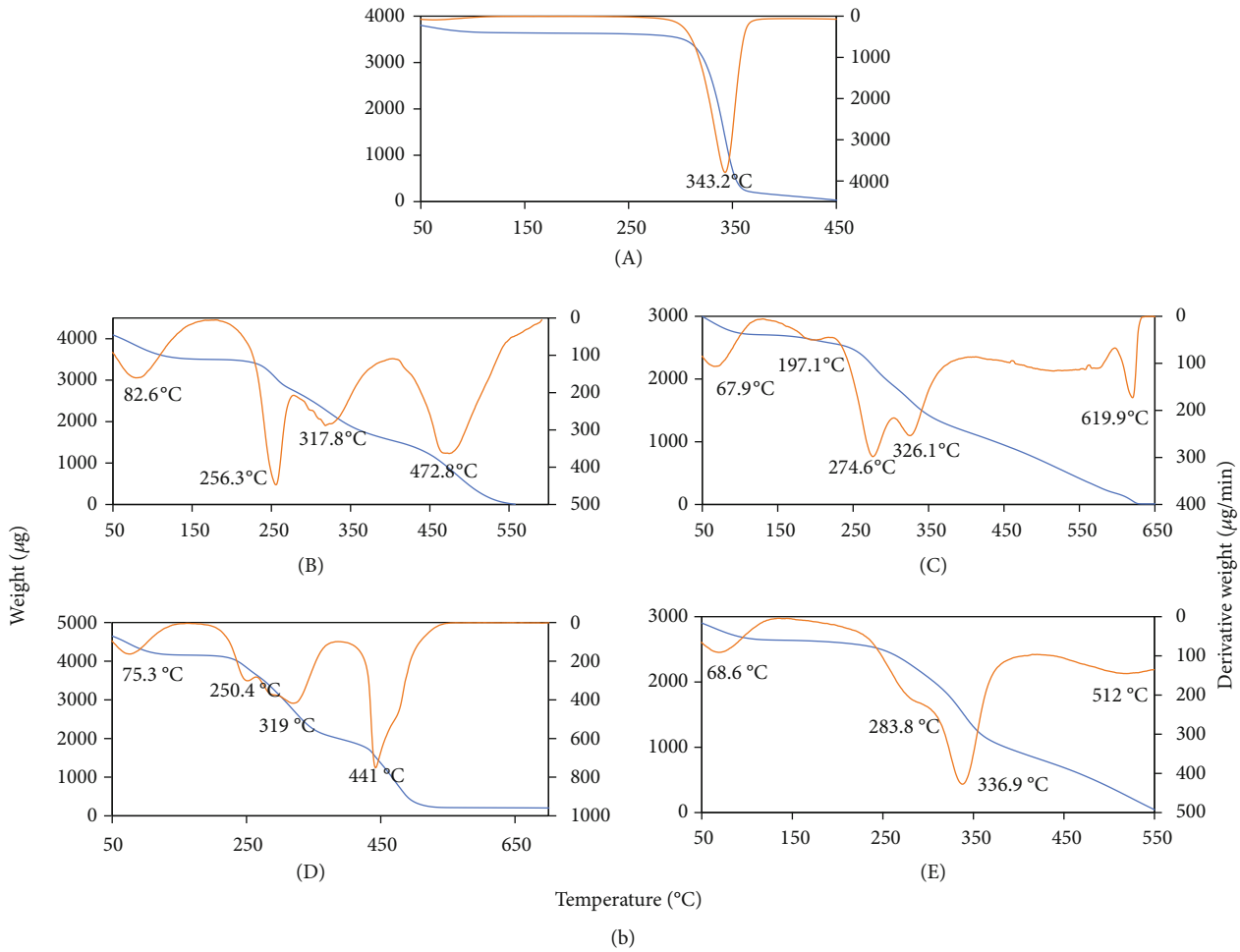

Figure 5: (a) DTA curves of hydrogels (A) CNC, (B) ALG-GEL, (C) CHI-GEL, (D) CNC-ALG-GEL, and (E) CNC-CHI-GEL at 20°C/min heating rate. (b) DTG curves of hydrogels (A) CNC, (B) ALG-GEL, (C) CHI-GEL, (D) CNC-ALG-GEL, and (E) CNC-CHI-GEL at 20°C/min heating rate.

the peak at $2\theta = 22^{\circ}$ of CNC-ALG-GEL was lesser as compared to that of CNC-CHI-GEL, which could be due to the difference in the percolation phenomenon of CNC in contact with alginate [8]. The intensity of the peak at $2\theta = 22^{\circ}$ of CNC-ALG-GEL was found to be increased as compared to that of CNC-CHI-GEL, due to the transcrystallization effect of nanocrystals. Furthermore, it can also be stated that the interaction between the CNC and the biopolymer matrix was one of the probable reasons for the increment of crystallinity [9]. However, XRD data in the present study revealed that the reinforcement of CNC does not change the structural uniformity of the hydrogel-based biopolymer matrix by improving the molecular ordering and mechanical properties as well as the amorphous nature of the polymer matrix.

3.5. Thermal Characteristics. DTG/DTA curves of hydrogel samples at 20°C/min heating rate under inert atmosphere are depicted in Figures 5(a) and 5(b). The thermal characteristic data illustrated that all the hydrogel samples have shown three major degradation steps. Thermal degradation of polymers includes dehydration followed by decomposition along with breakage of intra- and interlinkages in the structure of polymers [26]. The first degradation step of CNC was shown between 50°C and 300°C, which might be due to the loss of water bound to the polymer. The second degradation step was in the range of 300–360°C, and the maximum degradation temperature at this point was found to be 343°C. The final and third degradation step was found to be approximately at 450°C. The first degradation steps of hydrogels ALG-GEL, CHI-GEL, CNC-ALG-GEL, and CNC-CHI-GEL were found to be 82°C, 67°C, 75°C, and 68°C, respectively. The maximum degradation temperatures of hydrogels during the second step were observed to be 256°C, 274°C, 319°C and 336°C, respectively. The maximum degradation temperature of hydrogels hardly changes with the incorporation of CNC in the biopolymer matrix. It indicated that the CNC retained the thermal stability of hydrogels due to the strong interactions between CNC and biopolymers [27]. The significant weight loss of CHI-GEL and CNC-CHI-GEL hydrogels at the 200-400°C temperature range can be attributed to the depolymerization of chitosan

through deacetylation and cleavage of glycosidic linkages *via* dehydration and deamination, whereas in the case of ALG-GEL and CNC-ALG-GEL, it could be due to chain scission and ring opening reactions of alginate [9]. Maximum weight loss was observed to be in the second degradation step which could be attributed to degradation and dislocation of backbone linkages as well as functional groups of biopolymers [26]. The final and third degradation steps of hydrogels ALG-GEL and CHI-GEL were found to be at 472°C and 619°C, respectively, whereas for CNC-ALG-GEL and CNC-CHI-GEL hydrogels, they were at 441°C and 512°C, respectively. It can be observed that the reinforcement of CNC to the hydrogels has reduced the degradation temperature. This might be due to the decomposition of CNC derivatives that indicated the carbonization of polymeric biomaterial [28]. This difference in the degradation temperature and weight loss between the hydrogels might be due to the difference in the formation of hydrogen bonding between the CNC and molecules of biopolymers, and cross-linkers [29].

Figures 5(a) and 5(b) and Table 2 illustrate the T_o (onset temperature), T_m (melting temperature), and ΔH (enthalpy) of hydrogels. T_o, T_m, and ΔH (enthalpy) of polymeric blends usually represent the kinetic hindrances that take place during crystallization and melting. CNC showed a T_m value of 370°C that corresponds to the decomposition of glycosyl units and the formation of carbonaceous residues [30]. The CNC-CHI-GEL hydrogels reinforced with CNC were found to have a high T_m value compared to that of CHI-GEL, whereas CNC-ALG-GEL was marginally lesser than ALG-GEL. In a previous study by Rescignano et al., it was noted that the T_m values of chitosan and alginate biomaterials incorporated with CNC were found to be 289°C and 317°C, respectively [20]. In the present study, the T_m values of chitosan and alginate hydrogels reinforced with CNC were observed to be 359°C and 417°C, respectively. The disparity in T_m values might be due to the formation of intermolecular hydrogen interactions between chitosan, alginate, and CNC at elevated temperature. As the T_m value goes beyond the elevated temperature, the biopolymer gets the tendency to donate hydrogen bonds and results in the production of more -OH groups, and these groups facilitate more interaction and influence the melting temperature of biopolymeric materials [8]. Moreover, chemically modified CNC incorporated in biopolymers influence the T_m, due to strong interactions between chemically modified CNC and polymer matrices which could be originated from T_m difference [6]. Notably, the chemically modified CNC do not have any impact on the T_o of biopolymers [1]. The other resultant exothermic peaks of hydrogel membranes might be due to the decomposition of alginate as well as the breakdown of intermolecular structure of gelatin [31]. It is demonstrated from the present data that the biomaterial-based hydrogels reinforced with cellulose nanocrystals showed better thermal stability and miscibility as revealed by thermal gravity analysis.

3.6. Rheological Study. Different sorts of physicodynamic or computer rheological models such as Herschel–Bulkley, Newtonian, Bingham, Casson, and Power law were usually used to present the flow profile of blends and hydrogels to describe shear stress and shear behaviour. The Herschel–Bulkley rheological model is mostly preferred due to its accuracy. In the present study, the rheological Herschel–Bulkley model was used to analyse the experimental result data (shear stress and viscosity-shear rate) of hydrogel solutions (Table 3).The yield stress (T_o), flow behaviour index (η), and consistency coefficient (k) were also calculated using the software provided with the rheometer. The yield stress (T_o) represents the interaction potential of colloidal particles in the biopolymer and also plays an important role in demonstrating the macrolattice structure of biopolymers [32]. The rheological Herschel–Bulkley model exhibited yield stress values for hydrogel samples which were studied (Table 3). The T_o and consistency coefficient (k) values of ALG-GEL and CHI-GEL were found to have higher values as compared to those of CNC-ALG-GEL and CNC-CHI-GEL hydrogels, respectively. It has been stated that the method of analysis and experimental condition influences the yield stress [33]. Several research studies have conflated views on the yield stress which could be linked with the transition between liquid and solid states and/or two same fluids with different viscosities [34].

The ALG-GEL exhibited shear thickening and Newtonian behaviour, whereas the CHI-GEL exhibited shear thinning and pseudoplastic behaviour, which represents an irreversible structural breakdown (Figure 6). The Newtonian behaviour of ALG-GEL at low shear rates was characterized by shear rate-independent viscosity. The shear thinning behaviour of CHI-GEL indicates the disrupted intermolecular junctions with a slower rate of reformations, which tends to drop in viscosity at a lower shear rate [35]. As the shear rate increases, the viscosity of CNC-ALG-GEL and CNC-CHI-GEL hydrogels tends to decrease. This might be due to the distributed and weak nature of the hydrogel network,

Table 2: Thermal characteristics of CNC and hydrogels.

Samples	T_o (°C)	T_m (°C)	ΔH (mJ/mg)
CNC	313.2 ± 14.86	370.4 ± 16.82	−618 ± 23
ALG-GEL	230.4 ± 11.24	486.7 ± 17.80	−5675 ± 209
CHI-GEL	237.7 ± 12.45	340.9 ± 29.87	−889 ± 236
CNC-ALG-GEL	237.8 ± 13.56	471.1 ± 14.30	−4992 ± 215
CNC-CHI-GEL	246.9 ± 10.41	359.9 ± 13.74	−707 ± 55

Table 3: Herschel–Bulkley parameters for hydrogels.

Hydrogels	T_o	k	η'	R^2
CNC	0.03	0.74	1.38	0.99
ALG-GEL	0.14	1.40	1.04	0.99
CNC-ALG-GEL	0.04	0.96	1.26	0.99
CHI-GEL	0.08	20.5	0.80	0.99
CNC-CHI-GEL	0.06	11.7	1.06	0.99

T_o: yield stress; k: consistency coefficient; η: flow behavior index; R^2: regression coefficient.

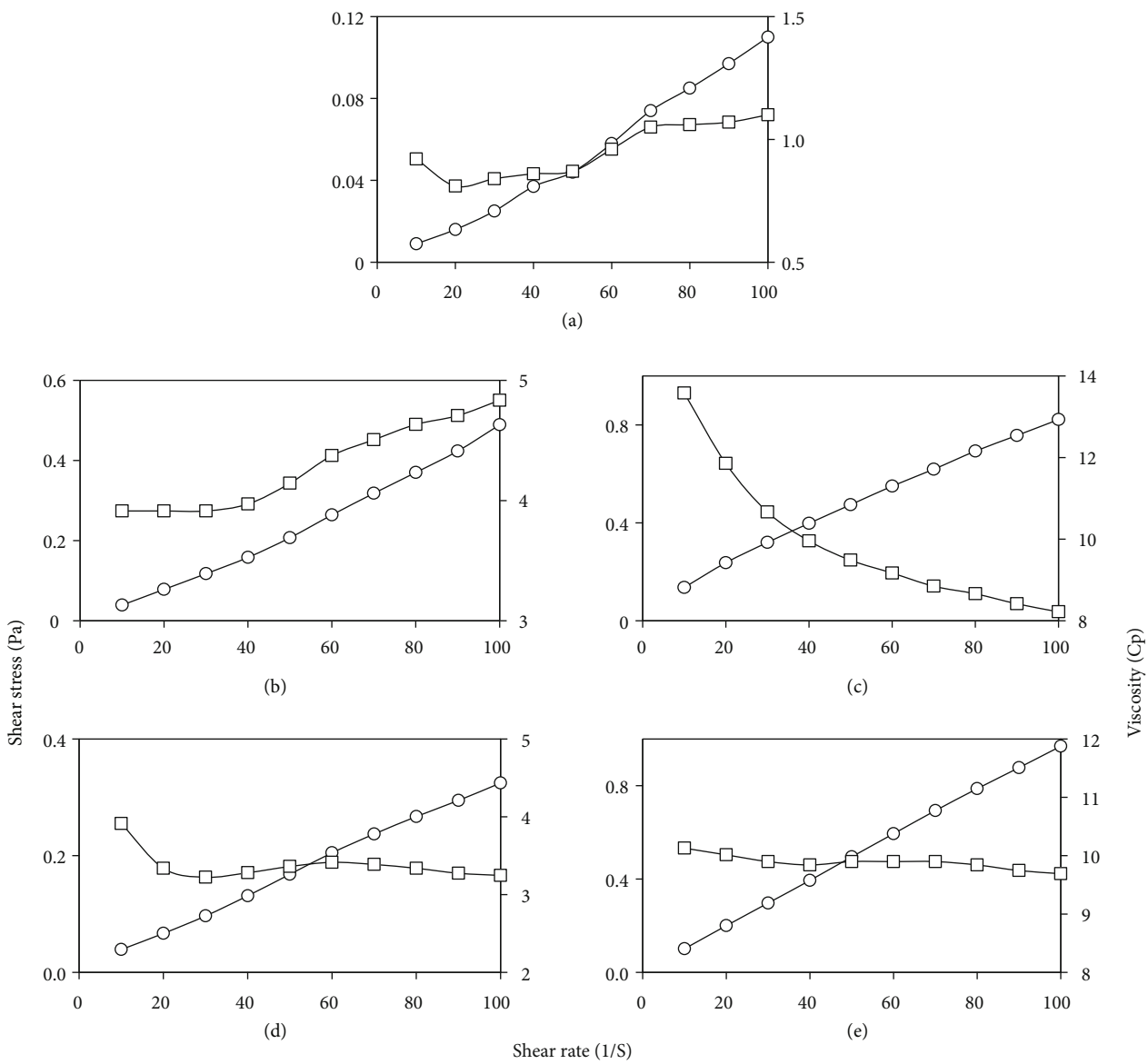

Figure 6: Flow properties (shear stress vs. shear rate and viscosity vs. shear rate) of hydrogels. (a) CNC, (b) ALG-GEL, (c) CHI-GEL, (d) CNC-ALG-GEL, and (e)CNC-CHI-GEL.

and this leads to release of the entrapped liquid which resists the flow behaviour, thus inducing the lower viscosity [36]. This nonlinear relationship represents the higher viscosity of hydrogels which is a strong indication on the impact of cross-linking [22]. The viscosity of a shear thinning liquid has an inversely proportional relationship with the shear rate, whereas a shear thickening liquid has a directly proportional relationship between viscosity and the shear rate [37]. Pseudoplastic nature is important for topical formulations that have viscous behaviour under static conditions; nevertheless, this viscous behaviour tends to decrease at a higher shear rate which results in better spreadability and improves the drug permeation of specific substances upon topical application [11]. By the reinforcement of CNC to hydrogels, the viscosity vs. shear rate curve of CNC-ALG-GEL and CNC-CHI-GEL hydrogels has transformed to a plateau shape, due to the breaking down of CNC domains by shearing force [38]. With regard to the flow behaviour index, $\eta = 1$ for a Newtonian fluid and $\eta < 1$ for a shear thinning fluid or rheofluid, whereas $\eta > 1$ for shear thickening or rheothickening fluid. In the present study, η values of CNC-ALG-GEL and CNC-CHI-GEL hydrogels indicated a Newtonian and shear thickening nature. This phenomenon of transition represents the network structure formed by CNC within alginate, chitosan, and gelatin which was constructed by strong hydrogen interactions and eventually maintains the viscosity [39, 40]. However, the increase in η values of CNC-ALG-GEL and CNC-CHI-GEL hydrogels was also an indication of the shear thickening nature [2]. The biomaterial-based hydrogels reinforced with CNC showed a dependent behaviour which results from rheological characterization.

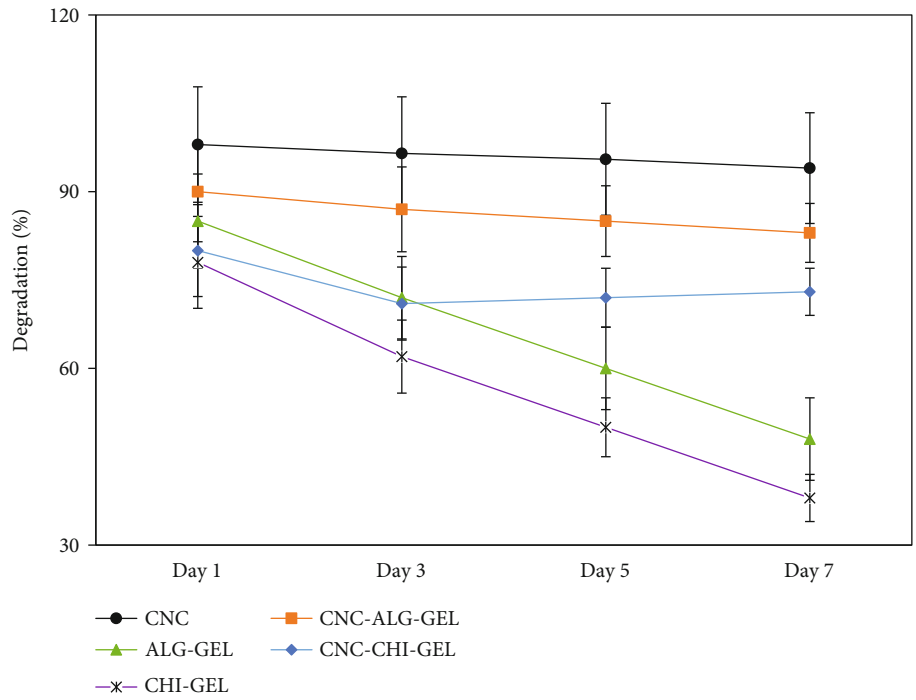

Figure 7: *In vitro* degradation of CNCs and hydrogels.

3.7. In Vitro Degradation. The ALG-GEL and CHI-GEL hydrogels were found to have 50% of weight loss from day 1 to day 7 (Figure 7). This illustrates that the majority of gelatin content in the respective hydrogel samples were susceptible to enzymatic degradation. In the hydrogel samples (CNC-ALG-GEL and CNC-CHI-GEL), 15% of weight loss were significantly observed from day 1 to day 7. In a study by Wang et al. [16], the hydrogels were prepared using alginate and gelatin biopolymers; moreover, the hydrogels without CNC were found to have 50% weight loss, and the hydrogels with CNC have significantly improved resistance to biodegradation. This improved resistance to enzymatic degradation might be due to homogenous dispersion and hydrophobicity [16]. It was believed that the CNC might have helped in creating the interpenetrated matrix between biomaterials alginate, chitosan, and gelatin due to cross-linking and can be expected to distribute uniformly by hydrogen bonding and hydrophobic interactions. Wen et al. [41] developed interpenetrated network (IPN) hydrogels with 25% of weight loss observed within 2 h of enzymatic degradation. They stated that the biomaterials blended with gelatin tend to have superior mechanical characteristics which resulted from interpenetrated matrix, and this provides good stability against degradation [41]. Furthermore, the crystallinity and hydrophilicity are important factors that influence the degradation rate. In addition, the surface hydrophilicity tends to cause the invasion of the degradation medium and water into the amorphous regions of CNC [42]. In this viewpoint of degradation, the biomaterial-based hydrogels reinforced with CNC are mostly recommended for bone and tissue engineering applications.

3.8. Cytotoxicity. The *in vitro* cytotoxicity of CNC and hydrogel membranes was investigated using the *L929* cell line by MTT assay, and absorbance was read at 570 nm to evaluate cell viability [43]. In this method, the viability of the *L929* fibroblast cell line was observed after 24 h of incubation. According to GB/T 16886.5-2003 (ISO 10993-5:1999), the biomaterial-based hydrogel membranes with cell viability more than 75% can be considered as noncytotoxic and are recommended for biomedical applications. The cell viabilities of ALG-GEL and CHI-GEL hydrogels were significantly higher than those of CNC ($p < 0.05$). The CNC-ALG-GEL and CNC-CHI-GEL hydrogel membranes reinforced with CNC had 96% and 97% cell viabilities, respectively, which were significantly higher than CNC, ALG-GEL, and CHI-GEL hydrogels ($p < 0.05$) (Figures 8(a) and 8(b)).

The alginate and chitosan bionanocomposite membranes reinforced with CNC enhanced the viability of *NIH-3T3* fibroblasts [16, 24]. In an another study by Shaheen et al., the chitosan-alginate-hydroxyapatite scaffolds fabricated with CNC were found to have 100% cell viability and promising cell growth and cell adherence [5]. In a previous study of our lab, promising biocompatibility characteristics of polyvinyl alcohol/starch polymer were proven [44]. It was noticed that the mechanical properties and zwitterion polymer network provide the suitable environment for cell growth and proliferation [23]. Interaction of viable cells with the substratum matrix of hydrogel membranes reinforced with CNC *via* physicobiochemical and molecular interactions and surface topological parameters has an essential role in the cytocompatibility of biomaterial membranes such as cell adhesion, differentiation, proliferation, and migration

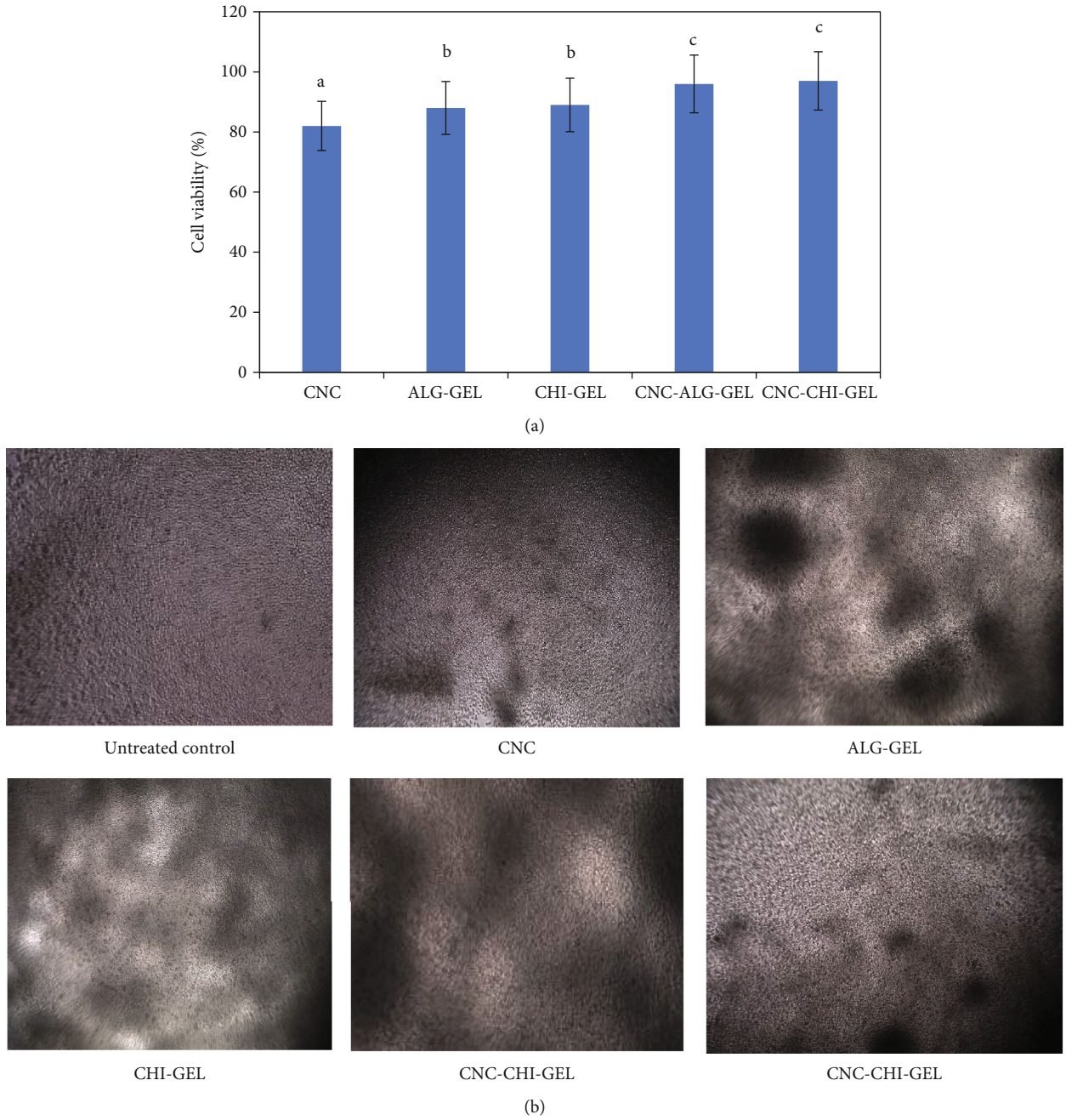

Figure 8: (a) Cell viability assay (different letters indicate significant difference; $p < 0.05$). (b) Fluorescence microscope images of CNC and hydrogel membranes at ×10 magnification.

[5]. Furthermore, the pore size of hydrogel membranes is mostly controlled by the zeta potential which enables the transportation of necessary bioactive molecules and migration of cells within the matrix of hydrogel membranes. In the present study, the zeta potential values of CNC-ALG-GEL, and CNC-CHI-GEL were quite different from those of ALG-GEL and CHI-GEL which might be due to the reinforcement of CNC. Surface charge modification by TEMPO was also most likely a probable reason for changes in zeta potential values. It was noted from a previous study that the CNC and gelatin promote the cell growth by forming mimetics of native bone tissue [45].

4. Conclusion

In the present study, biopolymer-based hydrogels reinforced with CNC were synthesized. Electrostatic chemical attractions, cross-linking of zinc ions, and intermolecular interactions were involved between CNC and alginate, chitosan, and gelatin used for the hydrogel preparation. These

biopolymer-based hydrogel membranes were characterized by desirable physicochemical and morphological properties. Surface charge modification and the reinforcement of CNC enhanced the crystallinity and stability against degradation. Cytotoxicity studies carried out with *L929* cell lines have confirmed its biocompatible nature for applications in tissue engineering, drug delivery, and biomedical fields. Also, hydrogels reinforced with CNC enabled effective cell adhesion, growth, and proliferation as evidenced in our study. However, further experimental studies need to be carried out for the applicability of these hydrogel membranes reinforced with CNC as a supportive biomaterial membrane in the treatment of burn wounds, skin implantations, *in vivo* drug delivery, and tissue transplantation.

Data Availability

Sufficient data have been included in the manuscript. Additional data can be kindly requested from the authors.

Conflicts of Interest

There is no conflict of interest to declare.

Acknowledgments

The authors would like to express their sincere gratitude to ICAR for providing funds to carry out the research work under the ICAR-National Fellow Scheme. The authors acknowledge the Director, ICAR-Central Institute of Fisheries Technology (ICAR-CIFT), Cochin, Kerala, India, for providing the facilities to carry out this work and also for granting permission to publish the data acquired from the study. The authors are grateful to Mrs. PA Jaya (Technical Officer), Mr. P. Suresh (Senior Technician), and Mrs. N. Lekha (Technical Officer) ICAR-Central Institute of Fisheries Technology (CIFT), Cochin, Kerala, for providing technical support to carry out the analyses.

References

[1] Y. Habibi, L. A. Lucia, and O. J. Rojas, "Cellulose nanocrystals: chemistry, self-assembly, and applications," *Chemical Reviews*, vol. 110, no. 6, pp. 3479–3500, 2010.

[2] S. D. Dutta, J. Hexiu, D. K. Patel, K. Ganguly, and K. T. Lim, "3D-printed bioactive and biodegradable hydrogel scaffolds of alginate/gelatin/cellulose nanocrystals for tissue engineering," *International Journal of Biological Macromolecules*, vol. 167, pp. 644–658, 2021.

[3] S. Y. Ooi, I. Ahmad, and M. C. I. M. Amin, "Cellulose nanocrystals extracted from rice husks as a reinforcing material in gelatin hydrogels for use in controlled drug delivery systems," *Industrial Crops and Products*, vol. 93, pp. 227–234, 2016.

[4] H. du, C. Liu, X. Mu et al., "Preparation and characterization of thermally stable cellulose nanocrystals via a sustainable approach of $FeCl_3$-catalyzed formic acid hydrolysis," *Cellulose*, vol. 23, no. 4, pp. 2389–2407, 2016.

[5] T. I. Shaheen, A. S. Montaser, and S. Li, "Effect of cellulose nanocrystals on scaffolds comprising chitosan, alginate and hydroxyapatite for bone tissue engineering," *International Journal of Biological Macromolecules*, vol. 121, pp. 814–821, 2019.

[6] S. P. Akhlaghi, R. C. Berry, and K. C. Tam, "Surface modification of cellulose nanocrystal with chitosan oligosaccharide for drug delivery applications," *Cellulose*, vol. 20, no. 4, pp. 1747–1764, 2013.

[7] Z. Hosseinidoust, M. N. Alam, G. Sim, N. Tufenkji, and T. G. van de Ven, "Cellulose nanocrystals with tunable surface charge for nanomedicine," *Nanoscale*, vol. 7, no. 40, pp. 16647–16657, 2015.

[8] T. Huq, S. Salmieri, A. Khan et al., "Nanocrystalline cellulose (NCC) reinforced alginate based biodegradable nanocomposite film," *Carbohydrate Polymers*, vol. 90, no. 4, pp. 1757–1763, 2012.

[9] H. Celebi and A. Kurt, "Effects of processing on the properties of chitosan/cellulose nanocrystal films," *Carbohydrate Polymers*, vol. 133, pp. 284–293, 2015.

[10] N. Lin, A. Gèze, D. Wouessidjewe, J. Huang, and A. Dufresne, "Biocompatible double-membrane hydrogels from cationic cellulose nanocrystals and anionic alginate as complexing drugs codelivery," *ACS Applied Materials & Interfaces*, vol. 8, no. 11, pp. 6880–6889, 2016.

[11] L. Esposito, A. I. Barbosa, T. Moniz et al., "Design and characterization of sodium alginate and poly(vinyl) alcohol hydrogels for enhanced skin delivery of quercetin," *Pharmaceutics*, vol. 12, no. 12, p. 1149, 2020.

[12] M. Karzar Jeddi and M. Mahkam, "Magnetic nano carboxymethyl cellulose-alginate/chitosan hydrogel beads as biodegradable devices for controlled drug delivery," *International Journal of Biological Macromolecules*, vol. 135, pp. 829–838, 2019.

[13] G. M. A. Ndong Ntoutoume, R. Granet, J. P. Mbakidi et al., "Development of curcumin-cyclodextrin/cellulose nanocrystals complexes: new anticancer drug delivery systems," *Bioorganic & Medicinal Chemistry Letters*, vol. 26, no. 3, pp. 941–945, 2016.

[14] P. Bertsch, L. Schneider, G. Bovone, M. W. Tibbitt, P. Fischer, and S. Gstöhl, "Injectable biocompatible hydrogels from cellulose nanocrystals for locally targeted sustained drug release," *ACS Applied Materials & Interfaces*, vol. 11, no. 42, pp. 38578–38585, 2019.

[15] M. Åhlén, G. K. Tummala, and A. Mihranyan, "Nanoparticle-loaded hydrogels as a pathway for enzyme-triggered drug release in ophthalmic applications," *International Journal of Pharmaceutics*, vol. 536, no. 1, pp. 73–81, 2018.

[16] K. Wang, K. C. Nune, and R. D. K. Misra, "The functional response of alginate-gelatin-nanocrystalline cellulose injectable hydrogels toward delivery of cells and bioactive molecules," *Acta Biomaterialia*, vol. 36, pp. 143–151, 2016.

[17] P. K. Dara, M. Raghavankutty, N. Sebastian et al., "Rheological, physico-chemical, and surface-active properties of gelatin extracted from bigeye tuna (Thunnus obesus) skin waste," *Journal of Aquatic Food Product Technology*, vol. 29, no. 5, pp. 428–444, 2020.

[18] P. K. Dara, M. Raghavankutty, G. Balaraman et al., "Biocompatibility and histopathological evaluation of chitosan nanoparticles grafted fish gelatin bio-nanocomposite membranes in rats," *Iranian Polymer Journal*, vol. 30, no. 9, pp. 953–964, 2021.

[19] B. Li, W. Xu, D. Kronlund et al., "Cellulose nanocrystals prepared via formic acid hydrolysis followed by TEMPO-

mediated oxidation," *Carbohydrate Polymers*, vol. 133, pp. 605–612, 2015.

[20] N. Rescignano, E. Fortunati, I. Armentano et al., "Use of alginate, chitosan and cellulose nanocrystals as emulsion stabilizers in the synthesis of biodegradable polymeric nanoparticles," *Journal of Colloid and Interface Science*, vol. 445, pp. 31–39, 2015.

[21] Y. Hu, X. Jiang, Y. Ding, H. Ge, Y. Yuan, and C. Yang, "Synthesis and characterization of chitosan-poly(acrylic acid) nanoparticles," *Biomaterials*, vol. 23, no. 15, pp. 3193–3201, 2002.

[22] R. Abouzeid, R. Khiari, D. Beneventi, and A. Dufresne, "Biomimetic mineralization of 3D printed alginate/TEMPO-oxidized cellulose nanofibril scaffolds," in *abstracts of papers of the American Chemical Society, vol. 257*, American Chemical Society, NW, WASHINGTON DC, USA, 2019.

[23] N. Chiaoprakobkij, S. Seetabhawang, N. Sanchavanakit, and M. Phisalaphong, "Fabrication and characterization of novel bacterial cellulose/alginate/gelatin biocomposite film," *Journal of Biomaterials Science, Polymer Edition*, vol. 30, no. 11, pp. 961–982, 2019.

[24] K. Madhusudana Rao, A. Kumar, and S. S. Han, "Polysaccharide based bionanocomposite hydrogels reinforced with cellulose nanocrystals: drug release and biocompatibility analyses," *International Journal of Biological Macromolecules*, vol. 101, pp. 165–171, 2017.

[25] P. Lu and Y. L. Hsieh, "Preparation and properties of cellulose nanocrystals: rods, spheres, and network," *Carbohydrate Polymers*, vol. 82, no. 2, pp. 329–336, 2010.

[26] S. Lopes, L. Bueno, F. D. Aguiar Júnior, and C. Finkler, "Preparation and characterization of alginate and gelatin microcapsules containing Lactobacillus rhamnosus," *Anais da Academia Brasileira de Ciências*, vol. 89, no. 3, pp. 1601–1613, 2017.

[27] Q. Li, J. Zhou, and L. Zhang, "Structure and properties of the nanocomposite films of chitosan reinforced with cellulose whiskers," *Journal of Polymer Science Part B: Polymer Physics*, vol. 47, no. 11, pp. 1069–1077, 2009.

[28] C. F. Bellani, E. Pollet, A. Hebraud et al., "Morphological, thermal, and mechanical properties of poly(ε-caprolactone)/poly(ε-caprolactone)-grafted-cellulose nanocrystals mats produced by electrospinning," *Journal of Applied Polymer Science*, vol. 133, no. 21, 2016.

[29] S. Parvez, M. M. Rahman, M. A. Khan et al., "Preparation and characterization of artificial skin using chitosan and gelatin composites for potential biomedical application," *Polymer Bulletin*, vol. 69, no. 6, pp. 715–731, 2012.

[30] S. S. Hindi, "Nanocrystalline cellulose: synthesis from pruning waste of Zizyphus spina christi and characterization," *Nanoscience and Nanotechnology*, vol. 4, no. 3, pp. 106–114, 2017.

[31] C. Xiao, H. Liu, Y. Lu, and L. Zhang, "Blend films from sodium alginate and gelatin solutions," *Journal of Macromolecular Science, Part A*, vol. 38, no. 3, pp. 317–328, 2001.

[32] V. Sharma, A. Jaishankar, Y. C. Wang, and G. H. McKinley, "Rheology of globular proteins: apparent yield stress, high shear rate viscosity and interfacial viscoelasticity of bovine serum albumin solutions," *Soft Matter*, vol. 7, no. 11, pp. 5150–5160, 2011.

[33] D. D. Christianson and E. B. Bagley, "Yield stresses in dispersions of swollen, deformable cornstarch granules," *Cereal chemistry*, vol. 61, no. 6, pp. 500–503, 1984.

[34] P. C. F. Møller, A. Fall, and D. Bonn, "Origin of apparent viscosity in yield stress fluids below yielding," *Europhysics Letters*, vol. 87, no. 3, article 38004, 2009.

[35] N. el Miri, K. Abdelouahdi, A. Barakat et al., "Bio-nanocomposite films reinforced with cellulose nanocrystals: rheology of film-forming solutions, transparency, water vapor barrier and tensile properties of films," *Carbohydrate Polymers*, vol. 129, pp. 156–167, 2015.

[36] B. V. Jyoti and S. W. Baek, "Rheological characterization of ethanolamine gel propellants," *Journal of Energetic Materials*, vol. 34, no. 3, pp. 260–278, 2016.

[37] Z. Liu, L. Zhang, A. Malfliet, B. Blanpain, and M. Guo, "Non-Newtonian behavior of solid-bearing silicate melts: An experimental study," *Journal of Non-Crystalline Solids*, vol. 493, pp. 65–72, 2018.

[38] D. Liu, X. Chen, Y. Yue, M. Chen, and Q. Wu, "Structure and rheology of nanocrystalline cellulose," *Carbohydrate Polymers*, vol. 84, no. 1, pp. 316–322, 2011.

[39] C. Qiao, G. Chen, J. Zhang, and J. Yao, "Structure and rheological properties of cellulose nanocrystals suspension," *Food Hydrocolloids*, vol. 55, pp. 19–25, 2016.

[40] P. K. Dara, A. Geetha, U. Mohanty et al., "Extraction and characterization of myofibrillar proteins from different meat sources: a comparative study," *Journal of Bioresources and Bioproducts*, 2021.

[41] C. Wen, L. Lu, and X. Li, "Mechanically robust gelatin–alginate IPN hydrogels by a combination of enzymatic and ionic crosslinking approaches," *Macromolecular Materials and Engineering*, vol. 299, no. 4, pp. 504–513, 2014.

[42] M. Cheng, Z. Qin, S. Hu, S. Dong, Z. Ren, and H. Yu, "Achieving long-term sustained drug delivery for electrospun biopolyester nanofibrous membranes by introducing cellulose nanocrystals," *ACS Biomaterials Science & Engineering*, vol. 3, no. 8, pp. 1666–1676, 2017.

[43] H. W. Sung, R. N. Huang, L. L. Huang, and C. C. Tsai, "In vitro evaluation of cytotoxicity of a naturally occurring crosslinking reagent for biological tissue fixation," *Journal of Biomaterials Science, Polymer Edition*, vol. 10, no. 1, pp. 63–78, 1999.

[44] P. K. Dara, M. Raghavankutty, G. K. Sivaraman et al., "Biomodulation of poly (vinyl alcohol)/starch polymers into composite-based hybridised films: physico-chemical, structural and biocompatibility characterization," *Journal of Polymer Research*, vol. 28, no. 7, pp. 1–12, 2021.

[45] J. M. Dugan, J. E. Gough, and S. J. Eichhorn, "Directing the morphology and differentiation of skeletal muscle cells using oriented cellulose nanowhiskers," *Biomacromolecules*, vol. 11, no. 9, pp. 2498–2504, 2010.

Hindawi
International Journal of Polymer Science
Volume 2021, Article ID 9930777, 12 pages
https://doi.org/10.1155/2021/9930777

Research Article

Antiskin Cancer and Antioxidant Activities of Formulated Agar from Brown Seaweed *Laminaria digitata* (Hudson) in Dimethyl Benzanthracene-Induced Swiss Albino Mice

Jeneesha George,[1] A. Thabitha,[1] N. Vignesh,[1] V. Manigandan,[1] R. Saravanan,[2] Ghaji Daradkeh,[3] and M. Walid Qoronfleh[4]

[1]*Department of Medical Biotechnology, Chettinad Academy of Research and Education (Deemed to be University), Kelambakkam, 603 103 Tamil Nadu, India*
[2]*Native Medicine and Marine Pharmacology Laboratory, Faculty of Allied Health Sciences, Chettinad Academy of Research and Education (Deemed to be University), Kelambakkam, 603 103 Tamil Nadu, India*
[3]*Department Nutrition, Hamad Medical Corporation–Al-Khor Branch, Doha, Qatar*
[4]*Research & Policy Department, World Innovation Summit for Health (WISH), Qatar Foundation, P.O. Box 5825, Doha, Qatar*

Correspondence should be addressed to R. Saravanan; saran_prp@yahoo.com and M. Walid Qoronfleh; walidq@yahoo.com

Received 23 March 2021; Revised 29 April 2021; Accepted 3 June 2021; Published 16 June 2021

Academic Editor: Antonio Caggiano

This study explores the antiskin cancer effect of formulated agar (FA) from *Laminaria digitata* on dimethyl benzanthracene-(DMBA-) induced skin cancer mice. The agar was extracted and formulated (emulgel), and FA was biochemically characterized. The *in vitro* cytotoxicity of FA was tested using NTT 3T3 mice fibroblast cells. The mice were divided into 5 groups: group 1 served as control mice, group 2 mice were considered as DMBA-induced cancer control, group 3 mice were FA pretreated (low dose) + DMBA-induced mice, group 4 mice were FA pretreated (high dose) + DMBA-induced mice, and group 5 were positive control + DMBA-induced mice. The behaviour and biochemical markers of cancer were significantly decreased in group 2 (DMBA-induced) mice, which were brought to near normalcy by FA pretreated mice (groups 3 and 4). The levels of p53 and keratin were significantly elevated in group 2 mice and these levels were decreased in 3 and 4 mice as well. The histopathological examination of DMBA-induced mice was shown degenerated cervical patches in the skin, cirrhosis in liver, oedema in the renal tissue, and swollen and damage in cardiac tissue, which were reduced for the mice applied with FA. This confirms that FA pretreatment offered potential antiskin cancer property.

1. Introduction

Worldwide, 18.1 million new cases and 9.6 million deaths are due to skin cancer [1]. In India, 63% of death is due to non-communicable diseases, and cancer is one of the dominating causes, accounting for 9%. These figures will nearly double by 2040; skin cancer is almost egregious malignancies among other common cancers though not ranked among the top ten common cancers [2]. There has been a continuous increase in the prevalence of skin cancers, especially that of cutaneous melanomas off the last few years. Despite lack of complete prevalence data, different cancer athenaeum in India announced an increasing incidence of skin cancer changing from 0.5 to 2 per 100 000 communities [3, 4]. Surgery and radiation therapy are the standard available treatments for cancer. However, the main drawback of these therapies includes damage to normal cells with a high proliferate index. Most chemotherapeutics are dispensed methodically and are cytotoxic to normal cells; hence, cancer case must undergo considerable morbidity. The traditional-

based topical administration of anticancer natural drug is a fascinating flipside for increasing drug directing and remedial benefits [5].

The dimethyl Benz (a) anthracene (DMBA) is a polycyclic aromatic hydrocarbon (PAHs), branded as an effective carcinogen and/or endocrine disruptors. PAHs are widely distributed in the environment as a result of incomplete combustion of fossil fuels and other organic molecules and are common contaminants of terrestrial and aquatic ecosystems [6]. Seaweeds are attractive sources of biomolecules such as proteins, polysaccharides, minerals, vitamins, steroids, and dietary fibers which are profitable resources for nutraceutical and pharmaceutical applications [7]. The brown seaweeds are the largest marine sources for polysaccharide extraction (44-53%) globally. Some of the valuable bioactivities revealed by the polysaccharides and their derivatives, both *in vivo* and *in vitro*, include immunomodulatory ability, anticancer, antiviral, anticoagulant, and/or antithrombotic properties. They are also proved to have potent antidislipidaemic, hypoglycaemic antioxidants, antibiotics, and anti-inflammatory effects. Previously, we have reported the antioxidant, anticoagulant, and mosquitocidal properties of phloroglucinol and some water-soluble polysaccharides from Indian brown seaweeds [8, 9]. But till now, there is no report on the anticancer activity of FA from seaweed (IP No. E-101/17997/dated 01.07.2019). Hence, the present study is aimed at finding out the antiskin cancer property of formulated agar from brown seaweed (*L. digitata*) against DMBA-induced mice model.

2. Materials and Methods

The study was conducted in accordance with the Basic & Clinical Pharmacology & Toxicology policy for experimental and clinical studies [9].

2.1. Seaweed Collection. Brown seaweed (*L. digitata*) was collected from Kanyakumari, (Lat. 8.0866 N and Long. 77.5544 E), Tamil Nadu, India, during December 2018–January 2019. The collected brown seaweed species were identified using the Central Marine Fisheries Research Institute (CMFRI) taxonomic manuals and bulletin. The collected samples were cleaned assiduously with seawater and distilled water and finally washed with distilled water. The processed seaweeds were shadow dried, powdered, and stored at -20°C for further study.

2.2. Extraction of Agar. A 10 g of powdered seaweed sample was transferred to the beaker and mix up with 100 ml of high-pure Milli-Q water then autoclaved at 121°C for 1 h for extraction of water-soluble polysaccharides. Further, the water-soluble polysaccharides were filtered through Whatmann No. 1 filter paper to eliminate seaweed debris present in the extract, and then, it was centrifuged at 5000 rpm for 15 min at RT. The filtered extract was kept at RT, and it gets gelated. The gelated samples were dried out at 60°C overnight and stored in -20°C for further experiments [10].

2.3. Formulation of Agar (FA). The carbopol 934 was liquefied slowly while stirring in 60 ml of Milli-Q water for 1 h to evade agglomeration. Carbopol was then neutralized with triethanolamine (5.6 ml) with stirring. This was followed by the addition of methylparaben (0.6 g) and propylparaben (0.07 g) with continuous exhaustive stirring until medium components were homogeneous, then mannitol (17.5 g), lysine (0.88 g), and glycerol (8.75 ml) were added; finally, the gelated agar (100 g) core component of the formulation was added. The mixture was mixed well, and it was stirred for 30 min (Magnetic stirrer, PCE Pvt. Ltd. India) until a clear consistent gel base was obtained. The formulated agar was stored in an air-tight container under freeze conditions [11].

2.4. Characterization of FA. Organoleptic characteristics of the FA, such as color, consistency texture, sterility, and homogeneity, were assessed by visual examination. Besides, several physicochemical characteristics were also analyzed [12–16]. The data represented here was for triplicate determinations.

2.5. FT-IR Spectroscopy of FA. The FT-IR spectroscopic analysis of FA from brown seaweed was performed using a Bruker Alpha instrument (USA) measured in the range of 4000 to 400 cm^{-1} at 30 scans at RT. The samples were thoroughly mixed up with KBr, and the spectra were taken [8].

2.6. Microstructure Studies of FA by Scanning Electronic Microscope (SEM). The morphological features of the FA were studied with a JSM-5600 LV scanning electron microscope (JEOL, Tokyo, Japan). The dried sample was mounted on a metal stub, and the images were taken at an accelerating temperature (200°C, 400°C, 600°C, and 1200°C) with magnifications 5.00 KX, 2.50X, 2.52 KX, and 1.00 KX [17].

2.7. MTT Assay of FA. The cell viability of FA was determined by MTT assay. Freshly cultured NIT 3T3 mouse fibroblast cell line cells were trypsinized, collected, counted, and seeded in a 96-well plate. After 24 h incubation, cells were treated with various concentrations of FA. Then, the cells were incubated in 5% CO_2 at 37°C for 24 h. Later, 100 μl of MTT was added, and incubation was extended for more 4 h. Finally, the medium was removed and 100 μl of DMSO were used to solubilize the formazan crystals. The samples were read at 570 nm (Tecan Multimode Multiwall Plate Reader, Austria). Percentage cytotoxicity was calculated as described earlier [10].

2.8. In Vivo Anticancer Assay. The skin cancer was experimentally induced in female Swiss albino mice following the ethical clearance obtained (IAEC4/Proposal: 31/A.Lr:13/Dated: 20.12.18). The animals were divided into 5 groups as mentioned in Table 1. Control mice received normal food and water *ad libitum*. The 5-FU (100 mg/100 ml acetone)-treated mice served as a positive control. The FA was applied topically weekly twice 30 min before exposure for 63 days. The physical parameters like measurement of tumor size, body weight, and food and water intake of the experimental mice groups were measured during the entire experimental period. At the end of the experimental period, the mice were sacrificed and the skin, liver, kidney, and heart were dissected, then the organs were stored under -20°C until further use.

Table 1: Experimental design.

Group 1	Normal control mice (normal diet and water)
Group 2	Cancer-induced mice (100 nM DMBA dissolved in 200 μl acetone was applied topically weekly twice for four weeks)
Group 3	FA (low dose)—60 mg/ml in 200 μl acetone was applied topically weekly twice for four weeks, 30 min before DMBA exposure (100 nM DMBA dissolved in 200 μl acetone was applied topically weekly twice)
Group 4	FA (high dose)—120 mg/ml in 200 μl acetone was applied topically weekly twice for four weeks, 30 min before DMBA exposure (100 nM DMBA dissolved in 200 μl acetone was applied topically weekly twice)
Group 5	Positive control: 5-FU-100 mg/ml in 100 ml acetone was applied topically weekly twice for four weeks, 30 min before DMBA exposure (100 nM DMBA dissolved in 200 μl acetone was applied topically weekly twice)

Table 2: Stability of FA.

S. no.	Parameters/tests	Stability of FA storage conditions		
		25°C ± 2°C Months (0–3)	32°C ± 2°C Months (0–3)	40°C ± 2°C Months (0–3)
1	Color	No change in color	No change in color	No change in color
2	Odor	No change	No change	No change
3	Homogeneity	Good	Good	Good
4	Consistency	Smooth	Smooth	Smooth
5	pH	6	6	6
6	Viscosity (m^2/s)	0.385	0.382	0.381
7	Microbial load (bacteria)	No microbial growth is observed at 24, 48, and 72 h	No microbial growth is observed at 24, 48, and 72 h	No microbial growth is observed at 24, 48, and 72 h
8	Sterility	No microbial contamination	No microbial contamination	No microbial contamination
9	Vibrational test	No phase of separation	No phase of separation	No phase of separation
10	Centrifugation test	No phase of separation	No phase of separation	No phase of separation

Time period (three months).

2.9. Measurement of Tumor in Experimental Mice. Measurement of tumor development and the effect of FA on tumor development was evaluated by using Vernier caliper. The length, width, and height of the tumor were measured for during the experimental days.

2.10. p53 Protein Level Measurement. Determination of p53 protein level in mice skin tissues and isolated cells were estimated by using mouse p53 ELISA kit.

2.11. Isolation and Determination of Primary Keratinocytes. The epidermis of experimental mice were isolated by incubation in dispase for up to 72 h that was cut subsequently into small pieces with sterilized scissors then incubated for 30 minutes in 0.025% DNase in DMEM at RT with gentle agitation. Afterwards, the mixture was filtered through a 100 mM cell strainer, and the cells were pelleted by centrifugation. Cells were resuspended in 3 : 1 defined keratinocyte serum-free medium containing appropriate growth supplements, seeded on plates previously coated with collagen, then characterized by spectroscopy [18].

2.12. Collagen and Elastin Contents Determination. The amount of collagen and elastin in the dermis was measured using a Sircol assay kit based on the fact that the sirius red dye binds to the side chains of the amino acids in collagen.

Table 3: Texture analysis of FA.

Moisture (%)	48.28 + 0.21
Hardness (g)	243.43 ± 0.60
Adhesiveness (N/mm)	61.50 ± 0.40
Cohesiveness	0.952 ± 0.0.12
Springiness (mm)	3.520 ± 0.012
Gumminess (N)	3.699 ± 0.10

Both soluble and covalently crosslinked insoluble collagen fractions were obtained by successive treatment of the skin with 10 volumes of 5 types of a buffer. The collagen extracted with buffers A and B was categorized as soluble collagen and that extracted with buffers C, D, and E were categorized as insoluble collagen [19, 20].

2.13. Enzymatic and Nonenzymatic Assessments. The levels of reduced glutathione (GSH), superoxide dismutase (SOD), catalase (CAT), and glutathione peroxidase (GPx) were measured in mice skin tissues determined by using commercial kits from Sigma, USA.

2.14. Histopathology. The skin, liver, kidney, and heart of each group of mice were fixed in 10% formalin for

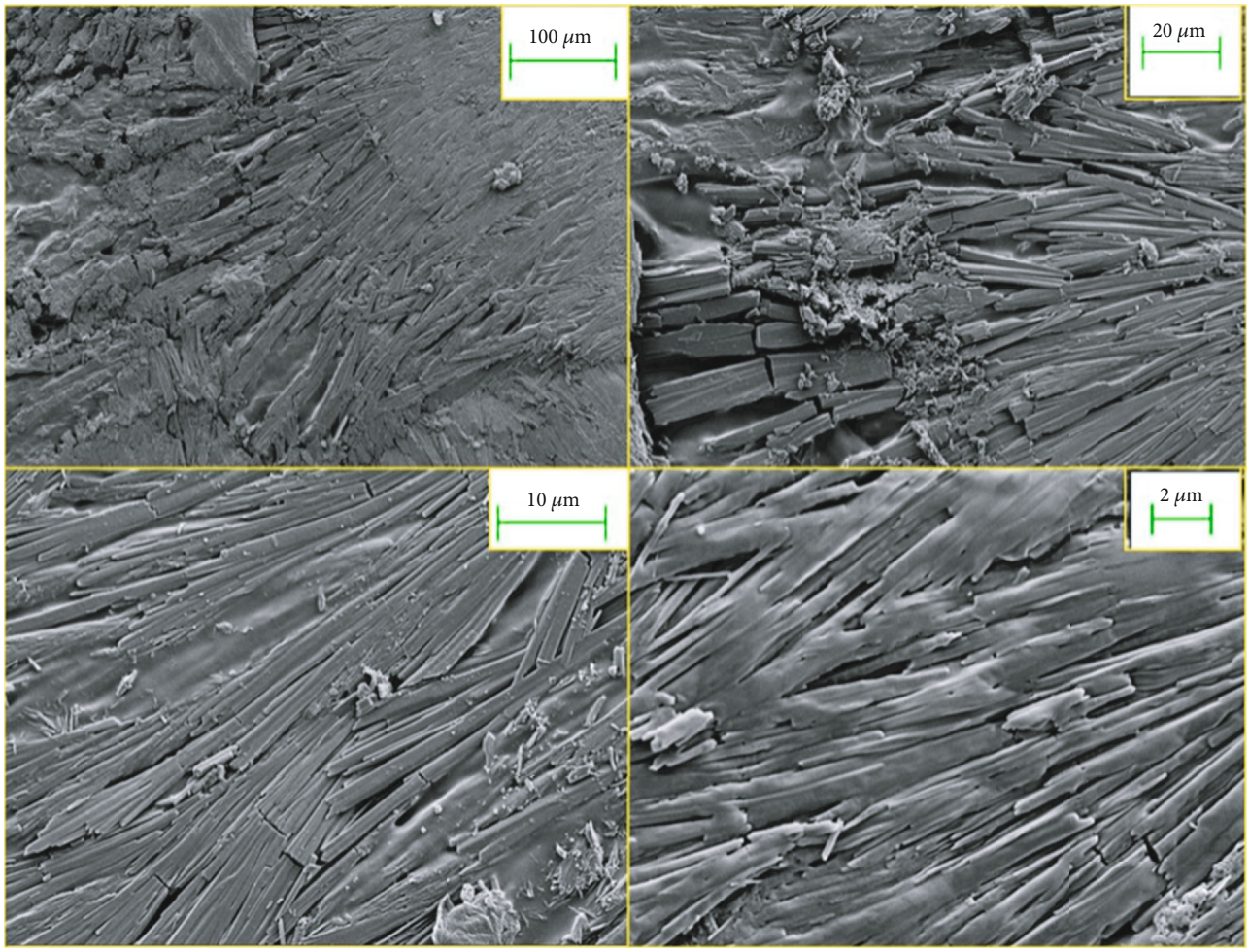

Figure 1: SEM of FA from brown seaweed (The FA (2-10 μm) exhibits regular, layered, patched and smooth, and flat continuous sheet appearance).

haematoxylin and eosin staining (H&E). Serial sections of 20 μm thickness were cut and mounted on slides and stained. The fixed samples were trimmed and dissected in the crosssections and were processed. The samples were fixed in stretches of formalin and alcoholic formalin, 95% alcohol, absolute alcohol, xylene, and liquid paraffin wax. Crosssections were selected from the three plates per sample. The morphological changes were detected under the microscope [21].

2.15. Statistical Analysis. All the statistical analyses were presented by using software using the SPSS software (SPSS, IBM, version 20.0). Each test is performed from all animals, and all the results were expressed as the means plus-minus their corresponding standard deviation (SD). A value of $p < 0.05$ was measured to specify a significant difference between groups.

3. Results and Discussion

3.1. Extraction Yield and FA. The agar yield from *L. digitata* was found to be 40%. This is considered the maximum yield when compared to a previous report [22], which indicated that the agar yield from brown seaweeds could vary. The yield difference is largely due to the species, season period, and geographical location. A cost-effective hot water extraction method with comparable yield was successfully developed for agar extraction and its formulation to develop antiskin cancer property of FA from brown seaweed (*L. digitata*) [23]. Screening for new drugs from natural sources mainly from marine environment to discover anticancer activities is valuable as they are likely to be more safe, robust, and effective. Since agents of synthetic origin may have various adverse effects. Natural products have been used as remedies for skin cancer prevention and other traditional treatments as well. Sulfated polysaccharides (SP) from marine sources were investigated to have good antioxidant, antitumor, and immunomodulating activities. It was suggested that, next to the pharmacological activities of SP, their physicochemical properties, like good water solubility, thickening, and solidity over a wide pH range, offer extra benediction for their use as a preservative in topical application products [10].

3.2. Characterization of FA. Stability studies of FA were essential to ensure product quality, efficacy, and safety. Thus, these studies tend to give the development and improvement

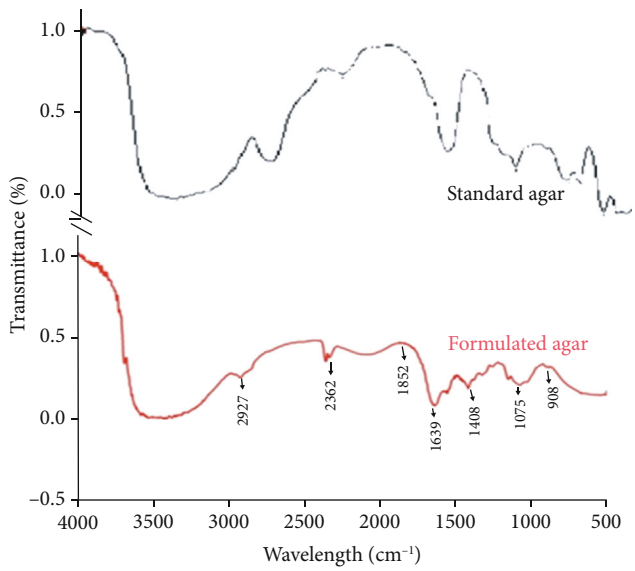

Figure 2: FT-IR spectrum of formulated agar.

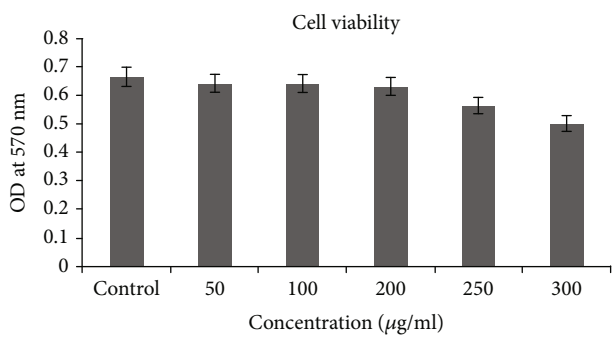

(a)

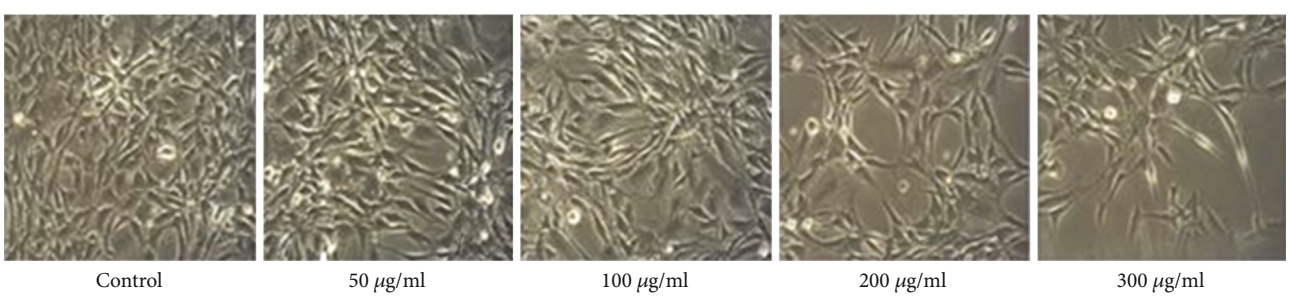

(b)

Figure 3: MTT assay of FA (Cells treated above 300 μg/ml concentration showed a significant ($p < 0.05$) death of cell; compared with control (a, b)).

of formulations, creating the product validity and observing its physical, chemical, and microbiological characteristics. The FA extracted from the *L. digitata* is slightly soluble in distilled water and its dispersal acquiesce a light brown color, slick solution. The FA was virtually insoluble in polar and nonpolar solvents like acetone, chloroform, and ethanol. Stability may be affected by environmental factors such as pH, light, temperature, air, and transport which can induce harsh damage on the product constituents. The FA stability parameters such as no color and odor change, good consistency, and homogeneity were smooth, and there was no microbial contamination. All these features indicate the sterility of FA in Table 2. The pH value of FA remains substantial during storage which was considered adequate to avoid the risk of irritation upon application to the skin. Hence, there was no change in the pH; the FA gel could be suitable for topical application. Centrifugation tests and vibrational tests are the main tools for estimating and predicting the shelf life of

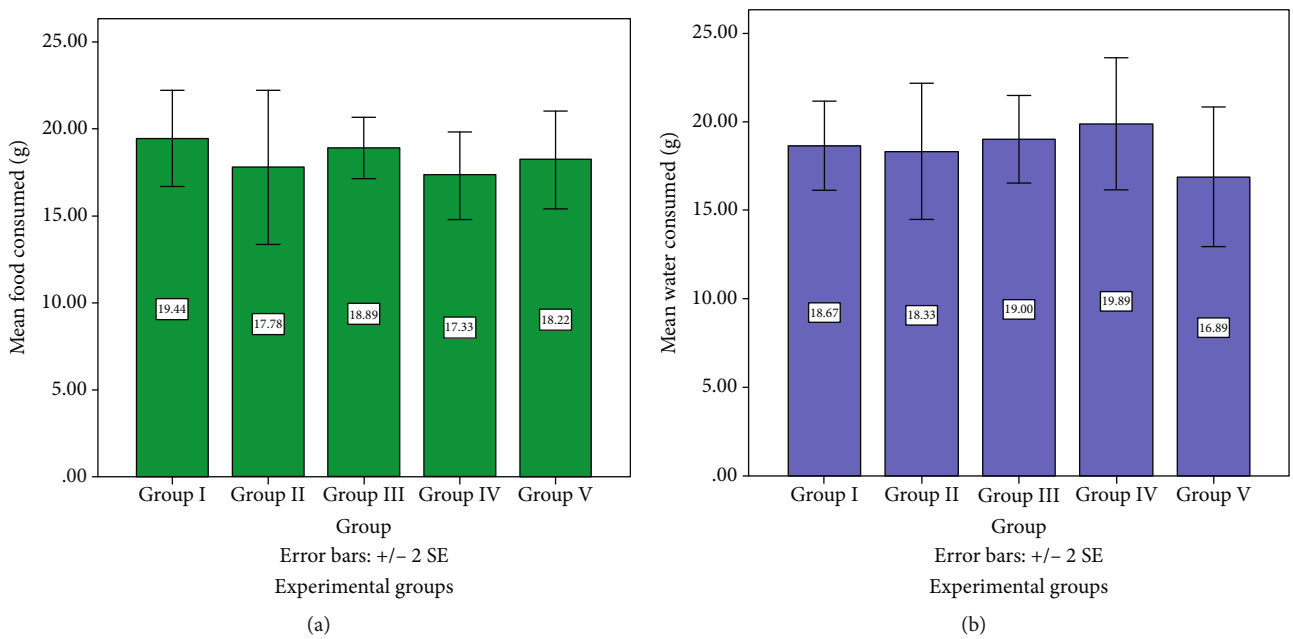

Figure 4: (a, b) Food and water intake of experimental mice (DMBA-induced mice significantly ($p < 0.05$) reduced the food and water intake; FA-treated mice significantly ($p < 0.05$) increased the food and water intake).

the formulated product. From our data, we found that the FA does not show any indication of phase separation during the study period, which are consistent with the findings of Andrade et al. [24].

3.3. Texture Analysis of FA. The texture analyses (moisture, hardness, adhesiveness, cohesiveness, and springiness) of FA were described in Table 3. The texture analysis results of FA are considered high when compared to the results of Reshma [23], who had extracted the agar by using hot water from brown seaweed. The difference in the texture numbers is likely due to the method of extraction and formulated nature of the sample. Texture analysis is one of the most essential unique inspection criteria for pharmaceuticals since it contributes important identification and exclamation knowledge. Characteristics with small intraclass variations and large interclass variations of differing textures are an essential product requirement. Here, we explored characteristics focused on those techniques that have been a standard in texture analyses or applied for repeated material examination.

3.4. Phytochemical Composition of FA. The phytochemical composition of FA includes crude protein amount (3.79%), total carbohydrates (12.33%), and element composition comprising of Ca (1.5%), P (0.18%), N (2.74%), K (2.99%), Mn (16.50 ppm), Zn (50.40 ppm), Fe (30.0 ppm), Cu (75.41 ppm), and Co (3.00 ppm), respectively. The element contents of FA were somewhat high when compared to the previous report of Fleurence et al. [25]. The observed difference in the mineral contents is owing to species difference and method selection for quantification. The mineral composition of FA grants antioxidant properties which could be partially responsible for its anticancer effect. Mineral composition typically is alerted by unusual environmental and physiological conditions, various processing techniques, and methods of mineralization. The macrominerals for example K, Ca, Na, and Mg are present in marine algae at very high levels than in land sources. Further, the level of Fe and Cu were reported to be higher in seaweeds than spinach and meat. The polysaccharides are major components of brown seaweed, accounting for 40% of the dry weight. The hot water extract of agar biomass is loaded in low molecular weight, water-soluble polysaccharides, (WSC) and insoluble in aqueous medium [10].

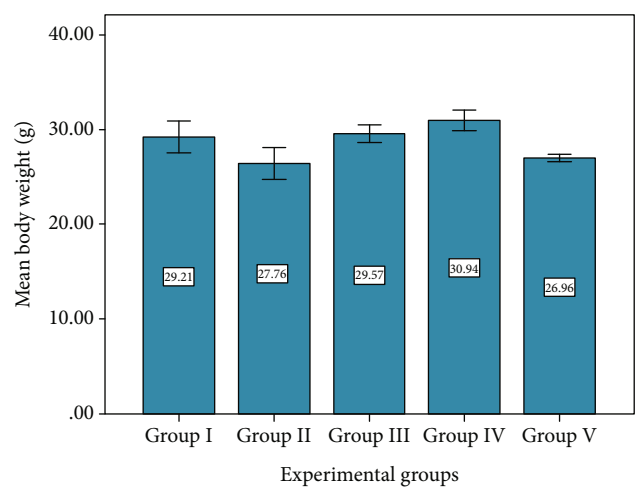

Figure 5: Body weight of experimental mice (DMBA-induced mice significantly ($p < 0.05$) reduced the body weight; FA-treated mice significantly ($p < 0.05$) increased the body weight).

3.5. Structural Characterization

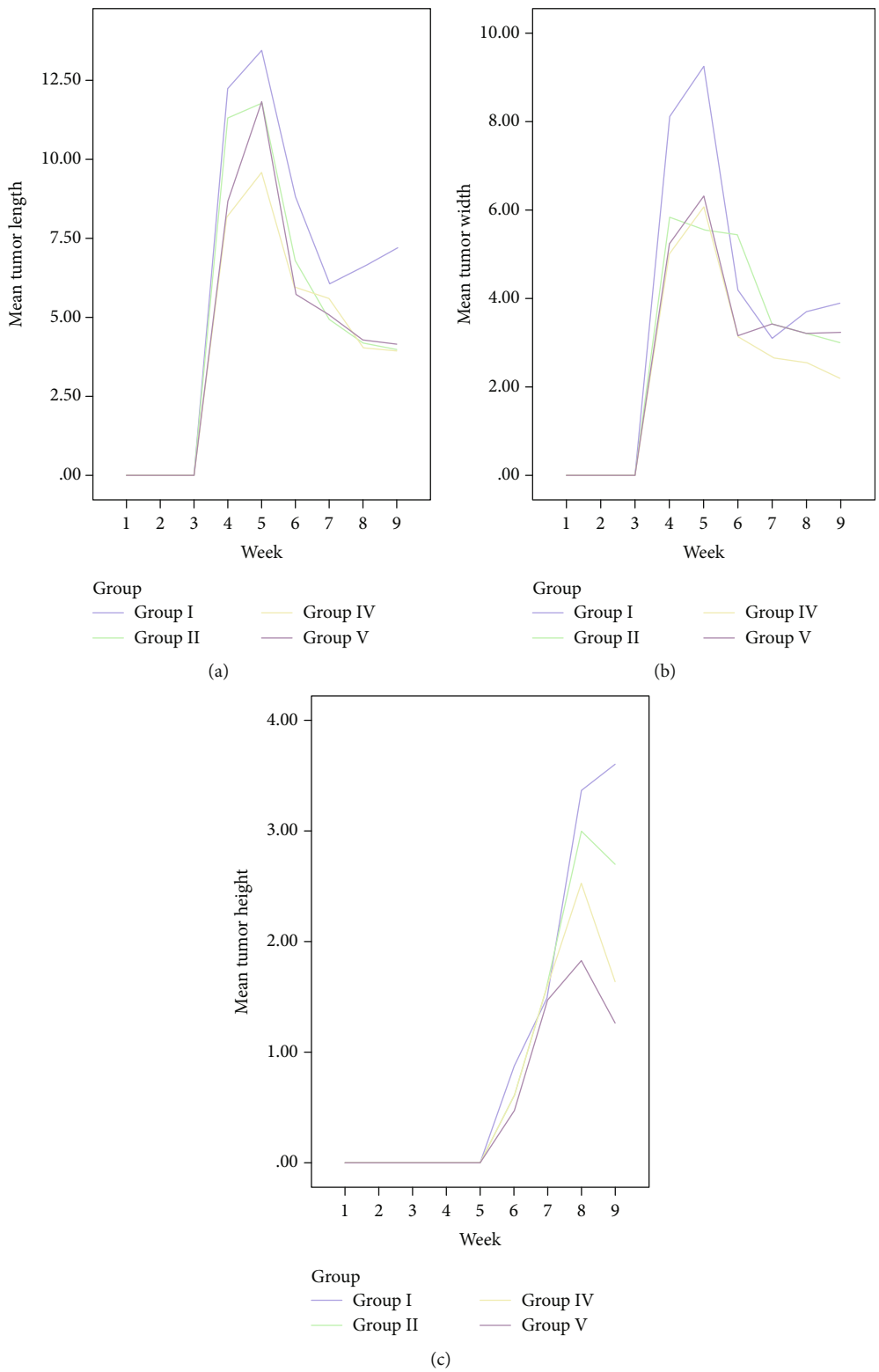

Figure 6: (a–c) Tumor measurement of experimental mice (DMBA-induced mice significantly ($p < 0.05$) increased the tumor size; FA-treated mice significantly ($p < 0.05$) decreased tumor size).

3.5.1. Analytical Method. The FA was dissolved in MilliQ water to bring about a homogeneous solution for scanning in a range of wavelengths between 200 and 700 nm, and it showed maximum absorbance at 280 nm. The UV absorbance of the present study was similar to the result of Azizi et al. [26], who have reported the aqueous extract polysaccharide from *S. muticum* recorded the same UV absorbance at 280 nm. UV-visible spectroscopy is widely used for the

investigation of chromophore associations of atoms identified by energetically absorbing electronic transitions. The UV-visible absorption spectrum of the FA calculated in the present study is displayed in Figure 1. Our data indicate that there was a significant amount of absorption in the UV region, particularly, the maximum absorption ranged from 280 to 350 nm. Further, there was a shoulder detected around 280 nm.

3.5.2. FT-IR Spectroscopy of FA. FT-IR spectroscopy is a promising method for the biochemical analysis of FA and other cellular materials. It affords objective assessment on the holistic biochemistry of a cell or formulated sample and has been practiced in many areas of biomedical research. The FT-IR spectrum of FA in the range 4000-500 cm^{-1} is depicted in Figure 2. Analysis of the given spectra, the peaks obtained were identified as C-H stretch (alkanes) that appeared in the range of 3000-2850 cm^{-1}, -C=C- stretch (alkenes) in the range of 1680-1640 cm^{-1}, C-N stretch in the range of 1250-1020 cm^{-1} that contributes aliphatic amines, and C=H bend (alkenes) in the range of 1000-650 cm^{-1}, when compared with standard agar. Sankar and Rhim et al. [27] reported similar types of FT-IR analyses conducted on both brown algae *S. wightii* and red algae *G. corticata* in between the ranges 4000 and 500 cm^{-1}.

3.5.3. SEM Analysis. SEM offers surface morphology evolution information due to 2D island nucleation and amalgam in FA and adsorbents. SEM images affirm various mount of layer-by-layer arrangement of FA. The step proliferation acceleration can be examined from these images. The vertical verdict was highly adequate to distinguish an atomic layer, while the lateral resolution was 2–100 nm, depending on the sheet appearance and dispatch intensity. The biological and natural source of a formulated material serves as a major determining factor on the basis of granule shape, morphology size, and morphology. The SEM of FA is shown in Figure 3; it exhibits regular, layered, patched, and smooth, flat continuous sheet appearance. It has an irregular geometrical shape with certain gaps on the surface and loosely superimposed. These properties could give significance when considering applications based on surface characteristics. These SEM pictures revealed the structure of the FA network. This intimate connection could also assist the physical stability of the formulated product. On comparison with a recent study by Kim et al. [7], fucoidan present in brown algae induces apoptosis of human colon cancer. In this study, the FA from brown seaweed was fractioned and evaluated for surface features and structural forms compound with smooth, flat continuous sheet appearance.

3.6. In Vitro Cell Viability Study (MTT Assay). The *in vitro* cell viability effects of FA on NIT 3T3 mouse fibroblast cells were assessed. The set of cells that were administrated with concentrations above 300 μg/ml exhibited significant death when compared to control group Figures 3(a) and 3(b). From this result, the LD_{50} of FA was calculated as 300 μg/ml. Fonseca et al. [28], reported the cytotoxicity effect of *Calendula officinalis* extract against UV-B-induced oxidative stress in the skin. The result indicated that above 500 μg/ml concentration, significant cell death was observed. UVA and UVB influence the skin surface and are moderately rejected by the stratum corneum of the epidermis and engrossed by epidermal melanin. Conversely, significant volumes run off the cell walls can activate DNA and cause damage to skin cells, inducing skin cancer.

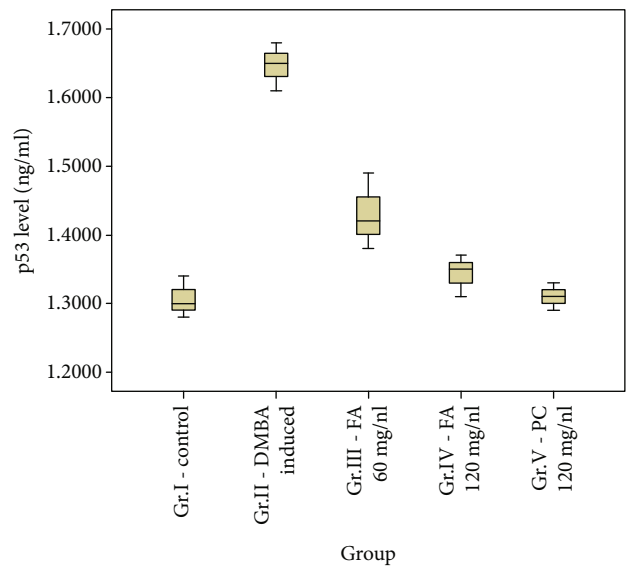

Figure 7: p53 level in skin of experimental mice (DMBA significantly ($p < 0.05$) increased the p53 level; FA-treated mice significantly ($p < 0.001$) reduced the p53 level).

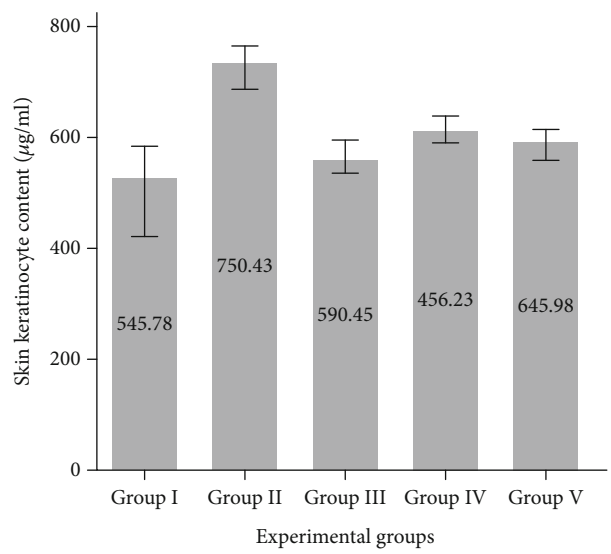

Figure 8: Keratinocyte contents in skin of experimental mice (DMBA-induced mice significantly ($p < 0.05$) lowers the keratinocytes, but it was increased in FA-treated groups).

3.7. Skin Irritation Test. The FA was evaluated for its skin irritant effect. No skin irritation was observed even after 10 days of study, demonstrating that the FA could be a safe material. Daniel et al. [29] reported that the UV-A sunscreen

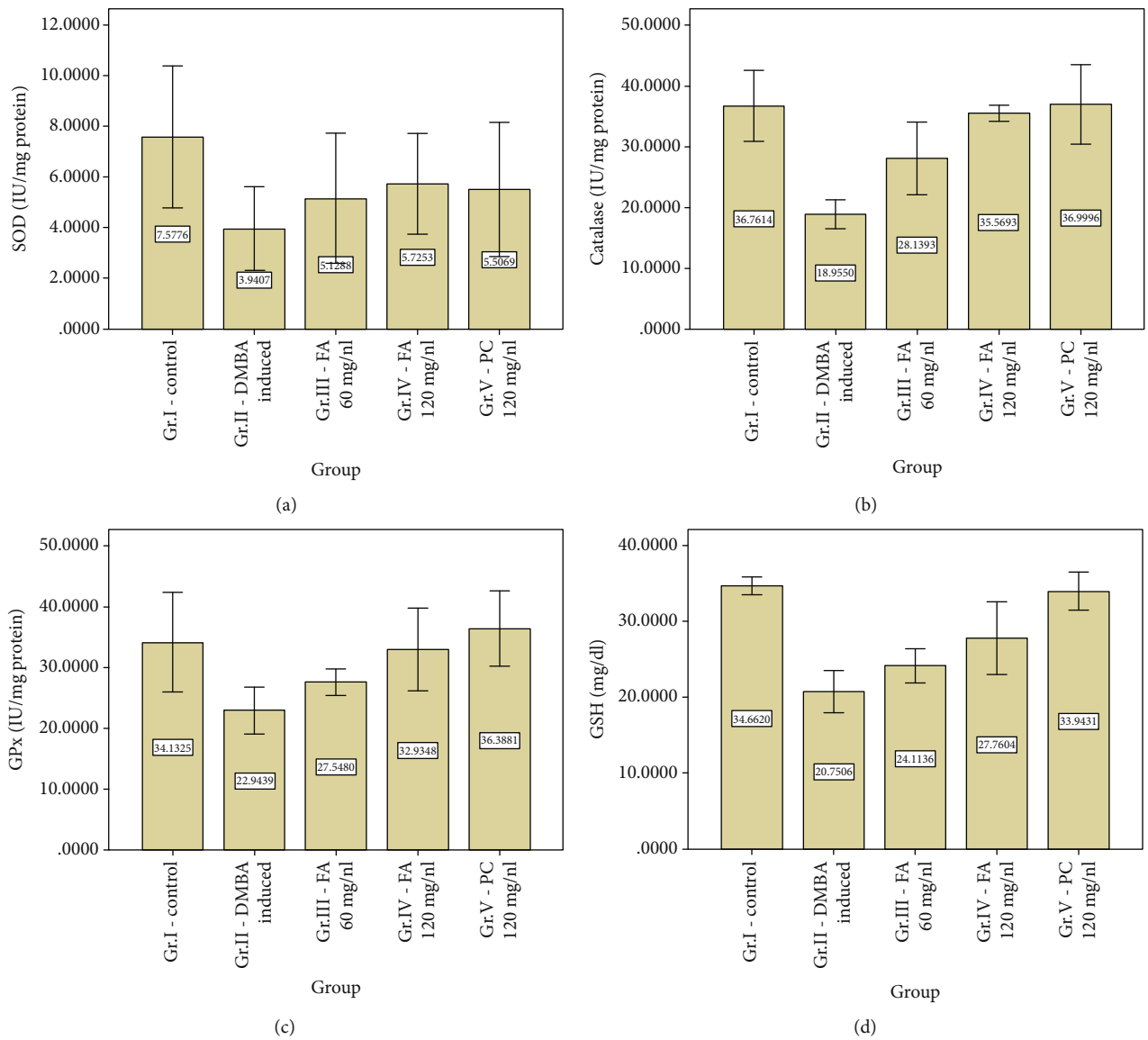

Figure 9: (a–d) *In vivo* antioxidant enzymes in skin tissues of experimental mice (The DMBA significantly ($p < 0.05$) decreased levels of SOD, CAT, GPx, and GSH, whereas, the FA enhanced the antioxidant enzymes activity of SOD, GSH, GPx, and CAT).

gel from red algae-formulated product did not show any skin irritation which corroborates our current data.

3.8. Physiological Observation Tumour Measurement. Experimental mice exhibited significant variations ($p < 0.05$) in food and water intake Figures 4(a) and 4(b). The water intake was significantly increased ($p < 0.05$) after DMBA administrated mice (group II, (from weeks 3 to 9)) on association with group I, II, and III mice. Later, the water intake becomes near normal after treatment with FA to mice groups III and IV Figure 4(b). Group II mice food intake is significantly reduced ($p < 0.05$) after induction of DMBA (weeks 3 to 9), and the food intake becomes near normal after topical treatment of FA to mice groups III and IV Figure 4(a).

Before animals were sacrificed, no mice died during the full experimental course. From the third week onwards, mice induced with DMBA (group II) presented evident cancer effects such as listlessness, lag in response, and slow movement, which continued up to nine weeks. The body weights of DMBA-induced mice were significantly decreased ($p < 0.05$) in group II when compared with control group (group I) and FA-treated groups (group III (60 mg/ml)) and group IV (120 mg/ml) mice Figure 5. Additionally, body weights of group II mice are significantly decreased ($p < 0.001$) when compared to other groups.

Measurements of tumor length, width, and height in group II mice were significantly maximum ($p < 0.001$) on comparison with groups III and IV (Figure 6). The present results confirm Swallow et al. [30] study, which stated that food intake, water intake, body weight measurement, lack of physical activities, physiological changes, and tumor measurement potentially play a major role in body composition. This study results suggested that all of the above-mentioned behaviors and detected changes were due to DMBA-induced mice skin cancer, whereas this was normalized in the FA topically applied mice.

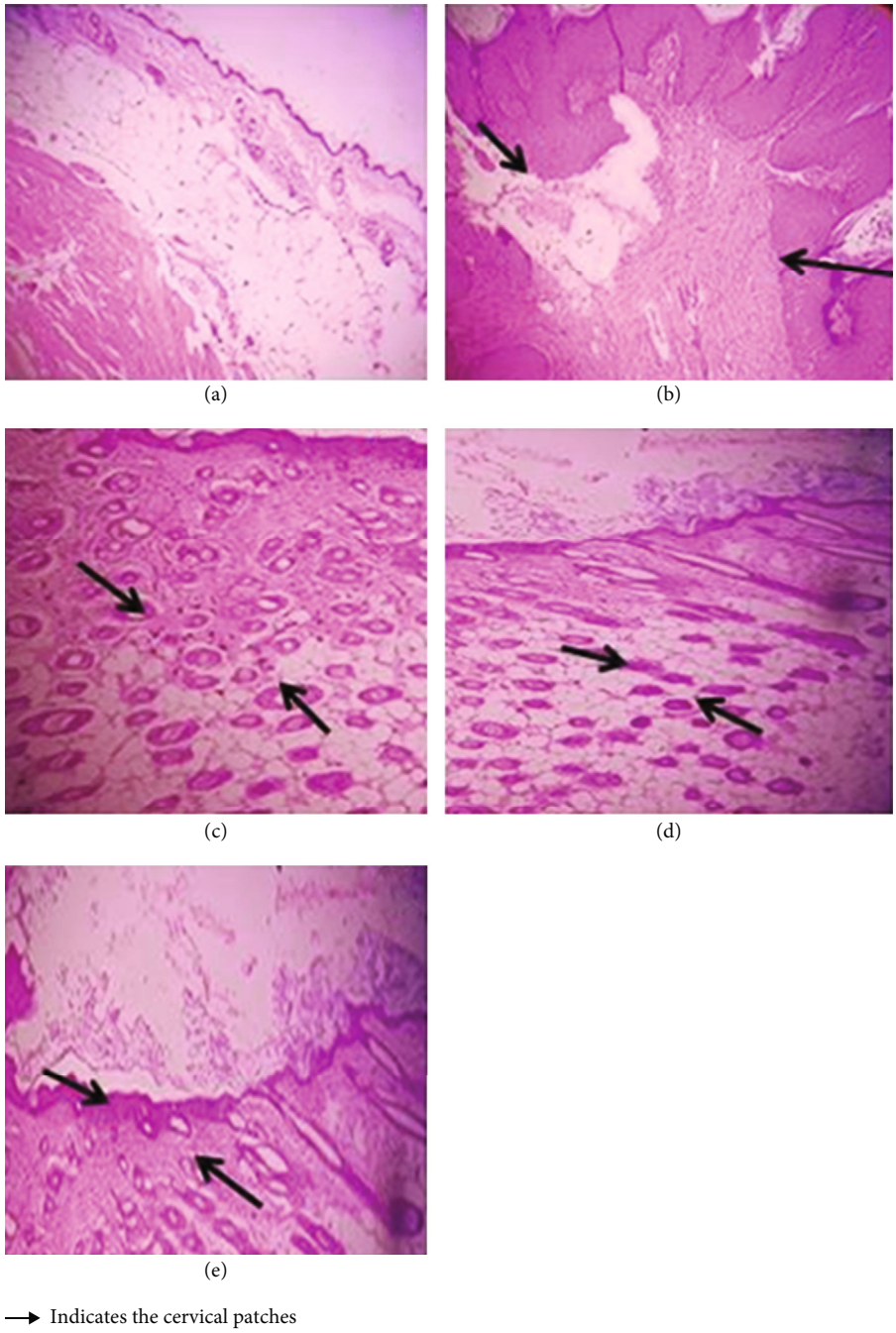

Figure 10: (a–e) Histological evaluation of skin tissue corresponding untreated, DMBA-induced group, FA-treated group, and positive control (The DMBA induced the degenerated cervical patches of the skin of mice; it was brought to normal by FA-treated mice).

3.9. p53 Level Analysis. The p53 protein level in group II mice showed significant elevation ($p < 0.001$) when compared with control and which was significantly reduced ($p < 0.001$) in other treated groups Figure 7. High expression of p53 protein and p53 alterations have been noticed in a great proportion of SCC and premalignant abrasions in renal allograft recipient cases. The p53 tumor suppressor gene was reported to have association with the cell cycle capture and inauguration of programmed cell death [31].

3.10. Keratinocytes Contents of the Skin. In the present investigation, significant loss of keratinocytes was found in the DMBA-induced mice ($p < 0.05$) than control mice. The FA administrated groups III and IV displayed significant improvement ($p < 0.05$) in keratinocyte content when compared to induced group mice Figure 8. Epidermis said to abide of multistate constantly renovating keratinocytes most of the time, and this structure forms the epidermal barrier which need to donate the self-protective responses against

various environmental factors (for example, cold, heat, radiation, trauma, and microbial infection to name a few). Increased level of keratinocytes indicates keratinocyte-connected cutaneous disorders, covering CSC, zoster herpes, and psoriasis [32].

3.11. In Vivo Antioxidant Enzymes Levels. The *in vivo* antioxidant defence system like SOD, CAT, GPx, and GSH in DMBA-induced mice exhibited a significant reduction ($p < 0.05$) in the skin tissues when compared to treated groups Figures 9(a) and 9(d). Cell life in an oxygenated background has necessitated the progression of effective cellular tactics to identify and detoxify metabolites of free radicals. These effects reported to disturb significantly the host of physiological practices and metabolic pathway locally bounded up with the skin cancer of the animal and skin or the change of its related disorders [33]. The results revealed significant rise ($p < 0.05$) in the activities of the primary antioxidant defence enzymes SOD, CAT, GPx, and GSH in the samples of topically applied mice group (groups III and IV) suggesting that the FA could enhance the antioxidant system in the skin of experimental mice. In particular, GSH estimation is an important indicator for quantifying the level of antioxidant activity. The GSH enzyme can be as curtained in almost every cell of the body and have tremendous antioxidant and detoxifying activity. GSH not only eradicates free radicals *in vivo* but also boosts the immunity level [34].

3.12. Histopathological Analysis. The paraffin sections of the skin, the liver, the heart, and the kidney of experimental mice are represented in Figure 10. From this result, the degenerated cervical patches of the skin tissue of the (DMBA) group II was more than that of groups I, III, IV, and V. The cervical patches of the skin were degenerated with skin cancer formation, whereas, these changes were regenerated in the skin cervical patches of formulated agar (group III and group IV)-treated mice. The DMBA-induced mice kidney showed oedema formation and treated mice seen as decrease of oedema. In the heart, the myofibrils were collapsed in the induced group, and in the treated group, showed the normalized myofibrils. The DMBA-induced mice showed significant liver cirrhosis, and these changes were nearly normalized in FA-treated mice.

4. Conclusion

Both the *in vitro* and *in vivo* findings of our present study revealed that FA from brown seaweed could act as a potent antiskin cancer agent and antioxidant. All these outcomes seem to be proposing that pretreatment of FA from *L. digitata* has a great development perspective for mitigation of the skin cancer induced by DMBA. However, there is a need to find the exact mechanism of action of FA, which warrants the need for extensive biochemical and molecular studies. The microbial load and UV-induced skin cancer activities of FA from brown seaweed are not analysed in this study, which could be tested in the future.

Data Availability

The data used to support the findings of this study are available from the authors upon request.

Additional Points

Animal Welfare. Animal use complied with institutional, national, and international guidelines including the Committee for the Purpose of Control and Supervision of Experiments on Animals (CPCSEA), Govt. of India guidelines. Guidelines of "*Guide for the Care and Use of Laboratory Animals*" (Institute of Laboratory Animal Resources, National Academic Press 1996; *NIH publication* number #85-23, revised 1996) were strictly followed throughout the study. Institutional Animal Ethical Committee (IAEC) approved this study. Research ethical clearance was obtained (IAEC4/-Proposal: 31/A.Lr:13/Dated: 20.12.18).

Ethical Approval

This research does not involve human participants, human material, or human data. This research involves experimental animals approved by the Institutional Animal Ethics Committee, Chettinad Academy of Research and Education (Deemed to be University), Kelambakkam-603 103, Tamil Nadu, India, and adhered to the Committee for the Purpose of Control And Supervision of Experiments on Animals (CPCSEA), Govt. of India guidelines.

Conflicts of Interest

All authors declare that there are no conflicts of/or competing interests.

Acknowledgments

The authors want to thank their respective institutions for their continued support. The technical and language editing done by The Editing Refinery, MD, USA, is highly appreciated. The Indian authors gratefully acknowledge the Department of Biotechnology, Ministry of Science and Technology, Govt. of India, New Delhi (BT/PR15676/AAQ/03/794/2016), for their financial support.

References

[1] S. Labani, S. Asthana, K. Rathore, and K. Sardana, "Incidence of melanoma and nonmelanoma skin cancers in Indian and the global regions," *Journal of Cancer Research and Therapeutics*, 2020.

[2] P. Mathur, K. Sathishkumar, M. Chaturvedi et al., "Cancer statistics, 2020: report from National Cancer Registry Programme, India," *American Society of Clinical Oncology*, vol. 16, pp. 1063–1075, 2020.

[3] G. Singh, P. W. Wong, J. Pecoriello et al., "Characterizing index keratinocytic carcinomas in commercially insured adults younger than age 50 years in the United States," *Journal of the American Academy of Dermatology*, vol. 83, no. 5, pp. 1458–1460, 2020.

[4] S. V. Deo, S. Hazarika, N. K. Shukla, S. Kumar, M. Kar, and A. Samaiya, "Surgical management of skin cancers: experience from a regional cancer centre in North India," *Indian Journal of Cancer*, vol. 42, no. 3, p. 145, 2005.

[5] G. Bertino, G. Sersa, F. De Terlizzi et al., "European Research on Electrochemotherapy in Head and Neck Cancer (EURECA) project: results of the treatment of skin cancer," *European Journal of Cancer*, vol. 63, pp. 41–52, 2016.

[6] K. Bernard, C. Forest, and X. Coumoul, "Dimethyl-Benz (a) anthracene: a mammary carcinogen and a neuroendocrine disruptor," *Biochimie Open*, vol. 3, pp. 49–55, 2016.

[7] S. K. Kim and I. Wijesekara, "Development and biological activities of marine-derived bioactive peptides: a review," *Journal of Functional Foods*, vol. 2, no. 1, pp. 1–9, 2010.

[8] K. Ramachandran, V. Manigandan, R. Sheeba, R. Saravanan, and P. R. Rajaian Rajesh, "Structural characterization and comparative biomedical properties of phloroglucinol from Indian brown seaweeds," *Journal of Applied Phycology*, vol. 28, no. 6, pp. 3561–3573, 2016.

[9] P. Tveden-Nyborg, T. K. Bergmann, and J. Lykkesfeldt, "Basic & clinical pharmacology & toxicology policy for experimental and clinical studies," *Basic & Clinical Pharmacology & Toxicology*, vol. 123, no. 3, pp. 233–235, 2018.

[10] M. Venkatesan, V. Arumugam, R. Pugalendi et al., "Antioxidant, anticoagulant and mosquitocidal properties of water soluble polysaccharides (WSPs) from Indian seaweeds," *Process Biochemistry*, vol. 84, pp. 196–204, 2019.

[11] E. A. Yapar, O. İnal, and M. S. Erdal, "Design and in vivo evaluation of emulgel formulations including green tea extract and rose oil," *Acta Pharmaceutica*, vol. 63, no. 4, pp. 531–544, 2013.

[12] J. P. Jadhav, S. S. Phugare, R. S. Dhanve, and S. B. Jadhav, "Rapid biodegradation and decolorization of Direct Orange 39 (Orange TGLL) by an isolated bacterium Pseudomonas aeruginosa strain BCH," *Biodegradation*, vol. 21, no. 3, pp. 453–463, 2010.

[13] A. N. Syad, K. P. Shunmugiah, and P. D. Kasi, "Seaweeds as nutritional supplements: analysis of nutritional profile, physicochemical properties and proximate composition of G. acerosa and S. wightii," *Biomedicine & Preventive Nutrition*, vol. 3, no. 2, pp. 139–144, 2013.

[14] V. C. Deuschle, R. A. Deuschle, M. R. Bortoluzzi, and M. L. Athayde, "Physical chemistry evaluation of stability, spreadability, in vitro antioxidant, and photo-protective capacities of topical formulations containing Calendula officinalis L. leaf extract," *Brazilian Journal of Pharmaceutical Sciences*, vol. 51, no. 1, pp. 63–75, 2015.

[15] M. Muehlbach, R. Brummer, and R. Eggers, "Study on the transferability of the time temperature superposition principle to emulsions," *International Journal of Cosmetic Science*, vol. 28, no. 2, pp. 109–116, 2006.

[16] M. Tomczykowa, M. Wróblewska, K. Winnicka et al., "Novel gel formulations as topical carriers for the essential oil of bidens tripartita for the treatment of candidiasis," *Molecules*, vol. 23, no. 10, p. 2517, 2018.

[17] S. Tajane, P. Dadhe, S. Mandavgane, and S. Mehetre, "Kinetic and thermodynamic azadirachtin extraction from whole neem fine powder formulation," *Indian Journal of Chemical Technology*, vol. 24, pp. 218–222, 2017.

[18] M. Dahlhoff, S. Muzumdar, M. Schäfer, and M. R. Schneider, "ERBB2 is essential for the growth of chemically induced skin tumors in mice," *Journal of Investigative Dermatology*, vol. 137, no. 4, pp. 921–930, 2017.

[19] S. Möllers, I. Heschel, L. H. Damink et al., "Cytocompatibility of a novel, longitudinally microstructured collagen scaffold intended for nerve tissue repair," *Tissue Engineering Part A*, vol. 15, no. 3, pp. 461–472, 2009.

[20] I. Stoilov, B. C. Starcher, R. P. Mecham, and T. J. Broekelmann, "Measurement of elastin, collagen, and total protein levels in tissues," *Methods in Cell Biology*, vol. 143, pp. 133–146, 2018.

[21] J. Sullivan-Brown, M. E. Bisher, and R. D. Burdine, "Embedding, serial sectioning and staining of zebrafish embryos using JB-4 resin," *Nature Protocols*, vol. 6, no. 1, pp. 46–55, 2011.

[22] R. Ahmad, M. Surif, N. Ramli, N. Yahya, A. R. Nor, and L. Bekbayeva, "A preliminary study on the agar content and agar gel strength of Gracilaria manilaensis using different agar extraction processes," *World Applied Sciences Journal*, vol. 15, no. 2, pp. 184–188, 2011.

[23] B. S. Reshma, *Antioxidant and Antiaging Properties of Aqueous Extract from Laminaria digitata (Hudson) in D-Galactose Induced Aging Mice*, M.Sc., Dissertation, Chettinad University, 2017.

[24] K. A. Martínez Andrade, C. Lauritano, G. Romano, and A. Ianora, "Marine microalgae with anti-cancer properties," *Marine Drugs*, vol. 16, no. 5, p. 165, 2018.

[25] J. Fleurence, "Seaweed proteins," *Trends in Food Science & Technology*, vol. 10, no. 1, pp. 25–28, 1999.

[26] S. Azizi, M. B. Ahmad, F. Namvar, and R. Mohamad, "Green biosynthesis and characterization of zinc oxide nanoparticles using brown marine macroalga Sargassum muticum aqueous extract," *Materials Letters*, vol. 116, pp. 275–277, 2014.

[27] S. Shankar and J. W. Rhim, "Preparation of nanocellulose from micro-crystalline cellulose: the effect on the performance and properties of agar-based composite films," *Carbohydrate Polymers*, vol. 135, pp. 18–26, 2016.

[28] Y. M. Fonseca, C. D. Catini, F. T. Vicentini, A. Nomizo, R. F. Gerlach, and M. J. Fonseca, "Protective effect of Calendula officinalis extract against UVB-induced oxidative stress in skin: evaluation of reduced glutathione levels and matrix metalloproteinase secretion," *Journal of Ethnopharmacology*, vol. 127, no. 3, pp. 596–601, 2010.

[29] S. Daniel, S. Cornelia, and Z. Fred, "UV-A sunscreen from red algae for protection against premature skin aging," *Cosmet Toiletries Manufacture Worldwide*, vol. 2004, pp. 139–143, 2004.

[30] J. Swallow, P. Koteja, P. Carter, and T. Garland, "Food consumption and body composition in mice selected for high wheel-running activity," *Journal of Comparative Physiology B*, vol. 171, no. 8, pp. 651–659, 2001.

[31] C. L. Benjamin and H. N. Ananthaswamy, "p53 and the pathogenesis of skin cancer," *Toxicology and Applied Pharmacology*, vol. 224, no. 3, pp. 241–248, 2007.

[32] K. Douroudis, K. Kingo, T. Traks et al., "Polymorphisms in the ATG16L1 gene are associated with psoriasis vulgaris," *Acta Dermato-Venereologica*, vol. 92, no. 1, pp. 85–87, 2012.

[33] H. Ye, K. Wang, C. Zhou, J. Liu, and X. Zeng, "Purification, antitumor and antioxidant activities in vitro of polysaccharides from the brown seaweed Sargassum pallidum," *Food Chemistry*, vol. 111, no. 2, pp. 428–432, 2008.

[34] G. Lavanya, S. P. Voravuthikunchai, and N. H. Towatana, "Acetone extract from Rhodomyrtus tomentosa: a potent natural antioxidant," *Evidence-based Complementary and Alternative Medicine*, vol. 2012, 8 pages, 2012.

Hindawi
International Journal of Polymer Science
Volume 2021, Article ID 5578032, 9 pages
https://doi.org/10.1155/2021/5578032

Research Article

Formulation of Insect Chitosan Stabilized Silver Nanoparticles with Propolis Extract as Potent Antimicrobial and Wound Healing Composites

Mohammed S. Al-saggaf

College of Science and Humanitarian Studies, Shaqra University, Quwaiiyah 11971, Saudi Arabia

Correspondence should be addressed to Mohammed S. Al-saggaf; dr.alsaggaf10@gmail.com

Received 27 February 2021; Revised 10 April 2021; Accepted 5 June 2021; Published 16 June 2021

Academic Editor: R. Saravanan

Skin wounds are frequently influenced with microbial infections and inflammation, which need innovative agents for disputing them. Chitosan (Csn) was extracted from larvae of BSF "black soldier fly, *Hermetia illucens*" and ethanolic propolis extract (Pro) was employed for synthesizing silver nanoparticles (Ag-NPs), using facile biogenic protocol. The BSF-Csn was acquired with a yield of 1.56%, 91.3% deacetylation degree, and 88.600 Dalton molecular weight. The Ag-NPs were effectually biosynthesized using Pro, with a mean diameter of 8.73 nm and zeta potential of -21.34 mV. The antimicrobial activities assessment of insect Csn, Pro, synthesized Ag-NPs with Pro, and their composite against skin pathogens (*Staphylococcus aureus* and *Candida albicans*) revealed the elevated efficiency of the individual agents and the superior action of their composite (Csn/Pro/Ag-NPs), with 26.3 and 23.4 mm inhibition zones and inhibitory concentrations of 35.0 and 45.0 μg/mL from the composite toward *S. aureus* and *C. albicans*, respectively, which exceeded the actions of commercial antibiotics. The treatment of rat's wounds with this composite promisingly led to faster healing of wounds and absence of inflammation and infection signs. The powerful actions of Csn/Pro/Ag-NPs as antimicrobial and wound healing composite strongly advocate their applications for skin protection, disinfection, and regeneration.

1. Introduction

Chitosan (Csn), the derived amino-polysaccharide from chitin deacetylation, is a superior biopolymer that has numerous applications in the biological and medical fields. Accordingly, more Csn extraction processes were greatly required from any potential source, including crustacean wastes, fungi, plants, or insects [1]. Crustacean are the foremost sources for Csn acquiring, but due to their seasonal limited supply, the Csn extractions from fungi and insects were explored as promising alternative sources [2]. The estimation of insect species number is ranging from 6 to 10 million, which exceeds all other animal species together [3]. The BSF could be cultivated for utilization as rich protein sources in animal, poultry, and fish feeding; these insects have also remarkable amounts of chitin in their exoskeleton, which are usable for Csn extraction [4, 5]. The Csn extraction was exploited from many insects, including *Apis mellifera*, *Calosoma rugosa*, *Schistocerca gregaria*, and *Hermetia illucens* "BSF, Black soldier fly" [2, 5–7]. The Csn bioactivities were recurrently verified as promising antimicrobial, clarifying, biochelating, antioxidant, antifungal, and healing accelerator agent [7–12]. The conjugating of Csn with other bioactive compounds and nanomaterials was proposed to augment its biological activity, e.g., antifungal and anticancerous activity [13, 14].

The nanotechnology and nanomaterials' applications in human daily life became an actuality, including their increasing usage in biomedical and health-related fields [15]. The nanomaterials' wide-ranging applications enforced the investigations for more efficient and ecofriendly methods to synthesized/manipulate these nanoforms [16]. The conventional synthesizing protocols (physical and chemical) have

several limitations in metal nanoparticles preparation, e.g., toxic chemicals, high-energy requirements, and expensive downstream processes [17].

The "Green synthesis/biosynthesis" strategies involve the employment of environmentally compatible agents/compounds from biological sources (plants, bacteria, biopolymers, fungi, etc.) for nanoparticles' synthesizing [16]; these auspicious strategies have many advantages over conventional methods, i.e., they produce speedy, eco-friendly, cost-effective, high yield, and safer nanoparticles [15].

Silver nanoparticles (Ag-NPs) are form the leading studied nanometals that have elevated potentialities for applying as powerful antimicrobial, anticancer, antioxidant, and wound-healing accelerator agents; they could be effectually synthesized via biogenic protocols, which augment their eco-friendly characteristics, biocompatibility, and safety toward human cells [18–24].

Numerous reports employed plant extracts/derivatives for synthesizing and stabilizing Ag-NPs, with elevated microbial-inhibition properties [17, 19, 25, 26]; the plants phytocompounds were serving as reducing/capping agents while reacting with $AgNO_3$ (the commonly exercised precursor for Ag-NPs synthesis), which can effectually increase the functionality, bioactivity, and eco-friendly attributes of the protocol.

Propolis (Pro) is the natural beehive resinous composite that is collected from exudates and buds of diverse plants by honeybees, amalgamated with wax, pollen and bees' enzyme. Pro exhibited numerous bioactive compounds and bioactivities and was effectually employed in plentiful pharmacological and biomedical applications [27], including its powerful antimicrobial action, inflammatory, antioxidant, and wound healing potentiality [28–30]. The bee Pro could efficiently synthesize metals' NPs (e.g., silver, gold, and selenium), stimulated by Pro content from biomolecules like flavonoids, alkaloids, phenols, terpenoids, and steroids [31–33].

Wound healing comprises complicated multistep processes affected with varied external and internal factors; skin injury is regularly accompanied by microbial infections and apparent inflammation [34]; these added aspects direct to further required therapies with an extended duration that include antimicrobial and anti-inflammatory agents. The misuse/overuse of antibiotics instigated the emergence of multiple resistant microbial pathogens that require innovative antimicrobial agent/compounds for their fighting [30].

The healing process of wounds comprises six steps: [1] inflammation, [2] cell's migration, [3] angiogenesis, [4] provisional matrix synthesis, [5] collagen deposition, and [6] reepithelization [35]. The Pro-based formulation proved its efficacy in reducing wounded areas, accelerating reepithelization, stimulating cellular proliferative, and decreasing healing time of cutaneous wounds [36, 37].

The current plan involved the extract insect Csn from BSF, to synthesized Ag-NPs using Pro extract, to evaluate their potentiality as antimicrobial candidates against skin pathogens and their capability for accelerating wound healing in rats.

2. Materials and Methods

2.1. Chitosan Extraction and Characterization. BSF "*Hermetia illucens* larvae" were achieved at their fifth instar from the "Experimental insect farm, University of King Abdulaziz, Jeddah, KSA." The majority of BSF oils and proteins were eliminated by oil-press process, and the insects' residues were washed with deionized water (DW) and lyophilized [3, 6]. The Csn extraction processes involved washing with DW and air drying after each step, which included (1) defatting with 10 folds (v/w) from methanol-chloroform mixture (3 : 7, respectively) and stirring for 4.5 h at 25 ± 2°C; (2) demineralization, using 2% HCl solution (12 folds, v/w) at 25 ± 2°C for 125 min; (3) deproteinization, with 10 folds (v/w) from NaOH solution (1.1 M) at 50 ± 2°C for 150 min; and lastly, (4) deacetylation, with 15 folds (v/w) from concentrated NaOH solution (60% w/v), at 25 ± 2°C for 35 min then heating to 110°C for 130 min. The resulted Csn was neutralized via repeated washing with DW then lyophilized.

2.2. Propolis Extraction. Collected propolis from apiaries in the Saudi Arabia southwestern regions was employed for extraction, which was conducted with 10 folds (v/w) from 70% methanol at 27 ± 2°C for 40 h, under shaking (220 x g). The extracted solution was statically kept at 4°C for further 24 h to precipitate propolis wax [27]. The solution was filtered, centrifuged (to eliminate the precipitated materials), and subjected to vacuum evaporation (Buchi, Flavil, Switzerland) at 42°C until dryness. The dried propolis extract (Pro) was redissolved in aqueous ethanol (40%) to have 10% concentration (w/v) [38].

2.3. Ag Nanoparticles Synthesis with Propolis Extract. Pro was diluted to 0.1% (w/v) using DW, and the solution pH was adjusted to 9.6 using NaOH solution (1.0 M). The $AgNO_3$ solution (0.1 M) was prepared in DW and 500 μL from it was slowly dropped into 10 mL of Pro solution with speed stirring at 40 ± 2°C. The color change to deep brown rapidly initiated (within 5 min of combination), which indicated Ag-NPs formation [31]. The produced Pro/Ag-NPs solution was then lyophilized and subjected for analysis.

2.4. Products' Physiognomies Characterization

2.4.1. UV-Visible (UV-vis) Analysis. The absorbance spectrum of Pro/Ag-NPs solution was spectrophotometrically measured (UV-2450, Shimadzu, Japan), at 200-800 nm range.

2.4.2. FTIR "Fourier-transform infrared spectroscopy" Analysis. The FTIR spectra of produced Pro, insect Csn and their composite were screened using FTIR spectrophotometer (JASCO 4100, Japan), at 450–4000 cm^{-1} wavenumber range. Homogeneous powdered materials, blended with KBr (potassium bromide), were examined and their transmittance spectra were plotted.

2.4.3. TEM "Transmission electron microscopy" Imaging. The size, structure, and morphology of the Pro-biosynthesized Ag-NPs were depicted using TEM "JEM-2100, JEOL, Japan", operated at 180 kV accelerating voltage and after sonication

of NPs solution in DW for 15 min, mounting onto grids of carbon-coated copper vacuum drying.

2.4.4. XRD "X-Ray Diffraction" Analysis. XRD analysis for Pro-biosynthesized Ag-NPs for purity measurements was made through a diffractometer (XRD-6000, Shimadzu, Japan), applying Cu-k_α radiation ($\lambda = 1.541$ Å) at 30 mA and 40 Kv in 10-80° range of 2θ.

2.4.5. Particle Size (Ps) Distribution and Zeta Potential (ζ) Determination. The surface charges (zeta potential, ζ) of Pro-biosynthesized Ag-NPs and their Ps distribution were analyzed using zeta plus (Brookhaven, USA).

2.5. Antimicrobial Potentiality Evaluation. The antimimicrobial potentialities of insect Csn, Pro, Pro/Ag-NPs, and their composites were qualitatively/quantitatively evaluated against the challenged skin pathogens, i.e., *Candida albicans* (ATCC-10231) and *Staphylococcus aureus* (ATCC-25923), as they are from the most invasive microbial pathogens to skin. The used media for maintaining and challenging microorganisms were Sabouraud Dextrose Broth/Agar (SDB and SDA, Merck, Germany) for the mycotic strain (*C. albicans*) and Nutrient Broth/Agar (NB and NA, Sigma-Aldrich, St. Louis, MO) for the bacteria strain *S. aureus*, respectively. The microorganisms were propagated and challenged aerobically at 37 ± 1°C.

2.5.1. Disc Diffusion. The qualitative assay, measuring appeared inhibition zones (IZ) following disc diffusion method, was conducted via plating microbial cultures onto appropriate solid media and positioning filter paper discs (6 mm diameter) that impregnated with 30 μL from each agent solution (with a concentration of 10%, w/v) onto the surface of inoculated plates. After incubation for 18-24 h, the appeared IZ around the discs was measured. Nystatin and Vancomycin were employed as standard antibiotics for comparison, using the same challenging conditions.

2.5.2. MIC "Minimum inhibitory concentration" Assay. The elucidated microdilution technique was followed for assessing the MICs of Csn, Pro, Pro/Ag-NPs, and their composites toward tested skin pathogens [8], using TTC "Triphenyl tetrazolium chloride, Merck, Germany" as an indicator for microbial survival. The successive concentration of 10-200 μg/mL from each agent in broth media (in 96 well microplates) was fixed and inoculated with ~10^7 CFU/mL from microbial cells, with the addition of 0.5% TTC. Samples from the colorless wells were subsequently plated onto agar media and incubated to verify the microbicidal action. The MICs were specified as the minimum concentration of a particular agent that prohibited microbial survival in microplates and on agar plates.

2.5.3. SEM "Scanning electron microscopy" Imaging. The SEM (Hitachi S-500, Japan) micrographs were captured for the exposed microbial cells, *C. albicans* and *S. aureus*, to Pro/Ag-NPs (at a concentration of 45.0 μg/mL in broth media), to elucidate the structural alterations in cells after treatment for 0, 4, and 8 h.

2.6. Wound Healing Potentiality of Composited Materials. Young Wistar healthy rats (average weight between 141 and 164 g) were individually housed under maintained conditions "25 ± 2°C; 12 h of light-dark cycle; 65 ± 3% relative humidity" in polyethylene clean cages. Animal's handling and practical experiments were implemented following the guidelines of "Saudi Ethical Committee for the care and use of laboratory animals" with the aid of two veterinarian technicians. The experiment period lasted for 14 days, with rats feeding on a customary pellet diet and free water access. After anesthesia induction via ketamine intramuscular injection (100 mg/kg body weight), wounds with semicircular areas of ~65 mm^2 were made on shaved rats' thoracic area. From the wounding day (day 0), the experimented composite [Csn (1%) + Pro/Ag – NPs (0.1%), dissolved in DW] was topically smeared every 12 h until complete epithelization (the Ag-NPs color intense became lesser after conjugating with Csn and Pro solutions). Wounds were digitally photographed daily, after precise cleansing of the wounded area with sterile saline solution (0.9% NaOH); the reductions and manifestation of wounded areas were appraised from the captured photographs.

2.7. Statistical Analysis. Trials were mostly triplicated; their means and SD "standard deviation" were computed (by Microsoft Excel 2016). T-test and One-way ANOVA were applied for statistical significance computation using the MedCalc software (V. 18.2.1, Mariakerke, Belgium) at $p \leq 0.05$.

3. Results and Discussion

Csn was promisingly extracted from BSF larvae with a final yield of 1.56%. Table 1 illustrated the obtained yields after each process in Csn extraction. The physiochemical attributes of BSF-Csn were the DD of 91.3%, a MW of 88.600 Dalton. Produced Csn had 97.8% solubility in 1% AC "acetic acid solution", without heating.

The BSF-derived chitin and Csn were reported as novel sources for these valuable compounds [4]; BSF requires specific extraction processes, e.g., defatting, due to their high contents of lipids [5]. The fifth instar in BSF larvae development was highly advised for Csn extraction, as after this stage, more pigments and melanin are found in covalently binding with chitin, which leads to poor color attributes for the product [4, 7].

The BSF-Csn spectrum (Figure 1-Csn) indicated typical bonds of standard Csn, illustrated in literature. The main designative bands were detected at 3456 cm^{-1} (NH_2), 2311 cm^{-1} (C—H), 1635 cm^{-1} (amide I, C=O), 1402 cm^{-1} (amide III, C—N), 1112 cm^{-1} (C—O), and 896 cm^{-1} (C—H), receptively. Additionally, the C—H stretching vibrations and C—O bending were also observed at 2879 cm^{-1} and 1069 cm^{-1}, respectively. The detected designative bands in BSF-Csn here are in accordance with former modern investigations concerned insect Csn extraction and characterizations from different types included mealworm, cicada slough, beetles "*Calosoma rugosa*," desert locust "*Schistocerca gregaria*," honey bee "*Apis mellifera*," grasshopper, silkworm chrysalis, and BSF [2, 3, 7].

Table 1: The obtained yields throughout insect chitosan extraction.

Extraction process	Weight after process*	Yield from previous row material (%)	Yield from initial row material* (%)
Oil press	43.2	8.64	8.64
Defatting	41.6	96.43	8.32
Demineralization	23.8	57.21	4.76
Deproteinization	11.6	48.57	2.32
Deacetylation	7.8	67.42	1.56

* The initial raw material weight was 500 g of complete insects.

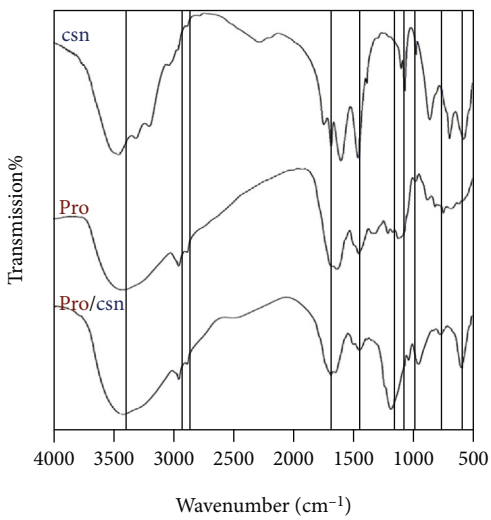

Figure 1: FTIR spectra of insect chitosan (Csn), propolis extract (Pro), and their composite (Pro/Csn).

For Pro (Figure 1-Pro), 889 cm-1 (C–H bonds of phenolic rings), 1151 and 1282 cm-1 (stretched C–O and C–N bond of amino acids aromatic), 1621 cm-1 (–COO^- carboxylate anion), 1654 and 2971 cm-1 (C=O of flavonoids), 2924 cm-1 (stretched CH_2 vibrations of phenolics), and broadband around 3432 cm-1 (Free N–H) [33, 39, 40].

Regarding the Csn/Pro composite spectrum (Figure 1-Pro/Csn), the interactions between Csn and Pro were evidently confirmed from appeared bands in the composite that belong to both constituting agents (indicated with vertical blue lines in figure).

The Ag-NPs were efficaciously synthesized using Pro extract, as evinced from their color changing from bale white to deep brown, after interaction with Pro solution (Figure 2-upper part). The observable color change after mixing of Pro and $AgNO_3$ solutions advocated the Ag^+ reduction to NP form that have free electrons and SPR "surface plasmon resonance" excitation absorption [41].

The UV-vis absorption spectrum of Pro-synthesized Ag-NPs revealed a distinctive apparent peak at 422 nm (Figure 2-lower part), which belong to the designative SPR for biogenic synthesized Ag-NPs (within 220-425 nm), performed formerly using varied plant extracts [19, 22, 25]. They reported also that SPR absorption band frequency/width are principally based on NPs size, shape, dielectric constants "the composition of the particles and surrounding medium" [41]. The detection of single SPR band frequently indicates the NPs spherical shape, while ≥ two SPR bands are mostly corresponding to anisotropic particles [42]. As the UV-vis spectroscopy is frequently distinguishing size-controlled NPs and their shapes in aqueous solutions, the current pattern could indicate the capability and efficiency of Pro solution to reduce Ag to Ag-NPs and advocate the phytosynthesis of NPs [31].

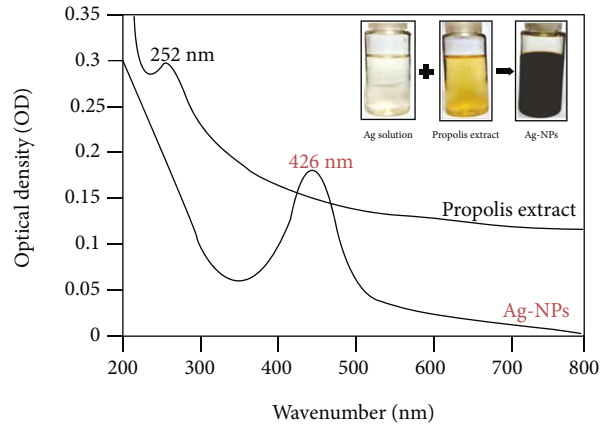

Figure 2: Visual guise and optical density of propolis extract and propolis-synthesized Ag-NPs.

The structural analysis of Pro-synthesized Ag-NPs revealed that NPs were well-distributed and spherically shaped (Figure 3(a)). The NPs diameter size ranged from 3.89 to 24.12 nm, with a mean diameter of 8.73 nm and median diameter of 8.42 nm. Additionally, the Pro-synthesized Ag-NPs had a ζ value of -21.34 mV.

The XRD analysis of phytosynthesized Ag-NPs disclosed clear peaks' existence at $2\theta = 38.13^\circ$, 44.28°, 64.61°, 77.42°, and 81.84°, which are accredited to (111), (200), (220), (311), and (222) reflections of fcc "face-centered cubic", respectively, indicating metallic Ag structure (Figure 3(b)). These attributes were formerly indicated for the biogenic synthesized Ag-NPs, especially using plants' extracts and phytochemicals [20, 22, 26, 43].

The surface of Ag-NPs was suggested as frequently carriers for negative charges, when dispersed in medium; these negative values reinforce the NPs repulsion and elevated stability [26].

The XRD pattern (Figure 3(b)) evidently exhibited the Ag-NPs crystalline nature, as expected from these biosynthesized NPs [22]. As the appeared peaks markedly indicate the NPs cubic crystallinity [20], Pro proved its capability as a promising candidate (from waste materials) for efficient Ag-NPs development.

The antimicrobial potentialities of insect Csn, Pro, synthesized Ag-NPs with Pro, and their composite against skin pathogens (*S. aureus* and *C. albicans*), comparing with customary (vancomycin and nystatin), are demonstrated in Table 2. The microbial inhibitory activities were observable for all examined agents; the most forceful treatment was the combined Csn+Pro+Ag-NPs, as it exhibited the least MIC

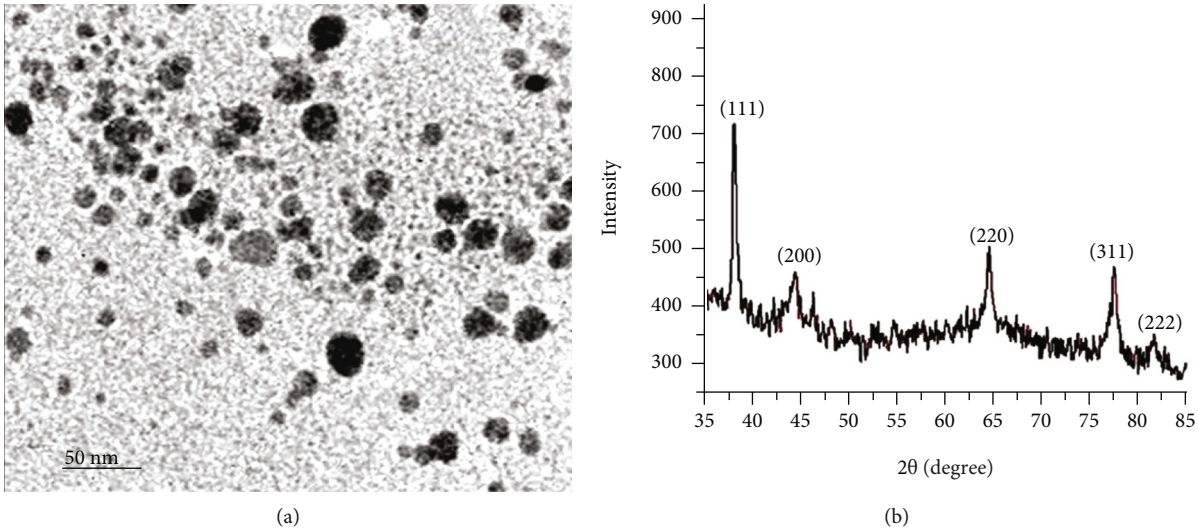

Figure 3: TEM depiction (a) and XRD analysis (b) of phytosynthesized Ag-NPs with propolis extract.

Table 2: Antimicrobial potentialities* of insect chitosan, propolis extract, synthesized Ag-NPs with propolis extract, and their composite against skin microbial pathogens.

Agents	*Staphylococcus aureus*		*Candida albicans*	
	IZ (mm)**	MIC (μg/mL)	IZ (mm)	MIC (μg/mL)
Chitosan	14.6 ± 2.1^{a}	85.0	9.9 ± 1.8^{a}	92.5
Propolis extract	17.3 ± 3.3^{a}	75.0	11.7 ± 2.1^{a}	85.0
Propolis/Ag-NPs	24.6 ± 3.2^{b}	37.5	19.1 ± 2.5^{b}	45.0
Chitosan/Propolis/Ag-NPs	26.3 ± 4.8^{b}	35.0	23.4 ± 2.2^{c}	45.0
Vancomycin	23.5 ± 3.7^{b}	40.0	ND	ND
Nystatin	ND	ND	19.8 ± 3.3^{b}	52.5

*IZ: appeared inhibition zones included diameter of assay disc; MIC: "minimum inhibitory concentrations." ** Within one column, dissimilar letters (superscript) indicate significant differences.

values and the largest ZOI diameters toward both microorganisms. The effect of Ag-NPs was very noticeable for inhibiting skin pathogens; the antibacterial actions (against *S. aureus*) of examined agents were more effectual than their antimycotic actions (against *C. albicans*).

The antimicrobial powers of phytosynthesized Ag-NPs were proved toward numerous pathogens; the assumed mechanisms depended on the NPs ability to attach and penetrate into microbial cells, disturb membrane permeability and interrupt respiration functions, disrupt DNA replication, and ATP production [17, 20, 22, 44, 45].

The observation of SEM micrographs of treated microorganisms with Pro-synthesized Ag-NPs appointed the consequences of NPs treatment on microbial topography and structure (Figure 4). The control cells in the initiation of exposure, i.e., *C. albicans* (Figure 4-C0) and *S. aureus* (Figure 4-S0), appeared with healthy normal structures and utterly smooth intact membranes. After 4 h of exposure (Figure 4-C4 and S4), the interactions between NPs and microbial cells' walls were noticeable, with the appearance of partial cell lysis, especially in *S. aureus* cells. The extension of NPs exposure to 8 h lead to complete cell lysis in *S. aureus* cells (Figure 4-S8) that released their interior contents and exploded, whereas the *C. albicans* cells were obviously deformed and many lysis signs were appeared in this stage (Figure 4-C0).

The attachments of Ag-NPs to microbial surfaces are mostly due to electrostatic attraction [46]; this nanoparticulate attribute was proposed as the leading basis for NPs bactericidal action [47]. Due to high electrostatic affinity and attractions of Ag^{+} ions towards sulfur proteins in cells' surface, the NPs can frequently adhere to cells' cytoplasm and walls, upsurge membranes' permeability and elasticity, which derive microbial casings' disruptions [23, 24]. Once the Ag^{+} ions get uptaken inside microbial cells, the deactivations of respiratory enzymes are occurred, leading to elevated ROS production and ATP release interruption [17]; these ROSs are aggressive factors for enforcing cellular membranes' disruption and DNA distortions. Furthermore, via denaturing the ribosomal cytoplasm components, Ag^{+} ions could competently hinder cellular protein synthesis [48]. Conversely, the biosynthesized Ag-NPs were reported to have elevated biocompatibility and minor toxicity toward mammalian natural cells, e.g., RBCs "red blood cells," PBMCs "peripheral

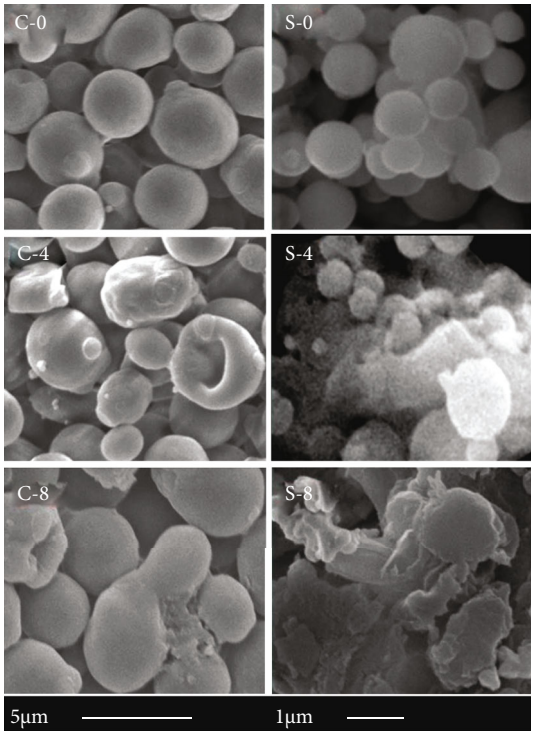

Figure 4: SEM micrographs of exposed *Candida albicans* (C) and *Staphylococcus aureus* (S) cells to synthesized Ag nanoparticles with propolis extract for 0, 4, and 8 h.

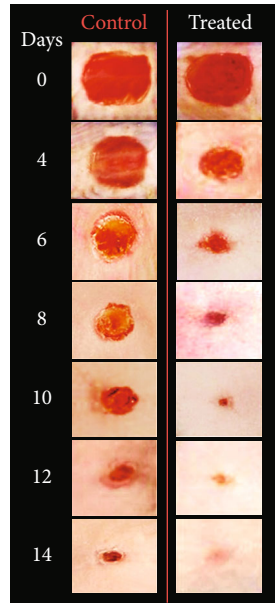

Figure 5: Consequence of treatment rats' skin wounds with chitosan/propolis extract/Ag-NPs composite (treated) on the healing rate of wounds during 14 days, compared to untreated (control) wounds.

blood mononuclear cells," and HEK "human embryonic kidney," which advocated their practical biomedical applications [23, 44, 45].

Ag-NPs themselves can eradicate exposed microbes; the cumulative NPs trigger cell's membranes denaturation and can permeate through these membranes to modify their structural arrangements [24]. The interior cell's organelles could be also ruptured after membranes' denaturation, and this promotes cell lysis/death [49]. The shape of Ag-NPs was demonstrated for influencing their bactericidal power [50], and the spherical shapes with tinier sizes provide more reactive contact facets that strengthen NPs activity [21].

The skin wounds' treatment with Csn/Pro/Ag-NPs composite promoted faster healing of wounded rats' skin during 14 days of local treatment (Figure 5). For the untreated group (Figure 5-control), no complete healing was observed after 14 days, and the mean wound size reduced from 65.4 mm^2 to 59.8, 41.3, 28.5, 22.7, 18.2, and 6.84 mm^2 after 4, 6, 8, 10, 12, and 14 days, respectively. The healing signs appeared much faster in the treated group with Csn/Pro/Ag-NPs composite (Figure 5-treated); the wounded parts became mostly healed after 12 days of treatment.

The composite-treated wounds had no signs of microbial contamination, pus formation, or bleeding throughout treatment, whereas untreated wounds exhibited remarkable inflammation and infection signs. By the 4th day onwards, Csn/Pro/Ag-NPs-treated wounds showed notable wound size reduction and distinguished closure, which were further progressed in the subsequent days of treatment.

The selection of *S. aureus* and *C. albicans* as models for skin pathogens based on their hazardous infections and contamination of epidermal wounds/burns, which resulted in many complications and disorders of infected parts [51]. Additionally, the inclusion of both bacterial and fungal skin pathogens in challenging trials can give more reliability and trustworthiness of the effectiveness and applicability of examined agents. Both *S. aureus* and *C. albicans* can possess the antimicrobial resistance, which require innovative microbicidal agents to overcome their skin wounds' infections [52, 53]. The combined presence of the two pathogens could increase their biofilm formation and antimicrobial resistance [54].

S. aureus is from the extremely dangerous pathogenic microorganism that threatens humans; the bacteria habitually located in skin and mucus membranes and could enter the bloodstreams through wounds and skin scratches [55]. In numerous skin and wound infections' studies, involving colonization and resistance characteristics, *S. aureus* was focused and reported to repeatedly cause severe bloodstream infections [51]. *C. albicans* was categorized among the hazardous fungal infections in diabetic ulcers and skin wounds, which remarkably delayed their healing [56, 57].

The usage of natural derivatives for wound treatments, as alternatives to chemotherapy, attained great concerns to manage skin infections and promote its regeneration [34]. Pro-based formulations were proposed as effectual treatments to accelerate the natural reorganization of injured tissues, through augmenting keratinocyte proliferation [58]. Even diabetic wounds were effectually healed with Pro via decrement the levels of MMPs "matrix metalloproteinases" and proinflammatory cytokines, enhancing the deposition of collagen I and VEGF "vascular endothelial growth factor"

in injured skin [28, 59], thus hastening the healing development. The healthy skin could too benefit from Pro protective properties, e.g., its persuasive anti-inflammatory, antimicrobial, photoprotective, and antioxidants activities [37, 60].

The wound size reduction and their closure are principally resulting from the antimicrobial and anti-inflammatory actions of the composite components, i.e., Csn, Pro, and Ag-NPs. The microbicidal activity of Ag-NPs could prevent wound microbial contamination, which consequently enabled tissue integrity restoring and resulted in adequate repairing of injured sites [22]. The Ag-NP potential role in rapid wound healing was reported to have dose-dependent manner with a healthier cosmetic appearance [61]. Besides, by their microbicidal potentials, Ag-NPs displayed positive consequences for deceasing wound inflammation through diminishing mast cell and lymphocyte infiltration and fibrogenic cytokines amendments [62]. Likewise, the potentiality of Ag-NPs in epidermal reepithelialization and dermal contraction throughout the healing process was the supposed factors for reproduction promotion, keratinocytes migration increment, and fibroblasts differentiation into myofibroblasts [18, 44, 61, 63].

Chitin and Csn were supposed to enhance the healing process in wounded skins. The multiple of mono-subunit (N-acetyl glucosamine), in these polymers' composition, is an imperative constituent in dermal tissue and has a vital necessity for repairing scar tissues [10, 64]. The Csn surface has numerous free amine groups, which can conjoin with blood acidic groups and enhance their coagulation [35, 65, 66]. Csn molecules (by their high positive charge) can effectively promote cells' growth and assist thrombosis/blood coagulation [12, 63, 67, 68], which greatly foster damaged tissue repairing.

4. Conclusion

The biosynthesis of Ag-NPs from Pro and extraction of insect Csn from BSF were promisingly attained in the current work. Csn was extracted from BSF "black soldier fly as an unconventional source for this polymer. The Pro-biosynthesis of Ag-NPs applied simple, direct, and eco-friendly protocol that generated the desired size, shape, and distribution of nanoparticles. The composite of these agents (Pro-synthesized Ag-NPs and Csn) exhibited powerful antimicrobial potentialities against skin pathogens (*C. albicans* and *S. aureus*) and high capability for fast wound healing, without the emergence of infection or inflammation signs, which strongly advocate their applications for skin protection, disinfection, and regeneration.

Data Availability

The datasets generated and/or analyzed during the current study are available from the corresponding author on reasonable request.

Conflicts of Interest

The author declares that they have no conflicts of interest.

References

[1] S. Kou, L. Peters, and M. Mucalo, "Chitosan: a review of sources and preparation methods," *International Journal of Biological Macromolecules*, vol. 169, pp. 85–94, 2021.

[2] Q. Luo, Y. Wang, Q. Han et al., "Comparison of the physicochemical, rheological, and morphologic properties of chitosan from four insects," *Carbohydrate Polymers*, vol. 209, pp. 266–275, 2019.

[3] T. Hahn, A. Roth, R. Ji, E. Schmitt, and S. Zibek, "Chitosan production with larval exoskeletons derived from the insect protein production," *Journal of Biotechnology*, vol. 310, pp. 62–67, 2020.

[4] A. Khayrova, S. Lopatin, and V. Varlamov, "Black soldier fly Hermetia illucens as a novel source of chitin and chitosan," *International Journal of Sciences*, vol. 8, no. 4, pp. 81–86, 2019.

[5] A. Mertenat, S. Diener, and C. Zurbrügg, "Black Soldier Fly biowaste treatment – assessment of global warming potential," *Waste Management*, vol. 84, pp. 173–181, 2019.

[6] N. H. Marei, E. A. El-Samie, T. Salah, G. R. Saad, and A. H. Elwahy, "Isolation and characterization of chitosan from different local insects in Egypt," *International Journal of Biological Macromolecules*, vol. 82, pp. 871–877, 2016.

[7] N. Marei, A. H. Elwahy, T. A. Salah, Y. El Sherif, and E. A. El-Samie, "Enhanced antibacterial activity of Egyptian local insects' chitosan-based nanoparticles loaded with ciprofloxacin-HCl," *International Journal of Biological Macromolecules*, vol. 126, pp. 262–272, 2019.

[8] A. A. Tayel, S. Moussa, W. F. El-Tras, D. Knittel, K. Opwis, and E. Schollmeyer, "Anticandidal action of fungal chitosan against Candida albicans," *International Journal of Biological Macromolecules*, vol. 47, no. 4, pp. 454–457, 2010.

[9] A. A. Tayel, M. M. Gharieb, H. R. Zaki, and N. M. Elguindy, "Bio-clarification of water from heavy metals and microbial effluence using fungal chitosan," *International Journal of Biological Macromolecules*, vol. 83, pp. 277–281, 2016.

[10] V. K. H. Bui, D. Park, and Y. C. Lee, "Chitosan combined with ZnO, TiO2 and Ag nanoparticles for antimicrobial wound healing applications: a mini review of the research trends," *Polymers*, vol. 9, no. 12, p. 21, 2017.

[11] S. Kim, "Competitive biological activities of chitosan and its derivatives: antimicrobial, antioxidant, anticancer, and anti-inflammatory activities," *International Journal of Polymer Science*, vol. 2018, Article ID 1708172, 13 pages, 2018.

[12] A. Moeini, P. Pedram, P. Makvandi, M. Malinconico, and G. G. d'Ayala, "Wound healing and antimicrobial effect of active secondary metabolites in chitosan-based wound dressings: a review," *Carbohydrate Polymers*, vol. 233, p. 115839, 2020.

[13] P. M. Matei, P. Martín-Ramos, M. S.-B. S. Hernández-Navarro et al., "Synthesis of chitosan oligomers/propolis/silver nanoparticles composite systems and study of their activity against Diplodia seriata," *International Journal of Polymer Science*, vol. 2015, Article ID 864729, 11 pages, 2015.

[14] A. I. Alalawy, H. A. El Rabey, F. M. Almutairi et al., "Effectual anticancer potentiality of loaded bee venom onto fungal chitosan nanoparticles," *International Journal of Polymer Science*, vol. 2020, Article ID 2785304, 9 pages, 2020.

[15] L. A. Kolahalam, I. K. Viswanath, B. S. Diwakar, B. Govindh, V. Reddy, and Y. L. N. Murthy, "Review on nanomaterials: synthesis and applications," *Materials Today: Proceedings*, vol. 18, pp. 2182–2190, 2019.

[16] R. G. Saratale, I. Karuppusamy, G. D. Saratale et al., "A comprehensive review on green nanomaterials using biological systems: recent perception and their future applications," *Colloids and Surfaces B: Biointerfaces*, vol. 170, pp. 20–35, 2018.

[17] C. A. Das, V. G. Kumar, T. S. Dhas et al., "Antibacterial activity of silver nanoparticles (biosynthesis): a short review on recent advances," *Biocatalysis and Agricultural Biotechnology*, vol. 18, p. 101593, 2020.

[18] T. Gunasekaran, T. Nigusse, and M. D. Dhanaraju, "Silver nanoparticles as real topical bullets for wound healing," *Journal of the American College of Clinical Wound Specialists*, vol. 3, no. 4, pp. 82–96, 2012.

[19] P. Logeswari, S. Silambarasan, and J. Abraham, "Ecofriendly synthesis of silver nanoparticles from commercially available plant powders and their antibacterial properties," *Scientia Iranica. F*, vol. 20, pp. 1049–1054, 2013.

[20] S. Bhakya, S. Muthukrishnan, M. Sukumaran, and M. Muthukumar, "Biogenic synthesis of silver nanoparticles and their antioxidant and antibacterial activity," *Applied Nanoscience.*, vol. 6, no. 5, pp. 755–766, 2016.

[21] V. E. dos Santos Junior, A. G. R. Targino, M. A. P. Flores et al., "Antimicrobial activity of silver nanoparticle colloids of different sizes and shapes against Streptococcus mutans," *Research on Chemical Intermediates*, vol. 43, no. 10, pp. 5889–5899, 2017.

[22] H. S. Al-Shmgani, W. H. Mohammed, G. M. Sulaiman, and A. H. Saadoon, "Biosynthesis of silver nanoparticles from Catharanthus roseus leaf extract and assessing their antioxidant, antimicrobial, and wound-healing activities," *Artificial cells, Nanomedicine, and Biotechnology*, vol. 45, no. 6, pp. 1234–1240, 2017.

[23] S. Khorrami, A. Zarrabi, M. Khaleghi, M. Danaei, and M. Mozafari, "Selective cytotoxicity of green synthesized silver nanoparticles against the MCF-7 tumor cell line and their enhanced antioxidant and antimicrobial properties," *International Journal of Nanomedicine*, vol. Volume 13, pp. 8013–8024, 2018.

[24] S. A. Ahmad, S. S. Das, A. Khatoon et al., "Bactericidal activity of silver nanoparticles: a mechanistic review," *Materials Science for Energy Technologies*, vol. 3, pp. 756–769, 2020.

[25] B. S. Maria, A. Devadiga, V. S. Kodialbail, and M. B. Saidutta, "Synthesis of silver nanoparticles using medicinal Zizyphus xylopyrus bark extract," *Applied Nanoscience*, vol. 5, no. 6, pp. 755–762, 2015.

[26] K. Anandalakshmi, J. Venugobal, and V. Ramasamy, "Characterization of silver nanoparticles by green synthesis method using Pedalium murex leaf extract and their antibacterial activity," *Applied Nanoscience*, vol. 6, no. 3, pp. 399–408, 2016.

[27] Y. Elnakady, A. Rushdi, R. Franke et al., "Characteristics, chemical compositions and biological activities of propolis from Al-Bahah, Saudi Arabia," *Scientific Reports*, vol. 7, no. 1, p. 41453, 2017.

[28] W. N. Hozzein, G. Badr, A. A. Al Ghamdi, A. Sayed, N. S. Al-Waili, and O. Garraud, "Topical application of propolis enhances cutaneous wound healing by promoting TGF-beta/Smad-mediated collagen production in a streptozotocin-induced type I diabetic mouse model," *Cellular Physiology and Biochemistry*, vol. 37, no. 3, pp. 940–954, 2015.

[29] I. Al-Ani, S. Zimmermann, J. Reichling, and M. Wink, "Antimicrobial activities of European propolis collected from various geographic origins alone and in combination with antibiotics," *Medicines*, vol. 5, no. 1, p. 2, 2018.

[30] E. Rojczyk, A. Klama-Baryła, W. Łabuś, K. Wilemska-Kucharzewska, and M. Kucharzewski, "Historical and modern research on propolis and its application in wound healing and other fields of medicine and contributions by Polish studies," *Journal of Ethnopharmacology*, vol. 262, p. 113159, 2020.

[31] N. Roy, S. Mondal, R. A. Laskar, S. Basu, D. Mandal, and N. A. Begum, "Biogenic synthesis of Au and Ag nanoparticles by Indian propolis and its constituents," *Colloids and Surfaces B: Biointerfaces*, vol. 76, no. 1, pp. 317–325, 2010.

[32] R. Shubharani, M. Mahesh, and V. Yogananda Murthy, "Biosynthesis and characterization, antioxidant and antimicrobial activities of selenium nanoparticles from ethanol extract of Bee Propolis," *Journal of Nanomedicine & Nanotechnology*, vol. 10, no. 1, p. 522, 2019.

[33] C. E. A. Botteon, L. B. Silva, G. V. Ccana-Ccapatinta et al., "Biosynthesis and characterization of gold nanoparticles using Brazilian red propolis and evaluation of its antimicrobial and anticancer activities," *Scientific Reports*, vol. 11, no. 1, pp. 1–16, 2021.

[34] M. F. Medellin-Luna, J. E. Castaneda-Delgado, V. Y. Martinez-Balderas, and A. R. Cervantes-Villagrana, "Medicinal plant extracts and their use as wound closure inducing agents," *Journal of Medicinal Food*, vol. 22, no. 5, pp. 435–443, 2019.

[35] D. Archana, J. Dutta, and P. K. Dutta, "Evaluation of chitosan nano dressing for wound healing: characterization, in vitro and in vivo studies," *International Journal of Biological Macromolecules*, vol. 57, pp. 193–203, 2013.

[36] A. M. Abu-Seida, "Effect of propolis on experimental cutaneous wound healing in dogs," *Veterinary Medicine International*, vol. 2015, Article ID 672643, 4 pages, 2015.

[37] A. A. Zohery, S. M. Meshri, M. I. Madi, S. S. Abd El Rehim, and Z. M. Nour, "Egyptian propolis compared to nanohydroxyapatite graft in the treatment of Class II furcation defects in dogs," *Journal of Periodontology*, vol. 89, no. 11, pp. 1340–1350, 2018.

[38] A. A. Tayel and W. F. El-Tras, "Plant extracts as potent biopreservatives for salmonella typhimurium control and quality enhancement in ground beef," *Journal of Food Safety*, vol. 32, no. 1, pp. 115–121, 2012.

[39] A. A. Righi, G. Negri, and A. Salatino, "Comparative chemistry of propolis from eight Brazilian localities," *Evidence-based Complementary and Alternative Medicine*, vol. 2013, Article ID 267878, 14 pages, 2013.

[40] N. Ibrahim, A. J. Zakaria, Z. Ismail, Y. Ahmad, and K. S. Mohd, "Application of GCMS and FTIR fingerprinting in discriminating two species of Malaysian stingless bees propolis," *International Journal of Engineering and Technology*, vol. 7, pp. 106–112, 2018.

[41] B. J. Wiley, S. H. Im, Z. Y. Li, J. McLellanm, A. Siekkinen, and Y. Xia, "Maneuvering the surface plasmon resonance of silver nanostructures through shape-controlled synthesis," *Journal of Physical Chemistry B*, vol. 110, no. 32, pp. 15666–15675, 2006.

[42] C. Udayasoorian, K. Vinoth Kumar, and R. M. Jayabalarishnan, "Extracellular synthesis of silver nanoparticles using leaf extract of Cassia auriculata," *Digest Journal of Nanomaterials and Biostructures*, vol. 6, pp. 279–283, 2011.

[43] A. Shah, S. Haq, W. Rehman, M. Waseem, S. Shoukat, and M. U. Rehman, "Photocatalytic and antibacterial activities of Paeonia emodi mediated silver oxide nanoparticles," *Materials Research Express*, vol. 6, no. 4, article 045045, 2019.

[44] M. Oves, M. Aslam, M. A. Rauf et al., "Antimicrobial and anticancer activities of silver nanoparticles synthesized from the root hair extract of Phoenix dactylifera," *Materials Science and Engineering: C*, vol. 89, pp. 429–443, 2018.

[45] M. Oves, M. A. Rauf, A. Hussain et al., "Antibacterial silver nanomaterial synthesis from Mesoflavibacter zeaxanthinifaciens and targeting biofilm formation," *Frontiers in Pharmacology*, vol. 10, p. 801, 2019.

[46] Y. W. Cao, R. Jin, and C. A. Mirkin, "DNA-modified core–shell Ag/Au nanoparticles," *Journal of the American Chemical Society*, vol. 123, no. 32, pp. 7961-7962, 2001.

[47] E. D. Matthew, N. M. Schaeublin, K. E. Farrington, S. M. Hussain, and G. R. Johnson, "Lysozyme catalyzes the formation of antimicrobial silver nanoparticles," *ACS Nano*, vol. 3, pp. 984–994, 2009.

[48] V. Pareek, R. Gupta, and J. Panwar, "Do physico-chemical properties of silver nanoparticles decide their interaction with biological media and bactericidal action? A review," *Materials Science and Engineering: C*, vol. 90, pp. 739–749, 2018.

[49] C. Liao, Y. Li, and S. C. Tjong, "Bactericidal and cytotoxic properties of silver nanoparticles," *International Journal of Molecular Sciences*, vol. 20, no. 2, p. 449, 2019.

[50] X. Hong, J. Wen, X. Xiong, and Y. Hu, "Shape effect on the antibacterial activity of silver nanoparticles synthesized via a microwave-assisted method," *Environmental Science and Pollution Research*, vol. 23, no. 5, pp. 4489–4497, 2016.

[51] A. L. Byrd, Y. Belkaid, and J. A. Segre, "The human skin microbiome," *Nature Reviews Microbiology*, vol. 16, no. 3, pp. 143–155, 2018.

[52] R. A. Proctor, "Challenges for a universal Staphylococcus aureus vaccine," *Clinical Infectious Diseases*, vol. 54, no. 8, pp. 1179–1186, 2012.

[53] L. Kalan and E. A. Grice, "Fungi in the wound microbiome," *Advances in Wound Care*, vol. 7, no. 7, pp. 247–255, 2018.

[54] E. F. Kong, C. Tsui, S. Kucharíková, D. Andes, P. Van Dijck, and M. A. Jabra-Rizk, "Commensal protection of Staphylococcus aureus against antimicrobials by Candida albicans biofilm matrix," *MBio*, vol. 7, no. 5, 2016.

[55] J. P. Rasigade and F. Vandenesch, "Staphylococcus aureus: a pathogen with still unresolved issues," *Infection, Genetics and Evolution*, vol. 21, pp. 510–514, 2014.

[56] L. Kalan, M. Loesche, B. P. Hodkinson et al., "Redefining the chronic-wound microbiome: fungal communities are prevalent, dynamic, and associated with delayed healing," *MBio*, vol. 7, no. 5, 2016.

[57] A. Kühbacher, A. Burger-Kentischer, and S. Rupp, "Interaction of Candida species with the skin," *Microorganisms*, vol. 5, no. 2, p. 32, 2017.

[58] E. Sehn, L. Hernandes, S. L. Franco, C. C. Goncalves, and M. L. Baesso, "Dynamics of reepithelialisation and penetration rate of a bee propolis formulation during cutaneous wounds healing," *Analytica Chimica Acta*, vol. 635, no. 1, pp. 115–120, 2009.

[59] D. S. Ernawati and A. Puspa, "Expression of vascular endothelial growth factor and matrix metalloproteinase-9 in Apis mellifera Lawang propolis extract gel-treated traumatic ulcers in diabetic rats," *Veterinary World*, vol. 11, no. 3, pp. 304–309, 2018.

[60] N. Saewan and A. Jimtaisong, "Natural products as photoprotection," *Journal of Cosmetic Dermatology*, vol. 14, no. 1, pp. 47–63, 2015.

[61] P. Y. Lee, C. M. Ho, and V. C. H. Lui, "Silver nanoparticles mediate differential responses in keratinocytes and fibroblasts during skin wound healing," *Chem Med Chem*, vol. 5, no. 3, pp. 468–475, 2010.

[62] J. Tian, K. K. Wong, C. M. Ho et al., "Topical delivery of silver nanoparticles promotes wound healing," *Chem Med Chem*, vol. 2, no. 1, pp. 129–136, 2007.

[63] T. D. Nguyen, T. T. Nguyen, K. L. Ly et al., "In vivo study of the antibacterial chitosan/polyvinyl alcohol loaded with silver nanoparticle hydrogel for wound healing applications," *International Journal of Polymer Science*, vol. 2019, Article ID 7382717, 10 pages, 2019.

[64] X. Zhao, B. Guo, H. Wu, Y. Liang, and P. X. Ma, "Injectable antibacterial conductive nanocomposite cryogels with rapid shape recovery for noncompressible hemorrhage and wound healing," *Nature Communications*, vol. 9, no. 1, pp. 1–17, 2018.

[65] J. Qu, X. Zhao, Y. Liang, T. Zhang, P. X. Ma, and B. Guo, "Antibacterial adhesive injectable hydrogels with rapid self-healing, extensibility and compressibility as wound dressing for joints skin wound healing," *Biomaterials*, vol. 183, pp. 185–199, 2018.

[66] B. Zhang, J. He, M. Shi, Y. Liang, and B. Guo, "Injectable self-healing supramolecular hydrogels with conductivity and photo-thermal antibacterial activity to enhance complete skin regeneration," *Chemical Engineering Journal*, vol. 400, p. 125994, 2020.

[67] M. Li, Y. Liang, J. He, H. Zhang, and B. Guo, "Two-pronged strategy of biomechanically active and biochemically multifunctional hydrogel wound dressing to accelerate wound closure and wound healing," *Chemistry of Materials*, vol. 32, no. 23, pp. 9937–9953, 2020.

[68] X. Zhao, Y. Liang, B. Guo, Z. Yin, D. Zhu, and Y. Han, "Injectable dry cryogels with excellent blood-sucking expansion and blood clotting to cease hemorrhage for lethal deep-wounds, coagulopathy and tissue regeneration," *Chemical Engineering Journal*, vol. 403, p. 126329, 2021.